UNIVERSITY OF SOUTHAMPTON

FACULTY OF ENGINEERING, SCIENCE AND MATHEMATICS

School of Chemistry

AN INVESTIGATION INTO THE USE OF MESOPOROUS PD FILMS AND SILICON MICROFABRICTED MICROHOTPLATES AS A METHANE SENSOR

By

Timothy Peter Dunford

Thesis submitted for the degree of Doctor of Philosophy
June 2006

UNIVERSITY OF SOUTHAMPTON

ABSTRACT

FACULTY OF ENGINEERING, SCIENCE AND MATHEMATICS

SCHOOL OF CHEMISTRY

Doctor of Philosophy

AN INVESTIGATION INTO THE USE OF MESOPOROUS PD FILMS AND SILICON MICROFABRICTED MICROHOTPLATES AS A METHANE SENSOR

By Timothy Peter Dunford

In this work nanostructured Pd films and silicon microfabricated microhotplates were used as a methane gas sensor. Mesoporous Pd films with an hexagonal array of pores (H_1-e Pd) were electrodeposited from an ammonium tetrachloropalladate dodecyl octa(ethylene oxide) template mixture in the hexagonal phase. The films were characterised using electrochemical techniques and found to have high surface areas of up to 56 $m^2 g^{-1}$. TEM analysis showed that the films had a regular array of pores with pore diameters of 3 nm.

H_1-e Pd films were electro-deposited from Brij®56 – ammonium tetrachoropalladate template mixtures onto microhotplates and found to give reproducible, stable catalytic responses to methane. H_1-e Pd films from $Pd(NO_3)_2$ precursors were found to have significantly greater initial catalytic activity. The maximum methane response was also greater.

The resistance of the methane responses to poisoning by hexamethyldisiloxane (HMDS) was also investigated. It was found that the response was rapidly and irreversibly poisoned. Attempts were made to improve the poison resistance. Mesoporous bi-layers with interconnecting pores were prepared by electodepositing mesoporous platinum on top of the palladium layer (H_1-e Pd-Pt bi-layer). Results indicated that the methane response of these H_1-e Pd-Pt bi-layers was poisoned more slowly.

The poisoning by HMDS in other flammable gases was also investigated. It was found that poisoning in n-butane was reversible whilst HMDS had negligible effect on the hydrogen response of mesoporous palladium catalysts.

Table of contents

Acknowledgements

I would like to thank City Technology for their support and keeping up with my incessant demand for microhotplates.

A big thank you to everyone in electrochemistry at Southampton. In particular for Liz for cutting my tea breaks short and Sergio for solving all my IT related nightmares. My biggest thanks are reserved for my supervisor Phil Bartlett for his endless patience and seemingly inexhaustible knowledge and my long suffering girlfriend Julie for all her support.

1. Introduction

This section outlines the need for flammable gas sensors, with particular focus on methane. It describes the various types of sensor available and their advantages.

1.1 Methane sensors

Historically, the mining industry was perhaps one of the first places to use gas sensors as a means of alerting miners to the possibility of an explosion due to the build up of flammable gases. During the twentieth century the use of organic fuels has increased enormously. There was hence a need to develop gas detectors for a wide range of flammable gases. The focus here will be on methane. In the 1970s 'town gas', produced from coal was widely replaced with natural gas [1] due to its significantly higher energy density. Natural gas is almost pure methane, with small amounts of other hydrocarbons. Methane becomes explosive when it reaches a concentration of 5 % in air, a level known as the lower explosion level (LEL). Furthermore, methane cannot be detected by the human senses. There is therefore a need for a sensor to alert to methane concentrations below the LEL to avoid the possibility of an explosion.

There are a number of different types of methane sensors. The focus here will be on solid state sensors which are thoroughly reviewed by Moseley.[2] This type of sensor is widely used due to low production costs and good reliability. There are three main types of solid state sensors; catalytic, solid electrolyte and semiconducting oxide gas sensors.[2]

Catalytic gas sensors were developed by Baker and Jones at the Health and Safety Executive laboratories in Sheffield.[2] These comprise a catalyst, heating element and a temperature sensor. The catalyst is heated to the temperature required to catalyse the oxidation of the gas by the heating element. As the catalyst oxidises the gas the temperature will increase resulting in a proportional increase in the resistance of the heating element. This type of device is fully discussed in the following section.

The key property of solid electrolyte sensors is the ability of the material to allow the conduction of ions but not of electrons. The solid electrolyte must provide two regions of different activity to the species under consideration. There is a high mobility pathway of the species between the two regions. This type of sensor

received considerable interest from the mid 1980s as legislation was introduced restricting emission levels of carbon monoxide, hydrocarbons and nitrogen oxides from automobiles.[2]

Finally, chemoresistive sensors employ semiconducting metal oxides whose electrical conductivity varies as the composition of the gas changes.[2] All three of the gas categories that need monitoring – oxygen, flammable and toxic gases can be monitored. Semiconductor gas sensors function as gas sensitive resistors. They represent a simple low cost and durable means of gas monitoring.

1.1.1 Pellistors

Pellistors are a common type of catalytic or calorimetric sensor. The first designs consisted of bare Pt coils and were operated between 800 and 1000 °C.[2] Operating temperatures were lowered by the use of finely distributed precious metal catalysts.[2] Modern devices comprise a platinum wire coil which is encapsulated within an alumina bead coated in palladium catalyst.[3] A diagram of a commercial pellistor is shown in fig 1.

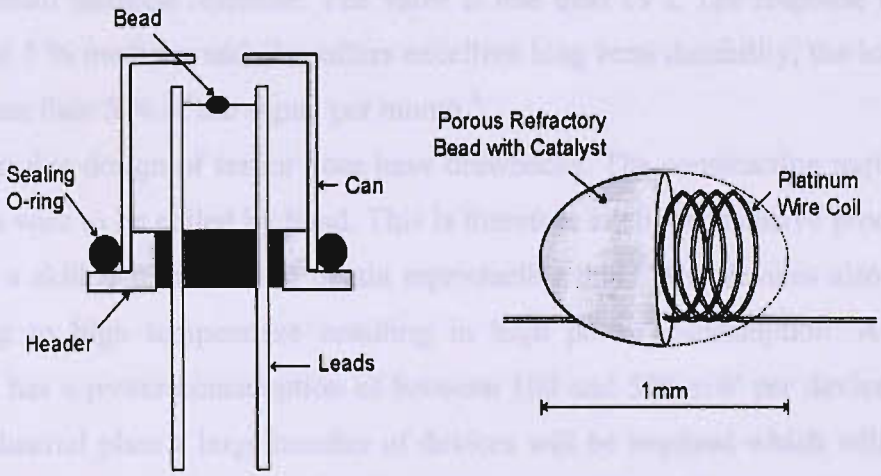

Fig 1. Diagram of a typical commercial pellistor. On the right the catalytic bead can be seen containing the coiled platinum wire heater element within the catalyst bead. On the left a cut-away view of a device shows the location of the bead within the can.[3]

Figure 1 shows the bead suspended between two leads and enclosed in a metal can. The main purpose of the can is to protect the relatively fragile bead. The

temperature of the catalyst is raised to an operating temperature of around 500 °C by applying a potential across the leads. Methane is then catalytically oxidised by the catalyst.

Pellistors are manufactured as pairs, comprising a sensitive (or catalytically active) element and a non-sensitive (or compensating) element. The sensitive element responds to gas whilst the compensating element allows for the effect of environmental changes. The two sensors are combined in a Wheatstone bridge arrangement, a detailed description of which is given in the experimental section. Once the two devices have heated up and stabilised the bridge output is set to zero using a trimming resistor. As the sensitive element oxidises methane its temperature increases relative to that of the compensating element. This can be used to trigger an alarm indicating the presence of methane. There is no need to amplify the signal as this can be up to a maximum of 50 mV per percent methane.

Commercial pellistors are relatively low in cost and easy to construct. The 90N device manufactured by City Technology has a very similar structure to that shown in fig 1. It has an operating voltage of 3.5 V and an output sensitivity of 30 to 40 mV / % methane. It also gives a rapid response. T_{90} is the time taken to reach 90 % of maximum methane response. The value is less than 15 s. The response is linear from 0 to 3 % methane and also offers excellent long term durability; the long term drift is less than 5 % of the signal per month.[4]

However, this design of sensor does have drawbacks. The construction requires the platinum wire to be coiled by hand. This is therefore a labour intensive process and requires a skilled technician to obtain reproducible coils. The devices also require powering to high temperature resulting in high power consumption. A typical pellistor has a power consumption of between 100 and 500 mW per device.[5,6] In a large industrial plant a large number of devices will be required which will add up to give a significant power consumption. Materials such as flame retardants, used in the very situations where such sensors are likely to be used can also poison the catalyst due to the additives they contain. Amongst the most effective poisons are halogenated hydrocarbons[2] and organosiloxanes.[7,8] A more detailed treatment of catalyst poisoning is given in section 5.1. A study by Gentry and Walsh[9] concluded that the best way to improve the poison resistance of pellistor type sensors, to HMDS in particular, was to increase porosity and dispersion of the catalyst. An

investigation by Moseley found that poison resistance was improved by using beads of very high surface area and by selecting the most appropriate catalyst.[2]

Commercial demands for low power, low cost devices have now exceeded the limitations of these pellistors. A new design is therefore required which involves minimal labour and production cost, low power consumption, high reproducibility and good poison resistance.

1.2 Catalytic oxidation of hydrocarbons

There have been extensive studies into the catalytic oxidation of hydrocarbons due to the considerable range of practical applications such as hydrocarbon detection,[10] odour control[11] and the removal of volatile organics from industrial processes such as polymer processing, coating, spray and offset printing[12] as well as from domestic heating systems,[13] industrial boilers[14] and gas turbines.[15,16] Much of the work has focused on methane as it is by far the largest constituent of natural gas used in combustion engines. Methane is harder to oxidise than higher chain hydrocarbons.[10,17,18] A study by Anderson[10] investigated the complete catalytic oxidation of 2-pentene, benzene and methane using a variety of supported catalysts including Pt and Pd. The results showed significantly higher temperatures were required for the oxidation of methane for all catalysts. Work by Burch *et al.*[18] concluded that the C-H bond in methane was the hardest to activate whilst ethane and butane were easier and higher hydrocarbons even easier still. Studies investigating the catalytic oxidation of alkanes have shown a trend between the ease of oxidation and the bond strength of the weakest C-H bond.[19-22] This therefore suggests that the rate determining step of the process is the activation of the C-H bond.

1.2.1 Oxidation of methane

The overall reaction for the complete oxidation of methane is shown in equation 1.[23]

$$CH_4 + 2O_2 \rightarrow CO_2 + 2H_2O, \quad \Delta H_{298} = -802.7 \text{ kJ mol}^{-1} \qquad \textbf{(1)}$$

The bond strength of a C-H bond in methane is 436 kJ mol^{-1}. The activation energy over certain crystal faces of transition metals is as low as 29 - 42 kJ mol^{-1}.[18] The

importance of the combustion of methane has resulted in a significant amount of research in identifying the optimal catalyst for this process.

1.2.2 Optimal catalyst material

Although we are primarily interested in the catalytic oxidation of methane the catalytic oxidation of other flammable gases will also be briefly discussed. There is now a growing consensus that palladium is the optimal choice for the catalytic oxidation of methane whilst platinum has been shown to be more effective for the combustion of higher hydrocarbons.[10,19,23,24 25]

1.2.3 Effect of the support

Existing commercial pellsitors such as the 90N device manufactured by City Technology contain palladium but also a number of other additives including zirconium and cerium. In the case of the City catalyst zirconium is added simply to fill out the volume needed for the construction of the bead. Other refractory type materials such as alumina and silica could also be used. Cerium is added as it was found to improve sintering of the bead which helps to improve baseline stability.[3] Much work has been carried out investigating the effect of additives on the catalytic performance of palladium catalysts, in particular the effect of the catalyst support. Most palladium catalysts are prepared by impregnating a support with palladium. Typically this support is alumina,[10,26-29] though Cullis and Willat[26] investigated the effect of using titania, thoria and tin oxide supports for palladium catalysts. The general consensus amongst these investigations was that catalytic activity is significantly affected by the choice of support.

Recently an investigation by Shi *et al.*[30] concluded that ZrO_2 significantly promotes the low temperature activity of Pd catalysts. It was proposed that the presence of more reactive PdO_x sites is the reason for the increased activity. This theory is backed up by results obtained by Epling and Hoflund[31] who reported that ZrO_2 could act as an oxygen reservoir and exhibited large oxygen mobility. It is therefore possible that ZrO_2 would be able to oxidise Pd atoms relatively easily, giving PdO, which is the optimal Pd state for methane oxidation, as discussed in the following section. Conversely an investigation by Ribiero *et al.* [29] reported that the turnover rate of methane oxidation over palladium catalysts does not depend on the particle size, Pd precursor and catalyst support. This is in stark contrast to the findings

outlined previously. Ribiero *et al.* propose that the significant variability in turnover rates is because the catalysts have not been completely activated.

1.2.4 Optimum state of Pd for the catalytic oxidation of methane

Palladium has been shown to be an ideal catalyst for the oxidation of methane. The optimal composition of palladium for the catalytic oxidation of methane has been the subject of considerable research. There are a number of possible states; metallic palladium, chemisorbed oxygen on palladium, a skin of palladium oxide on a core of palladium and finally bulk palladium oxide. In the case of the latter it is possible that different oxide states are formed though these are not typically defined. Burch and Urbano[19] compared the catalytic activity of oxygen chemisorbed on metal to that of oxide ions for palladium supported on alumina. Catalytic activity was measured at 300 °C and results indicated that metallic palladium was not active whilst pre-oxidised palladium was. Burch also carried out an investigation in which the oxygen uptake and the evolution of methane oxidation were compared at a constant temperature of 300 °C as a function of time.[32] At this temperature a chemisorbed layer of oxygen was formed quickly and catalytic activity was low. It was therefore concluded that chemisorbed oxygen on metallic Pd had low activity. Sustained exposure to oxygen resulted in the oxidation of the palladium to a state close to that of bulk oxide in a few minutes. Maximum activity was achieved when 70-75 % of the Pd had been oxidised. It was therefore concluded that palladium oxide was the most active state.

Farrauto *et al.*[33] prepared palladium catalysts by impregnating an alumina support with a 10 % solution of $Pd(NO_3)_2$. Thermogravimetric analysis revealed that on heating to temperatures above 800 °C PdO decomposed to give metallic Pd. By 850 °C this process was complete, though heating was continued to 1000 °C. At 750 °C the percentage conversion of methane, presumably to carbon dioxide and water, due only to the alumina support was 100 %. It was therefore deduced that the catalytic contribution from the Pd was effectively zero. The temperature was then allowed to cool. A sharp weight gain indicating the formation of palladium oxide started at 650 °C and ended at 530 °C. A regain in the catalytic activity from the catalyst was noted to start at 680 °C and peaked at 600 °C. It was therefore concluded that metallic Pd was inactive towards methane oxidation and that the presence of palladium oxide was essential. From these results it would appear that metallic Pd is not required for the oxidation of methane.

Burch and Hayes[24] attempted to determine the optimum state of a Pd catalyst by carrying out various pretreatments of the Pd catalyst. The results showed that the reduced Pd and the reduced Pd with chemisorbed oxygen layers had low activity. The results showed a levelling off of catalytic activity as the extent of oxidation continued. This indicates that bulk PdO is no more active than PdO on a Pd core. Another study by Burch *et al.*[34] reported that the combustion of methane by Pd catalysts increased steadily as Pd was progressively and fully oxidised to PdO.

Conversely, research by other workers found metallic Pd to be the most active phase. Cullis and Willat[26] reported that reduced palladium on alumina is more active at 400 °C than the oxidised form. Oh *et al.* [35] also found that reduced Pd shows superior activity. Their finding is supported by the findings of Hicks *et al.*[36] Work by Lyubovsky and Pfefferle[37] also found that metallic Pd did show catalytic activity to methane. Furthermore they reported that it gave a faster reaction rate than PdO.

Finally Thevenin *et al.* concluded that in the presence of excess oxygen both metallic palladium and palladium oxide are present in the optimal form of the catalyst.[38]

It should be noted that in many of these studies the surface was not characterised under reaction conditions. The actual composition of the catalyst was therefore unknown. It is very possible that some of the metallic Pd catalysts could well have a surface comprising some PdO. Conversely PdO catalysts may have also contained islands of metallic Pd. It does however seem that the general consensus is that the PdO is the optimum catalyst at lower temperatures (<1075K) whilst it is possible that metallic Pd may show some catalytic activity at higher temperatures.[39]

A study by Hoflund *et al.* [40] investigated the active state of Pd catalysts by studying Pd catalysts before and after methane oxidation using electron energy loss spectra (ELS) and X-Ray photoelectron spectroscopy (XPS). ELS is sensitive to both the filled and unfilled levels near the Fermi level which are directly involved in chemical bonding. ELS is therefore a powerful tool in determining chemical environment. It can also provide depth sensitive information by varying the power of the primary beam energy. The results indicated that a layer of PdO formed over Pd under reaction conditions and there was no significant amount of Pd present in the outer layers. This therefore suggests that PdO is the active state and furthermore suggests the presence of metallic Pd is not required. This has implications on the mechanism of methane oxidation which are discussed in the next section.

1.2.5 Mechanism of methane oxidation over Pd catalysts

In this section the possible mechanisms for the oxidation of methane over Pd catalysts will be presented. A number of authors have concluded that the first step of methane oxidation over oxide based catalysts involves the formation of methyl radicals via surface assisted hydrogen abstraction.[41-45] Studies by Lunsford and various co-workers[41-43] showed that only one of the methane C-H bonds was broken in the initial step of dissociative adsorption. There are two likely mechanisms for the breaking of the C-H bond.[24] The heterolytic mechanism involves deprotonation and the formation of CH_3^-. These react with oxygen to give methyl radicals. [46-48] The alternative, homolytic splitting involves the abstraction of a hydrogen radical by a partially reduced oxygen species.[49,50] There is disagreement over which mechanism occurs.

The activation of the C-H bond by Pd catalysts was investigated by Burch and Hayes.[24] It was reported that the mechanism will depend on the active state of the Pd catalyst which was discussed in section 1.2.4. The results obtained by Burch and Hayes indicated that the active site for C-H bond activation was PdO comprising of a Pd^{2+} - O^{2-} couple. This is consistent with the findings of Choudhary and Rane[46] and Finocchio.[51] In both of these studies a heterolytic mechanism involving a cation-oxide anion couple in which the proton links to the oxide ion was proposed. A schematic of the mechanism suggested by Choudhary and Rane[46] is shown in fig 2.

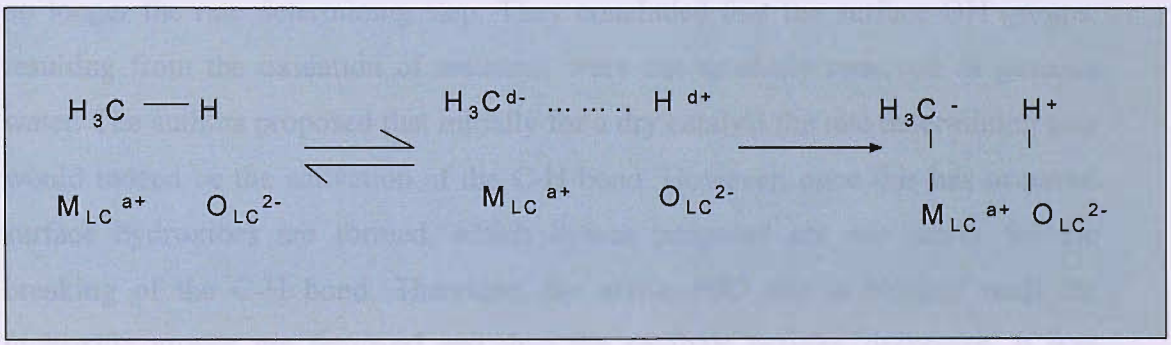

Fig 2. Schematic of the heterolytic splitting of the methane C-H bond by a surface acid base pair as proposed by Choudhary and Rane. M_{LC}^{a+} and O_{LC}^{2-} represent low co-ordination metal cation and oxygen anion sites. These function as the Lewis acid and Lewis base sites respectively.

In section 1.2.4 it was reported that there was a consensus that PdO was the optimum state of the catalyst. PdO is thermodynamically stable in air up to 800 °C.[24] It is therefore clear that for a heterolytic mechanism to occur the partially charged metal ions must be exposed at the surface. Burch and Hayes concluded that a heteroyclic mechanism was possible on even a fully oxidised Pd catalyst due to the crystalline nature of the oxide. Pt on the other hand does not form a similar stable oxide phase and so for a heterocyclic mechanism to occur the surface would have to be only partially covered in chemisorbed oxygen.

In section 1.2 it was proposed that the rate determining step was the cleavage of the C-H bond. Burch and Hayes[24] proposed that it is necessary to also consider the removal of the products of the reaction, CO_2 and H_2O. A number of studies have shown that CO_2 and, to a more significant extent, H_2O have an inhibitory effect on the catalytic oxidation of methane over Pd catalysts.[24,29,52] Conversely, results obtained by Cullis and Willat[53] indicated that whilst relatively large amounts of water and CO_2 did inhibit the catalytic activity, concentrations of water comparable to those formed by the total oxidation of methane did not have any appreciable effect on the activity of the catalyst. Results obtained by Burch and Hayes[24] indicated that water had a significant inhibitory effect, especially at temperatures of 275 °C and below. The effect was however, reversible; removal of water from the gas supply resulted in a return of catalytic activity. The authors therefore proposed that under normal reaction conditions the water formed by the oxidation of methane might have such a significant inhibitory effect that the activation of the C-H bond is no longer the rate determining step. They concluded that the surface OH groups, resulting from the oxidation of methane, were not as easily removed as gaseous water. The authors proposed that initially for a dry catalyst the rate determining step would indeed be the activation of the C-H bond. However, once this has occurred surface hydroxides are formed, which it was proposed are not active for the breaking of the C-H bond. Therefore, the active PdO site is blocked until the hydroxide groups are removed and thus the catalytic activity decreases. It was therefore proposed that the actual rate determining step in the oxidation of methane over Pd catalysts was the removal of the surface hydroxide groups. In a later study by Burch *et al.* [18] experiments were carried out at very short contact time using very dry gas mixtures. The results showed that the initial activity of dry PdO/Al_2O_3 was significantly greater than that of the catalysts exposed to the gas mixture. It was

therefore concluded that the breaking of the surface O-H bond was slower than the cleavage of a C-H bond.

In work by Fujimoto *et al.*[54] the presence of oxygen vacancies was proposed on PdO_x surfaces. This is consistent with the findings of Thevenin *et al.* who concluded that both metallic palladium and palladium oxide were present in the optimal Pd catalyst.[38] It was proposed that activation of methane occurred on site pairs consisting of oxygen atoms from surface PdO and oxygen vacancies. A schematic showing the proposed reaction is shown in fig 3. It can be seen that the methane molecule interacts with the Pd catalysts at an oxygen vacant site. A hydrogen atom is then removed from the methane molecule by interaction with an adjacent PdO site.

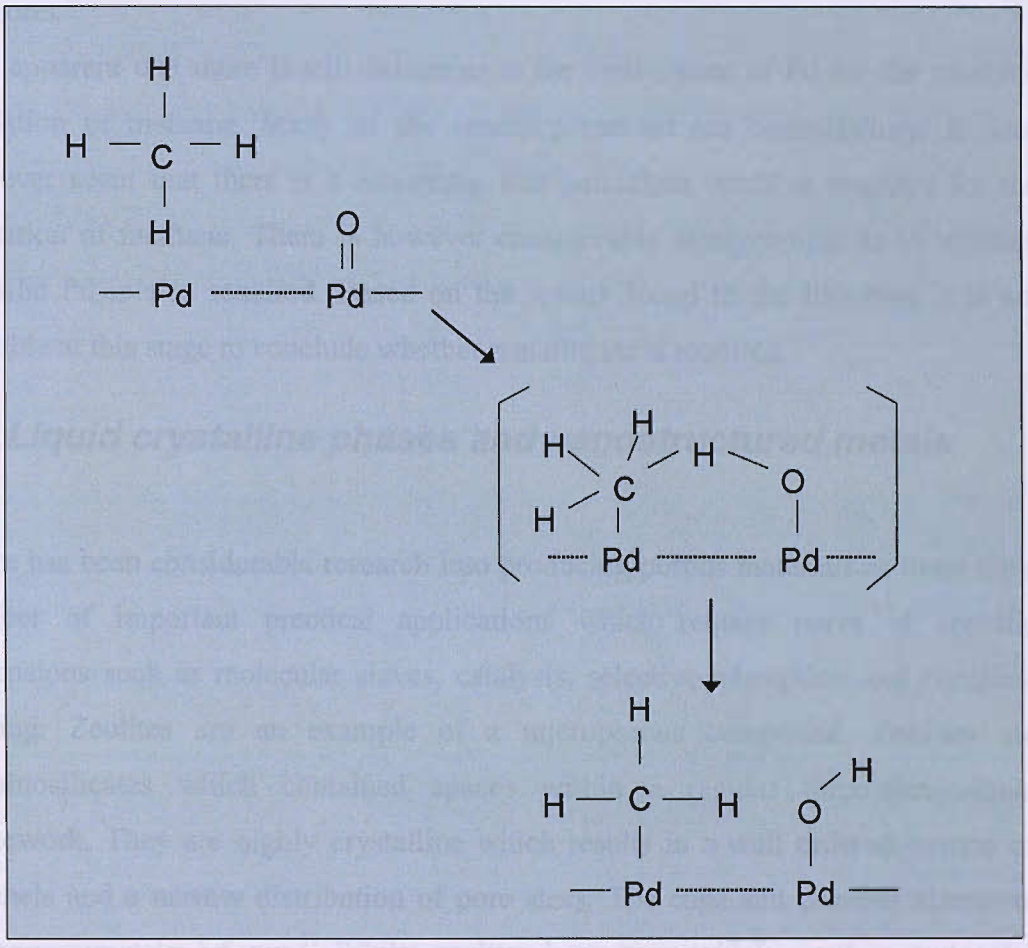

Fig 3. Schematic of the reaction scheme proposed by Fujimoto et al.[54] The methane molecule interacts with the Pd catalyst at an oxygen vacancy. A hydrogen atom is removed via interaction with an adjacent PdO site.

In section 1.2.4 the active state of palladium catalysts for methane oxidation was determined by Hoflund *et al.*[40] using EPS and XPS techniques as PdO. The results indicated that there was no metallic Pd in the outer layers. This is in direct contrast to the mechanism in fig 3 which requires a metallic Pd site. On this basis it was proposed that the mechanism would involve both methane and oxygen chemisorbing on PdO. It was proposed that methane would adsorb dissociatively forming a methoxy species and a hydroxyl group. The adsorbed radicals subsequently react with chemisorbed oxygen to produce CO_2 and H_2O.[23] Other hydrogen atoms would then be removed resulting in the formation of more hydroxyl groups which would react to from water. This proposed mechanism is consistent with results obtained by Epling and Hoflund using Pd catalysts on zirconia supports.[31]

It is apparent that there is still debate as to the active state of Pd for the catalytic oxidation of methane. Many of the results presented are contradictory. It does however seem that there is a consensus that palladium oxide is required for the oxidation of methane. There is however considerable disagreement as to whether metallic Pd is also required. Based on the results found in the literature it is not possible at this stage to conclude whether metallic Pd is required.

1.3 Liquid crystalline phases and nanostructured metals

There has been considerable research into producing porous materials as there are a number of important practical applications which require pores of specific dimensions such as molecular sieves, catalysis, selective adsorption and chemical sensing. Zeolites are an example of a microporous compound. Zeolites are aluminosilicates which contained spaces within a regular three-dimensional framework. They are highly crystalline which results in a well ordered system of channels and a narrow distribution of pore sizes. The cage and channel diameters are approximately 1.5 nm.[55] Whilst zeolites have been widely used as molecular sieves[55] and also for selective catalytic applications[56] the pore size is too narrow for many applications. Consequently, there was demand for materials with pores in the 2 – 50 nm range, which are defined as mesoporous by the IUPAC definitions.[57] In recent years mesoporous materials have been obtained using liquid crystal

templating techniques. Liquid crystals are introduced in the following section and liquid crystal templating methods in section 1.3.2.

1.3.1 Liquid Crystals

In order to define liquid crystals it is perhaps useful to consider solids and liquids. Crystals consist of molecules which generally have both orientational and positional order. Liquids comprise a random arrangement of molecules which diffuse randomly throughout their container. Liquid crystal phases could be thought of as existing between solids and liquids in terms of molecular order. These phases have less order than a solid but more than that of a liquid. These phases are formed by molecules self assembling into organised mesophases. The mesophase formed depends on the ambient conditions and the type of liquid crystal. There are two classes of liquid crystals; thermotropic where the phase formed depends on the temperature and lyotropic where the mesophase is determined by the concentration of molecules in a solvent such as water as well as temperature.[58]

Lyotropic liquid crystalline phases are formed by amphiphile molecules comprising a hydrophobic tail and a hydrophilic head group. In the presence of a polar solvent such as water these can self assemble as a result of the electrostatic interactions between the molecules and the solvent. Amphiphiles are often referred to as surfactants. Fig 4 shows a schematic of an amphiphile molecule.

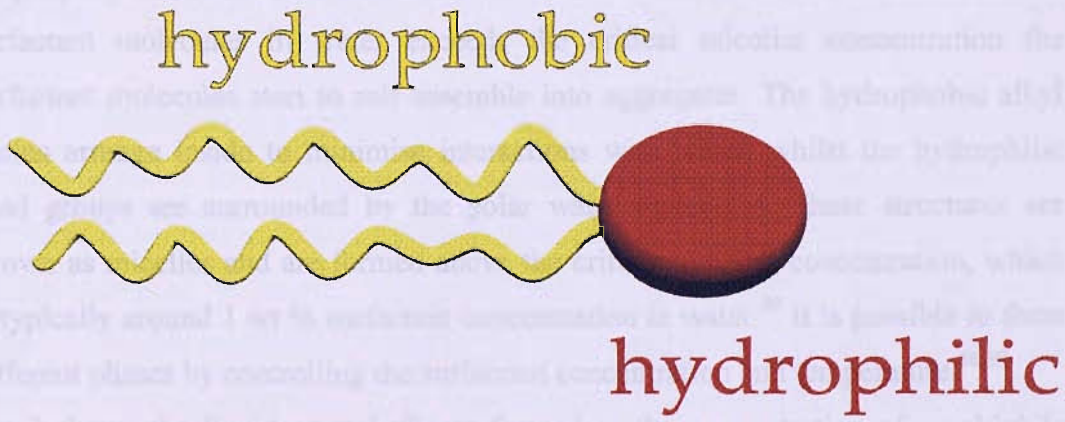

Fig 4 Schematic of an amphiphile molecule showing the hydrophobic hydrocarbon chain and hydrophilic head group. .

There are two main groups of surfactant; ionic and non-ionic. Sodium dodecyl sulfate is an example of an ionic surfactant and comprises a non-polar hydrocarbon chain and a polar head group, in this case the sulfate group.

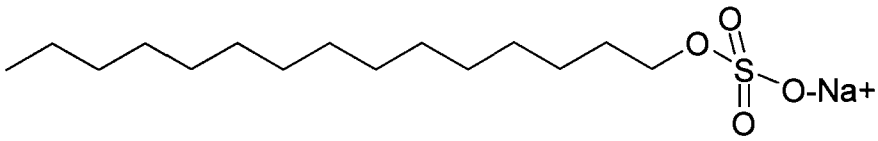

Fig 5 Schematic of sodium dodecyl sulfate

Non-ionic surfactants comprise a hydrophilic polar head group consisting of ethylene glycol groups and a hydrophobic alkyl chain.[59]

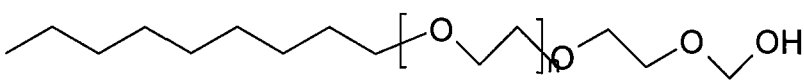

Fig 6. Schematic of non-ionic surfactant.

Amphiphile surfactant molecules are mixed with water. When the concentration of surfactant molecules in water exceeds the critical micellar concentration the surfactant molecules start to self assemble into aggregates. The hydrophobic alkyl chains arrange inside to minimise interactions with water, whilst the hydrophilic head groups are surrounded by the polar water molecules. These structures are known as micelles and are formed above the critical micellar concentration, which is typically around 1 wt % surfactant concentration in water.[59] It is possible to form different phases by controlling the surfactant concentration and temperature.[56,59]
Fig 7 shows the liquid crystal phases formed as the concentration of amphiphile surfactant molecules was increased above the critical micellar concentration. It can be seen that the micellar phase is formed at relatively low amphiphile concentration. As previously indicated this consists of spheres with the hydrophilic head groups on the outer surface and the hydrophobic alkyl chains on the inside. As the amphiphile concentration is increased the hexagonal (H_1) phase is formed. This consists of

surfactant molecules arranged in cylinders of infinite length. The outer surface consists of the head groups which are surrounded by water, whilst the hydrophobic alkyl chains pack inside the cylinders. This structure is also found in the cubic (V_1) phases. The former consist of cylinders of surfactant molecules arranged in an hexagonal array whilst the cubic phase is formed by cylinders.

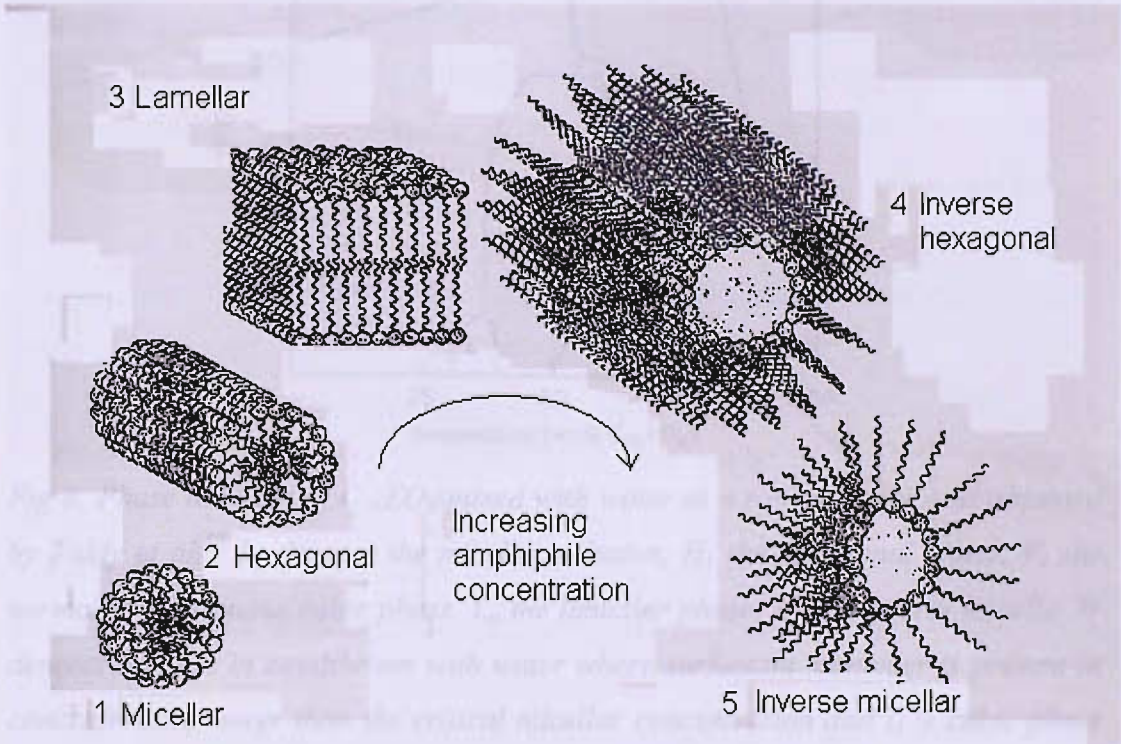

Fig 7. Diagram showing the meso-phases formed as the amphiphile concentration is increased.

As the concentration of amphiphile surfactant is further increased it can be seen that a third phase is formed comprising a sandwich arrangement of a bi-layer of surfactant molecules separated by layers of water. As the surfactant concentration is further increased an inverse hexagonal phase is formed. This comprises water molecules within a cylinder formed by the polar head groups. Finally, at very high surfactant concentration the inverse micellar phase is formed. This consists of water trapped inside the micelles surrounded by the polar head groups.

In order to be able to obtain the desired phase it is necessary to determine the temperature and surfactant concentrations at which the phase changes take place. This can be undertaken with the use of an optical microscope and a polarised light source. Tiddy *et al.*[60] investigated the phase behaviour of a range of common

surfactants including octaethyleneglycol monohexadecyl ether ($C_{16}EO_8$). The phase diagram is shown in fig 8.

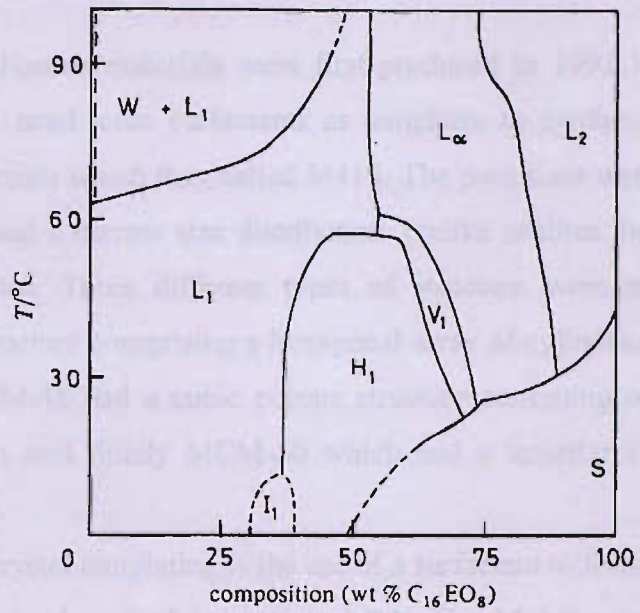

Fig 8. Phase diagram of $C_{16}EO_8$ mixed with water at a range of ratios as obtained by Tiddy et al.[60] L_1 denotes the micellar solution, H_1 the hexagonal phase, V_1 the normal bi-continuous cubic phase, L_α the lamellar phase, L_2 the inverse micelle. W denotes a phase in equilibrium with water where surfactant monomer is present at concentrations lower than the critical micellar concentration and I_1 is cubic phase of close packed sperhical micelles. S indicates the presence of a solid. The dashed lines indicate boundaries that were not accurately determined.

Fig 8 shows that the micellar solution exists over a wide temperature and composition range. At room temperature (25 °C) it exists up to approximately 40 wt. % $C_{16}EO_8$. The hexagonal phase is also formed over a wide temperature and composition range. At room temperature it is formed between approximately 40 and 65 wt. % $C_{16}EO_8$. The cubic phase exists over a narrow range on the shoulder of the hexagonal phase. The solid phase is formed predominantly below room temperature above 50 wt. % $C_{16}EO_8$. The lamellar phase is formed at surfactant concentrations from approximately 50 to 80 wt. % surfactant above 30 °C.

1.3.2 Liquid crystal templating

Mesoporous siliceous materials were first produced in 1992 by Mobil scientists. Kresge[61] *et al.* used ionic surfactants as templates to synthesise the mesoporous silciceous materials which they called M41S. The pore sizes were in the range of 25 to 100 Å and had a narrow size distribution. Unlike zeolites the walls are made of amorphous silica. Three different types of structure were made by the Mobil scientists; a structure comprising a hexagonal array of cylindrical pores was named MCM-41, MCM-48 had a cubic porous structure consisting of an interconnected channel system and finally MCM-50 which had a lamellar structure comprising sheets of silica.

Key to liquid crystal templating is the use of a surfactant to form micelles and liquid crystal phases as described in section 1.3.1. The Mobil scientists used cationic alkyltrimethylammonium ions comprising alkyl chains of between 8 and 18 carbon atoms in length. The Mobil method used low surfactant concentrations and the H_1 phase comprising cylindrical pores in a hexagonal arrangement is not formed at low concentrations. Following considerable research it appears that the micelles self assemble in the template mixture resulting in the observed pore topology. In the synthesis of MCM-41 it was proposed that electrostatic interactions between the headgroups and the silicate species resulted in the formation of a biphasic reaction mixture.[59] The solution was comprised mainly of water but also contained small regions of micelles surrounded by silica with the hexagonal order observed in MCM-41.

1.3.2.1 True liquid crystal templating using high surfactant concentrations

True liquid crystal templating uses higher surfactant concentrations. This method has a number of distinct advantages over the low concentration method used by the Mobil scientists. Perhaps the most significant advantage is that the final structure is known from the phase used in the reaction. This is in stark contrast with the Mobil

method in which there is no reliable method of predicting the structure of the final product. Another advantage is that it is possible to produce inverse phases using the direct templating method. Finally and also of key practical importance is the ability to produce mesoporous materials other than inorganic oxides. In the Mobil method the choice of materials is restricted due to the inherent necessity of the headgroup precursor interactions. In the direct templating method non-ionic surfactants are used thus these charge interactions are no longer necessary. This is of great practical importance as it facilitates the production of mesoporous structures in materials other than silica. In 1995 Attard *et al.*[62] synthesised mesoporous silica using non-ionic polyoxyethylene surfactants. Tetramethoxysilane was used as the silica precursor. One drawback of this method is that under acidic conditions hydrolysis of the precursor results in the production of methanol. This compromises the liquid crystal phase and was therefore removed using a gentle vacuum. Following further condensation which results in the reformation of the mesoporous material, calcination of the silica results in the destruction of the template giving well ordered porous silica. Later, Attard *et al.* [63] produced mesoporous platinum by reducing H_2PtCl_6 using polyoxyethylene as the surfactant. The Pt salt was dissolved in the aqueous regions of lyotropic liquid crystal phases. Mesoporous Pt films were produced with pores of 3 nm in diameter arranged in an hexagonal array. The production of mesoporous metal films Pt in particular, is of great practical significance as high surface area Pt films have a wide range of possible uses, in particular in catalytic applications. These include the production of nitric acid from ammonia[64] and in car exhaust catalytic converters for the reduction of NO_x species. They are also used in the catalytic hydrogenation of olefins as well as in electrical equipment.[65]

1.3.2.2 Electrodeposition of mesoporous metal films using true liquid crystal templating

In 1997 Attard *et al.*[66] reported the electrodeposition of mesoporous Pt with pores arranged in an hexagonal array. The plating mixture used was similar to that used in previous work[63] where Pt was chemically reduced. In this case the Pt precursor, hexachloroplatinic acid was electrochemically reduced to give Pt metal. A schematic outlining the key steps used in the method followed by Attard *et al.* in the

electrodeposition of a meosoporous metal film onto an Au electrode is shown in fig 9.

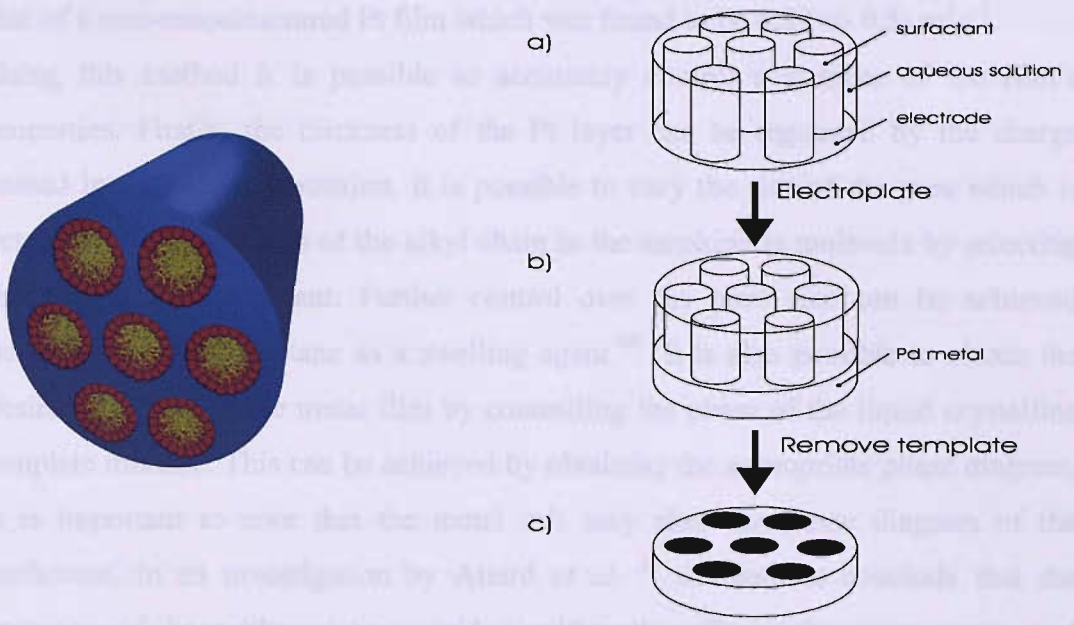

Fig 9. The schematic on the left shows the hexagonal phase with the aqueous solution containing the metal salt in blue surrounding the surfactant amphiphiles. The schematic on the right shows the key steps in the electrodeposition of a mesoporous metal. The cylinders represent the micellar rods in liquid crystalline phase.[67]

Fig 9 outlines the key stages in the electrodeposition of a mesoporous Pd film with an hexagonal array of pores though the same procedure applies for the electrodeposition of Pt. In step a) the template mixture is applied to the surface of the Au electrode. It can be seen that the template mixture contains cylinders of surfactant with the metal salt in the surrounding aqueous regions. In step b) Pd metal is electrodeposited onto the Au electrode by reducing the Pd salt. This is done by applying a suitable electrode potential. Having electrodeposited the Pd onto the Au electrode the surfactant is then removed using copious amounts of water, leaving the mesoporous Pd film. TEM studies confirmed that the film electrodeposited by Attard *et al.* was nanostructured with pores of 25 Å in diameter arranged in an

hexagonal array. Similar films were produced using $C_{16}EO_8$ in which the surfactant was swelled with heptane and $C_{12}EO_8$. The pore diameters were found to be 35 and 17.5 Å respectively. Electrochemical measurements were carried out to determine the electro-active surface area. A high surface area is important for potential use in a range of applications such as catalysis. The specific surface area of the mesoporous Pt film was calculated to be 22 (+/- 2) m^2g^{-1}. This compares very favourably with that of a non-nanostructured Pt film which was found to be 4.5 (+/- 0.5) m^2g^{-1}.

Using this method it is possible to accurately control a number of the film's properties. Firstly, the thickness of the Pt layer can be regulated by the charge passed in the electrodeposition. It is possible to vary the size of the pore which is determined by the length of the alkyl chain in the amphiphile molecule by selecting the appropriate surfactant. Further control over the pore size can be achieved through the use of heptane as a swelling agent.[66] It is also possible to obtain the desired structure in the metal film by controlling the phase of the liquid crystalline template mixture. This can be achieved by obtaining the appropriate phase diagram. It is important to note that the metal salt may alter the phase diagram of the surfactant. In an investigation by Attard *et al.* [68] the authors conclude that the presence of hexachloroplatinic acid significantly affects the temperature and composition ranges of the liquid crystalline phases. The report concluded that the Pt salt particularly improved the stability of the micellar cubic and hexagonal phases. In the case of ammonium tetrachloropalladate used for the electrodeposition of Pd films, Marwan[69] reported that the salt had no effect on the phase boundaries.

1.4 Electrochemistry of noble metals

The electrochemical characteristics of mesoporous Pt films have been studied by Attard *et al.* following their electrodeposition.[66,68] The cyclic voltammetry of a mesoporous Pt film with an hexagonal array of pores had well resolved voltammetric features corresponding to the formation and removal of platinum oxide and hydride.[66] The areas under the platinum hydride formation and removal and the deposition charge were used to calculate the specific surface area. As reported the films were found to have high surface areas by electrochemical characterisation.

There have been limited studies on the electrochemistry of mesoporous Pd. Much of the work has focussed on the ability of hydrogen to enter rapidly into the palladium

bulk,[70] a trait not shared with platinum. Work by Cioffi *et al.* [71] investigated the electrochemical synthesis of palladium nano-particles which were then deposited electrochemically or embedded into a polypyrrole film. Cyclic voltammetric studies were carried out which revealed a significant difference in the behaviour of bulk palladium and nanostructured palladium on the anodic scan. In particular the peak corresponding to the formation of palladium oxide for the nanostructured palladium film was more pronounced and a larger charge passed compared to that of bulk palladium. Curiously, a similar charge was passed in the reduction of palladium oxide for both films. The authors were not able to explain this result.

Bartlett *et al.*[67] investigated the electrochemistry of H_I-e Pd films on Au electrodes. The films had high electroactive surface areas. In the oxide region on the anodic scan the formation of the oxide began at 0.1 V vs. SMSE with two peaks well resolved at approximately 025 and 0.4 V vs. SMSE. On the cathodic scan the surface oxide was removed at 0.0 V vs. SMSE. The hydrogen potential region was investigated in detail. At a low scan rate of 20 mV / s on the cathodic scan a sharp pair of peaks was well resolved at -0.45 V vs. SMSE, then a smaller, broader pair of peaks at -0.52 V vs. SMSE and a rapidly increasing current at the cathodic sweep potential limit at -0.625 V vs. SMSE. Cyclic voltammetry was also carried out on polycrystalline wire. The voltammetry in the hydrogen potential region contained a broad and unresolved feature. The first pair of peaks at -0.45 V vs. SMSE was attributed to the formation and removal of adsorbed hydrogen. Similar features were obtained in work by Baldauf and Kolb[72] in studies of thin Pd films of between 1 and 10 monolayers equivalence deposited on Pt single crystals. The current for the formation of adsorbed hydrogen can be well resolved on thin films because the current due to the formation of absorbed hydrogen does not dominate the voltammogram as is the case for bulk palladium.[67] The remaining pairs of peaks were attributed to the formation of absorbed hydrogen. The first pair at -0.52 V vs. SMSE correspond to the formation of the Pd α-hydride phase and the start of the formation of the formation of the β-hydride phase.

Guerin and Attard[73] electrodeposited mesoporous Pd-Pt alloy films with pores arranged in an hexagonal array. The authors carried out cyclic voltammetry studies which exhibited different characteristics to those of bulk palladium films. Bulk palladium only shows peaks corresponding to the absorption of hydrogen into the bulk. The mesoporous films had three peaks of which two were attributed to the

adsorption and absorption of hydrogen. During voltammetric cycling in acid palladium will be removed and subsequently replated.[74] After several voltammetric cycles the replated palladium will start to form islands of palladium. It was proposed that these palladium islands will also show adsorption and absorption features.

1.5 Summary

In this chapter the need for a methane sensor and the shortcomings of existing technology were introduced. There is a commercial need for a more power efficient, reproducible and more poison resistant methane sensor. Analysis of the literature revealed palladium to be the optimal catalytic material for the oxidation of methane whilst the consensus indicates platinum is more effective at the oxidation of higher hydrocarbons. The requirement for good poison resistance of the catalyst is a major consideration. Studies of the literature suggested that the best way to achieve this was high porosity, a large surface area and good dispersion of the most appropriate catalyst. High porosity and a large surface can be achieved by the electrodeposition of mesoporous metal films using liquid crystal templating. This method also allows accurate control over the thickness of the film which will help to ensure good reproducibility between catalyst films.

The optimal catalytic state of palladium for the oxidation of methane was also investigated. There is still considerable debate concerning the optimal state, though there is now a growing consensus that palladium oxide is the most active state.

1.6 Outline

In chapter 3 the electrodeposition of mesoporous palladium films using $C_{12}EO_8$ for the first time as well as from Brij®56 is reported. The film was then characterised using electrochemical methods as well as SEM and TEM. In chapter 4 the electrodeposition of mesoporous palladium films onto micro-hotplates and their response to methane is described. An investigation was then carried out into the effect of chlorine in the palladium precursor. In chapter 5 the resistance of mesoporous palladium films to poisoning is investigated and various possible ways of improving the poison resistance are explored. In chapter 6 the response and poisoning to flammable gases other than methane is presented. Finally chapter 7 concludes by presenting the best case device produced during these studies.

2 Experimental

2.1 Chemicals and materials

Aqueous solutions were made using purified water from a Whatman STILLplus system. The following chemicals were used as received; sulphuric acid (Analar BDH), ammonium tetrachloropalladate (99.998 % Alfa Aesar), Brij® 56 (Aldrich), octaethylene glycol monododecyl ether ($C_{12}EO_8$, Fluka), heptane (99% Lancaster) and palladium (II) nitrate hydrate (97% Aldrich). Reference electrodes were prepared using potassium chloride (Analar BDH), mercury (II) chloride (Analar BDH), mercury (electronic grade, 99.998 % Alfa Aesar), sodium sulphate (Analar BDH), mercurous sulphate (Fluka).

All glassware was soaked overnight in Decon 90 diluted with deionised water before being thoroughly rinsed in deionised water. The glassware was then dried in a glass drying oven prior to use.

2.2 Instrumentation

An EG&G Model 263A potentiostat / galvanostat was used for carrying out the electrochemical experiments. Gold electrodes were made from 1 mm diameter gold wire sealed in glass. These were polished using 25 μm, 1.0 μm and finally 0.3 μm alumina slurry. A platinum wire gauze was chosen as the counter electrode. This was cleaned with Decon solution before being rinsed with deionised water. Immediately prior to use the gauze was heated with a butane gas gun to remove any contamination. A platinum wire coil used in the droplet setup described in fig 11 was cleaned in the same way. For the reference electrode a home-made saturated calomel electrode (SCE) was used for the depositions. A home-made saturated mercury sulphate (SMSE) was used for the cyclic voltammetry experiments in sulphuric acid, unless otherwise indicated. When not in use, the SCE reference electrodes were stored in saturated potassium chloride solution and the SMSE in saturated potassium sulfate solution.

2.3 Preparation of the liquid crystalline template mixtures

2.3.1 Nanostructured Pd with hexagonal topology using Brij 56

Mesoporous metal films were electrodeposited from a mixture consisting of a non-ionic surfactant, the metal precursor, water and heptane. The mixture will be referred to as the templating mixture or bath. The templating mixture used to deposit the H_1-e Pd films consisted of 12 wt. % $(NH_4)_2PdCl_4$, 39 wt. % water, 2 wt. % heptane and 47 wt.% Brij®56. The components were added in the order given. The templating mixtures were warmed in an oven at 40 °C for ten minutes and then thoroughly mixed to ensure a homogeneous mixture. The mixture was kept sealed during the heating process to prevent water evaporation which would alter the composition. The heating and stirring process was repeated two more times to ensure a homogeneous mixture. When the mixture had cooled the phase was checked using an Olympus BH-2 polarising light microscope to ensure it was in the hexagonal phase at room temperature. The temperature was raised using a Linkman TMS90 heating stage and a heating ramp rate of 5 °C was used.

2.3.2 Nanostructured Pt with hexagonal topology

The template bath for electrodeposition of mesoporous Pt consisted of hexachloroplatinic acid, water and Brij® 56 in the ratio of 1:1:1.5. The template bath was made up in the same way as the Pd mixture as described in the previous section.

2.3.3 Nanostructured Pd with cubic topology

The template bath used for the electrodeposition of nanostructured Pd with cubic topology consisted of 12 wt. % $(NH_4)_2PdCl_4$, 39 wt. % water, 2 wt. % heptane and 47 wt. % Brij®56. The template bath was made up using the method described in section 2.3.1. Electrodepositions were carried out at 41 °C.

2.3.4 Nanostructured Pd with hexagonal topology using $C_{12}EO_8$

The template bath consisted of 12 wt. % $(NH_4)_2PdCl_4$, 39 wt. % water, 2 wt. % heptane and 47 wt. % $C_{12}EO_8$. The template bath was made up using the method described in section 2.3.1.

2.3.5 Nanostructured Pd from chlorine free precursor with hexagonal topology using Brij®56

The template bath consisted of 12 wt. % palladium nitrate hydrate, 39 wt. % water, 2 wt. % heptane and 47 wt. % Brij®56. The template bath was made up using the method described in section 2.3.1.

2.4 Electrochemical deposition of nanostructured metal films onto 1 mm diameter gold electrodes

Mesoporous Pd films were electrodeposited onto 1 mm gold diameter electrodes embedded in resin. The electrode surface was polished prior to each deposition using 25, 1 and subsequently 0.3 μm alumina powder on polishing cloth. Following the polishing regime the electrode surface was voltammetrically cycled in 1 M sulphuric acid to confirm a clean electrode surface. The mesoporous Pd films were electrodeposited onto the gold electrode by applying a potential step from 0.4 to 0.1 V versus SCE. Mesoporous Pt films were electrodeposited by potential step from 0.5 to -0.1 V vs. SCE. The charge passed was displayed on the potentiostat allowing control over the film thickness. Following deposition the surfactant was removed using purified water or iso-propanol which was stirred using a magnetic stirrer bar.

2.5 Cyclic voltammetry of nanostructured metal films on 1 mm diameter gold disc electrodes

Electrochemical measurements of the mesoporous Pd were carried out using cyclic voltammetry in 1 M sulphuric acid. The acid was first bubbled with argon for at least 15 min to displace dissolved oxygen. Argon was chosen preferentially to nitrogen as argon being heavier than air forms a layer on top of the acid solution thus preventing more oxygen from dissolving into the solution. The electrochemically active surface area of the mesoporous Pd was then determined from the charge involved in the oxide stripping peak calculated by potential cycling in sulphuric acid. The specific surface area was calculated from the charge using the Rand and Wood's conversion factor of 424 μC cm^{-2}.[75]

2.6 Electrodeposition and electrochemical characterisation of mesoporous metal films on SRL microhotplate devices

The same chemicals were used as in the deposition onto the 1 mm diameter gold disc electrodes. It was not possible to polish the gold surface prior to deposition. However, the devices were soaked in isopropanol to remove any possible contamination. A cyclic voltammogram was then obtained to ensure a clean surface. The setup is shown in fig 11. A glass pipette with a frit at one end was used to house the electrolyte (1 M sulphuric acid) and the reference electrode. A platinum wire used as the counter electrode was fastened to the glass pipette using PTFE tape. The wire ran to the base of the pipette and looped around the outside of the frit. A drop of 1 M sulphuric acid was carefully placed onto the frit. The microhotplate was placed into a connection box located on an xyz micro-adjust stage. The stage was then raised with the aid of a microscope to ensure that the gold electrode on the device came into contact with the drop of sulphuric acid. A photo of an SRL 136 microhotplate in the zero insertion force connection box is shown in fig 10.

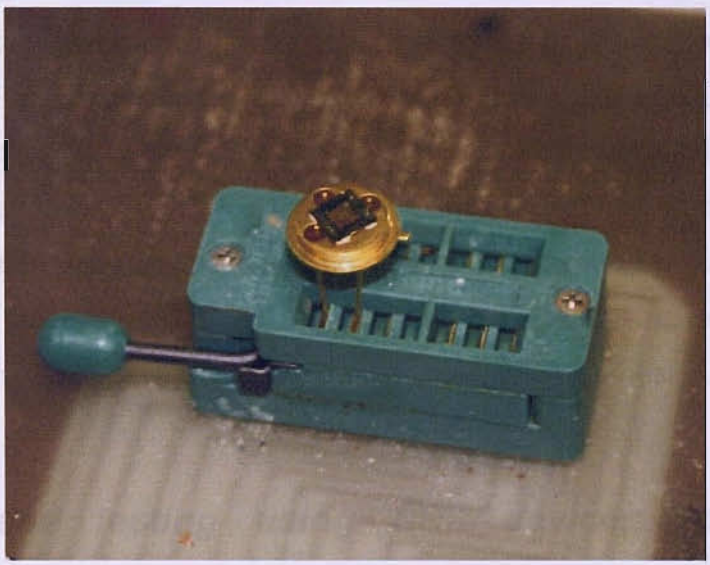

Fig 10 Photo of an SRL136 micro-hotplate in a zero insertion force connection box.

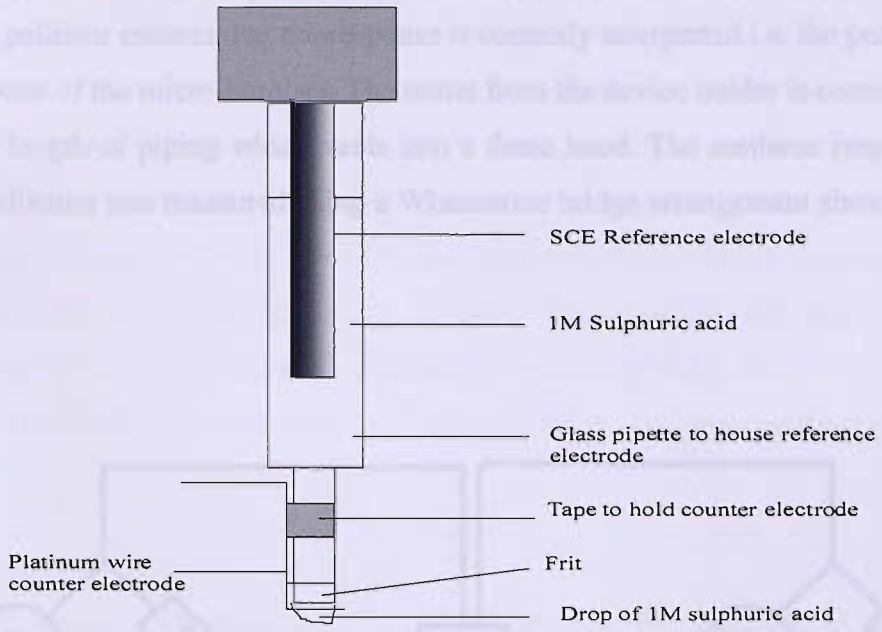

Fig 11 Diagram of apparatus used for cyclic voltammetry of micro-hotplates.

Electrodeposition was carried out by wrapping a platinum gauze counter electrode around an SCE reference electrode and generously coating the platinum gauze in the template mixture. A blob of template mixture was carefully applied to the gold working electrode of the device and very gently spread and compressed in an attempt to ensure good coverage and no air bubbles. Electrodeposition of Pd was carried out by potential step from 0.4 to 0.1 V vs. SCE. Following electrodeposition the surfactant was removed from the pores by soaking in isopropanol.

2.7 Methane testing using SRL devices coated with nanostructured metal films

2.7.1 Gas Testing Rig description

The gas testing rig consists of a cylinder of 2.5% methane in air (supplied by BOC special gases) connected via Tygon® plastic tubing to a 3 position tap. A cylinder of synthetic air (BOC special gases) was connected via mains metal piping and plastic tubing to the tap. The tap makes it possible to select methane or air. The outlet of the tap is connected via a gas flow meter to a device holder (supplied by City Technology). The device holder holds 2 sensors; a 90N or 200N standard pellistor

used as a reference and an SRL 136 or other type device under investigation. The standard pellistor ensures that the response is correctly interpreted i.e. the polarity of the response of the micro-hotplate. The outlet from the device holder is connected to a 10 cm length of piping which vents into a fume hood. The methane response of planar pellistors was measured using a Wheatstone bridge arrangement shown in fig 12.

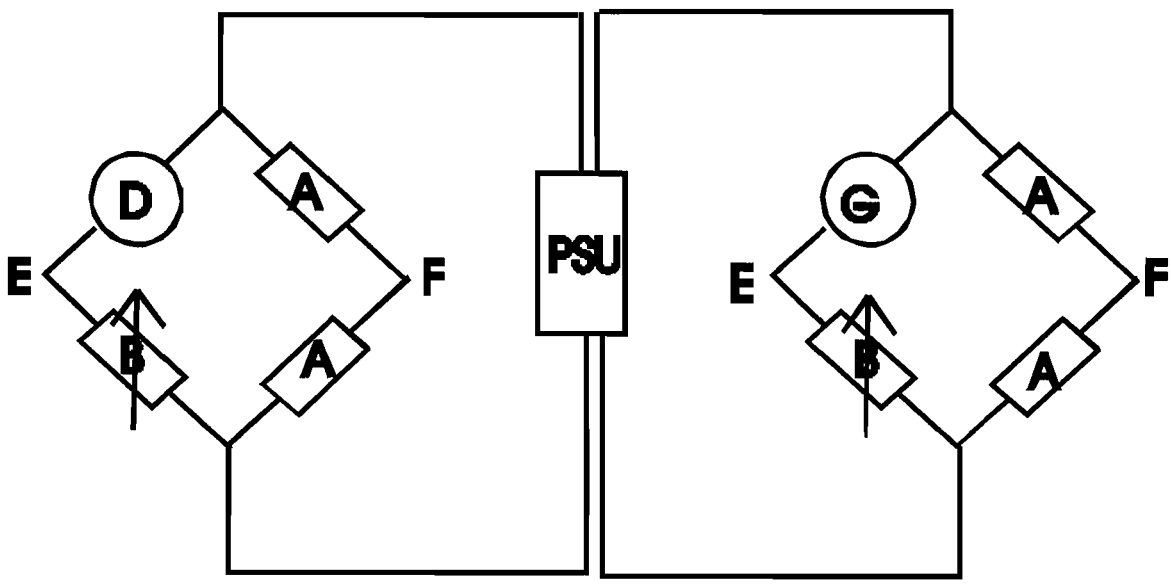

Fig 12. Diagram of the Wheatstone bridge arrangements used in the gas testing rig to test for methane gas.

Key:

PSU; Power Supply Unit, dual source power supply unit.

A; 1kΩ resistor

B; Variable resistor

D; Standard pellistor, type 90N or other

E and F; Points where the potential can be measured to check resistances of B and D are the same

G; Sensor to be tested

The potential was supplied by a GW GPQ3030D Dual Power Supply. The potential across D was slowly increased. When describing the voltage applied to a device this refers to the voltage from the power supply. For a 90N commercial sensor which

requires a potential of 1.75 V a potential of 3.5 V was used as half the potential will be dropped across the resistor, B. At the same time as increasing the potential the resistance of B was increased so that there is zero potential dropped across EF- i.e. the same potential was lost across D and B (or G and B). Synthetic air was then passed over the device and the potential across EF rechecked. Methane gas was then passed through the device holder. The potential response was then monitored to show the response of the sensor to methane. The response was measured by connecting across the Wheatstone bridge (EF) as shown in fig 12 to a Picologger data recorder. This was connected to a PC onto which the data was displayed and saved.

2.8 Poison testing of microhotplate devices using hexamethyldisiloxane (HMDS)

Devices were poison tested at City Technology. The poison testing rig comprised an inflatable plastic bag which was filled with methane before injecting the appropriate amount of HMDS with a syringe via a subaseal, to give the desired concentration of typically 6 ppm. The bag was connected via a tube to a 3 position tap which in turn was connected via a section of tubing to the device holder. Air and methane were also connected to the tap, making it possible to select the desired gas.

3 Preparation and characterisation of electrodeposited mesoporous palladium films

3.1 Introduction

The aim in this section is to produce and characterise high surface area mesoporous Pd films so that their use as catalysts in methane gas sensors can subsequently be investigated. The mesoporous Pd film will be used in conjunction with silicon microhotplates which are fully described in section 4.1.1. Previous work by Marwan[69] reports the electrodeposition of mesoporous palladium onto 1 mm diameter gold disc electrodes and onto similar microhotplates. Mesoporous Pd films with a hexagonal array of pores, with surface areas of up to 91 m^2 g^{-1} were produced. Electrodeposited mesoporous Pd films with a hexagonal array of pores will be referred by the nomenclature H_1-e Pd. The Pd films were electrodeposited from a template bath comprising an aqueous solution of ammonium tetrachloropalladate as the source of Pd ions and Brij®56 or $C_{16}EO_8$ as the non-ionic surfactants. The template baths also contained heptane which was included to swell the size of the pores.

Here we report the first use of $C_{12}EO_8$ as an alternative surfactant to $C_{16}EO_8$. $C_{12}EO_8$ and $C_{16}EO_8$ are highly purified single length alkyl chain surfactants. They differ in that $C_{12}EO_8$ has a shorter alkyl chain length which will result in a smaller pore diameter compared to $C_{16}EO_8$. These will be compared to similar Pd films electrodeposited from template baths based on the cheaper, polydisperse commercial surfactant Brij®56. Marwan[69] investigated the composition of Brij®56 using mass spectrometry and reported the most common constituent to be $C_{16}EO_8$, comprising 8 % of the total. There were many different components differing in the length of the alkyl chain and the number of ethylene oxide groups.

3.2 Phase behaviour

The aim was to electrodeposit nanostructured Pd films from a template mixture in the hexagonal phase giving a mesoporous Pd film with a hexagonal array of pores. A detailed description of the various lyotropic liquid crystalline phases is given in section 1.3. The composition and temperature range over which the hexagonal phase exists was identified by producing a phase diagram. This was achieved by producing a range of different compositions and identifying the phase boundaries using an optical microscope as the temperature was slowly increased. The phase diagram of the Pd $C_{12}EO_8$ system is shown in fig 13.

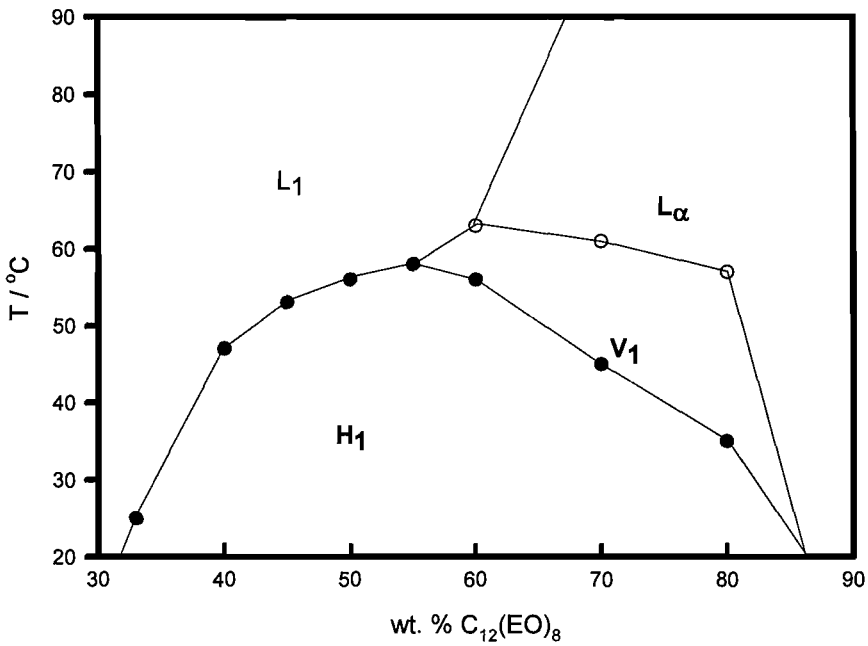

Fig 13. Pseudo binary phase diagram of a aqueous solution of 1.4 mol l^{-1} ammonium tetrachloropalladate in $C_{12}(EO)_8$ and heptane. Note that the lines are added as a visual aid. The weight to weight ratio between $(NH_4)_2PdCl_4$ and water was kept constant at 0.4. The same ratio of $C_{12}EO_8$ to heptane was kept constant at 22. The weight % of $C_{12}EO_8$ was increased from 33 to 80 %. L_1 refers to the micellar solution, H_1 to the hexagonal phase, V_1 the cubic phase and L_α the lamellar phase.

Figure 13 shows the phase diagram of an aqueous solution of ammonium tetrachloropalladate in $C_{12}EO_8$ and heptane. A full description of lyotropic liquid

crystalline phases is given in section 1.3.1. In fig 13 it can be seen that the hexagonal phase, denoted H_1, which consists of an hexagonal array of micelles arranged in cylinders has a broad composition range at room temperature and is formed up to approximately 57 °C. The cubic phase denoted, V_1, consists of two intertwined cylinders of surfactant molecules which meander 3 dimensionally, but do not interconnect and have multiple pore openings. It can be seen that the V_1 phase has a narrow composition range and is not formed at room temperature. The micellar solution, L_1, is formed over a small composition range at room temperature, but above 55 °C the phase exists over a significantly wider composition range. The lamellar phase, L_α, consists of horizontal sheets of amphiphile molecules separated by aqueous regions containing the Pd salt. Again, the phase is formed over a narrow composition range at room temperature but over a much wider range of compositions above 60°C.

The phase diagram in fig 13 is very similar to that of ammonium tetrachloropalladate in an aqueous solution of $C_{16}EO_8$ and heptane obtained by Marwan.[69] The phase diagram in fig 13 is also similar to that obtained by Mitchell *et al.* for the $C_{12}EO_8$ system.[60] This suggests that addition of the Pd salt does not affect the phase behaviour of the surfactant. This is in sharp contrast to the behaviour of Pt salts. In an investigation by Attard *et al.*[66] it was noted that the addition of hexachloroplatinic acid to a $C_{16}EO_8$ – water system had a significant effect on the phase boundaries. It was concluded that this was a result of interactions between the Pt salt and the ethylene oxide head groups. Mitchell *et al.*[60] carried out an extensive investigation into the phase behaviour of a range of pure polyoxyethylene surfactants. Generally, fig 13 is similar to the phase diagram obtained for $C_{12}EO_8$ though there are some differences. It is noted that they obtained data down to 0 °C. At these lower temperatures they report the existence of a close packed spherical micelle cubic phase denoted I_1, over a composition range 30 to 45 wt. % $C_{12}EO_8$ at 0 °C. They also found that solid surfactant was formed above concentrations of 65 wt. % surfactant at 0 °C. They report the H_1 phase existing between approximately 40 and 70 wt % $C_{12}EO_8$ at 30 °C, whereas in fig 13 it can be seen that the H_1 phase is formed at 35 wt. % $C_{12}EO_8$ and exists up to 85 wt. % $C_{12}EO_8$. Fig 13 and the results obtained by Mitchell *et al.* both support the formation of the cubic, (V_1) phase over a narrow composition range on the right

shoulder of the hexagonal phase though Mitchell *et al.* reported the existence of the V_1 phase down to 15 °C. The most significant difference between the two phase diagrams is that Mitchell *et al.* report the formation of the L_α phase over a significantly smaller composition range of between approximately 75 and 77 wt. % $C_{12}EO_8$. Furthermore they found it only existed below 30 °C. As indicated previously the initial aim is to deposit H_1-e Pd. Based on fig 13 and the results of Mitchell *et al.* a concentration of 50 wt. % $C_{12}EO_8$ at 25 °C will result in the template bath being in the hexagonal phase.

For means of comparison a phase diagram was also obtained of an aqueous solution of ammonium tetrachloropalladate in Brij®56 and heptane. The diagram is shown in fig 14.

A comparison of figs 13 and 14 reveals that the two phase diagrams are very similar, though it is noted that some of the phase changes occur at slightly different temperatures. Fig 14 is also very similar to the ammonium tetrachloropalladate Brij®56 system phase diagram obtained by Marwan.[69] It is noted that Marwan also reported differences in the temperature of the phase changes when comparing the Brij®56 and $C_{16}EO_8$ systems.

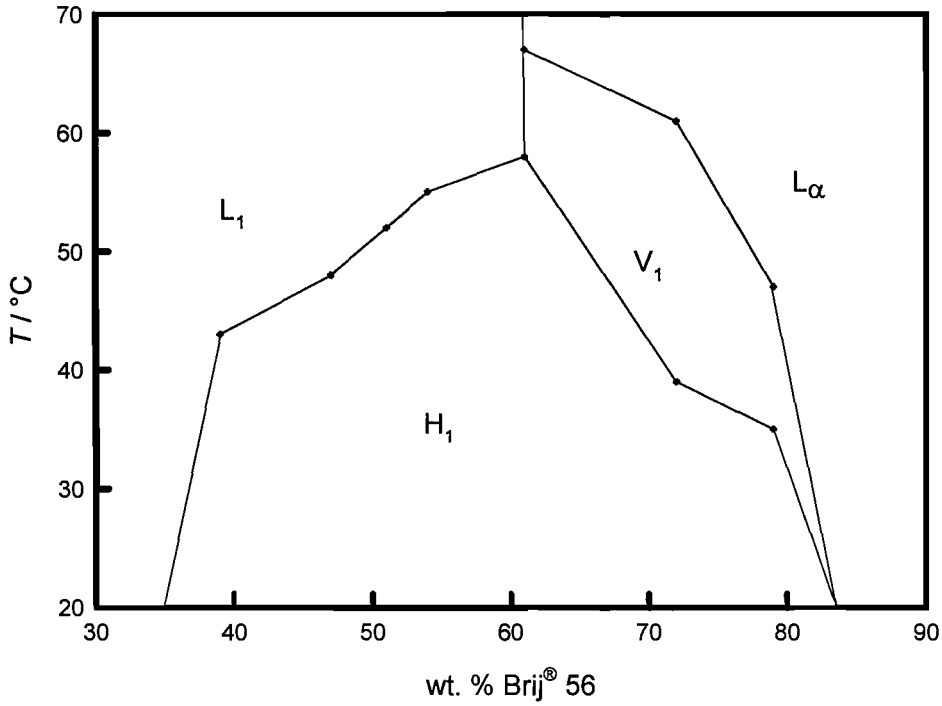

Fig 14. Pseudo binary phase diagram of an aqueous solution of 1.4 mol l^{-1} ammonium tetrachloropalladate in Brij®56 and heptane. Note that the lines are added as a visual aid. The weight to weight ratio between $(NH_4)_2PdCl_4$ and water was kept constant at 0.4. The same ratio $C_{12}EO_8$ to heptane was kept at 22. The weight % of Brij®56 was increased from 20 to 80 %. L_1 refers to the micellar solution, H_1 to the hexagonal, V_1 the cubic phase and L_α the lamellar phase.

3.3 Electrodeposition

The aim in this section was to electrodeposit mesoporous Pd from the template mixture in the hexagonal phase. A template mixture was made up of 47 wt % $C_{12}EO_8$, 2 wt % heptane 12 wt% $(NH_4)_2$ $PdCl_4$ and 38 wt% water based on the phase diagram in fig 13. In order to verify the electrode potential required for the reduction of the Pd salt to Pd metal on gold, a cyclic voltammogram of the template mixture was carried out.

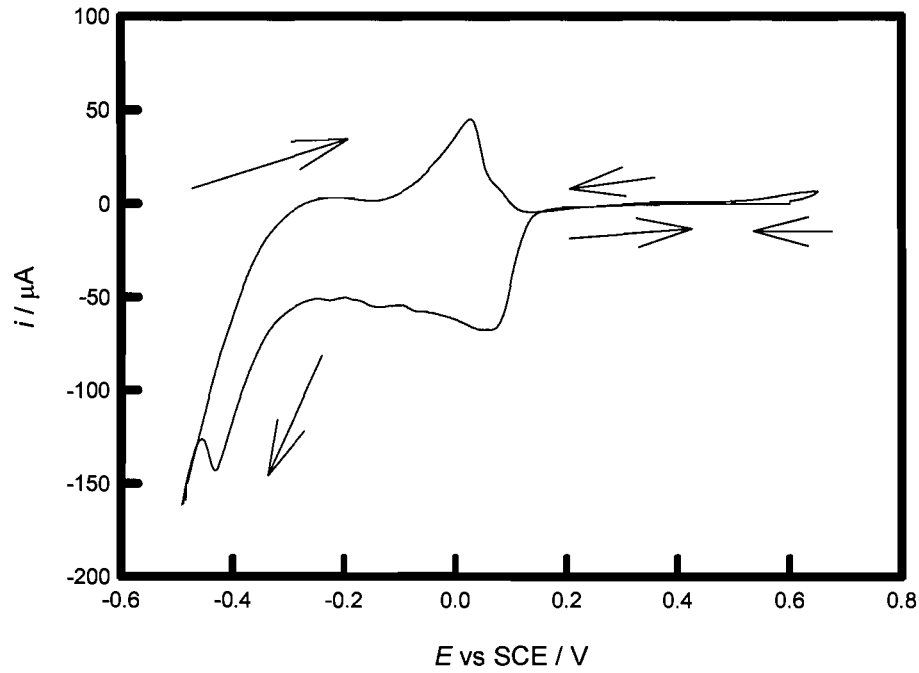

Fig 15. Cyclic voltammogram of $C_{12}EO_8$ template mixture on a clean Au 1 mm diameter electrode. The template mixture comprised 47 wt % $C_{12}EO_8$, 2 wt % heptane 12 wt % $(NH_4)_2$ $PdCl_4$ and 39 wt % water. A scan rate of 100 mV / s was used. The first scan is shown. The scan was started at 0.4 V vs. SCE and was carried out at room temperature (25 °C).

The cyclic voltammogram in fig 15 shows the electroreduction of the Pd salt in the $C_{12}EO_8$ template mixture on a gold electrode. The arrows indicate the sweep direction. The scan was started at 0.4 V vs. SCE and swept to -0.5 V vs. SCE which will be referred to as the forward scan. The potential was then swept up to 0.65 V vs. SCE and then back down to 0.4V. It can be seen that between 0.4 and 0.2 V vs.

SCE there is very little current flowing. After approximately 0.2 V on the cathodic scan the reduction current increases slowly at first before increasing more rapidly, becoming linear with potential beyond approximately 0.13 V until approximately 0.03 V vs. SCE. It can be seen that the maximum reduction current in this region occurs at around 0.03 V vs. SCE. There is now a large negative current indicating that the reduction of the palladium salt is occurring rapidly. In previous work by Marwan[69] and Guerin [5]a deposition potential of 0.1 V vs. SCE was used for the electrodeposition of H_1-e Pd onto gold electrodes. It can be seen from the cyclic voltammogram in fig 15 that it would be possible to use a smaller potential, up to around 0.03 V vs. SCE, which would result in a larger current flowing. It would therefore be possible to electrodeposit a given amount of charge in a shorter time. However, a study by Elliott *et al.*[76] investigated the effect of electrodeposition conditions on the properties of a mesoporous Pt film. They report that using a deposition potential of -0.1 V vs. SCE resulted in an ordered nanostructure. Increasing the overpotential to a deposition potential of -0.2 V vs. SCE resulted in a disordered nanostructure. Further increasing the overpotential to a more negative potential than -0.2 V vs. SCE resulted in no observable nanostructure. It was proposed that the disordered nanostructure obtained by depositing at -0.2 V vs. SCE was the result of side reactions such as the evolution of hydrogen gas. At potentials of -0.3 and -0.4 V vs. SCE a decrease in surface area was observed which was attributed to the increasing dominance of other reactions such as proton reduction. This also accounts for thinner films obtained as the faradaic efficiency will have decreased. At these more negative potentials hydrogen evolution becomes even more significant and resulted in the loss of nanostructure. The results indicated that in the case of Pt precise conditions were required for the successful electrodeposition of a nanostructured metal film and that it was not possible to easily increase the rate of electrodeposition by using a greater overpotential for the deposition. Although these studies were carried using Pt the findings may also apply to the electrodeposition of Pd. For this reason a potential of 0.1 V vs. SCE was used for the electrodeposition of Pd onto Au, as this has already been shown to give well ordered nanostructures by Marwan[69] and Guerin.[5]

Referring to fig 15 it can be seen that there a number of other voltammetric features that require explanation. On the cathodic scan the reduction of Pd^{2+} begins at approximately 0.2 V vs. SCE. After increasing to a maximum at around 0.03 V vs.

SCE the current remains fairly constant until around -0.25 V vs. SCE. The charge passed in this region will be referred to as Q_1. Between -0.25 and -0.45 V vs. SCE on the cathodic scan the current increases steadily. Between these potentials it is proposed that $PdH_{0.6}$ is formed,[69] the charge passed in this region will be referred to as Q_2. It is proposed that hydrogen gas evolution occurs at the cathodic potential limit. On the anodic scan there is a peak at 0.03 V vs. SCE. It is proposed that this corresponds to the stripping of $PdH_{0.6}$ to Pd. The charge passed under this peak will be referred to as Q_3. The charge passed for the formation and stripping of the hydride should be equal, so $Q_2 = Q_3$. Q_3 can then be equated to Q_1 assuming a maximum hydride loading ratio of 0.6; $Q_3 = 0.6 / 2\ Q_1$. The relevant areas under the cyclic voltammogram were calculated and were found to support this theory to a good approximation.

To investigate the effect of the surfactant on the cyclic voltammogram and on the deposition potential a cyclic voltammogram of an aqueous solution of ammonium tetrachloropalladate was carried out and is shown along with the cyclic voltammogram of the ammonium tetrachloropalladate – Brij®56 template mixture in fig 16.

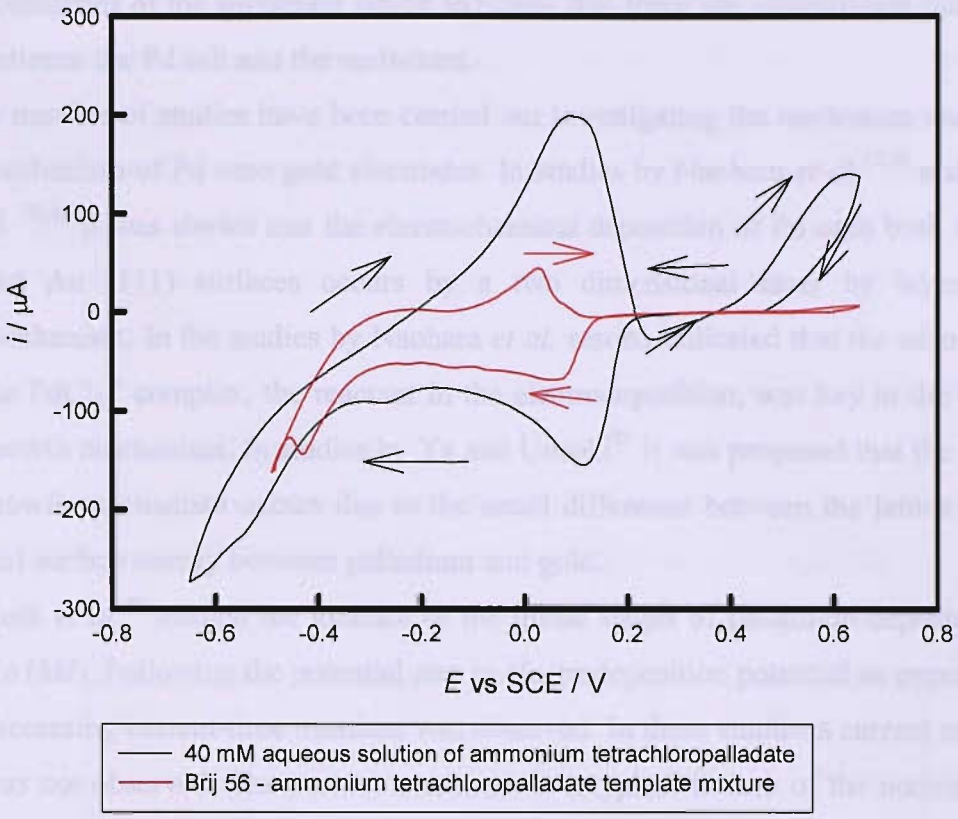

Fig 16. Cyclic voltammograms of a 40 mM solution of ammonium tetrachloropalladate on an Au 1 mm diameter electrode and of a Brij®56 – ammonium tetrachloropalladate mixture. The same composition was used as in fig 15. A scan rate of 100 mV / s was used in each case. The scans were started at 0.4 V vs. SCE and were scanned initially in the cathodic direction. Scans were carried out at room temperature (25 °C).

It can be seen that there are a number of differences between the cyclic voltammograms. On the cathodic scan of the cyclic voltammogram of the ammonium tetrachloropalladate - Brij®56 mixture there is a reduction current with a linear region between 0.3 and 0.0 V vs. SCE. A maximum reduction current of -67.5 μA was recorded at 0.06 V vs. SCE. In the case of the aqueous solution a maximum reduction current of -154.9 μA was recorded at 0.12 V vs. SCE. A larger maximum reduction current was expected as the surfactant may reduce the mobility of the Pd ions. However, there is also a shift in potentials of the reduction currents. This could be a kinetic effect due to the surfactant affecting the rate of electron transfer. It could also be a thermodynamic effect with the surfactant affecting the

thermodynamic equilibrium of the Pd and tetrachloropalladate ion. However, it has been shown that the addition of the Pd salt has minimal effects on the phase boundaries of the surfactant which indicates that there are insignificant interactions between the Pd salt and the surfactant.

A number of studies have been carried out investigating the nucleation and growth mechanism of Pd onto gold electrodes. In studies by Naohara *et al.*[77,78] and Kolb *et al.* [79,80] it was shown that the electrochemical deposition of Pd onto both Au (100) and Au (111) surfaces occurs by a two dimensional layer by layer growth mechanism. In the studies by Naohara *et al.* results indicated that the adsorption of the $PdCl_4^{2-}$ complex, the reactant in the electrodeposition, was key in the epitaxial growth mechanism. In studies by Ye and Uosoki[81] it was proposed that the epitaxial growth mechanism occurs due to the small difference between the lattice constant and surface energy between palladium and gold.

Kolb *et al.*[80] studied the kinetics of the initial stages of palladium deposition onto Au (*hkl*). Following the potential step to electrodeposition potential an exponentially decreasing current-time transient was observed. In these studies a current maximum was not observed. The current maximum is a typical feature of the nucleation and growth mechanism.[82] This is inconsistent with the findings of Uosaki *et al.* [77,78] who observed using in situ STM measurements that some nuclei were formed as soon as the potential was stepped into the potential region where palladium deposition occurs. It was therefore concluded that an instantaneous nucleation mechanism occurs. The same authors carried out another study using cyclic voltammetry and potentiostatic measurements.[82] This study confirmed their other findings, that the deposition of palladium onto Au(111) occurs via instantaneous nucleation and 2D growth with overlap of the nuclei. It is noted that these studies were carried out using a solution of 0.1 M H_2SO_4 containing 0.1 mM K_2PdCl_4. The authors reported that increasing the concentration of Pd resulted in poor agreement between the experimental and theoretical results.

There have been several studies on the effect of surfactant on the electrodeposition of palladium. Tsirlina *et al.*[83] studied the effect of adding polyethylene glycol to a $PdCl_2$ solution for the electrodeposition of Pd. In this case low surfactant concentrations were used hence liquid crystal formation was unlikely. The current transients obtained resembled those of polymer-free solutions. The palladium deposits obtained had very high surface areas of up to 50 m^2g^{-1}. In another study by

the same group [84] the effect of the molecular weight of the polyethylene glycol polymer used was investigated. The results showed that the magnitude of the current peak in the current transient decreased as the molecular weight of the polymer used was increased. For a low molecular weight (M_w = 600) the current increased rapidly to a peak of approximately 1.3 mA before gradually decreasing to a plateau. For the highest molecular weight surfactant used (M_w = 40,000) the current increased only gradually to around 0.4 mA and then stayed constant at this value. It was concluded that increases in the molecular weight of the polymer resulted in the blocking of active centres. This is consistent with the results in fig 16 which show a higher reduction current for the reduction of the Pd salt in the aqueous solution compared to that in the template mixture.

H_I-e Pd films were electrodeposited onto gold 1 mm diameter electrodes from both $C_{12}(EO)_8$ and Brij®56 template baths. The current transients are shown in fig 17.

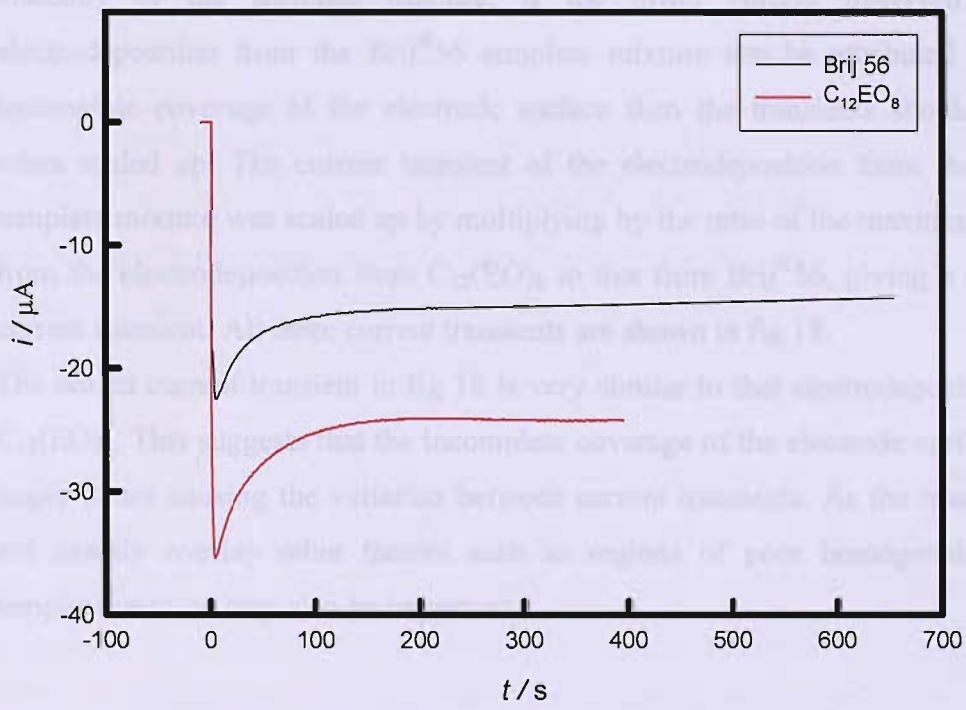

Fig 17. Current transients of the electrodeposition of H_I-e Pd onto a 1 mm diameter Au disc electrode from both the standard Brij® 56 template bath and that of the $C_{12}EO_8$ bath with the same composition. Electrodeposition was carried out by applying a potential step of 0.4 to 0.1 V vs. SCE. In each case a total deposition charge of 3.5 mC was passed. Electrodepositions were carried out at room temperature.

Fig 17 shows the current transients for the electrodeposition of H_1-e Pd onto a 1 mm Au disc electrode from both the Brij®56 and the $C_{12}EO_8$ bath. A faradaic efficiency of 100 % is assumed based on the result obtained by Marwan of 95-98 % using electro quartz crystal microbalance (EQCM) techniques.[69] In both cases a charge of 3.5 mC was passed. In both cases the current has a maximum soon after the potential step before the current decays to a plateau region. This is consistent with the results obtained by Uosaki *et al.*[82]. It can be seen that the current transient for the $C_{12}EO_8$ bath has a higher peak value of approximately -37 μA compared to approximately -22 μA for the Brij®56 template bath. The current in the plateau region is also higher. During the investigations many electrodepositions were carried out and it was noted that different current transients were obtained for replicate measurements. SEM revealed that parts of the gold electrode were not covered by palladium. It is proposed that this is the result of some areas of the electrode not being covered by the template mixture. This is due to the high viscosity of the template mixture. If the lower current observed for the electrodeposition from the Brij®56 template mixture can be attributed solely to incomplete coverage of the electrode surface then the transients should overlay when scaled up. The current transient of the electrodeposition from the Brij®56 template mixture was scaled up by multiplying by the ratio of the maximum current from the electrodeposition from $C_{12}(EO)_8$ to that from Brij®56, giving a scaled up current transient. All three current transients are shown in fig 18.

The scaled current transient in fig 18 is very similar to that electrodeposition from $C_{12}(EO)_8$. This suggests that the incomplete coverage of the electrode surface is the major factor causing the variation between current transients. As the transients do not exactly overlay other factors such as regions of poor homogeneity in the template mixture may also be important.

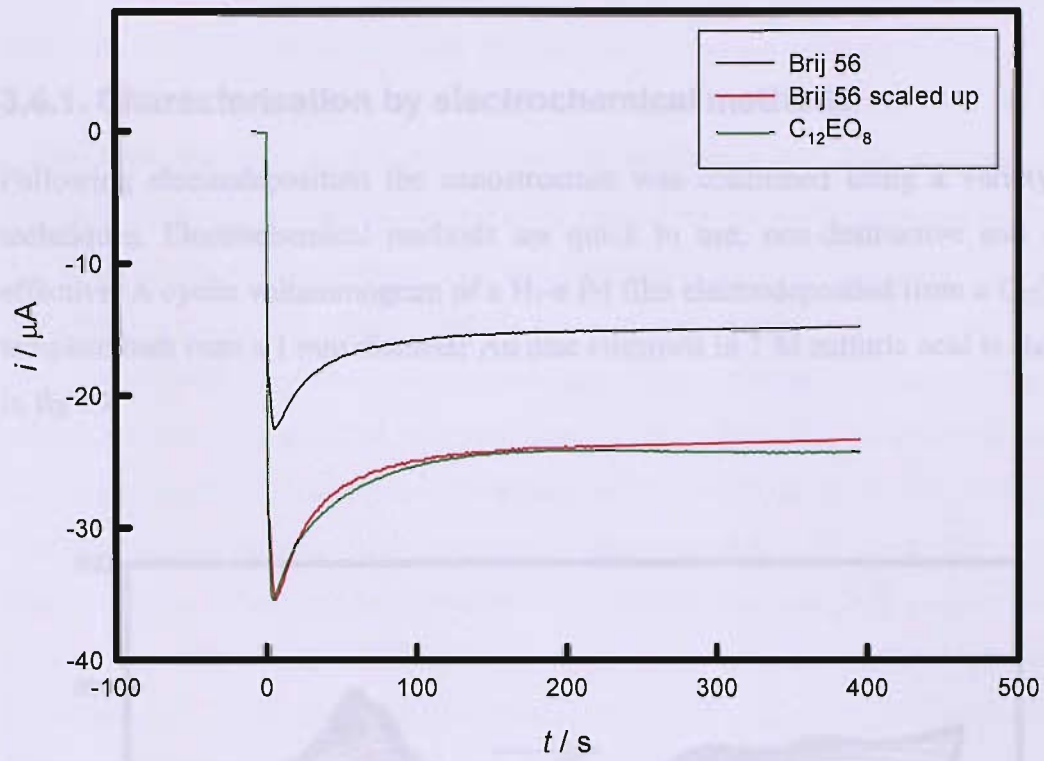

Fig 18. Current transients of the electrodeposition of H_1-e Pd onto a 1 mm diameter Au disc electrode from the Brij®56 $C_{12}EO_8$ template bath. Electrodeposition conditions are described in fig 17. The scaled up current transient was calculated using the ratio of the maximum current of the $C_{12}(EO)_8$ electrodeposition to the maximum current of the Brij®56 electrodeposition.

Following electrodeposition the surfactant was removed from the pores of the electrodeposited Pd metal by soaking in iso-propanol for 1 h. Marwan[69] carried out similar studies. Following a 10 min water soak results indicated that there was still significant amounts of surfactant remaining in the pores. However, soaking for 1 h removed the majority of the surfactant. During these investigations it was found that iso-propanol was significantly more effective at removing the surfactant than water and that stirring was also beneficial.

3.4 Characterisation of H1-e Pd

3.4.1. Characterisation by electrochemical methods

Following electrodeposition the nanostructure was confirmed using a variety of techniques. Electrochemical methods are quick to use, non-destructive and cost effective. A cyclic voltammogram of a H_1-e Pd film electrodeposited from a $C_{12}EO_8$ template bath onto a 1 mm diameter Au disc electrode in 1 M sulfuric acid is shown in fig 19.

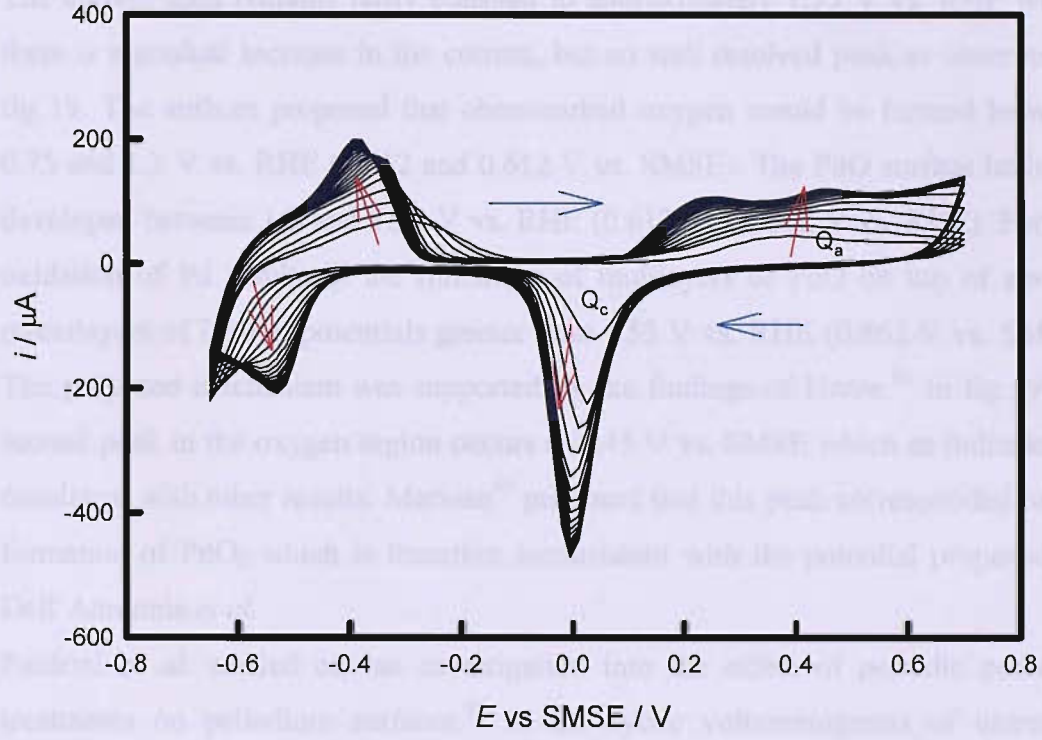

Fig 19 Cyclic voltammograms of mesoporous palladium electrodeposited onto a 1 mm diameter Au disc electrode from the standard Brij®56 templating mixture. The H_1-e Pd film was electrodeposited by applying a potential step of 0.4 to 0.1 V vs. SCE at room temperature. A deposition charge of 3.5 mC was passed in the deposition. The cyclic voltammogram was carried out at room temperature at a scan rate of 200 mV/s, starting from 0.0 V vs. SMSE, in 1 M sulfuric acid which was first deoxygenated for 15 min with argon.

The cyclic voltammogram in fig 19 shows the first twenty voltammetric cycles of a H_1-e Pd film in 1 M sulfuric acid. The scan was started at 0 V vs. SMSE. The blue

arrows indicate the sweep direction and the red arrows show the direction of increasing voltammetric cycle number. It can be seen that the current increases with scan number, before stabilising after approximately ten voltammetric cycles.

A similar cyclic voltammogram was obtained by Marwan[69] from a H_1-e Pd film electrodeposited from an ammonium tetrachloropalladate - $C_{16}EO_8$ template bath. The formation of a surface oxide begins at around 0.1 V vs. SMSE. It can be seen that there are two peaks, one at 0.25 and the second at 0.45 V vs. SMSE. Cyclic voltammograms of non mesoporous Pd films do not contain these features,[85] or if they are present they are not as prominent.[75] Dall'Antonia *et al.* investigated palladium electrodes in 0.5 M sulphuric acid. In the cyclic voltammograms obtained the oxygen region is characterised by a peak at 0.8 V vs. RHE (0.112 V vs. SMSE). The current then remains fairly constant to approximately 1.55 V vs. RHE where there is a gradual increase in the current, but no well resolved peak as observed in fig 19. The authors proposed that chemisorbed oxygen would be formed between 0.75 and 1.3 V vs. RHE (0.012 and 0.612 V vs. SMSE). The PdO surface lattice is developed between 1.3 and 1.55 V vs. RHE (0.612 and 0.862 V vs. RHE). Further oxidation of Pd results in the formation of mulilayers of PdO on top of several monolayers of PdO at potentials greater than 1.55 V vs. RHE (0.862 V vs. SMSE) The proposed mechanism was supported by the findings of Hoare.[86] In fig 19 the second peak in the oxygen region occurs at 0.45 V vs. SMSE which as indicated is consistent with other results. Marwan[69] proposed that this peak corresponded to the formation of PdO_2 which is therefore inconsistent with the potential proposed by Dall'Anotonia *et al.*

Perdriel *et al.* carried out an investigation into the effect of periodic potential treatments on palladium surfaces.[87] In the cyclic voltammograms of untreated palladium electrodes a broad peak corresponding to the formation of palladium oxide was observed at 0.86 V vs. RHE (0.72 V vs. SMSE). The current then increased steadily from approximately 1.0 V vs. RHE (0.312 V vs. SMSE). When palladium electrodes were subject to repetitive square wave potential sweeps a 2^{nd} peak at 1.1 V vs. RHE (0.412 V vs. SMSE) was well resolved. This is consistent with the second peak at 0.45 V vs. SMSE in fig 19. It was concluded that the applications of periodic potentials to Pd electrodes in 1 M sulphuric acid resulted in a number of modifications to the palladium surface. These modifications involved different types of roughening and faceting and were mainly the result of the

electrodissolution-electrodeposition of palladium and the oxide layer formation-electroreduction process. Rand and Woods carried out an investigation into the dissolution of platinum, palladium, rhodium and gold in 1 M sulphuric acid.[75] A number of studies reported that the charge corresponding to the formation of palladium oxide, Q_A in fig 19, was greater than the charge corresponding to the removal of the palladium oxide, Q_C. [64,88-91] Results obtained by Rand and Woods showed that this difference was due to metal dissolution. [75] The investigation also concluded that an anodic mechanism was responsible for the dissolution of palladium. This may involve either direct dissolution of the metal:

$$Pd \rightarrow Pd^{2+} + 2e^- \qquad \textbf{(2)}$$

Or may proceed via an intermediate surface oxide:

$$Pd + H_2O \rightarrow PdO + 2H^+ + 2e^- \qquad \textbf{(3a)}$$
$$PdO + 2H^+ \rightarrow Pd^{2+} + H_2O \qquad \textbf{(3b)}$$

The amount of metal dissolution per voltammetric cycle was significantly higher for palladium compared to the other metals investigated. Much of the palladium will redeposit during the cathodic scan. This will result in surface roughening. It is also noted that Rand and Woods used a lower potential limit of 0.4 V vs. RHE, whilst the investigation by Perdriel *et al.* [87] used a lower limit of 0.33 V vs. RHE. Rand and Woods report that below 0.3 V palladium absorbs significant amounts of hydrogen which causes appreciable roughening to the surface. It is possible that the use of the smaller lower potential limit and hence the resulting hydrogen absorption is partially responsible for the resolution of the peak at 1.1 V vs. RHE noted by Perdriel *et al.* Although this peak can be seen in the cyclic voltammograms obtained by Rand and Woods it is significantly less prominent. In summary the presence of two peaks in the oxygen potential region at 0.25 and 0.45 V vs. SMSE is consistent with results in the literature. It is proposed that the two peaks correspond to the formation of different palladium surface oxide states.

Referring to fig 19 it can be seen that there is a sharp peak at approximately 0.0 V vs. SMSE which is consistent with the results obtained by Marwan[69] using similarly prepared H_1-e Pd films. In the cyclic voltammograms obtained by Dall'Antonia *et*

al. a similarly sharp peak was obtained but occurred at 0.52 V vs. RHE, (-0.168 V vs. SMSE).[92] This peak corresponds to the reduction of PdO. It is noted that Dall'Antonia *et al.* propose that this peak corresponds to the reduction of only PdO. It is proposed that the reduction of PdO_2 occurs between 1.4 and 1.2 V vs. RHE on the cathodic scan.

In fig 19 the hydrogen region occurs between -0.4 V vs. SMSE on the cathodic scan and -0.2 V vs. SMSE on the anodic scan. It can be seen that on the cathodic scan there is a peak at -0.55 V and another feature at the potential limit. On the anodic scan there is only one well resolved peak at -0.4 V vs. SMSE. In a similar study by Marwan using a scan rate of 20 mV / s a peak at approximately -0.6 V vs. SMSE on the anodic scan was also well resolved. It is proposed that this peak may have been resolved in these studies had a lower scan rate been used. A number of studies have been carried into the absorption and adsorption of hydrogen on transition metal electrodes. It has been shown that the hydrogen electrode reaction on transition metal electrodes can take place in both acidic and alkaline media by the Volmer-Heyrovsky-Tafel mechanism.[93-95] The first step of this process is the Volmer reaction and involves the adsorption of hydrogen onto the metal surface from H atoms originating from H_2O or H_3O^+:

$$H_3O^+ + e^- \rightarrow H^\bullet_{ads} + H_2O \qquad \textbf{(4)}$$

Hydrogen evolution then occurs either electrochemically by the Heyrovsky mechanism shown in equation 5 or chemically by the Tafel reaction shown in equation 6.

$$H^\bullet_{ads} + H_3O^+ + e^- \rightarrow H_2 + H_2O \qquad \textbf{(5)}$$

$$H^\bullet_{ads} + H^\bullet_{ads} \rightarrow H_2 \qquad \textbf{(6)}$$

Adsorbed hydrogen is then able to permeate into the metal lattice to form α and β hydride.[94] It is still unclear how exactly hydrogen enters the metal from the adsorbed state. It has been suggested by Conway *et al.*[93] that this occurs via an intermediate hydrogen subsurface state:

$$PdH_{ads} \rightarrow PdH_{diss} \rightarrow PdH_{abs} \qquad \textbf{(7)}$$

There are several potential problems with this proposed mechanism. Firstly, it is unclear how PdH_{diss} is affected by electrode potential. Furthermore, it is possible that PdH_{ads} equilibrates with PdH_{diss}. This mechanism is also unknown.[94]

Calculating the surface area

The area under a defined part of a cyclic voltammogram is equal to the amount of charge passed;

$$Q = \int i\,dt \qquad \textbf{(8)}$$

Where Q is the charge passed in μC, i the current in μA and t time in s.

The charge passed in the removal of the surface oxide which occurs at 0.0 V vs. SMSE on the backward scan, is related to the surface area of the Pd film by the Rand and Wood's constant of 424 μC cm^{-2} for a palladium film.[75] Thus the area under the surface oxide stripping peak is proportional to the surface area of the Pd film. It can then be noted that the electrochemically active surface area of the H_I-e Pd film in fig 19 increases with each voltammetric cycle. The surface area of the H_I-e Pd film calculated after the first voltammetric cycle was found to be approximately one quarter of the area after 20 voltammetric cycles. It is proposed that the increase in surface area is due to a number of factors. Firstly, despite washing in isopropanol there may be surfactant remaining in the pores. This will block the pores and prevent the electrolyte from accessing the entire nanostructure. It is possible that voltammetric cycling in sulphuric acid removes the surfactant, resulting in an increase in the electroactive surface area. Rand and Woods carried out an investigation into the dissolution of Pt, Pd, Rh and Au in 1 M sulphuric acid.[74] They consider the charge under the oxide formation region (0.1 to 0.65 V vs. SMSE), Q_o^a and the charge under the oxide stripping peak (0.1 to -0.15 V vs. SMSE), Q_o^c. They report that $Q_o^a > Q_o^c$. A This has been reported previously by a number of authors[96,97] but the possibility that metal dissolution was responsible was generally overlooked.[74] In the investigation by Rand and Woods the Pd electrode was voltammetrically cycled between 0.33 to 1.54 V vs. RHE (-0.35 to 0.86 V vs. SMSE) at 40 mV / s. They concluded that the difference between the total anodic and cathodic charges on a voltammetric cycle corresponds to the amount of metal in the solution which was not replated. They investigated the dependence of the charge difference (Q_o^a - Q_o^c) on the anodic potential limit. They report that with an anodic

potential limit of approximately 0.95 V vs. RHE (0.27 V vs. SMSE) the charge difference was zero. This indicates that the onset of Pd dissolution commences at approximately 0.27 V vs. SMSE. Referring to fig 19 it can be seen that a peak which was attributed to the formation of Pd oxide occurs at this potential. Indeed it was established by Vetter and Berndt that the initial stage of oxygen adsorption occurs at the potential of electrodissolution of palladium as described by:

$$Pd \leftrightarrow Pd^{2+} + 2e^{-} \qquad \textbf{(9)}$$

Bolzan *et al.*[85] investigated the electrodissolution of palladium in sulphuric acid using a rotating disc electrode. Using a rotating disc electrode means that replating of the palladium does not occur as the Pd that has been dissolved during the anodic scan will be swept away from the electrode by the perturbation of the solution.[85] The report concluded that Pd electrodissolution occurs in different potential regions. At low potentials Pd electrodissolution occurs as a competitive process with the formation of an oxide layer. Key to these two processes is the reversible oxidation of water

$$Pd + H_2O \leftrightarrow Pd(OH) + H^{+} + e^{-} \qquad \textbf{(10)}$$

The electrodissolution reaction proceeds as follows[85]

$$Pd(OH) \Leftrightarrow Pd(OH)^{+} + e^{-} \qquad \textbf{(11)}$$

$$Pd(OH)^{+} \leftrightarrow Pd^{2+}_{(aq)} + OH^{-} \qquad \textbf{(12)}$$

As indicated the dissolution reaction is in competition with the formation of the oxide layer which proceeds from equation 10 as follows:

$$Pd(OH) \Leftrightarrow Pd(O) + H^{+} + e^{-} \qquad \textbf{(13)}$$

$Pd(O) \rightarrow$ Oxygen containing layer.

The investigation by Bolzan also reports that at high positive potentials the rate of electrodissolution is enhanced.

Marwan [69] investigated mass loss in a H_1-e Pd film voltammetically cycled in sulphuric acid using electroquartz crystal microbalance techniques (EQCM). It was

concluded that Pd was lost with the formation of the surface oxide layer at approximately 0.1 V vs. SMSE on the forward (anodic) scan and continuing until approximately 0.05 V vs. SMSE on the backward (cathodic) scan. At this point the removal of the oxide begins and mass gain occurs as Pd is replated. The investigation agrees with the findings of Rand and Woods,[75] that mass loss exceeds mass gain.

The dissolution and subsequent partial replating of Pd will increase the surface area of the film in two ways. Firstly, the surface will be roughened as a result of replating. Secondly, as Pd electrodissolution occurs and subsequently does not replate, the diameters of the pores will increase. It is proposed that this will result in an increase in the electroactive surface area, as despite a loss of mass of Pd there will actually be more Pd in contact with the electrolyte. This is at odds with the conclusion reached by Marwan[69], who proposed that a loss of Pd would result in a decrease in the electroactive surface area. It is proposed that as the pore diameter increases the amount of Pd in contact with the electrolyte increases until the maximum surface area is obtained when the pores are as large as possible and there is the minimum amount of material between the pores. If voltammetric cycling were continued there may eventually be a dramatic decrease in surface area as there is insufficient Pd between the pores, resulting in the collapse of the nanostructure.

It was noted earlier that the surface area of the Pd film increased by approximately 4 times. In this discussion it was proposed that the loss of Pd from the pore walls would result in an increase in the surface area. Marwan[69] reported the pores to have a diameter of 2.5 nm and the pore separation to be 2.5 nm. Similar values were obtained here using TEM and are presented in section 3.4.3. If we take the loss of Pd to the limit where the pores are as large as possible then we estimate the increase in surface area to be approximately 50 %. It can therefore be reasonably concluded that the increase in surface area due to loss of Pd accounts for only a small amount of the total increase in surface area. It is probable that the majority of the increase in surface area is due to surfactant being removed from the pores, surface roughening and electrolyte filling the pores.

As indicated earlier Rand and Woods reported that adsorption and the subsequent removal of hydrogen from the Pd film results in a marked roughening of the surface.[75] It was for this reason that the hydrogen region was omitted from the potential range used in their investigations. The cyclic voltammogram in fig 19

includes the hydride region, therefore the Pd film will have been roughened not only by the dissolution and replating in the oxide potential range, but also by the absorption and subsequent removal of hydrogen. This roughening of the surface will further increase the electroactive surface area.

Cyclic voltammograms were carried out at a slower scan rate of 10 mV / s so as to better resolve the peaks in the hydrogen potential region Cyclic voltammograms of H_I-e Pd deposited from both the $C_{12}EO_8$ and the Brij®56 template mixtures are shown in fig 20.

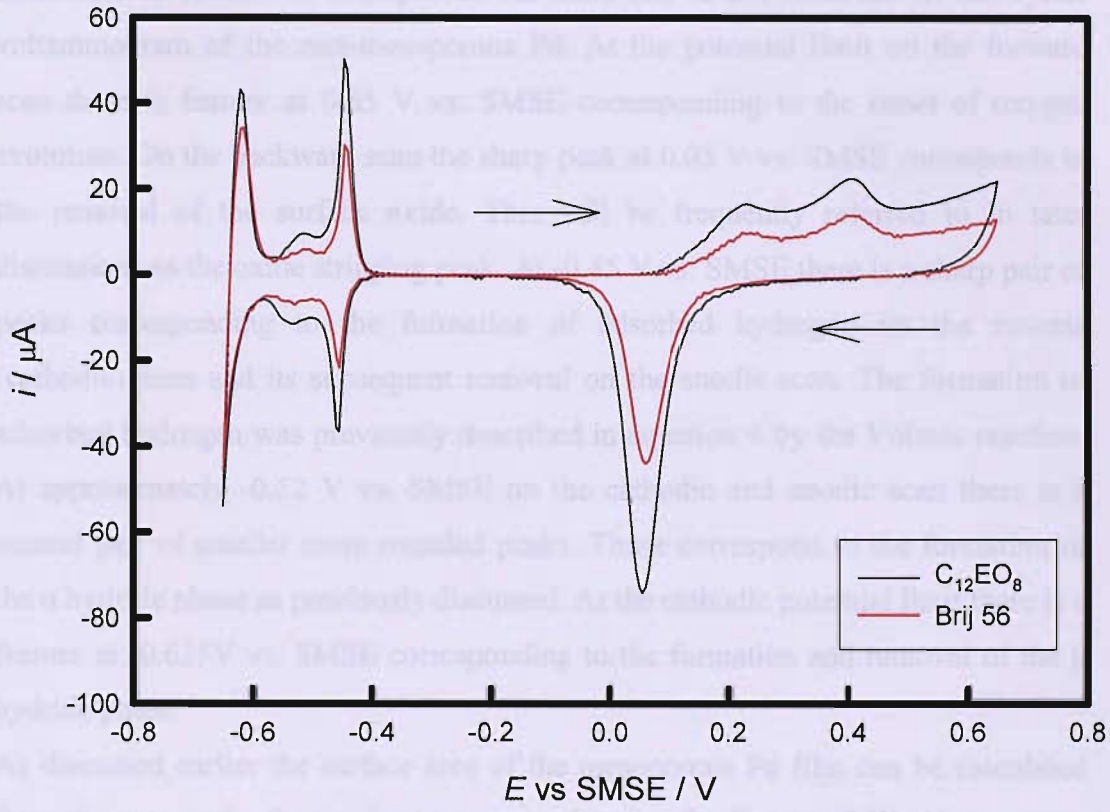

Fig 20 Cyclic voltammograms of H_I-e Pd on a 1mm diameter Au disc electrode deposited from Brij®56 and $C_{12}EO_8$ template mixtures. Both H_I-e Pd films were electrodeposited by applying a potential step of 0.4 to 0.1 V vs. SCE. A deposition charge of 3.5 mC was passed in each case. The cyclic voltammograms were carried out at a scan rate of 20 mV/s starting at 0.0 V vs. SMSE in 1 M sulphuric acid. The 3rd voltammetric cycle is shown in each case. The sulphuric acid was deoxygenated for 15 min with argon prior to the cyclic voltammograms being undertaken. The Au electrode was polished prior to electrodeposition using 1 and subsequently 0.3 µm alumina. A cyclic voltammogram of the Au electrode in 1 M sulphuric acid was then carried out to confirm a clean surface.

The cyclic voltammograms in fig 20 show H_1-e Pd on a gold electrode in 1 M sulphuric acid. The cyclic voltammograms were started at 0.0 V vs. SMSE. The black arrows indicate the sweep direction. It can be seen that the cyclic voltammograms of the two mesoporous Pd films electrodeposited from Brij®56 and $C_{12}EO_8$ respectively are very similar and that all the features occur at similar potentials. The formation of the surface oxide begins at around 0.15 V vs. SMSE on the forward scan. There are two peaks associated with the formation of the surface oxide; one at 0.22 V vs. SMSE and a second at 0.4 V vs. SMSE. This is a characteristic feature of mesoporous Pd films and is not observed in the cyclic voltammogram of the non-mesoporous Pd. At the potential limit on the forward scan there is feature at 0.65 V vs. SMSE corresponding to the onset of oxygen evolution. On the backward scan the sharp peak at 0.05 V vs. SMSE corresponds to the removal of the surface oxide. This will be frequently referred to in later discussions as the oxide stripping peak. At -0.45 V vs. SMSE there is a sharp pair of peaks corresponding to the formation of adsorbed hydrogen on the reverse (cathodic) scan and its subsequent removal on the anodic scan. The formation of adsorbed hydrogen was previously described in equation 4 by the Volmer reaction. At approximately -0.52 V vs. SMSE on the cathodic and anodic scan there is a second pair of smaller more rounded peaks. These correspond to the formation of the α hydride phase as previously discussed. At the cathodic potential limit there is a feature at -0.625V vs. SMSE corresponding to the formation and removal of the β hydride phase.

As discussed earlier the surface area of the mesoporous Pd film can be calculated from the area under the oxide stripping peak using the Rand and Woods constant. The specific surface area has units of $m^2\ g^{-1}$. This is a useful figure as it allows for a comparison of the surface areas of films of varying deposition quantities. This can be calculated as the mass of Pd can be easily calculated from the charge passed in the electrodeposition. A Faradaic efficiency of 100 % is assumed. The specific surface area of the H_1-e Pd from the $C_{12}EO_8$ template bath was calculated to be 56 $m^2\ g^{-1}$. The H_1-e Pd from the standard Brij®56 template bath had a specific surface area of 31 $m^2\ g^{-1}$. There is a significant difference in the specific surface areas of the two films. The H_1-e Pd electrodeposited from the $C_{12}EO_8$ should theoretically have a smaller surface area as the pores have a smaller diameter due to the shorter alkyl

chain length. However, experiments revealed a significant variation in the surface area of similarly prepared H_1-e Pd films. It is proposed that this is a result of a number of factors including imperfect nanostructures and regions of inhomogeneity in the template mixture. Imokawa[98] investigated H_1-e Pd films electrodeposited using $C_{16}EO_8$ and Brij®56. The surface areas were calculated using the charge under the oxide stripping peak to be 58 and 28 m^2g^{-1} respectively. These values are very similar to those obtained here using $C_{12}EO_8$ and Brij®56. It was concluded that the difference was not due to the amount of Pd as there was no appreciable difference in the amount of hydrogen absorbed into the two films. It was concluded that the difference was due to differences in the nanostructure and it was proposed that the film deposited from the Brij®56 template mixture may have a less regular structure.

Having compared the cyclic voltammograms of H_1-e Pd from the two different template baths a cyclic voltammogram of non-mesoporous Pd was carried out for comparison. It is shown along with the cyclic voltammogram of H_1-e Pd from the $C_{12}EO_8$ template bath in fig 21.

The surface area of the non-mesoporous Pd catalyst was calculated from the area under the oxide stripping peak to be 0.94 $m^2\ g^{-1}$ compared to 54 $m^2\ g^{-1}$ for the H_1-e Pd film. Comparing the two cyclic voltammograms in fig 21 it can be seen that the cyclic voltammogram of the non-mesoporous Pd does not have the well resolved peaks in the hydride region seen in the cyclic voltammograms of H_1-e Pd. The acid cyclic voltammogram therefore gives the first evidence that H_1-e Pd films have been successfully deposited using $C_{12}EO_8$ for the first time.

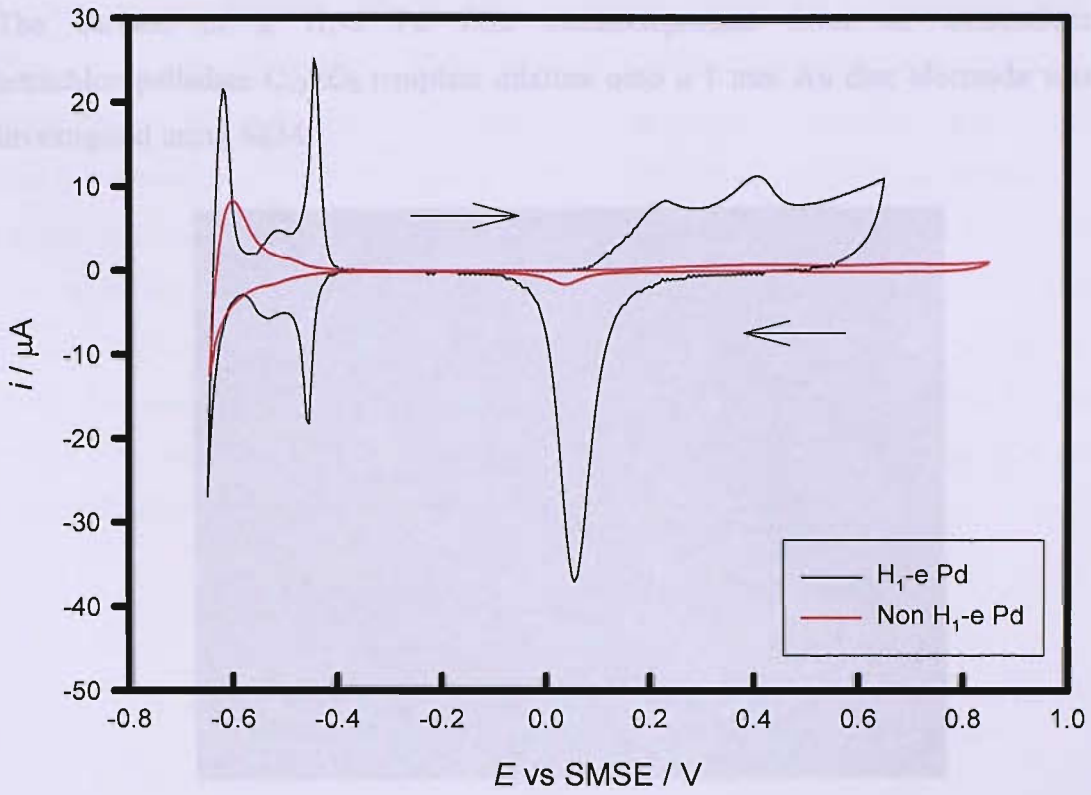

Fig 21 Cyclic voltammograms of mesoporous and non-mesoporous palladium electrodeposited onto a 1 mm diameter Au disc electrode. The H_1-e Pd was electrodeposited from a $C_{12}EO_8$ template mixture consisting of 47 wt % surfactant. The non-mesoporous Pd was electrodeposited from a solution containing 50 mM $(NH_4)_2PdCl_4$, 1 M HCl and 1M NH_4Cl. Both Pd films were electrodeposited by applying a potential step of 0.4 to 0.1 V vs. SCE. A deposition charge of 3.5 mC was passed in both cases. The cyclic voltammograms were carried out at a scan rate of 10 mV/s in 1 M sulphuric acid which was first deoxygenated for 15 min with argon. The scan shown is the fifth voltammetric cycle in each case.

3.4.2 Characterisation by SEM

The surface of a H_1-e Pd film electrodeposited from an ammonium tetrachloropalladate $C_{12}EO_8$ template mixture onto a 1 mm Au disc electrode was investigated using SEM.

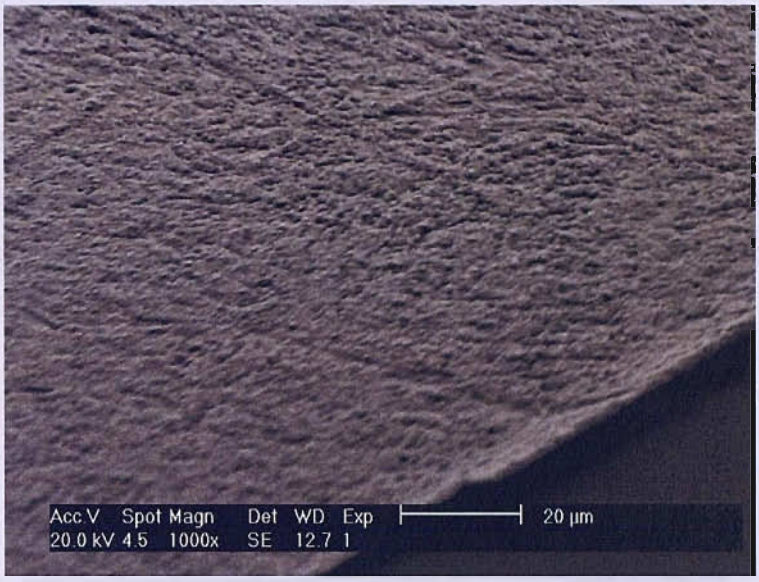

Fig 22 SEM image of a H_1-e Pd electrodeposited onto a 1 mm Au disc electrode. Electrodeposition was carried out by applying a potential step from 0.4 to 0.1 V vs. SCE. A charge of 3.5 mC was passed. The template mixture comprised ammonium tetrachloropalladate, water, heptane and $C_{12}EO_8$ in the standard composition as described in fig 15.

The SEM image in fig 22 shows that the surface of the H_1-e Pd film is fairly smooth and there is complete coverage over this area of the electrode. Investigating other areas of the film revealed that the film was typically smooth, though the Au electrode was not completely covered. The SEM does not give sufficient resolution to confirm the nanostructure. It can be seen that the film is thicker at the edge of the electrode. It is proposed that this is a result of radial diffusion at the edge of the electrode. This edge effect was observed by Imokawa[98] using microelectrodes and non-mesoporous Pd films. It was found that by increasing the deposition potential (decreasing the overpotential) reduced the edge effect.

3.4.3 Characterisation by TEM

Further evidence is needed to show that a nanostructured film has been produced from the $C_{12}EO_8$ template bath. TEM is a useful tool as it allows visual confirmation of the nanostructure. Furthermore, measurement of the pore dimensions is possible. The disadvantages of this technique are that it is expensive, difficult to prepare the sample and results in the destruction of the film. The TEMS shown here are of Pd films electrodeposited onto Au electrodes. Following electrodeposition the film was scraped off the electrode using a scalpel into a container containing a droplet of water. The water droplet was placed onto a TEM grid using a micro-pipette before evaporating the water to leave the Pd particles. A TEM image of a mesoporous Pd film electrodeposited from the $C_{12}EO_8$ template bath is shown in fig 23.

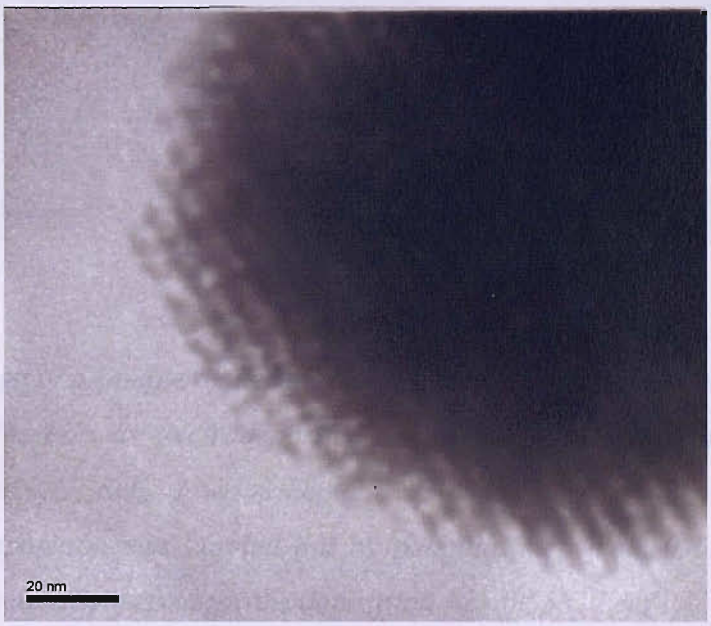

Fig 23 TEM image of a sample of mesoporous Pd scraped from a 1 mm diameter Au disc electrode. The Pd was electrodeposited onto the Au electrode from a template mixture of 47 wt% $C_{12}EO_8$, 2 wt % heptane 12 wt% $(NH_4)_2$ $PdCl_4$ and 39 wt% water. Electrodeposition was carried out by potential step from 0.4 to 0.1 V vs. SCE. The charge density passed for the deposition was 0.55 C / cm^2.

The TEM image shown in fig 23 was taken by with the help of Dr. Barbara Cressey. At the edge of the sample pores in the Pd can be seen. The order of the pores is well resolved and it can be seen that there is good long range order. The dark area of the film is nanostructured though it is too thick to allow the beam to penetrate. The pore

repeat distance was calculated to be approximately 6 nm. TEM images were taken at other areas of the sample. An example is shown in fig 24.

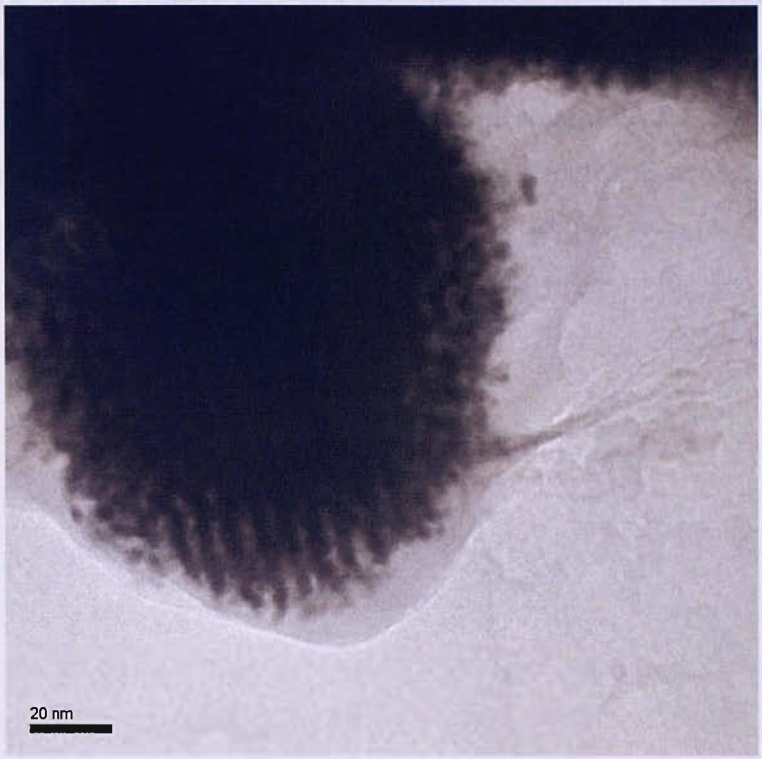

Fig 24 TEM image of a sample of mesoporous Pd scraped from a 1 mm diameter Au disc electrode. The Pd was electrodeposited onto the Au electrode from a template mixture of 47 wt% $C_{12}EO_8$, 2 wt % heptane 12 wt% $(NH_4)_2$ $PdCl_4$ and 39 wt% water. Electrodeposition was carried out by potential step from 0.4 to 0.1 V vs. SCE. The charge density passed for the deposition was 0.55 C / cm^2.

From the TEM in fig 24 the pores were measured to be 3 nm in diameter and the pore walls 2 nm thick. The distance between pore centres was again calculated to be approximately 6 nm. The TEM of the sample in fig 23 clearly shows that the pores are well ordered and of a regular size, therefore confirming its nanostructure.
Attard *et al.*[66] prepared mesoporous Pd films using $C_{12}EO_8$ based templates. In this case a pore diameter of 17.5 Å (+/- 2 Å) was measuerd. In our template mixture heptane was included. Heptane is hydrophobic and swells the surfactant thus increasing the pore diameter. Even so the value obtained here for the pore diameter seems large.

The H_1-e Pd film electrodeposited from a $C_{12}EO_8$ template bath has been investigated using a variety of techniques. It has been shown by electrochemical methods to have a high surface area and have the characteristic features associated with a nanostructured Pd cyclic voltammogram. TEM has shown the film to have a regular array of pores. In the next chapter mesoporous Pd films will be electrodeposited onto microhotplate devices for use as a methane sensor.

4 Mesoporous Pd films used as part of a catalytic methane sensor

4.1 Introduction

In the previous chapter the electrodeposition and characterisation of mesoporous Pd onto gold electrodes was reported. In this section the electrodeposition of H_1-e Pd onto microhotplates is investigated. As described in chapter 1 the motivation is to produce a methane sensor using mesoporous Pd catalysts.

4.1.1 Silicon microfabricated microhotplates

Palladium catalyses the oxidation of methane at temperatures of 500 °C and above.[33] Therefore a method of heating the Pd film is required. For a sensor to have commercial viability it must have low power consumption, be possible to produce the devices in large quantities and at low cost and with a high degree of reproducibility.

One of the drawbacks of pellistor technology is the high power consumption. Recently efforts in catalytic gas sensor research have focussed on addressing this issue.[2] In order to achieve low power consumption it is necessary to achieve good thermal isolation between the sensing element and its housing whilst maintaining good mechanical stability. [99] During the last number of years significant progress has been made in micromachining technology. To achieve thermal isolation devices have been made with dielectric membranes separating the sensing element from the housing. These membranes have low thermal conductivity which reduces power consumption to between 30 and 150 mW.[99] The membranes are manufactured from silicon nitride which has a high tensile strength giving the membrane good mechanical stability.[99]

Krebs and Grisel[100] manufactured a device on silicon with thin film deposition and silicon micromachining techniques. Their device housed the sensor and reference on the same chip. This device required a power of 50-60 mW at 500 °C [101] which compares very favourably with the figure of 250 mW for a typical pellistor.[2] Another advantage of silicon micro-machined micro-hotplates is their fast thermal time constants,[99] silicon micromachined devices have thermal time constants in the

milliseconds range.[2] The definition of the thermal time constant is the amount of time required for a sensor to change by 63.2 percent when subjected to a step function change in temperature.[102] This introduces the possibility of pulse powering which would give significantly reduced power consumption. Aigner *et al.*[103] investigated pulse powering using silicon microhotplates. They reported that modulation of temperature at frequencies up to 100 Hz was possible. This gave power consumptions of as low as 40 mW at 300 °C.

Briand *et al.*[104] report the design and manufacture of microhotplates using backside silicon micromachining in KOH. They found that the devices could withstand temperatures up to 700 °C which was of benefit when annealing the coating materials. They applied a 2 % Pd doped tin oxide coating which was annealed by heating at 600 °C for 10 s. This was then operated at approximately 400 °C in 4000 ppm methane and found to give an increase in resistance of 1×10^5 ohms, which represents an increase of 26 %. It is noted that both the baseline in air and the response to methane were unstable. The authors report that annealing at 700 °C decreased the baseline drift, though did result in significant electronic noise. This was a result of contact problems between the substrate and the gas sensitive layer as a result of the bending caused during the annealing process. The bending was observed under an optical microscope to be 400 μm at 700 °C for a membrane of 1 mm by 1 mm.

Capone *et al.*[105] produced a sensor for analysing CO and CH_4 gas mixtures using a sol gel fabricated Pd-doped SnO_2 film on a silicon microhotplate. The Si_3N_4 membrane was 1 x 1 mm^2 and 0.85 mm thick. The sensor was operated at 350 °C. The report concluded that it was possible to combine thick film technology necessary to produce highly sensitive elements with micromachined susbstrates for low cost and low power consumption.

Cerdà *et al.*[106] report on the deposition of gas sensitive layers on silicon micromachined hotplates using a wet chemical deposition method. Physical deposition methods such as chemical vapour deposition, sputtering and ion beam assisted deposition have potential problems such as stabilisation of the material both on the surface and in the bulk as the treatment temperatures are insufficient. Furthermore, there are problems in adding the catalytic additives and their activation.[106] Wet chemical methods are based on the addition of material using a micro-pipette to deposit a small amount of paste made of the stabilising elements

and the catalytic additives in the form of nanopowders. Using this method it is possible to exert control over the properties of the nanopowders characteristics such as grain size, the quantity of catalyst, activation treatment, porosity and thickness. The device gave reproducible methane responses though the results show that the response in methane was not stable.

4.1.2. Description of microhotplates used in these investigations

The development of silicon microfabrication technology has made it possible to produce a large number of devices at low cost with a high degree of reproducibility. Features can be made with dimensions in the nanometer scale. The micro-hotplates described here were developed in collaboration between City Technology and the Universities of Southampton and Warwick. Figure 25 shows a top view of a silicon micromachined microhotplate.

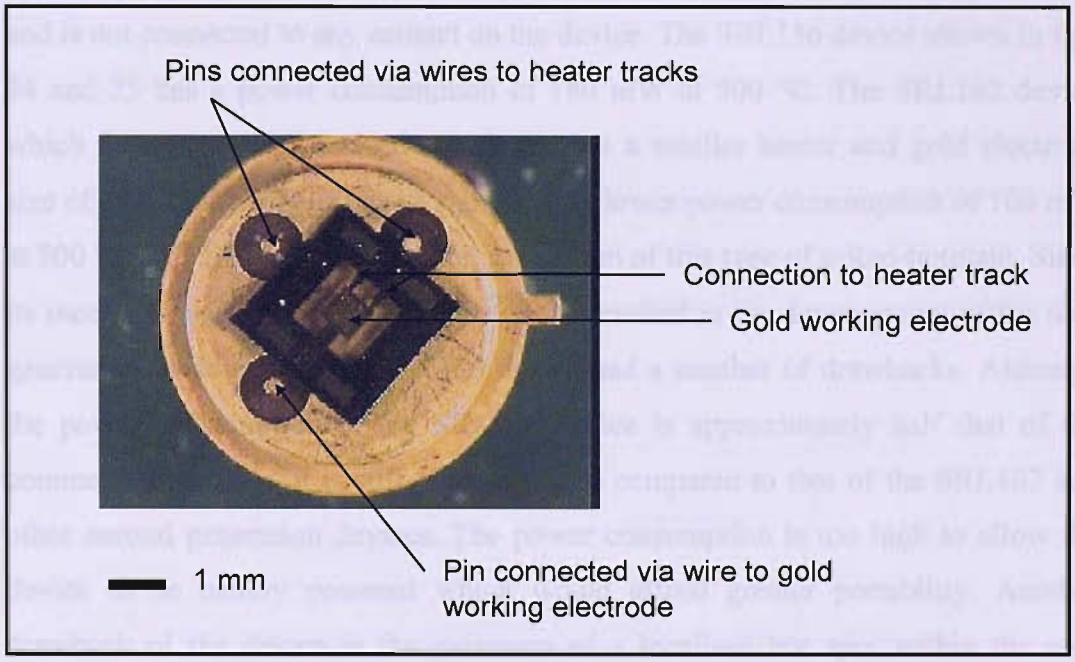

Figure 25 Top view of an SRL136 microhotplate.

The microhotplate consists of a thin membrane structure and uses a <100> silicon wafer as the inert substrate. The membrane is 2 mm by 2 mm in size. The membrane comprises a 250 nm thick Pt heater which is sandwiched between two layers of silicon nitride. The top layer is 500 nm thick and the bottom layer 250 nm thick. The Pt heater track follows a rectangular meander. The microhotplate features a square gold working electrode in the centre of the device. The electrode is 750 μm

by 750 μm and 300 nm thick. The electrode was patterned by a lift off process. The purpose of the Au electrode is to provide a platform onto which the catalyst layer can be applied. In these investigations H_1-e Pd films were electrodeposited onto the electrode. To facilitate this, the electrode is connected via a track and a bonded wire to the pin head shown in the bottom left hand corner of fig 25. The pin extends into a leg which protrudes beneath the bottom of the device. This was then inserted into a zero insertion force socket and connected to the potentiostat. This arrangement ensures that the rest of the device is insulated from the current that passes during electrodeposition.

The catalyst film is heated by a resistive Pt heater track which is sandwiched between two layers of silicon nitride. This is connected via tracks and wires to the pins in the top left and top right of the device. Again, the pins extend through the header unit into legs that protrude beneath the device. These can be connected to a power supply to raise the temperature of the catalyst layer. The 4^{th} leg is a dummy and is not connected to any contact on the device. The SRL136 device shown in figs 24 and 25 has a power consumption of 180 mW at 500 °C. The SRL162 device which features a similar sized membrane but a smaller heater and gold electrode size of 570 μm by 570 μm has a significantly lower power consumption of 106 mW at 500 °C. The SRL136 was the first generation of this type of micro-hotplate. Since its inception work carried out by Lee[107] has resulted in the development of the next generation of devices. The SRL 136 device had a number of drawbacks. Although the power consumption of the SRL136 device is approximately half that of the commercial pellistor, it is still relatively high compared to that of the SRL162 and other second generation devices. The power consumption is too high to allow the device to be battery powered which would afford greater portability. Another drawback of the device is the existence of a localised hot spot within the area defined by the gold electrode. This results in an uneven catalyst reaction to methane.[107] Although ultimately achieving a lower power consumption is the goal it requires a smaller electrode area and also a thinner membrane. Both of these requirements make electrodepositions harder; the thinner membrane makes the device more fragile and the smaller electrode area makes it harder to apply the template mixture. For the purpose of these experiments the use of SRL136 devices is acceptable.

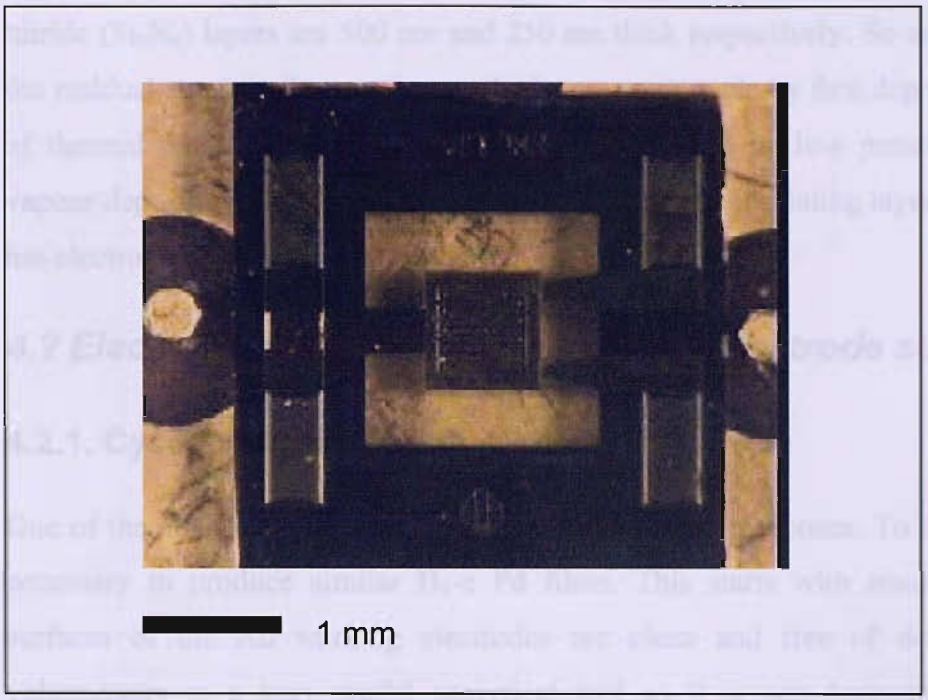

Fig 26. Close up photo of a SRL 136 micro-machined substrate mounted on a TO5 header. The Au working electrode can be seen in the centre of the device.

The photo in figure 26 is a close up of the working electrode. The meander heater track can be seen through the Au electrode. The heater track connections can clearly be seen on the right of working electrode. The connection to the working electrode can be seen on the left hand side of the device.

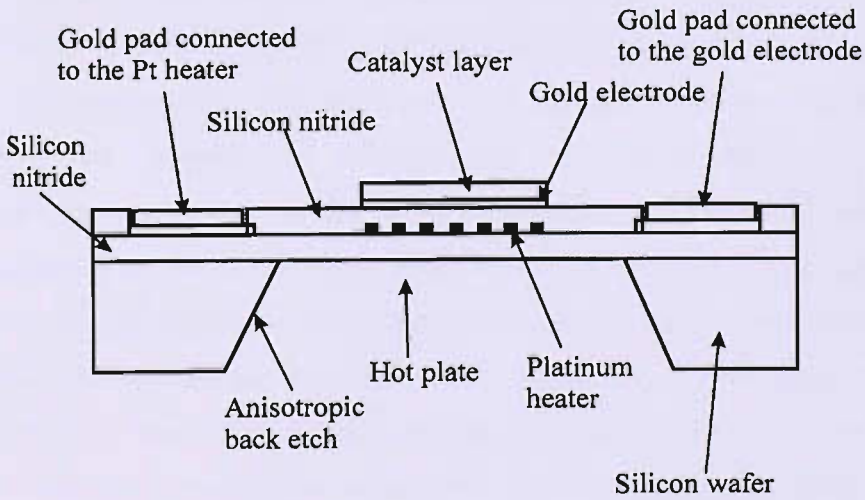

Fig27 .Cross section of a silicon microhotplate.

Figure 27 shows a cross section of a microhotplate. The top and bottom silicon nitride (Si_3N_4) layers are 500 nm and 250 nm thick respectively. So as to minimise the residual stress in the membrane, the layers were made by first depositing 80 nm of thermal oxide before silicon nitride was deposited by low pressure chemical vapour deposition. The silicon nitride layer provides an insulating layer between the hot electrode layer and the substrate.

4.2 Electrochemical characterisation of electrode surface

4.2.1. Cyclic voltammogram of the Au electrode

One of the aims was to achieve reproducible methane responses. To do this it was necessary to produce similar H_1-e Pd films. This starts with ensuring that the surfaces of the Au working electrodes are clean and free of defects. Cyclic voltammetry is a very useful analytical tool as it is non-destructive which is essential as the devices will subsequently be used for electrodepositing and ultimately gas testing. Furthermore the technique will not apply any significant force to the device which is important given the inherent fragility of the membrane. As well as confirming a clean electrode surface, direct comparisons can be made with cyclic voltammograms of 1 mm diameter Au disc electrodes which will highlight any contamination or defects.

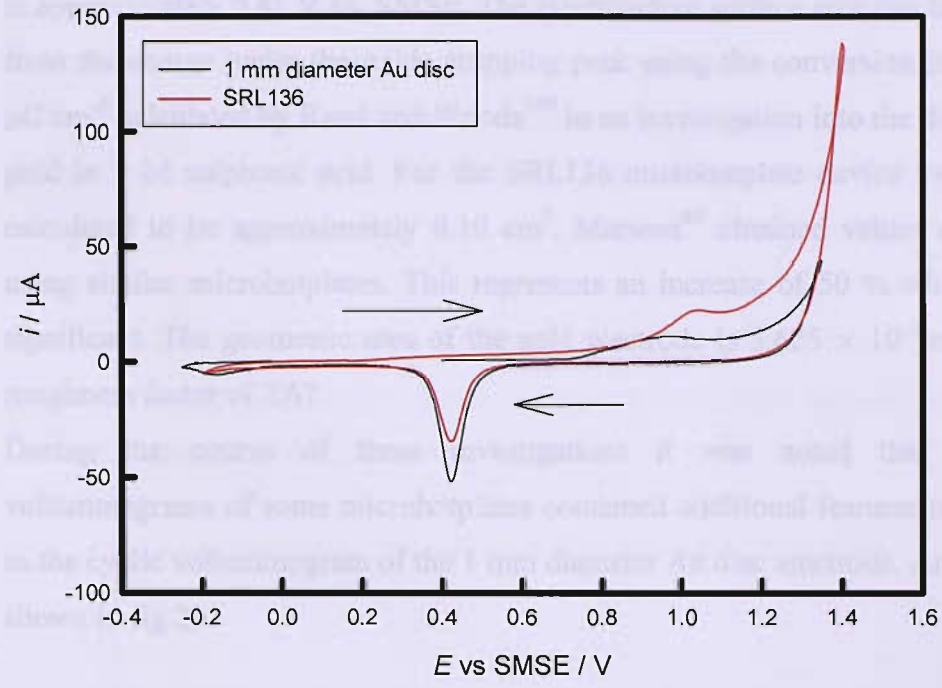

Fig 28. Cyclic voltammograms of the gold electrode of a SRL 136 device and a 1 mm diameter Au disc electrode at 100 mV / s in 1 M sulphuric acid. The cyclic voltammograms were started at 0.2 V vs. SMSE and were carried out at room temperature (25 °C).

Figure 28 shows the cyclic voltammograms of the gold electrode of an SRL 136 device and a 1 mm diameter Au disc electrode in 1 M sulphuric acid. The experiment was carried out using the droplet setup which is described in section 2.1.1. The two cyclic voltammograms are similar, there are no extra peaks indicating the presence of contamination or surface defects. The cyclic voltammograms are also similar to those obtained by Marwan[69] using similar microhotplates as well as those obtained in studies by Hoare[108] using gold wires. The oxide stripping peaks both occur at approximately 0.41 V vs. SMSE. However the peak resulting from the formation of the surface oxide which occurs at 0.9 V vs. SMSE on the 1 mm Au electrode is shifted by approximately 0.15 V to 1.05 V vs. SMSE. Some differences in the voltammetry may be expected due to the differences in the gold surfaces. The Au wire has a polished polycrystalline surface whilst the Au electrode on the microhotplate consists of evaporated gold and cannot be polished which will result in the surface consisting of lumps of Au. It can be seen

that on the forward (anodic) scan the formation of gold oxide begins at around 0.8 V vs. SMSE. On the backward (cathodic) scan the removal of the surface oxide occurs at approximately 0.41 V vs. SMSE. The electroactive surface area can be calculated from the charge under the oxide stripping peak using the conversion factor of 386 $\mu C\ cm^{-2}$ calculated by Rand and Woods[109] in an investigation into the dissolution of gold in 1 M sulphuric acid. For the SRL136 microhotplate device used this was calculated to be approximately 0.10 cm^2. Marwan[69] obtained values of 0.15 cm^2 using similar microhotplates. This represents an increase of 50 % which is fairly significant. The geometric area of the gold electrode is $5.625 \times 10^{-3}\ cm^2$ giving a roughness factor of 2.67.

During the course of these investigations it was noted that the cyclic voltammograms of some microhotplates contained additional features not observed in the cyclic voltammogram of the 1 mm diameter Au disc electrode. An example is shown in fig 29.

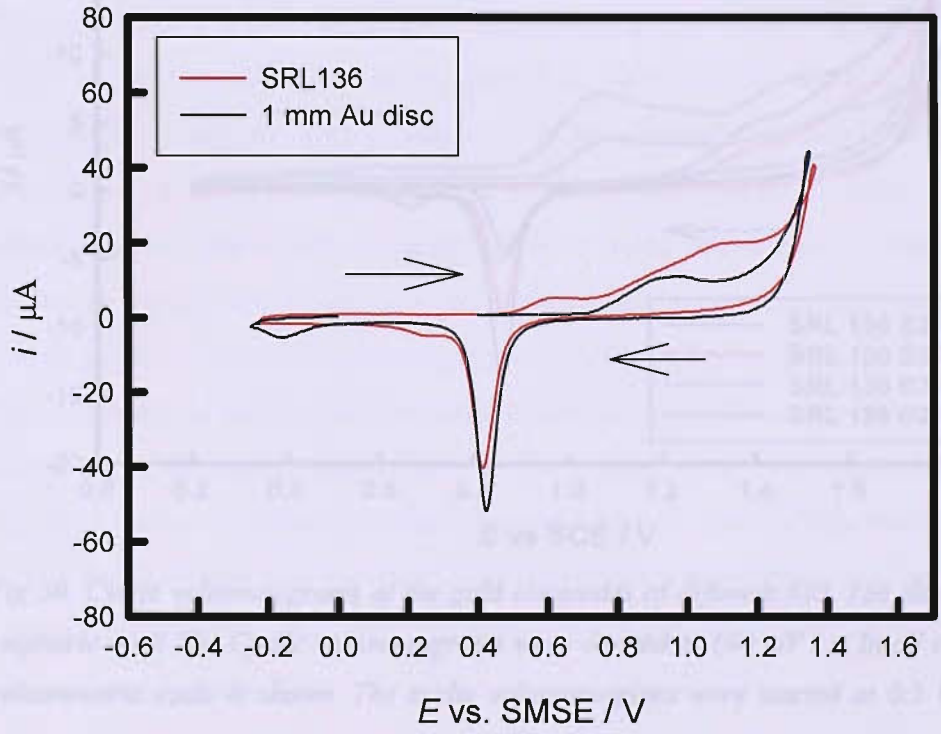

Fig 29 Cyclic voltammograms of SRL 136 and gold disc electrode in 1 M sulphuric acid at 200 mV / s. In both cases the fifth voltammetric cycle is shown. The cyclic voltammograms were started at 0.2 V vs. SMSE and were carried out at room temperature (25 °C).

Figure 29 shows the cyclic voltammograms of a 1 mm diameter Au disc electrode and the Au electrode of an SRL136 microhotplate device in 1 M sulphuric acid. It can be seen that the cyclic voltammogram of the device has an extra feature at approximately 0.6 V vs. SMSE on the forward (anodic) scan. This is not present in the cyclic voltammograms of the Au electrode or the microhotplate device shown in fig 28. Examination of the electrode surface under a microscope did not reveal any obvious surface contamination so it is unclear what is responsible for this extra feature. Comparing the relative size of the voltammetric feature corresponding to the contaminant to those of the Au electrode it is noted that it is relatively small. Further examples of microhotplates containing additional features in their acid cyclic voltammograms are shown in fig 30.

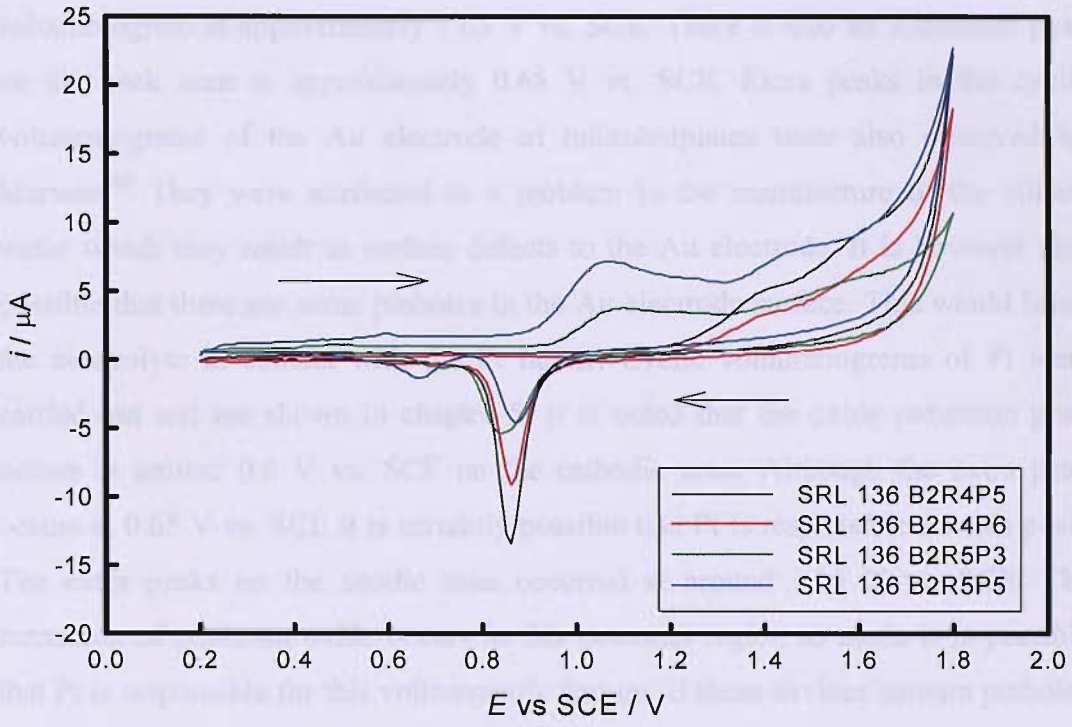

Fig 30. Cyclic voltammograms of the gold electrodes of different SRL 136 devices in 1 M sulphuric acid. The Cyclic voltammograms were carried at 100 mV / s. In all cases the 5th voltammetric cycle is shown. The cyclic voltammograms were started at 0.2 V vs. SMSE and were carried out at room temperature (25 °C).

It can be seen that the oxide stripping peak which occurs at approximately 0.85 V vs. SCE, differs significantly in size. As indicated previously the surface area of the Au electrode can be calculated using the charge under the oxide stripping peak. It can therefore be ascertained that there is a significant variation in the surface area of

the Au electrodes. This is despite the electrodes having the same geometric area. The largest surface, that of device SRL136B2R4P5 was calculated to be 0.05 cm^2 whereas the smallest, that of device SRL136B2R5P5 was calculated to be approximately 0.014 cm^2. That is approximately 14 % of the area of the device calculated from fig 27. Marwan[69] reported a variation of only 0.1 cm^2 in the surface area of the Au electrodes calculated using this method. It is not immediately clear why there should be such a significant variation in surface area of some of the devices. It is possible that there is some photoresist remaining on the surface of the Au electrode. This would act as a barrier and thus decrease the electroactive surface area. It is possible that a manufacturing problem may be responsible.

It is noted that the cyclic voltammograms of devices SRL 136B2R5P3 and SRL136B2R5P5 have additional peaks on the forward scan on the cyclic voltammogram at approximately 1.05 V vs. SCE. There is also an additional peak on the back scan at approximately 0.65 V vs. SCE. Extra peaks in the cyclic voltammograms of the Au electrode of microhotplates were also observed by Marwan.[69] They were attributed to a problem in the manufacture of the silicon wafer which may result in surface defects to the Au electrode. It is however also possible that there are some pinholes in the Au electrode surface. This would bring the electrolyte in contact with the Pt heater. Cyclic voltammograms of Pt were carried out and are shown in chapter 5. It is noted that the oxide reduction peak occurs at around 0.6 V vs. SCE on the cathodic scan. Although the extra peak occurs at 0.65 V vs. SCE it is certainly possible that Pt is responsible for this peak. The extra peaks on the anodic scan occurred at around 1.05 V vs. SCE. The formation of platinum oxide occurs in this potential region so again it is possible that Pt is responsible for this voltammetric feature. If these devices contain pinholes in the Au electrode then this may compromise later investigations. For this reason devices containing these extra voltammetric features were discarded and not used in further investigations.

4.3 Electrodeposition of H_1-e Pd onto microhotplate devices

Deposition transient

Once a clean gold electrode had been obtained the next step was to apply the mesoporous Pd film onto the gold working electrode of the microhotplate device. This was done by electrodeposition. The principal advantage of this method is that it allows control over the thickness of the film. This means different thickness films can be produced but it also ensures that batches of films of similar thickness can be produced. This method also does not use any chemicals that may damage the device. A deposition potential of 0.1 V vs. SCE was used as determined in section 3.3 and a deposition charge of 5.0 mC was passed. In initial experiments it was decided to use Brij®56 rather than the $C_{12}EO_8$ template bath characterised in Chapter 3. Both surfactants have been shown to give mesoporous Pd films, but the Brij®56 surfactant is significantly cheaper. A typical current transient of the deposition of H_1-e Pd onto the Au electrode of an SRL136 microhotplate from a template bath comprising 47 wt. % Brij®56, 2 wt % heptane 12 wt % $(NH_4)_2$ $PdCl_4$ and 39 wt % water is shown in fig 31.

The current transient for the electrodeposition of H_1-e Pd onto a microhotplate shown in fig 31 is very similar to that obtained for the electrodeposition of H_1-e Pd onto a 1 mm diameter Au disc electrode shown in fig 17. It is noted that the maximum current in the transient in fig 31 is significantly smaller than that obtained when using the 1 mm diameter Au disc electrode. The area of the Au electrode on the device is smaller, 0.5625 mm^2 compared to 0.785 mm^2. So the microhotplate device has an area 0.7 times that of the Au disc electrode. However, a typical current transient for a deposition onto a 1 mm diameter Au disc electrode had a maximum current of around 30 μA.

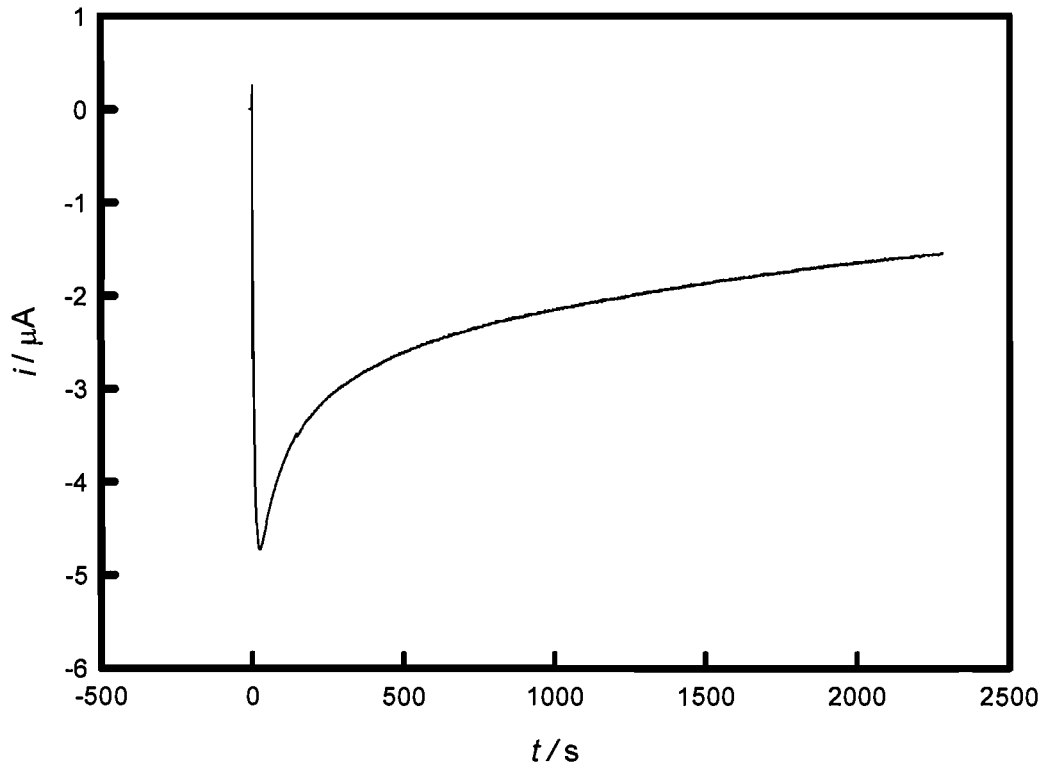

Fig 31. Current transient for the electrodeposition of H_1-e Pd onto an SRL136 microhotplate. The electrodeposition was carried out by applying a potential step from 0.4 to 0.1 V vs. SCE. A deposition charge of 5.0 mC was passed. The template bath comprised 47 wt. % Brij®56, 2 wt % heptane 12 wt % $(NH_4)_2$ $PdCl_4$ and 39 wt % water. The Au electrode had previously been voltammetrically cycled in 1 M sulphuric acid to ensure a clean surface. The surface was then cleaned in iso-propanol and dried in a glass drying oven at 40 °C.

One explanation for the small current is the difficulty of setting up the deposition onto the microhotplates. The membrane of the device is very thin and consequently very fragile. When depositing on the 1 mm Au electrode the electrode can be pushed into the template bath, shearing the template mixture and ensuring no air bubbles and good contact with the template mixture. When depositing on devices a small spatula was used to add a small amount of template mixture to the electrode. This was then carefully spread over the Au electrode in an attempt to ensure good coverage. The high viscosity of the mixture meant it was likely that there would be bubbles in the mixture and that the Au electrode would not be fully covered. The photo in fig 32 shows an example of a H_1-e Pd film on an SRL136 microhotplate.

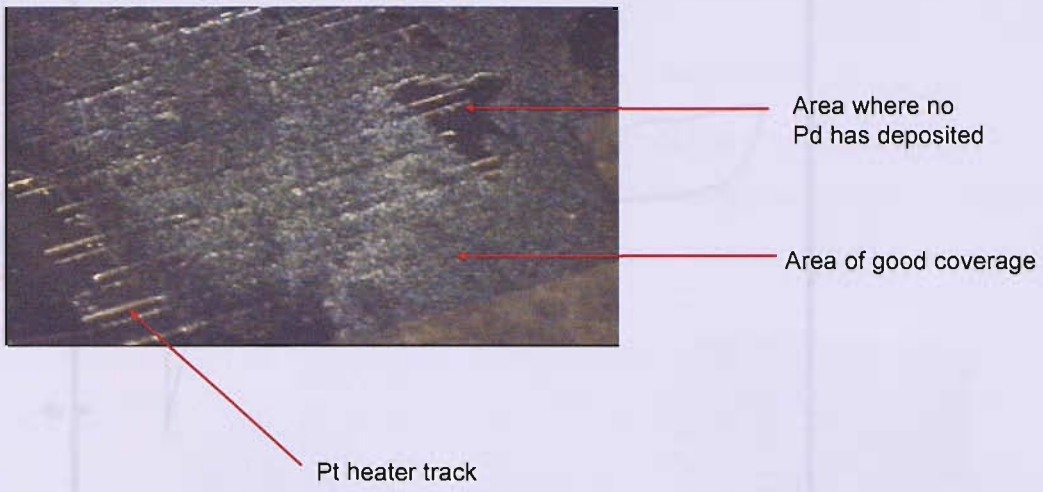

Fig 32 Photo showing H_I-e Pd electrodeposited onto the surface of the Au electrode of an SRL 136 device. The H_I-e Pd was electrodeposited by applying a potential step from 0.4 to 0.1 V vs. SCE. A deposition charge of 5 mC was passed. Following electrodeposition the surfactant was removed by soaking in isopropanol for 1 h.

Examining the H_I-e Pd film in fig 32 it can be seen that some areas of the electrode remain uncovered following electrodeposition.

Following Pd electrodeposition the surfactant was removed by suspending the device upside down in iso-propanol for one hour. The solution was stirred gently using a magnetic stirrer and bar to accelerate the removal of surfactant from the pores.

4.4 Characterisation of Pd on microhotplate device

4.4.1 Electrochemical characterisation of Pd

Once the Pd film had been electrodeposited onto the microhotplate device it was necessary to confirm that it was indeed nanostructured. Cyclic voltammetry is a non destructive technique that would confirm a high surface area. The presence of the characteristic features of a nanostructured Pd cyclic voltammogram would further suggest that the Pd was nanostructured. A cyclic voltammogram of an H_I-e Pd film on an SRL136 microhotplate is shown in figure 33.

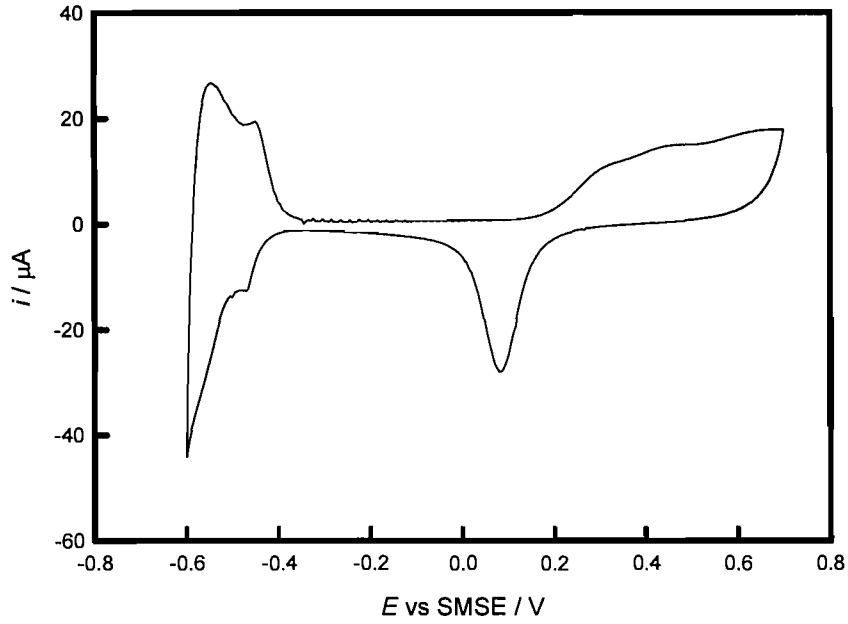

Fig 33. Cyclic voltammogram of an H_1-e Pd film electrodeposited onto a SRL136 microhotplate device as per fig 31. The cyclic voltammogram shows the 15th voltammetric cycle and was carried out at 20 mV / s in 1 M sulphuric acid, starting at 0.0 V vs. SMSE.

The cyclic voltammogram in fig 33 shows the fifteenth voltammetric cycle of an H_1-e Pd film in 1 M sulphuric acid on an SRL136 micro-hotplate device. The maximum Pd surface area was calculated from the charge under the oxide stripping peak using the Rand and Wood's[74] constant to be 18.9 $m^2 g^{-1}$. The magnitude of the surface area suggests that the Pd film is indeed mesoporous. In addition the cyclic voltammogram exhibits the characteristic features of H_1-e Pd. There are two peaks in the oxide region at approximately 0.25 and 0.45 V vs. SMSE. These are not shown in the cyclic voltammogram of non-mesoporous Pd. In addition the resolution of the two sets of peaks in the hydride region are not observed in the cyclic voltammogram of a non activated, low surface area Pd film as indicated in section 3.4.1. A comparison with the cyclic voltammograms in fig 20 of H_1-e Pd films electrodeposited on Au disc electrodes from both $C_{12}EO_8$ and Brij®56 template baths reveals similar features in the oxide potential region though the peaks at 0.25 and 0.45 V vs. SMSE are not as well resolved in fig 33. In the hydride potential region in fig 20 there are three distinct sets of peaks at -0.45, -0.52 and 0.625 V vs. SMSE. In fig 33 there are only two well resolved peaks at approximately -0.45 and -0.6 V vs. SMSE. It is possible that this is caused by an

imperfect nanostructure possibly due to the added difficulties in electrodepositing on the microhotplates.

4.4.2 Characterisation of H_1-e Pd surface by SEM

A number of H_1-e Pd films on microhotplates were examined using SEM in order to examine the surface, particularly with regard to its roughness and the coverage of the electrode surface. Figure 34 shows an SEM image taken of the Pd surface.

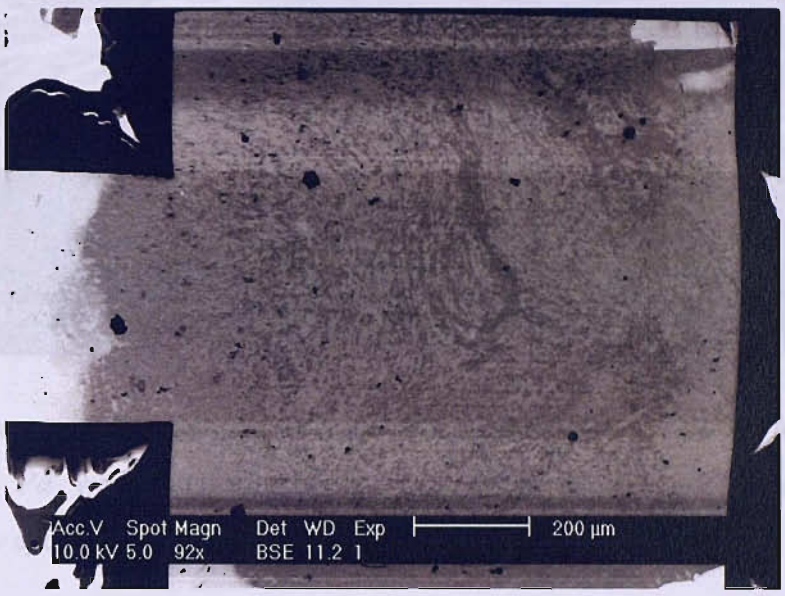

Figure 34. SEM image of the Pd surface at 92 times magnification. The H_1-e Pd was electrodeposited as per fig 31. The Pd was then voltammetrically cycled in 1 M sulphuric acid over 8 voltammetric cycles.

Figure 34 shows that Pd coverage of the square Au electrode is fairly good. The white areas indicate areas of the Au electrode that have not been covered by the Pd. It can be seen that there are small areas in the top right and bottom left and right corners. It is also noted that the Pd deposition extends a short way along the connecting bridge on the left of the electrode. The deposition of Pd onto the remaining section of the bridge is prevented by the incorporation of a passivation layer on top of the device.[107] It is not anticipated that Pd on this part of the bridge will cause any problems.

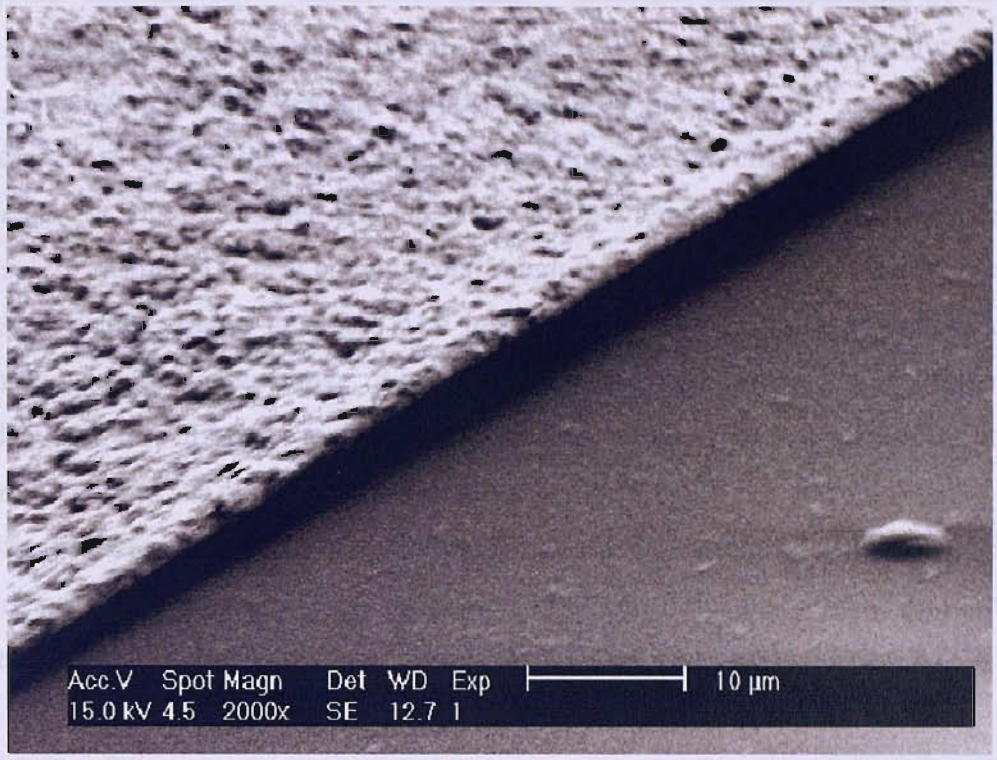

Fig 35 SEM image of the Pd surface at 2000 times magnification at a tilt angle of 65°. The H_1-e Pd was electrodeposited as per fig 31. The Pd was then voltammetrically cycled in 1 M sulphuric acid over 8 voltammetric cycles.

It can be seen that the surface is fairly smooth. The true thickness of the layer was calculated from the observed thickness using the tilt angle of 65° to be approximately 6.2 µm. It can be seen that the film is thicker at the edge of the electrode. A significantly greater edge effect was obtained by Imokawa[98] with non-mesoporous Pd films on microelectrodes. When the deposition potential was increased to 0.3 V vs. SCE the effect was not observed. It is proposed that the greater thickness at the edge may be the result of radial diffusion.

4.5 Methane response of H_1-e Pd films on microhotplates

There is the possibility that the H_1-e Pd film will not be catalytically active. If this is the case then the sign and magnitude of the response need to be anticipated so as to prevent the possibility of misinterpreting the result.

Heat loss from the device will occur via conduction, convection and radiation. The microhotplates used here have membranes made from silicon nitride which has very

low thermal conductivity.[110] Krebs and Grisel[100] measured the temperature of the silicon substrate using a thermocouple to be 31 °C at an operating temperature of 400 °C, illustrating the excellent thermal isolation of the membrane.

Baroncini *et al.* carried out an investigation into the thermal characterisation of a microheater for micromachined gas sensors.[111] At low temperatures the heat losses can be solely attributed to heat conduction through the membrane, the heater and the air.[111] As the temperature increases heat losses due to convection increase as the surrounding gas begins to move. As a result convection becomes the dominant method of heat loss at higher temperatures, though heat losses due to radiation also begin to increase as the temperature increases.

It is assumed that natural convection will be the dominant heat loss mechanism. It is therefore necessary to consider the relative thermal capacities of methane and air. The thermal capacity c_p, of air and methane can be calculated using equation 14.[141]

$$\mathbf{c_p = a + bT + cT^{-2}} \qquad \mathbf{(14)}$$

Where, T is the temperature in Kelvin and a, b and c are constants.

For air a = 28.1, b = 1.97 x 10^{-3} K^{-1}, c = 4.8 x 10^{6} K^{2} and for methane, a = 23.64, b = 47.86 x 10^{-3} K^{-1}, c = -1.92 x 10^{5} K^{2}

So at 500 °C or 773 K the thermal capacity of air and methane were calculated to be 37.65 J K^{-1} mol^{-1} and 60.33 J K^{-1} mol^{-1} respectively.

Consequently, for a catalytically inactive Pd film, methane will absorb more thermal energy than air as it has a higher thermal capacity. As the temperature of the device decreases so will its resistance. The potential across the Wheatstone bridge will therefore decrease. This will be referred to as a thermal response.

The catalytic oxidation of methane is an exothermic reaction:[112]

$$\mathbf{CH_4 + 2\ O_2 \rightarrow CO_2 + 2\ H_2O + heat}\ ,\ \mathbf{\Delta H_{298}} = -802.7\ \text{kJ mol}^{-1}$$

When Pd catalyses the oxidation of methane the temperature of the Pd increases, resulting in an increase of the resistance of the device. This will cause an increase in

the potential across the Wheatstone bridge arrangement. Such a response will be referred to as a catalytic response.

4.5.1 Methane response of a bare micro-hotplate device

A control experiment was carried out to determine the response of a catalytically inactive micro-hotplate. This was achieved by heating a micro-hotplate in air then recording the response to methane. The methane response is shown in fig 36. This magnitude and sign of this response can later be used as a reference to compare with the methane responses of Pd catalysts.

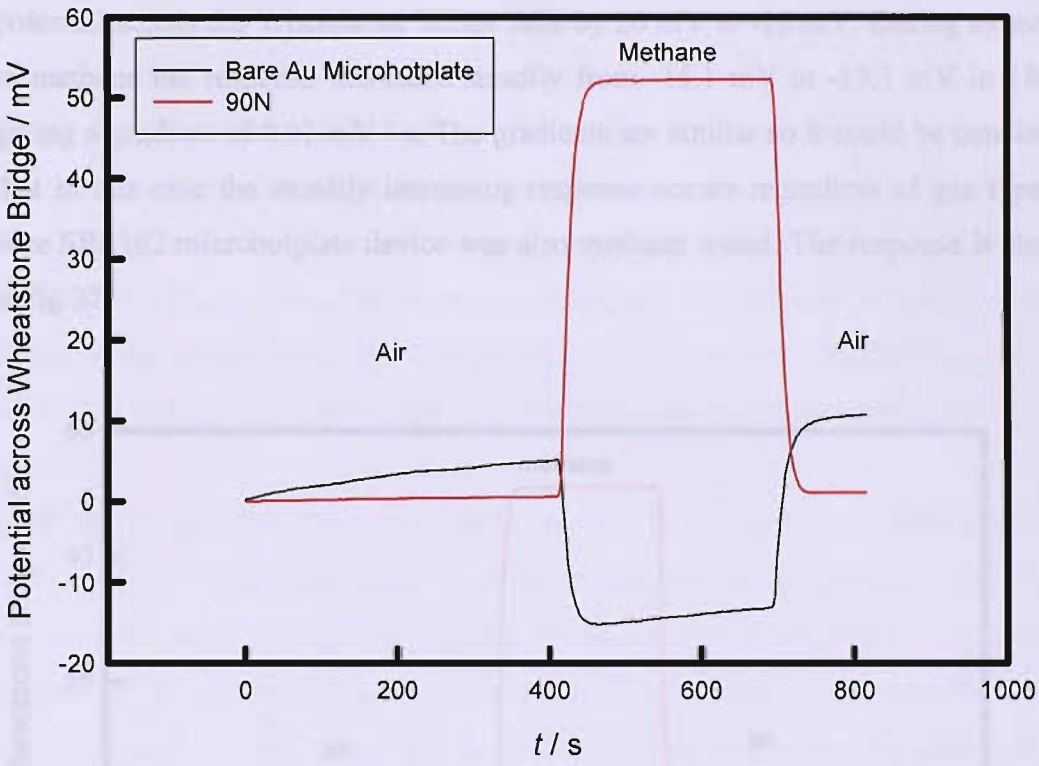

Fig 36 Response of a bare SRL136 microhotplate device to methane. The device was powered by 15.0 V from the power supply and a flow rate of 400 cm^3 min^{-1} was used. The device was powered in air for 1 h prior to this result being obtained.

Fig 36 shows the response of a bare gold electrode on an SRL136 device to methane at approximately 500 °C. The response of a 90N commercial pellistor is also shown for reference. The 90N is a commercial pellistor manufactured by City Technology. It consists of a platinum wire coil embedded in a 1 mm diameter bead of catalytic material. A diagram and description of the device are shown in fig 1. A 90N will always be used as a reference in methane testing to ensure the polarity of the

response is correctly interpreted. The magnitude of the 90N methane response is also stable and so may be used to explain any unexpected results. It can be seen that the baseline in air of the microhotplate is not stable and increases gradually during exposure to both air and methane. This must be attributable to the device as no catalyst layer has been applied. In this case the baseline steadily increases with time. The SRL136 devices are manufactured by City Technology. Some baseline drift is anticipated due to annealing of the various components.[3] In this case the baseline increases from 0.2 to 5.1 mV in 400 s, giving a gradient of 0.0125 mV / s. After approximately 400 s the supply was switched to methane, 2.5 % in air, again using a flow rate of 400 cm^3 min^{-1}. It can be seen that when exposed to methane, the potential across the Wheatstone bridge falls by 20 mV to -15 mV. During exposure to methane the response increased steadily from -15.1 mV to -13.1 mV in 180 s, giving a gradient of 0.01 mV / s. The gradients are similar so it could be concluded that in this case the steadily increasing response occurs regardless of gas type. A bare SRL162 microhotplate device was also methane tested. The response is shown in fig 37.

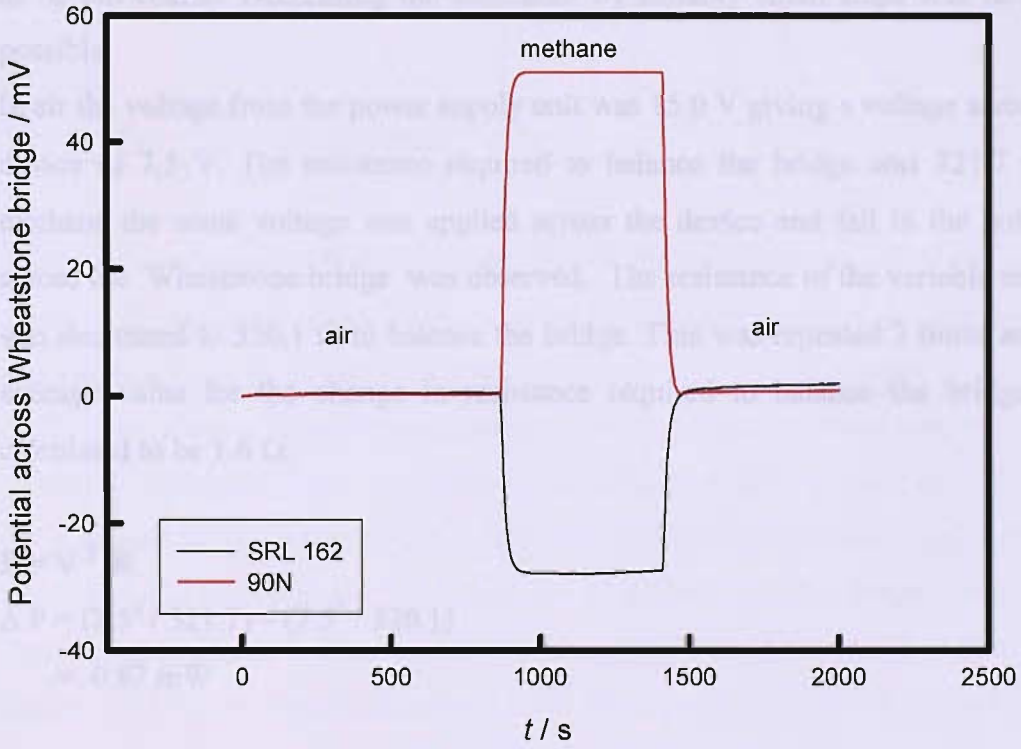

Fig 37 Response of a bare SRL162 microhotplate device to methane. The device was powered to 14.0 V from the power supply and a flow rate of 400 cm^3min^{-1} was used.

The SRL162 device has a smaller electrode area than the SRL136 device. It requires less power to reach the desired operating temperature of 500 °C. A potential of 14 V was used compared to 15 V for the SRL136 in fig 36. It can be seen that the baseline is stable and is comparable to that of the 90N. The magnitude of the negative methane response is -28 mV, 8 mV more than the SRL136 in fig 36. This suggests that the SRL162 is at a slightly higher temperature. Following exposure to methane the air baseline returns to almost the same potential it was at prior to exposure to methane.

The magnitudes of purely thermal methane responses have been established as -20 mV for an SRL136 and -28 mV for an SRL162. These figures can be used later when analysing any negative responses of Pd catalysts.

It was decided to convert the voltage changes of a device when exposed to methane to heat fluxes by carrying out experiments to determine the amount of energy removed by methane. This was done by determining the power needed to return the Wheatstone bridge potential to the air baseline. Initially the intention was to increase the voltage supplied by the power supply. However, the adjustment proved to be too coarse. Decreasing the resistance by suitably small steps was however possible.

In air the voltage from the power supply unit was 15.0 V giving a voltage across the device of 7.5 V. The resistance required to balance the bridge was 321.7 Ω. In methane the same voltage was applied across the device and fall in the potential across the Wheatstone bridge was observed. The resistance of the variable resistor was decreased to 320.1 Ω to balance the bridge. This was repeated 3 times and the average value for the change in resistance required to balance the bridge was calculated to be 1.6 Ω.

$$\mathbf{P = V^2/R}$$

$$\Delta P = (7.5^2 / 321.7) - (7.5^2 / 320.1)$$

$$= 0.87 \text{ mW}$$

These calculations have given a value for the heat removed from the microhotplate by methane of approximately 1 mW. This compares to a value of approximately 175 mW required to heat the device to 500 °C in air.

4.5.2 Methane response of H_1-e Pd

Having established the magnitude of a purely thermal methane response it was now possible to methane test Pd films. A H_1-e Pd film was electrodeposited onto an SRL136 device and prepared using the standard preparation method of removing the surfactant using iso-propanol for 1 h and then voltammetric cycling in 1 M sulphuric acid until the maximum surface area was obtained, typically after five to ten voltammetric cycles. The device was placed in the cell holder along with a commercial 90N device supplied by City Technology to be used as a reference. The methane responses after 10 min in air and then 30 minutes in air are shown in fig 38A and 38B respectively.

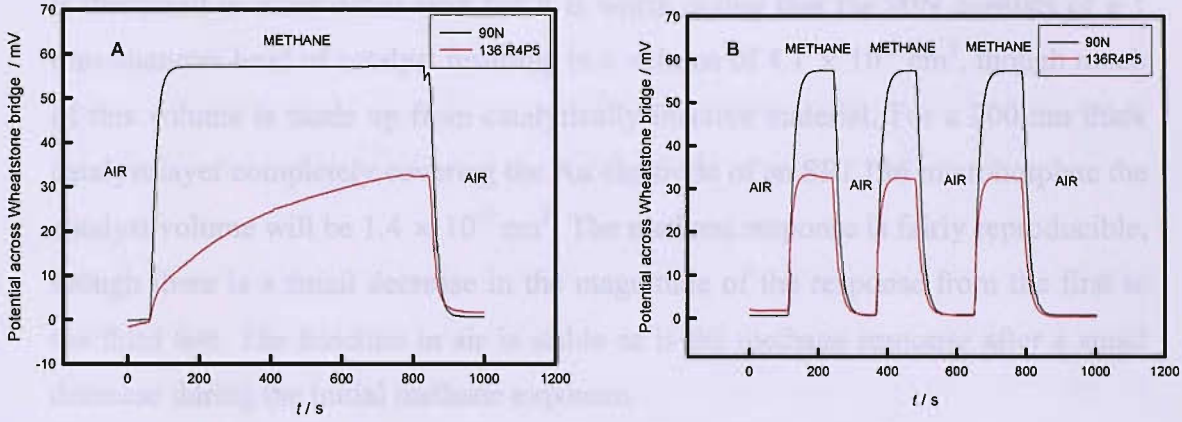

Figure 38 Responses of H_1-e Pd on an SRL136 microhotplate to 2.5 % methane in air after 10 min in air in fig 38 A and after 30 min total in fig 38 B. The H_1-e Pd was electrodeposited by potential step from 0.4 to 0.1 V vs. SCE from the standard Brij®56 ammonium tetrachloropalladate template mixture at room temperature. A deposition charge of 5 mC was passed. The surfactant was removed by soaking in iso-propanol for 1 h. The H_1-e Pd film was then voltammetrically cycled in 1 M sulphuric acid over 8 cycles at a scan rate of 100 mV / s. The temperature of the device was gradually raised by slowly increasing the power to 7.5 V across the device, 15.0 V from the power supply. A gas flow rate of 400 cm^3 min^{-1} was used for both methane and air. A 3 position tap was used to manually select the gas type.

Fig 38A shows the methane response of a H_1-e Pd catalyst after 10 min in air. It can be seen that the methane response increases gradually stabilising at a maximum of

30 mV after 800 s. This indicates that when the catalyst was first exposed to methane it had relatively weak methane sensitivity. It can be seen that the catalytic activity gradually increases as the catalyst is exposed to methane. When the response reaches a plateau this indicates that the catalyst has achieved its maximum catalytic activity. Following this test the supply was switched back to air. After 30 min in air the device was retested. It can be seen in fig 38B that the response is positive and increases rapidly to the maximum value of 30 mV. There has therefore been no increase in the magnitude of the response as a result of the extra time powered up, though the initial response to methane is much more rapid and similar to that of the 90N in that respect. The reasons for the low initial catalytic activity are discussed in the following section. The magnitude of the methane response is relatively small when compared to the 60 mV response of the 90N. However, the relative maximum responses will depend on the geometry of the two catalysts. This is discussed in more detail later but it is worth noting that the 90N consists of a 1 mm diameter bead of catalyst resulting in a volume of 4.1×10^{-3} cm^3, though much of this volume is made up from catalytically inactive material. For a 200 nm thick catalyst layer completely covering the Au electrode of an SRL136 microhotplate the catalyst volume will be 1.4×10^{-7} cm^3 The methane response is fairly reproducible, though there is a small decrease in the magnitude of the response from the first to the third test. The baseline in air is stable as is the methane response after a small decrease during the initial methane exposure.

4.5.3 Initial methane response of H_1-e Pd films

In the previous section a positive methane response was recorded. It was noted that the initial response to methane increased gradually. Some H_1-e Pd catalysts gave a negative response when first exposed to methane, before the response increased gradually. An example is shown in fig 39.

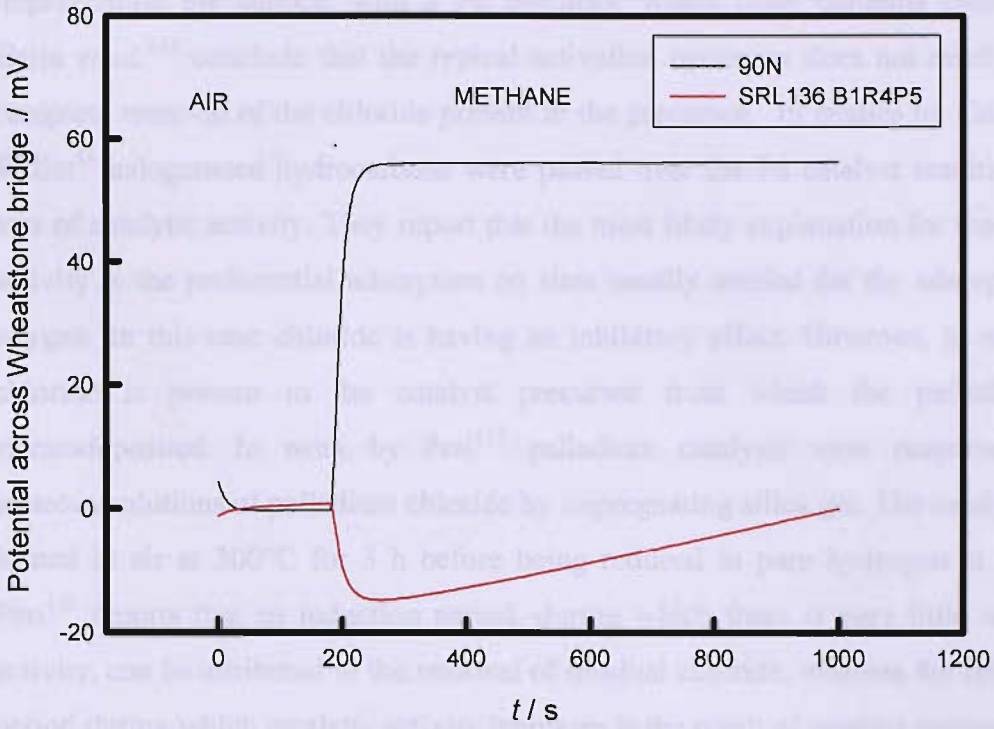

Figure 39 Response of H_1-e Pd on an SRL136 microhotplate to 2.5 % methane in air after 10 min in air. The H_1-e Pd film was prepared as per fig 38.

The 90N commercial pellistors manufactured by City Technology are subject to a significant activation period. Typically this consists of 10 hours powered in air then 10 hours in methane. The methane response shown in fig 38b was recorded after 30 min powered in air. Following this test the device was powered in air for a further 4.5 h. After a total of 5 h the device was retested. There was no increase in the magnitude of the methane response. However, the short period of time prior to methane testing may be responsible for the low initial activity.

A time dependent activation period of Pd catalysts for methane oxidation has been reported by a number of authors. An induction period was described by Peri[113] as a period of time where the catalyst is exposed to reaction conditions during which no catalytic activity is observed. Activation is defined as a period of time when the catalyst's activity increases steadily with time. These definitions will be used in future discussions.

Hicks *et al.*[28,36] proposed that chloride remained in the Pd particles from the $PdCl_2$ precursor and this was responsible for the low initial methane activity.[36] The effect of chloride on Pd catalysts for the oxidation of methane has been extensively

investigated. Typically Pd catalysts are formed on a support. They are prepared by impregnating the support with a Pd precursor which often contains chloride.[114] Gelin *et al.*[114] conclude that the typical activation treatment does not result in the complete removal of the chloride present in the precursor. In studies by Cullis and Willat[53] halogenated hydrocarbons were passed over the Pd catalyst resulting in a loss of catalytic activity. They report that the most likely explanation for the loss of activity is the preferential adsorption on sites usually needed for the adsorption of oxygen. In this case chloride is having an inhibitory effect. However, in our case chloride is present in the catalyst precursor from which the palladium is electrodeposited. In work by Peri[113] palladium catalysts were prepared from aqueous solutions of palladium chloride by impregnating silica gel. The catalyst was heated in air at 300°C for 3 h before being reduced in pure hydrogen at 275°C. Peri[113] reports that an induction period, during which there is very little catalytic activity, can be attributed to the removal of residual chloride, whereas the activation period during which catalytic activity increases is the result of catalyst restructuring, catalyst redispersion under reaction conditions and a change in the catalyst oxidation state under reaction conditions. The report concluded that the presence of chloride was not responsible for the low catalytic activity during the activation period. Baldwin and Burch[27,115] also proposed that restructuring of the PdO may be responsible for the observed activation period. In section 1.3.3 the optimal active state of Pd catalysts was discussed and it was concluded that both Pd and PdO were required. During the restructuring process described by Baldwin and Burch the optimal active state of the Pd film was being achieved. A study by Burch and Hayes[19] investigated the methane combustion of a 4 % Pd / Al_2O_3 catalyst with time on stream. The report concluded that the observed increase in activity with time on stream was due to the progressive oxidation of metallic Pd. The results indicated that a steady state of activity was attained after 10 min, which corresponded to the equivalent of having taken up 4 monolayers of oxygen.

Of considerable significance to these investigations were the findings by Roth *et al.*[116] In their investigation two types of catalyst were prepared, termed Pd-Cl and Pd-NO_3 by impregnation of the support with H_2PdCl_4 and $Pd(NO_3)_2$ respectively. The catalysts were tested at increasing temperatures from 150°C to 600°C for 3 h at each temperature. They report that the catalytic activity of Pd-NO_3 was higher for

each temperature than the chlorine containing catalyst. They also found that the activity of the Pd-Cl catalyst increased over the 3 h at each temperature whereas the activity of the Pd-NO_3 catalyst decreased over the 3 h. The superior catalytic performance is attributed to an inhibitory effect caused by residual chlorine. Furthermore, they report that at least 10 h at 600°C are required to remove all chloride from the catalyst.

A study by Tonetto *et al.* [117] also investigated the effect of chlorine on the activity of Pd catalysts and found that the catalyst prepared without chlorine had the greatest activity which is consistent with the work of Roth *et al.*[116] They also found that in a sample prepared with chlorine the activity increases during the reaction. This is also consistent with the results of Roth *et al.* [116] but not entirely consistent with the conclusions of Peri.[113]

In conclusion the literature suggests that palladium catalysts initially exhibit low activity to methane due to two main factors. Firstly, chlorine present in the Pd precursor inhibits initial activity relative to a Pd catalyst prepared from a chlorine free Pd precursor. Activity of the Cl containing Pd catalyst does increase to a similar level of the Cl free catalyst after a lengthy activation period. Secondly, there is also evidence that catalytic activity is low whilst catalyst restructuring occurs.

The plot in fig 39 shows the initial methane response of a H_1-e Pd film electrodeposited from the standard Brij®56 ammonium tetrachloropalladate template bath containing chloride ions. The initial negative response was followed by a gradual increase in the response as the potential across the Wheatstone bridge became less negative. The device was powered in methane for a further 1 h. After this time the device was retested. The methane response is shown in fig 40.

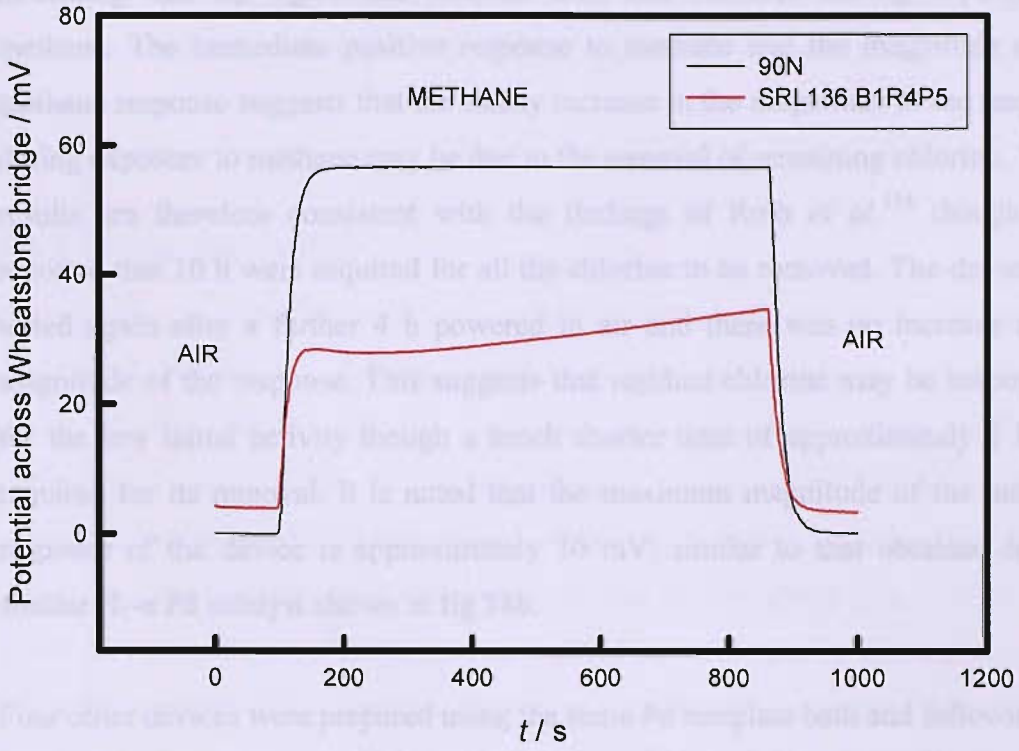

Fig 40. Response of H_1-e Pd on an SRL136 microhotplate to 2.5 % methane in air after 1 h in air. The device was methane tested after 10 min in air. The response is shown in fig 39. The H_1-e Pd film was prepared as per fig 38.

Fig 40 shows the methane response of device SRL136B1R4P5 to methane following 1 h in air. It can be seen that the response of the device is now immediately positive when exposed to methane. It is noted that the baseline in air has increased from 0 to 5 mV as a result of the baseline drift. It is possible that the microhotplate device rather than the H_1-e Pd catalyst is responsible for this as illustrated by the response of a bare gold device in fig 36. Baseline drift could be caused by a number of factors. As indicated earlier annealing of the components in the device can cause baseline drift. In this case this seems unlikely as there is little drift in air in this case. It is possible that the drift is the result of disturbances in the gas flow rate although a flow meter was used to monitor the flow rate and also the 90N baseline is stable. After rising rapidly when first exposed to methane, the response flattens before increasing steadily. When the gas supply was switched back

to air the response dropped rapidly to a similar level before methane testing, indicating that no significant baseline drift has occurred during exposure to methane. The immediate positive response to methane and the magnitude of the methane response suggests that the steady increase in the magnitude of the response during exposure to methane may be due to the removal of remaining chlorine. These results are therefore consistent with the findings of Roth *et al,*[116] though they reported that 10 h were required for all the chlorine to be removed. The device was tested again after a further 4 h powered in air and there was no increase in the magnitude of the response. This suggests that residual chlorine may be responsible for the low initial activity though a much shorter time of approximately 1 h was required for its removal. It is noted that the maximum magnitude of the methane response of the device is approximately 30 mV, similar to that obtained from a similar H_1-e Pd catalyst shown in fig 38b.

Four other devices were prepared using the same Pd template bath and following the same procedure. They all exhibited similar behaviour; an initial negative methane response followed by a gradual increase in the response during exposure to methane for 1 h. This result is consistent with those obtained by Peri and Lund[113] who reported that during the induction period there was no catalytic activity whilst chlorine was removed. The gradual increase in methane response then observed is consistent with the results of Roth *et al.*[116] and Tonetto *et al.*[117] However, the rate at which activity increases is fairly rapid. Roth *et al.* reported that 10 h was required for all chlorine to be removed. The maximum catalytic activity of the H_1-e Pd catalysts was typically reached after 10 minutes in methane. It is possible that exposure to methane is key in the activation rather than the total time powered up.
In order to further investigate the relationship between initial methane activity and residual chlorine catalysts were prepared from a chlorine free Pd precursor.

4.6 Mesoporous Pd catalyst from chlorine free Pd precursor

In section 4.5.2 it was reported that the H_1-e Pd catalysts gave a catalytic response to methane gas. It was noted that the initial response to methane was often negative before gradually increasing to give a positive, catalytic methane response. Reports in the literature suggest that chlorine in the Pd precursor may inhibit the catalytic

activity. To investigate if this is occurring H_1-e Pd films were electrodeposited from chlorine free precursors. Initially the H_1-e Pd films were electrodeposited onto 1 mm diameter Au disc electrodes in order to characterise the film and confirm its nanostructure.

4.6.1 Phase behaviour

Phase diagrams of Brij®56 with ammonium tetrachloropalladate have already been determined. However, in this case the Pd salt is being changed to palladium (II) nitrate hydrate. As this is the first time mesoporous Pd films have been electrodeposited using this Pd salt the effect of this particular salt on the phase boundaries is unknown. The first step was therefore to construct a phase diagram so that the template mixture composition required for the hexagonal phase was known. It was decided to use Brij®56 rather than $C_{12}EO_8$ due to the higher cost of the latter. The structure type of the electrodeposited metal is determined by the phase of the liquid crystalline template. This is governed by the concentration of the non-ionic surfactant and the temperature. A diagram showing the phases of palladium nitrate (II) hydrate in Brij®56, water and heptane is shown in fig 41. It can be seen that the hexagonal phase is formed over surfactant concentrations of between 35 and approximately 83 wt. % in water at 20 °C. The hexagonal phase is stable up to approximately 54 °C with a surfactant concentration of 60 wt. %. The cubic phase denoted V_1 does not exist at room temperature. It is formed over the right hand shoulder of the hexagonal phase.

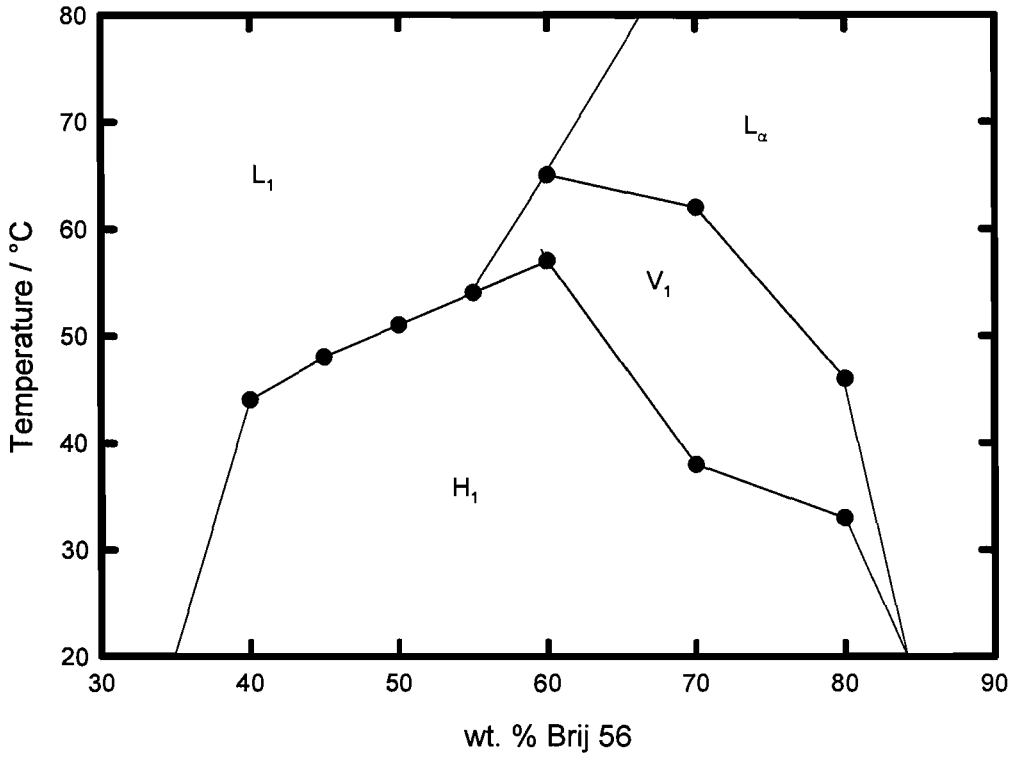

Fig 41. Pseudo binary phase diagram of an aqueous solution of 1.4 mol l^{-1} palladium (II) nitrate hydrate in Brij®56 and heptane. Note that the lines are added as a visual aid. The weight to weight ratio between palladium (II) nitrate hydrate and water was kept constant at 0.4. The same ratio of Brij®56 to heptane was kept constant at 22. The weight % of Brij®56 was increased from 35 to 80 %. L_1 refers to the micellar solution, H_1 to the hexagonal phase, V_1 the cubic phase and L_α the lamellar phase.

The micellar solution, L_1, is formed at room temperature over surfactant concentrations of 30 to 35 wt. %. Above 50 °C the micellar solution exists over a range of surfactant concentrations of between 20 and 55 wt. %. The Lamellar phase, L_α is formed at high surfactant concentrations, above approximately 84 wt. % at room temperature. It is also formed over a wider composition range of approximately 60 to 90 wt % surfactant above 60 °C.

A comparison of fig 41 with the phase diagram of the ammonium tetrachloropalladate Brij®56 system revealed that the two systems are very similar. The phase diagrams were overlayed and are shown in fig 42.

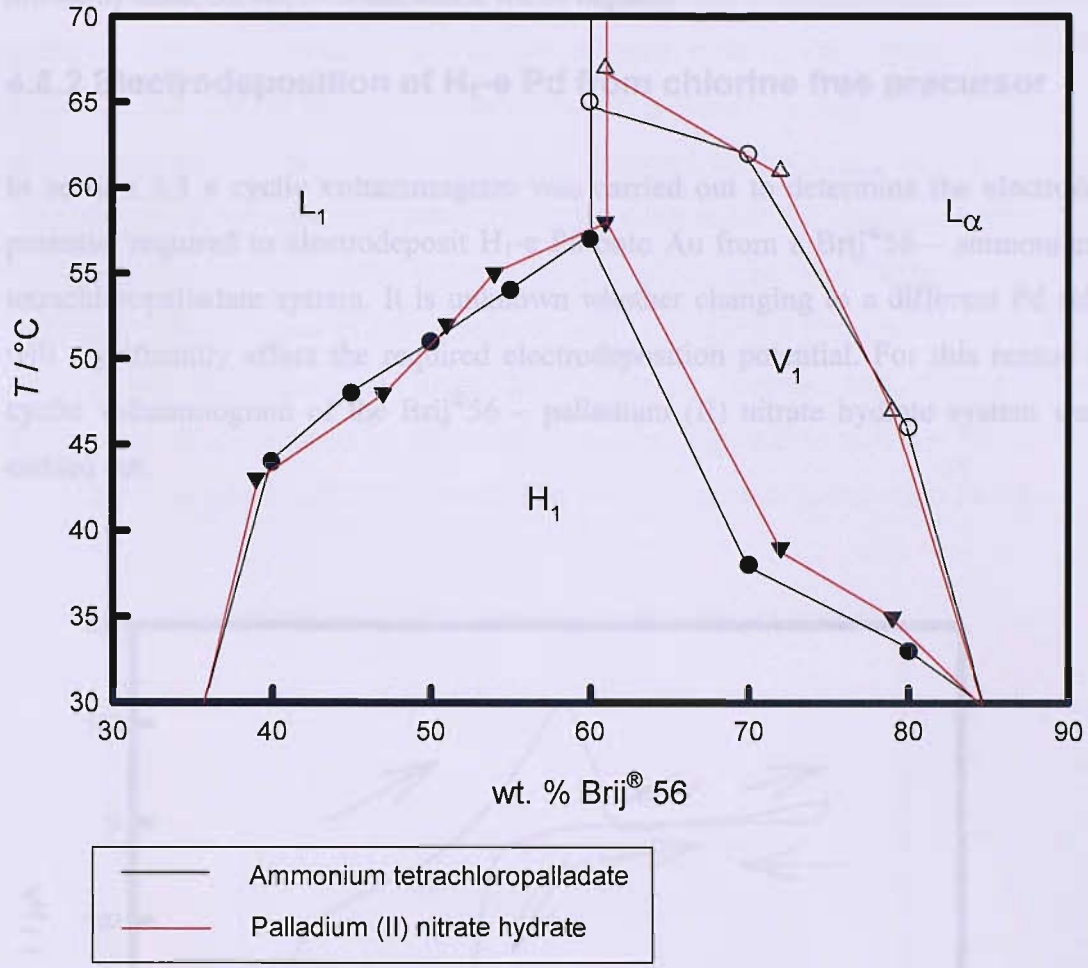

Fig 42. Pseudo binary phase diagrams of aqueous solution of 1.4 mol l^{-1} palladium (II) nitrate hydrate and ammonium tetrachloropalladate in Brij®56 and heptane. Note that the lines are added as a visual aid. The weight to weight ratio between electrolyte and water was kept constant at 0.4. The ratio of $C_{12}EO_8$ to heptane was kept constant at 22. The weight % of Brij®56 was increased from 35 to 80 %. L_1 refers to the micellar solution, H_1 to the hexagonal phase, V_1 the cubic phase and L_α the lamellar phase.

It can be seen in fig 42 that the two phase diagrams have very similar phase boundaries. The main change is a shift of the hexagonal / cubic phase boundary. Initially the aim is to electrodeposit H_1-e Pd from the Brij®56 – palladium nitrate (II) hydrate system. It can be seen from figs 41 and 42 that at room temperature there is a very wide composition range that will give the hexagonal phase. In order to make a good comparison, the same composition used for the standard H_1-e Brij®56 ammonium tetrachloropalladate bath was used. The composition used for

the electrodeposition of H_1-e Pd was 47 wt. % Brij®56, 12 wt. % palladium (II) nitrate hydrate, 39 wt. % water and 2 wt. % heptane.

4.6.2 Electrodeposition of H_1-e Pd from chlorine free precursor

In section 3.3 a cyclic voltammogram was carried out to determine the electrode potential required to electrodeposit H_1-e Pd onto Au from a Brij®56 – ammonium tetrachloropalladate system. It is unknown whether changing to a different Pd salt will significantly affect the required electrodeposition potential. For this reason a cyclic voltammogram of the Brij®56 – palladium (II) nitrate hydrate system was carried out.

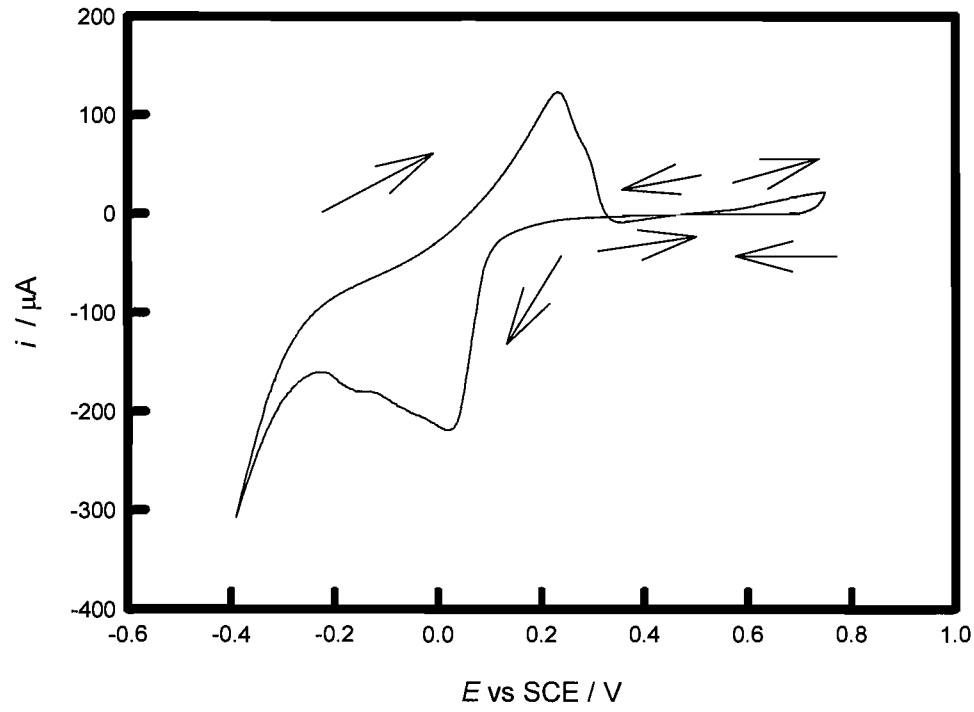

Fig 43. Cyclic voltammogram of Brij®56 – palladium (II) nitrate hydrate mixture on an Au 1 mm diameter electrode. The template mixture comprised 47 wt % Brij®56, 2 wt % heptane 12 wt % palladium (II) nitrate hydrate and 39 wt % water. A scan rate of 100 mV / s was used. The scan was started at 0.4 V vs. SCE and was carried out at room temperature (25 °C).

It can be seen that the cyclic voltammogram in fig 43 is similar to that of the Brij®56 – ammonium tetrachloropalladate system shown in fig 16. The reduction of the Pd salt commences around 0.2 V vs. SCE and the reduction current increases as

the potential was further decreased. There is a linear region between approximately 0.15 and 0.05 V vs. SCE on the cathodic scan. It was noted that the open circuit potential for the palladium (II) nitrate hydrate system was typically 0.55 V compared to 0.4 V for the ammonium tetrachloropalladate system.

A 1 mm diameter Au disc electrode was prepared by polishing with 1 μm and subsequently 0.3 μm alumina powders on polishing pads. The electrodes were then thoroughly washed in purified water to remove all alumina. The electrode was then voltammetrically cycled in 1 M sulphuric acid to confirm a clean surface. An H_1-e Pd film was electrodeposited from the Cl free Pd template bath onto a 1 mm diameter Au disc electrode by applying a potential step of 0.55 to 0.1 V vs. SCE. A deposition charge of 5 mC was passed. The current transient is shown in fig 44.

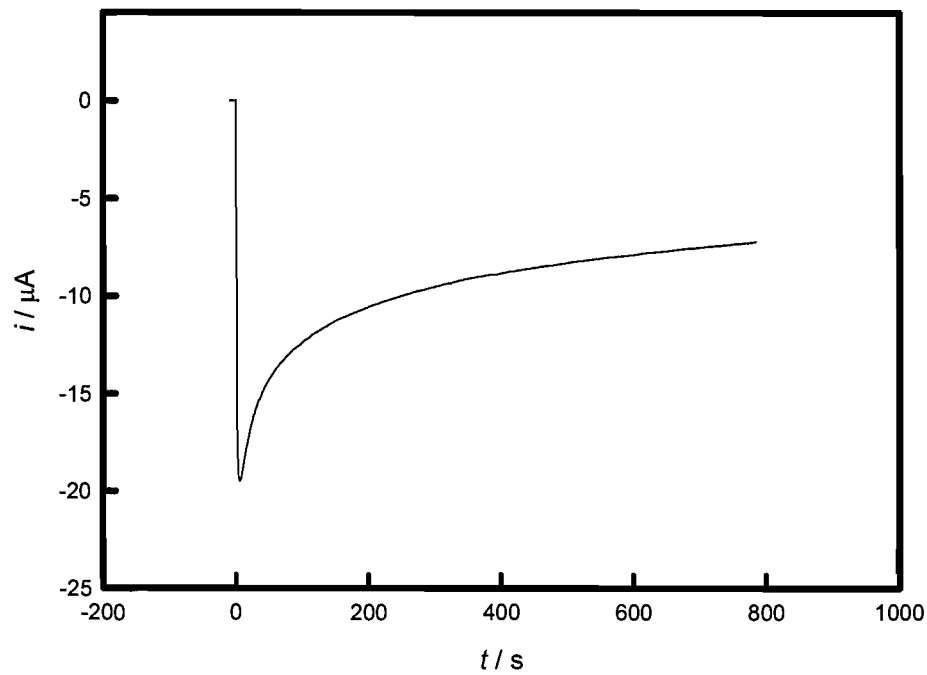

Fig 44. Graph showing the electrodeposition of H_1-e Pd from chlorine free template bath onto a 1 mm diameter Au disc electrode by potential step from 0.5 to 0.1 V vs. SCE. A deposition charge of 5 mC was passed. The composition of the template mixture is described in fig 43.

The current transient in fig 44 shows the electrodeposition of H_1-e Pd onto a 1 mm diameter Au disc electrode. The current transient shows an immediate increase in current to approximately -30 μA when the potential is stepped from 0.55 to 0.1 V vs. SCE. The magnitude of the current then decreases quickly. After approximately 300 s the current decreases at a near constant rate. The cyclic voltammogram in fig

43 indicates that if a more negative electrode potential was used a larger reduction current would be obtained. This suggests that the electrodeposition at 0.1 V vs. SCE is kinetically controlled. Even so the rapid decrease in the magnitude of the current is probably due to the depletion of Pd ions close to the electrode surface. The shape of the transient is very similar to that obtained using the standard template mixture shown in fig 17 in section 3.3, however, the magnitude of the current peak is slightly larger for the deposition from the ammonium tetrachloropalladate salt at -23 μA compared with -20 μA for the palladium (II) nitrate hydrate salt in fig 44. Examining the cyclic voltammograms in figs 15 and 43 it is noted that the current at the deposition potential of 0.1 V vs. SCE used for the electrodeposition of Pd from both precursors were very similar at -41.2 μA for palladium (II) nitrate hydrate and -42.4 μA for ammonium tetrachloropalladate. It is therefore likely that the difference in the magnitudes of the currents is due to differences in surface coverage.

4.6.3 Characterisation of H_1-e Pd from chlorine free precursor

Having electrodeposited Pd from the H_1 phase it was necessary to confirm the film has the expected structure.

4.6.3.1 Electrochemical characterisation

Following electrodeposition the surfactant was removed from the pores by soaking the film in iso-propanol for 1 h. A cyclic voltammogram was then obtained in 1 M sulphuric acid. The electrolyte was deoxygenated by bubbling argon through the solution for fifteen minutes prior to carrying out the cyclic voltammogram which is shown in fig 45.

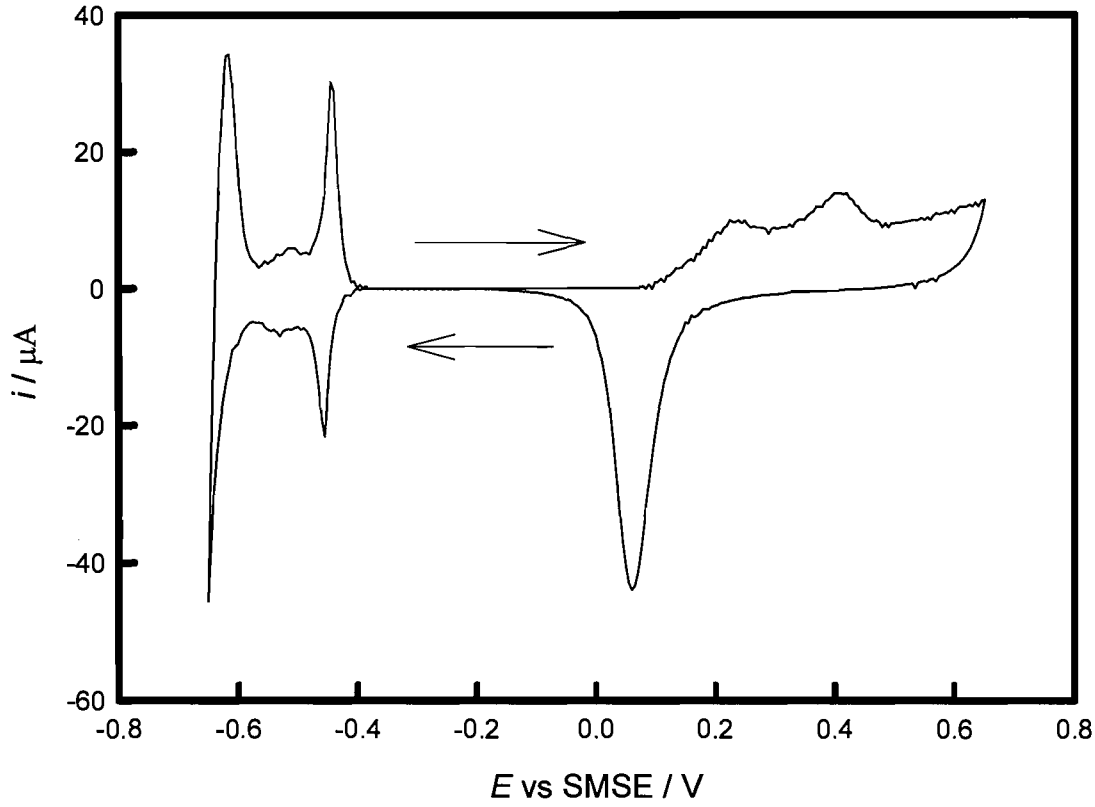

Fig 45. Cyclic voltammogram of H_1-e Pd in 1 M sulphuric acid on a 1 mm Au disc electrode. For electrodeposition details please refer to fig 44. The cyclic voltammogram was carried out at 10 mV/s from -0.6 to 0.65 V vs. SMSE, starting at -0.2 V vs. SMSE at room temperature. The tenth voltammetric cycle is shown.

Fig 45 shows the cyclic voltammogram of H_1-e Pd electrodeposited from a chlorine free template bath consisting of 47 wt % Brij®56, 12 wt. % palladium (II) nitrate hydrate, 39 wt. % water and 2 wt. % heptane. The cyclic voltammogram is similar to that in fig 20, section 3.4.1, of an H_1-e Pd film electrodeposited onto a 1 mm diameter Au disc electrode from the Brij®56 ammonium tetrachloropalladate template mixture. The peaks in the hydride region, between -0.4 and -0.65 V vs. SMSE are well resolved, indicative of the presence of a nanostructure. In addition there are two peaks corresponding to the formation of Pd oxide on the forward (anodic) scan 0.25 and 0.45 V vs. SMSE, a characteristic not observed in the acid cyclic voltammogram of low surface area Pd films. The surface area was calculated from the charge under the oxide stripping peak using the Rand and Woods constant[109] to be 34 m^2g^{-1}. The high surface area is further evidence that the Pd film is nanostructured.

4.6.3.2 Characterisation by TEM

The cyclic voltammogram in fig 46 indicated that the Pd film had the high surface area and characteristic features of a nanostructured Pd film. TEM was carried out to provide further evidence of the films nanostructure. TEM images are shown in fig 46 and 47.

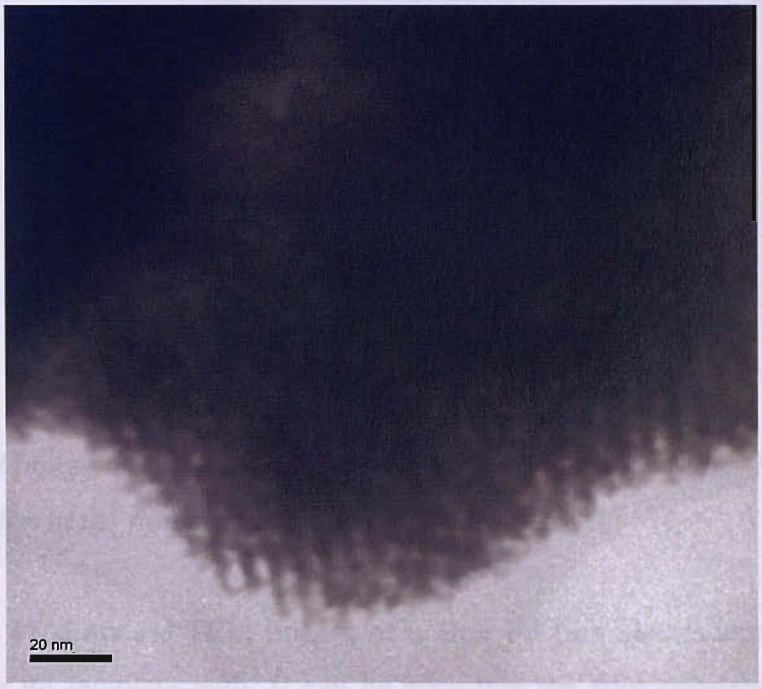

Fig 46. TEM image of a sample scraped from a mesoporous Pd film. The Pd was electrodeposited onto a 1 mm diameter Au disc electrode by potential step from 0.4 to 0.1 V vs. SCE. A deposition charge of 0.55 C / cm^2 was passed. The surfactant was subsequently removed by soaking in iso-propanol for 1 h. The Pd was then allowed to dry. A scalpel was used to scrape the Pd from the Au electrode into a small plastic container. A small droplet of water was added and the drop then added to a TEM grid. The grid was placed in a drying oven to allow the water to evaporate.

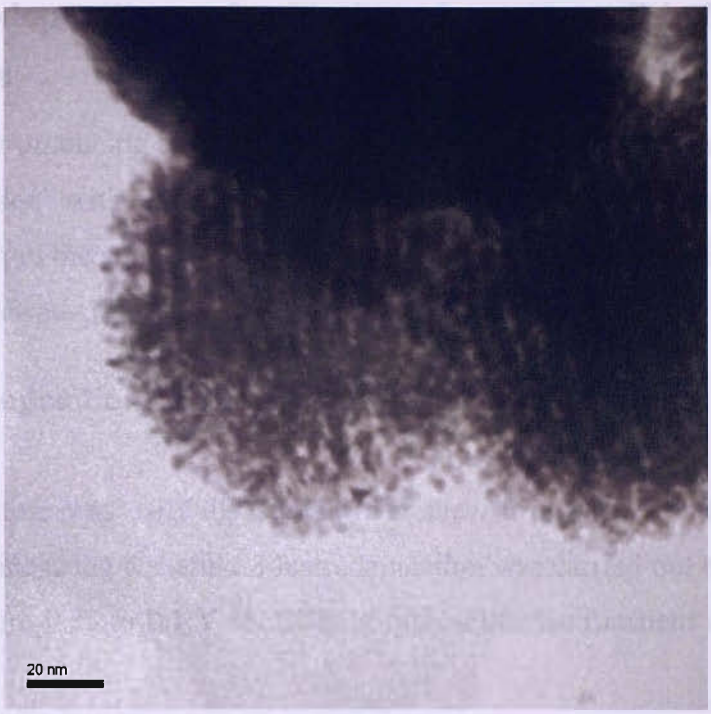

Fig 47. TEM image of a sample scraped from a mesoporous Pd film. For details of the preparation of the film please refer to fig 46.

Figs 46 and 47 show the TEM images of a H_I-e Pd film electrodeposited from a chlorine free Pd template bath. It can be seen that the film consists of regularly arranged pores. The diameter of the pores was calculated to be approximately 2.7 nm using scan image software. An error margin of +/- 0.3 nm is proposed as the edges of the pores are not well defined making accurate measurement difficult. Within the limits of experimental error this is consistent with the value of 2.5 nm obtained by J. Marwan[69] for H_I-e Pd films electrodeposited from ammonium tetrachloropalladate Brij®56 template bath. The centre to centre distance was calculated to be approximately 6.3 nm. In this case the error is not as significant as the distance can be calculated from the repeat distance of a number of pores, thus reducing the error.

In this section the electrodeposition of H_I-e Pd from palladium (II) nitrate hydrate has been reported for the first time. The results indicate that a high surface area Pd film with a regular array of pores was obtained. It can therefore be concluded that H_I-e Pd films can be electrodeposited from the palladium (II) nitrate hydrate bath equally as well as from the ammonium tetrachloropalladate bath more commonly used.

4.6.4 Electro-deposition of chlorine free H_1-e Pd films on microhotplates

The motivation for producing an H_1-e Pd film from a chlorine free precursor was to make a comparison with the initial methane response of a H_1-e Pd film electrodeposited from the ammonium tetrachloropalladate -Brij®56 template bath. In this section the electrodeposition onto microhotplates is reported.

4.6.4.1 Electrodeposition of H_1 Pd from Cl free template bath

The template mixture was carefully spread over the Au electrode of an SRL136 microhotplate device using a spatula. Electrodeposition was carried out by applying a potential step from 0.55 to 0.1 V vs. SCE. A typical current transient is shown in fig 48.

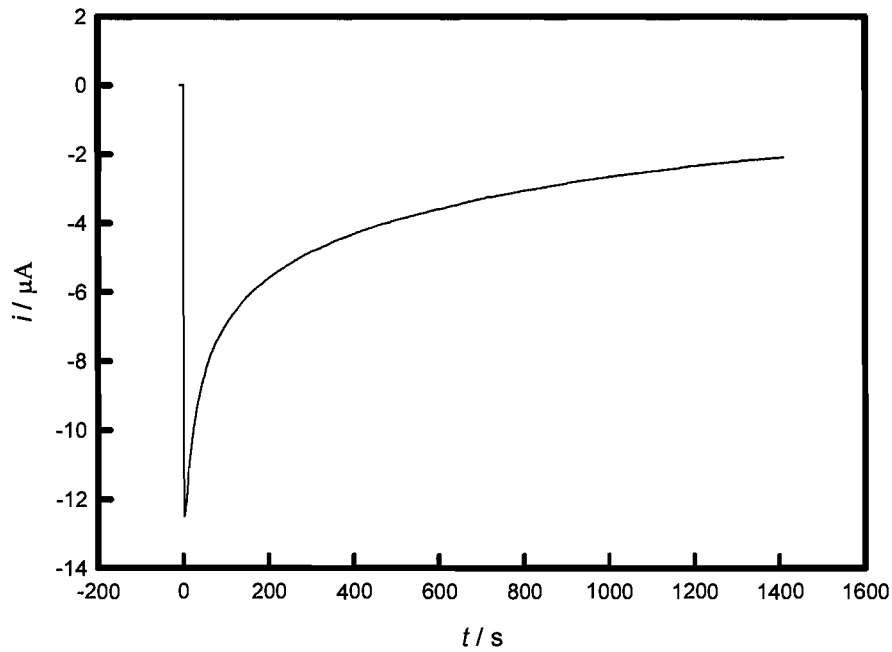

Fig 48 Graph showing the electrodeposition of H_1-e Pd onto an SRL136 microhotplate. Please refer to fig 44 for electrodeposition details. A deposition charge of 3.5 mC was passed.

Fig 48 shows a current transient of the electrodeposition of H_1-e Pd onto an SRL136 microhotplate from a Brij®56 palladium (II) nitrate hydrate template bath. Comparing the transient with that of the electrodeposition of H_1-e Pd from the ammonium tetrachloropalladate Brij®56 template bath, shown in fig 31 it can be

seen that the shape of the transients are similar but the current in this case is significantly greater. This is likely to be due to better coverage of the electrode surface. As already discussed, similar currents were obtained in the cyclic voltammograms of the two palladium salts at the deposition potential of 0.1 V vs. SCE which suggests similar kinetics for the two depositions assuming the electrodes were fully covered in the cyclic voltammograms.

4.6.4.2 Electrochemical characterisation of H_1-e Pd from Cl free Pd precursor on microhotplates

An acid cyclic voltammogram of the H_1-e Pd film on the SRL136 microhotplate was carried out to determine the surface area of the film which will help to confirm the Pd film's nanostructure. The eighth voltammetric cycle is shown in fig 49.

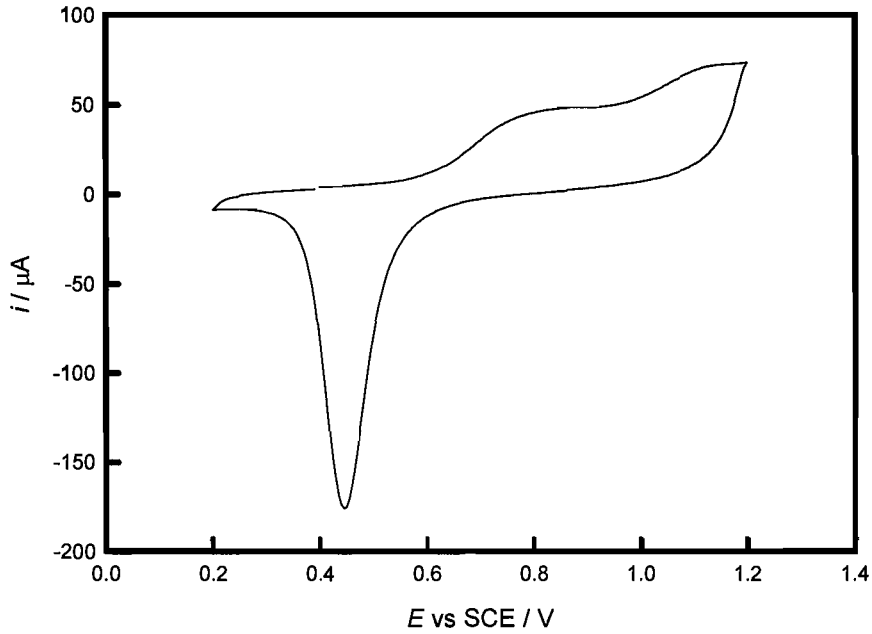

Fig 49. Cyclic voltammogram of H_1-e Pd in 1 M sulphuric acid. Please refer to fig 48 for deposition conditions. The cyclic voltammogram was started at 0.4 V vs. SCE and a scan rate of 100 mV / s was used. The cyclic voltammogram was carried out at room temperature, 25 °C.

The potential range was limited to the oxide potential region though it can be seen that this is similar to that obtained for the H_1-e Pd film electrodeposited onto a microhotplate from the ammonium tetrachloropalladate Brij®56 template mixture shown in fig 33. The surface area was calculated from the charge under the oxide stripping peak and the Rand and Woods constant[109] to be 27 $m^2 g^{-1}$. This value is

similar to that obtained for H_1-e Pd deposited from the same template bath onto a 1 mm diameter Au disc electrode described in section 4.6.3 which suggests that the film is nanostructured.

4.6.4.3 Initial Methane response of H_1-e Pd from Cl free Pd precursor

H_1-e Pd films deposited onto microhotplates from the chlorine free Pd template bath were methane tested with the aim of comparing the initial methane response with that of an H_1-e Pd film electrodeposited from the ammonium tetrachloropalladate Brij®56 template bath.

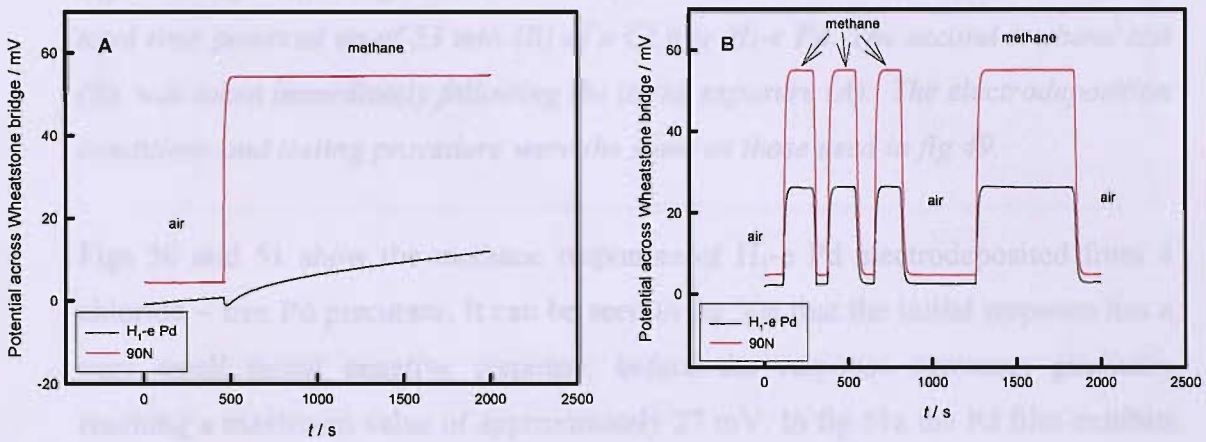

Fig 50 Graphs showing the methane responses after 10 min in air (A) and after a total time powered up of 33 min (B) of a Cl-free H_1-e Pd film. The second methane test, B was taken immediately following the initial exposure. Following electrodeposition as described in fig 48, the H_1-e Pd film was then voltammetrically cycled in 1 M sulphuric acid over 8 cycles at a scan rate of 100 mV / s. The temperature of the device was gradually raised by slowly increasing the power to 15.0 V from the power supply. A gas flow rate of 400 cm^3 min^{-1} was used for both methane and air.

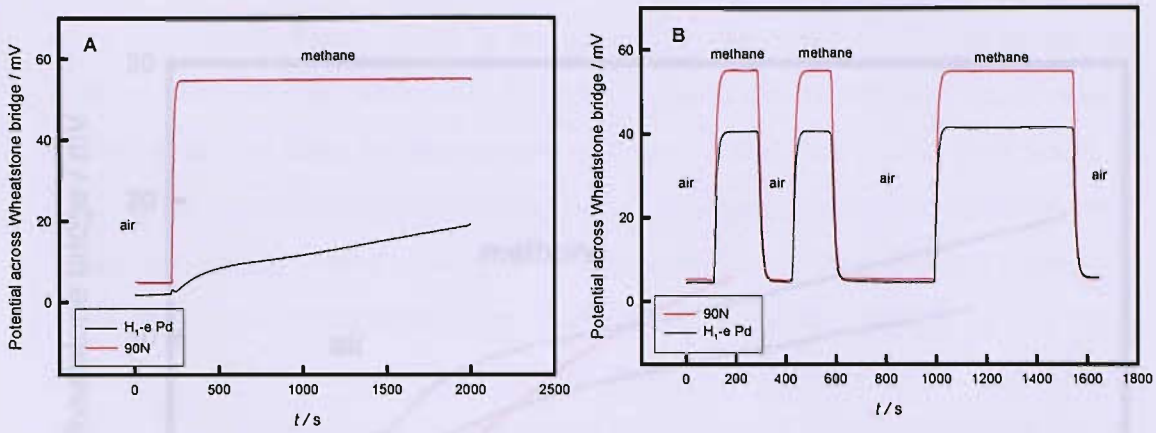

Fig 51. Graphs showing the methane responses after 10 min in air (A) and after a total time powered up of 33 min (B) of a Cl free H_1-e Pd. The second methane test (B), was taken immediately following the initial exposure (A). The electrodeposition conditions and testing procedure were the same as those used in fig 49.

Figs 50 and 51 show the methane responses of H_1-e Pd electrodeposited from a chloride – free Pd precursor. It can be seen in fig 50a that the initial response has a very small initial negative response, before the response increases gradually reaching a maximum value of approximately 27 mV. In fig 51a the Pd film exhibits a gradual increase in catalytic activity Following 20 min continuous exposure to methane the catalyst has reached full activity. Both devices were retested after a further 4 h and there was no increase in the magnitude of the response.

It can be seen that the methane response in fig 50a is initially negative before becoming positive. The negative response cannot be attributed to the presence of chlorine as the palladium was electrodeposited from a chlorine free precursor. A direct comparison of the initial activity of two H_1-e Pd films electrodeposited from a Pd precursor and two H_1-e Pd films electrodeposited from a Cl-free Pd precursor is shown in fig 52.

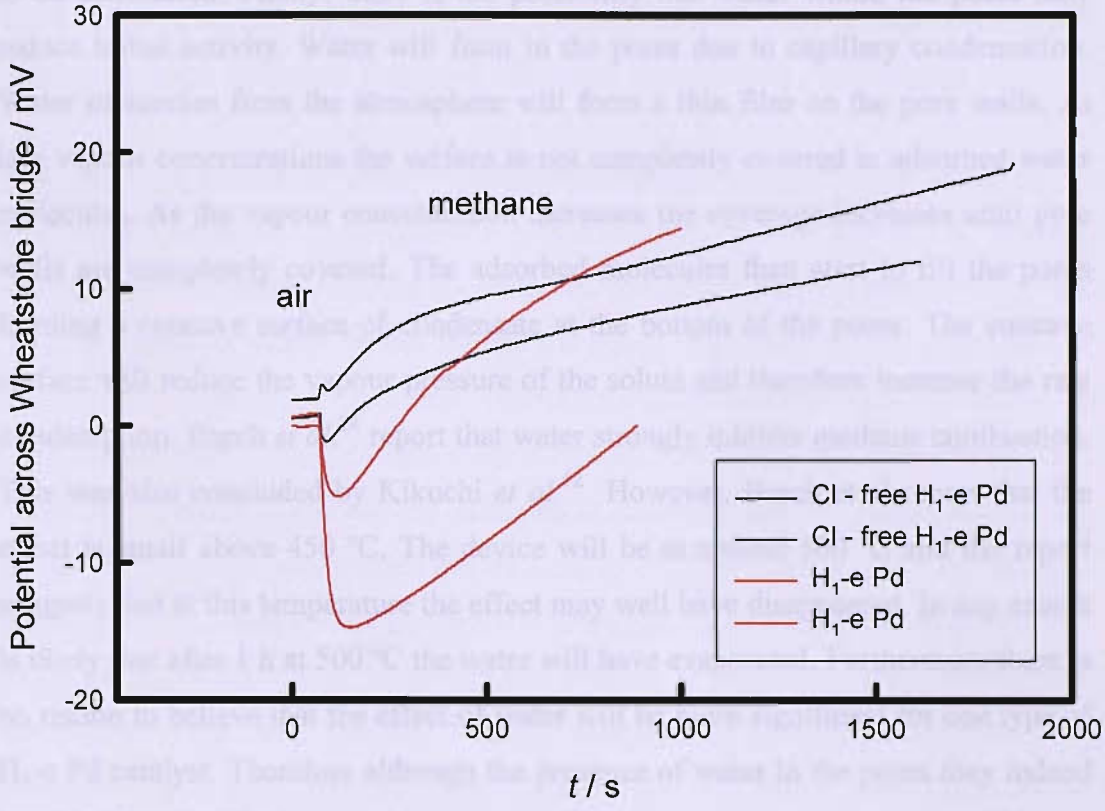

Fig 52. Graph showing the initial activity of H_1-e Pd catalysts prepared from Cl-free and Cl-containing Pd precursors. The Cl-containing Pd catalysts were electrodeposited onto SRL136 microhotplates as described in fig 39.The Cl-free Pd catalysts were electrodeposited onto SRL136 microhotplates as described in fig 50.

Fig 52 shows significantly greater initial activity for the two H_1-e Pd films electrodeposited from the Cl-free Pd precursors. One of the graphs has a small negative response but the magnitude is less than 2 mV and the bridge potential returns to the baseline in under 2 min. In contrast the magnitudes of the negative responses of the H_1-e Pd films electrodeposited from ammonium tetrachloropalladate are significantly larger at -14.6 and -5.0 mV respectively. In addition it takes longer for catalytic activity to be obtained; approximately 14 and 5 min respectively. It is therefore proposed that Cl in the Pd precursor does have an inhibitory effect on initial activity of electrodeposited mesoporous Pd films as the initial negative response, where it occurs, is significantly smaller and is overcome much more quickly. It is believed that the gradual increase in catalytic activity is a period of activation during which restructuring of the Pd catalyst is occurring.

There are a number of other factors which may influence catalytic activity that need to be considered. Firstly, there is the possibility that water within the pores may reduce initial activity. Water will form in the pores due to capillary condensation. Water molecules from the atmosphere will form a thin film on the pore walls. At low vapour concentrations the surface is not completely covered in adsorbed water molecules. As the vapour concentration increases the coverage increases until pore walls are completely covered. The adsorbed molecules then start to fill the pores forming a concave surface of condensate at the bottom of the pores. The concave surface will reduce the vapour pressure of the solute and therefore increase the rate of adsorption. Burch *et al.*[24] report that water strongly inhibits methane combustion. This was also concluded by Kikuchi *et al.*[52] However, Burch et al report that the effect is small above 450 °C. The device will be at around 500 °C and the report suggests that at this temperature the effect may well have disappeared. In any case it is likely that after 1 h at 500 °C the water will have evaporated. Furthermore there is no reason to believe that the effect of water will be more significant for one type of H_1-e Pd catalyst. Therefore although the presence of water in the pores may indeed have a detrimental effect on catalytic activity it should have a similar effect on different H_1-e Pd films. Carbon dioxide has also been shown to have an inhibitory effect on the methane activity of Pd catalysts. [24] However, CO_2 would have a constant inhibitory effect and not just on initial activity. It is also highly probable that it would have a similar effect on the two types of H_1-e Pd film studied here.

It seems highly plausible that the initial negative response is due to the presence of choride whilst the slow gradual increase in activity is due to restructuring of the catalyst. It is however curious that the initial methane response is negative even though the H_1-e Pd films have been at temperature for 1 h prior to exposure to methane. The increase in activity following the initial negative response is fairly rapid. It can be seen in fig 51 that within 500 s there is a positive 10 mV response. This suggests that the initial exposure to methane may have some effect on the Pd film which accelerates the activation process. A further point that needs to be remembered is that it is not known whether there is indeed chloride present in the Pd films electrodeposited from the ammonium tetrachloropalladate template mixture. However, the results do suggest that the H_1-e Pd films from the palladium nitrate (II) hydrate template mixture give better initial activity. In the next section the relative maximum catalytic activities are investigated.

4.6.4.4 Comparison of the magnitude of methane responses of H_1-e Pd catalysts form chlorine free and chlorine containing precursors

In the previous section the effect of chloride in the palladium precursor on the initial methane response was investigated. It was concluded that the low initial methane activity was attributable to Cl in the Pd precursor though catalyst restructuring was occurring simultaneously. In this section the effect of chloride on the magnitude of the methane response of 'seasoned' palladium catalysts is reported. The aim is to establish whether Cl has an inhibitory effect by comparing the magnitude of the methane responses of the two Pd catalysts at different methane concentrations. A similar investigation was carried out by Roth *et al.*[116] In this study the Pd catalysts were not electrodeposited but prepared by impregnation of the support with H_2PdCl_4 and $Pd(NO_3)_2$. They tested the catalysts in methane at increasing temperatures from 150 to 600 °C and found that the Cl-free Pd catalyst gave superior performance.

Three standard H_1-e Pd and three Cl-free H_1-e Pd films were prepared by electrodeposition from the ammonium tetrachloropalladate and palladium (II) nitrate hydrate template baths. The electro-deposition charge was kept constant at 5 mC. The devices were exposed to increasing concentrations of methane from 0.5 to 2.5 % in air. The methane responses are shown in fig 53.

Fig 53 shows the maximum methane response of each H_1-e Pd film at each concentration of methane. It can be seen that the H_1-e Pd catalysts from the Cl-free Pd precursor gave larger responses at each methane concentration.

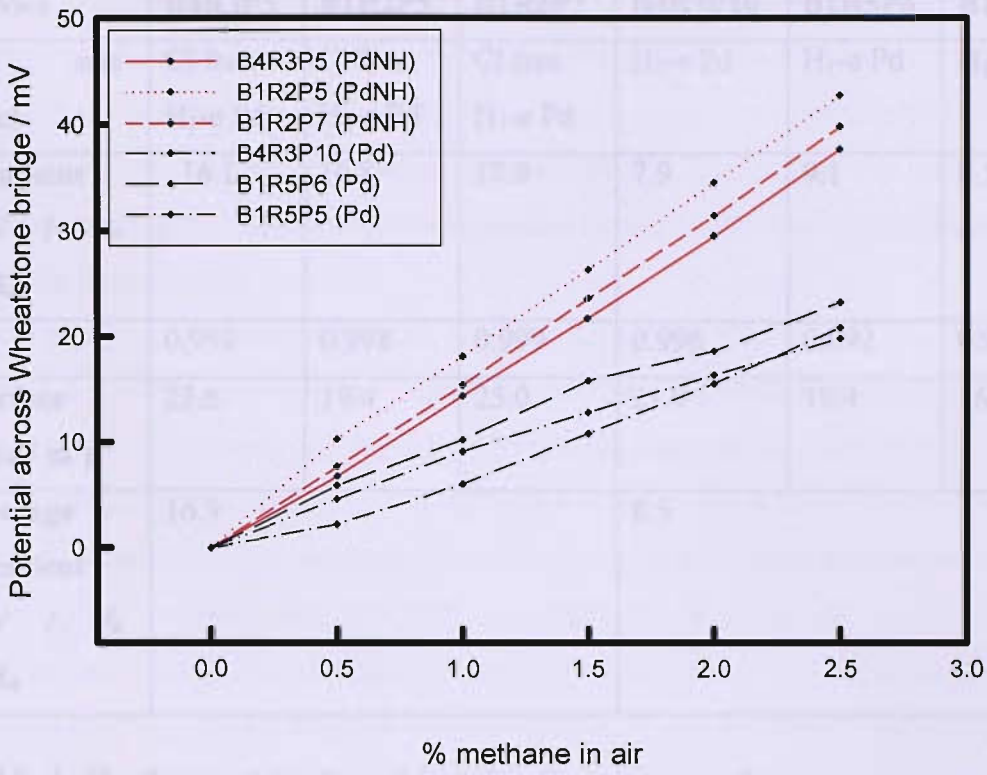

Fig 53. Graph showing the linearity of methane response of mesoporous Pd catalysts. In each case 5 mC of Pd was electrodeposited from the template mixture at room temperature. H_I-e Pd films were electrodeposited from the ammonium tetrachloropalladate template mixture by applying a potential step from 0.4 to 0.1 V vs. SCE. The electrodeposition of Cl- free H_I-e Pd films is described in fig 48. In both cases the Pd films were washed in iso-propanol for 1 h to remove the surfactant. The H_I-e Pd films were then voltammetrically cycled in 0.1 M sulphuric acid over 10 voltammetric cycles.

Linear regression was carried out to calculate the gradient and the R^2 value of the graphs which are given in table 1.

Device	B4R3P5	B1R2P5	B1R2P7	B4R3P10	B1R5P6	B1R5P5
Pd salt used	Cl free H_1-e Pd	Cl free H_1-e Pd	Cl free H_1-e Pd	H_1-e Pd	H_1-e Pd	H_1-e Pd
Gradient / mV / % CH_4	16.1	16.8	17.9	7.9	9.1	8.5
R^2	0.999	0.998	0.999	0.996	0.992	0.985
Surface area / m^2g^{-1}	23.6	19.4	25.0	21.9	19.4	16.5
Average Gradient / mV / % CH_4	16.9			8.5		

Table 1. Gradients of the line of best fit of maximum methane response against methane concentration for H_1-e Pd catalysts electrodeposited from chlorine free and chlorine containing precursors. The R^2 value is was calculated using data analysis in excel.

Table 1 shows the gradients of the linear regression from the graph of methane response against concentration of methane in air. A higher gradient indicates a higher catalytic activity. It can be seen from the R^2 values in table 1 that with the exception of the device B1R5P5, all the graphs can be described as linear. Examining the gradients from the methane responses of the Cl free H_1-e Pd catalysts it can be seen that the gradients of the three results are all similar. The gradients of the methane response from the standard H_1-e Pd catalyst were also all similar. This suggests that the results are reproducible. The specific surface areas of each Pd film were also calculated using the charge under the oxide stripping peak. It can be seen that the surface areas of the Pd films are all of a similar magnitude, indicating that the lower gradients of the Pd films electrodeposited from the Cl-containing Pd precursors are not a result of variation in surface areas.

Comparing the average gradients it can be seen that the Cl free H_1-e Pd catalysts have significantly higher sensitivity to methane. The average gradient for the Cl-

free H_I-e Pd catalysts is 16.9 mV / % methane compared with 8.5 mV / % methane for the standard H_I-e Pd catalyst. This equates to an increase of nearly 100 %. It could therefore be reasonably concluded that chlorine in the Pd precursor inhibits the methane activity of palladium catalysts. Again, it must be remembered that it is not known whether there is indeed chloride in the Pd catalyst. An alternative explanation might be that the electrodeposition from the nitrate salt might produce a more reactive catalyst.

These results are consistent with the work by Roth *et al.*[116] discussed previously in section 4.5.1. Their investigation tested the catalysts at different temperatures from 150 to 600°C and concluded the chlorine free palladium catalyst was superior. It is noted that Roth *et al.* found that at least 10 h were required for all chlorine to be removed from palladium catalysts made from chlorine containing precursors though it is again stressed that the catalysts prepared by Roth *et al.* were not electrodeposited as is the case here. As already indicated the H_I-e Pd catalysts were retested after 4 h and no increase in methane activity was observed. To confirm this result the H_I-e Pd films electrodeposited from the Pd precursor containing Cl tested in fig 26 were left powered up in air and retested for methane after 12 h. There was no increase in the magnitude of any of the methane responses. Indeed 2 of the methane responses had decreased by several mV. The observed decrease in methane sensitivity is consistent with work by Euzen *et al.*[118] A more in depth examination into the loss of methane activity over time is reported in section 4.7.

It has been reported that the use of different palladium precursors results in the formation of palladium oxide species with different characteristics.[119,120] This will affect the thermal stability of the catalyst and the catalytic behaviour.[121] Simplicio *et al.*[121] investigated the effect of the palladium precursor on methane combustion over PdO supported on alumina.[121] Catalysts were prepared using palladium nitrate, palladium acetylacetonate and palladium chloride by impregnating an alumina support. These were labelled PAN, PAA and PAC respectively. A fourth catalyst was made using a solution of palladium acetylacetonate in ethylene glycol and labelled PAAP. The results showed that the palladium oxide decomposed at increasing temperatures in the following order: PAC, PAN, PAA, PAAP. TEM and XRD experiments were also carried out and revealed that the particle size decreased in this order. This indicates that the palladium precursor affects the particle size which itself influences the decomposition temperature of the oxide. Methane

activity of the different catalysts was also compared using the temperature corresponding to 10 % conversion, T_{10}. PAA had the lowest T_{10} of 270 °C, then PAAP at 328 °C, PAN at 334 °C and PAC at 378 °C. The palladium catalyst prepared from the chlorine precursor showed the least activity and was reported to have chloride on the surface even after calcination at 600 °C. These results were consistent with the XRD and TPD profiles and clearly indicated a relationship between PdO particle size and methane conversion. The most active catalysts had the smallest PdO particle size and the highest PdO dispersion as well as the highest PdO decomposition temperature. Although the report found chloride still present in the PdO catalyst prepared from the chloride precursor, the results suggest that particle size and dispersion may be equally, if not more important. The results are consistent with those obtained here and those obtained by Roth *et al.* indicating that Pd catalysts prepared from chloride containing Pd precursors have lower activity than those prepared from chloride free precursors.

In summary the results obtained here indicate that H_1-e Pd films from the chloride-free palladium (II) nitrate hydrate salt have better initial activity and also greater maximum sensitivity. The higher initial activity is consistent with the results obtained by Roth *et al.*[116] and the greater maximum sensitivity is consistent with the results obtained by Simplicio *et al.*[121] It is conceded that there is no evidence that there is residual chloride in the Pd catalysts deposited from ammonium tetrachloropalladate precursor. However, the results remain consistent with those of Simplicio *et al.* and suggest that the possibility of residual chloride may be the key factors.

4.7 Response longevity

The commercial 90N pellistor produces a reproducible methane response with a loss of less than 5 % of activity over a period of a month.[4] An investigation was carried out to investigate the longevity of the methane response of H_1-e Pd catalysts. Fig 54 shows the methane response of a mesoporous Pd catalyst electrodeposited from the standard ammonium tetrachloropalladate – Brij®56 template mixture. The palladium film was electrodeposited by potential step from 0.4 to 0.1 V vs. SCE. A deposition charge of 3.5 mC was passed. The surfactant was removed by soaking in iso-

propanol for 1 h before the palladium was voltammetrically cycled in 1 M sulphuric acid over ten voltammetric cycles at 100 mV/s in the oxide potential region only.

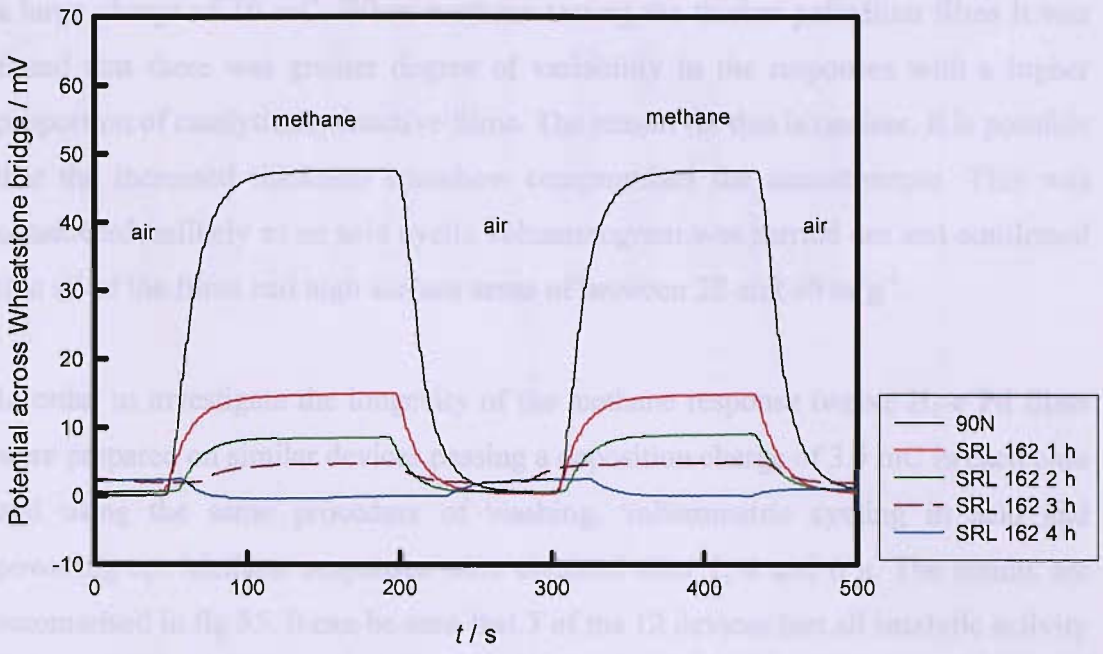

Fig 54 Graph showing the methane response of H_1-e Pd on an SRL 162 device after 1, 2, 3 and 4 h powered up. The temperature of the SRL162 device was gradually raised by slowly increasing the power to 7.0 V across the device, 14.0 V from the power supply. A gas flow rate of 400 cm^3 min^{-1} was used for both methane and air. A 3 position tap was used to manually select the gas type. The palladium film was electrodeposited at room temperature by applying a potential step from 0.4 to 0.1 V vs. SCE. A deposition charge of 3.5 mC was passed. The surfactant was removed by soaking in iso-propanol before the palladium was voltammetrically cycled in 1 M sulphuric acid over ten voltammetric cycles at 100 mV/s in the oxide region only.

In fig 54 it can be seen that the Pd catalyst on an SRL162 microhotplate initially has a moderate response following 1 h in air of approximately 15 mV. Following the recording of this response the gas supply was switched back to air before the device was retested in methane after another hour, after a total of 2 h powered up. It is noted that after a total of 4 h powered up the Pd catalyst has lost all catalytic activity and now gives a negative response to methane. Euzen *et al.*[118] report that for a methane concentration of 2.75 % catalytic activity of a palladium catalyst fell by 20 % over 15 h. It was proposed that the loss of activity was attributed to the conversion of Pd to bulk PdO and sintering of the metal. If it is simply a case of

losing catalytically active sites then it seems reasonable that as the film is mesoporous, a thicker film will have better durability as more active sites will be available. To investigate this theory thicker H_I-e Pd films were prepared by passing a large charge of 10 mC. When methane testing the thicker palladium films it was found that there was greater degree of variability in the responses with a higher proportion of catalytically inactive films. The reason for this is unclear. It is possible that the increased thickness somehow compromises the nanostructure. This was considered unlikely as an acid cyclic voltammogram was carried out and confirmed that all of the films had high surface areas of between 22 and 30 m^2g^{-1}.

In order to investigate the longevity of the methane response twelve H_I-e Pd films were prepared on similar devices passing a deposition charge of 3.5 mC in each case and using the same procedure of washing, voltammetric cycling in acid and powering up. Methane responses were obtained after 1, 4 and 6 h. The results are summarised in fig 55. It can be seen that 3 of the 12 devices lost all catalytic activity within 6 h whilst the remaining 9 lost little catalytic activity. It is noted that the devices that lost all methane activity also had the lowest initial methane response recorded after 1 h. It was considered possible that surface area may have some bearing on response longevity, so the surface area was calculated for each Pd film using the area under the oxide stripping peak and the Rand and Woods constant.[109] The results do not suggest that surface area is a factor in determining the longevity of the response. It can be seen that the devices 8 and 11 have similar surface areas yet device 8 gave an initial response of 28.5 mV after 1h and a response of 26.4 mV after 6 h. Device 11 however only gave an initial response of 9.3 mV which had become a negative response after 4 h.

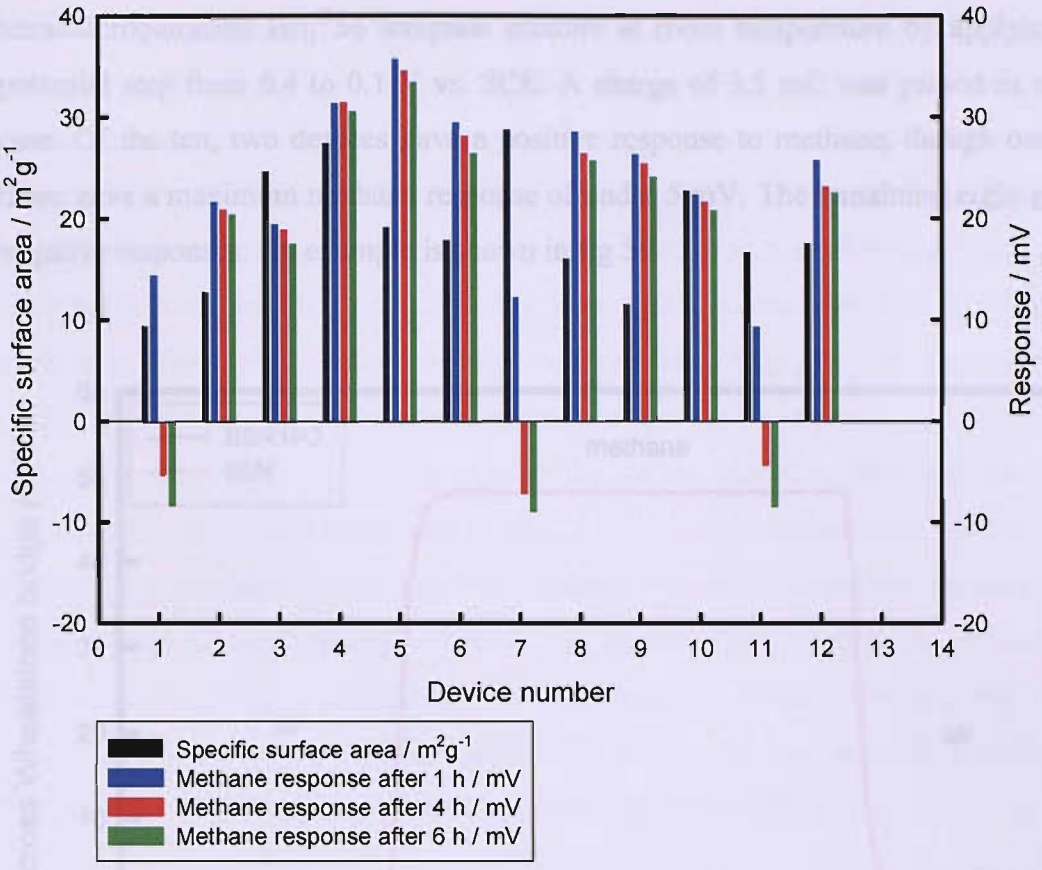

Fig 55 Summary of methane responses of H_1-e Pd films electrodeposited from a Brij®56 ammonium tetrachloropalladate template bath at room temperature. A deposition charge of 3.5 mC was passed by potential step from 0.4 to 0.1 V vs. SCE. Following deposition the films were soaked in iso-propanol for 1 h, before being voltammetrically cycled in 1 M sulphuric acid over ten voltammetric cycles. Devices were powered at 14.0 V in air flowing at 400 cm^3 min^{-1}.

It is unclear why similarly prepared H_1-e Pd films should exhibit such differing methane longevities, despite in some cases having similar surface areas. It still seems likely that the decrease in activity is due to the conversion of palladium to palladium oxide, though it is unclear why this should occur on some palladium films and not others.

4.8 Effect of acid cycling of Pd film on methane response

Previous work by Guerin[5] and Marwan[69] suggested it was necessary to voltammetrically cycle the Pd film in acid in order to get a positive methane response. Investigations were carried out to determine whether acid cycling was

required. Initially ten H_1-e Pd films were electrodeposited from the ammonium tetrachloropalladate Brij®56 template mixture at room temperature by applying a potential step from 0.4 to 0.1 V vs. SCE. A charge of 3.5 mC was passed in each case. Of the ten, two devices gave a positive response to methane, though one of these gave a maximum methane response of under 5 mV. The remaining eight gave negative responses. An example is shown in fig 56.

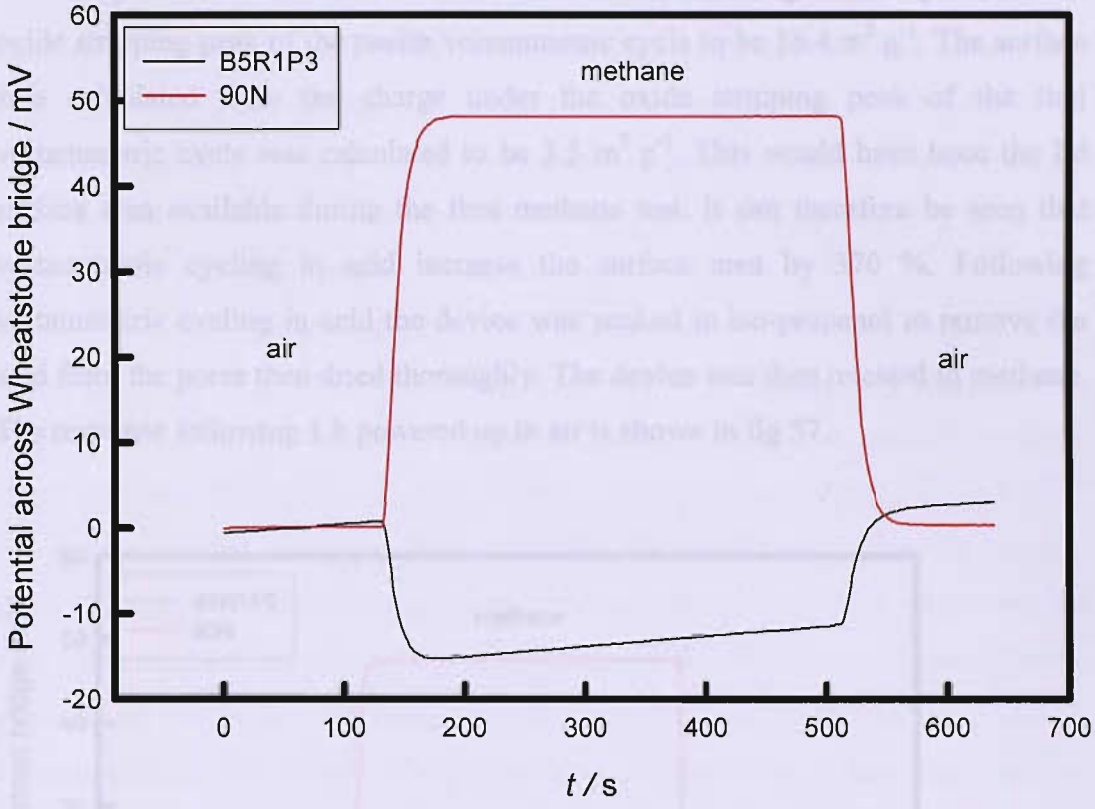

Fig 56. Response of an H_1-e Pd film that was not voltammetrically cycled to methane. For details of the preparation of the film please refer to fig 55.

Fig 56 shows the methane response of an H_1-e Pd film that was not voltammetrically cycled to methane. It is noted that the methane response increases gradually. The gradient of the methane response was calculated to be very similar to that of the baseline in air, suggesting that the response is not increasing due to an increase in catalytic activity but due to baseline drift. The device was left powered in air for a further 1 h when it was retested. A similar response was obtained. It was therefore concluded that the H_1-e Pd film was not active for the catalytic oxidation of methane.

Following the negative methane response the device was powered down. It was decided to carry out a cyclic voltammogram in acid of the H_1-e Pd film to determine the surface area and to investigate whether a subsequent methane test yielded a positive response. The cyclic voltammogram was restricted to the palladium oxide region of 0 to 0.65 V vs. SMSE, using a scan rate of 100 mV / s. The charge under the oxide stripping peak, used to calculate the surface area, was observed to increase with each voltammetric cycle over the first twelve voltammetric cycles before stabilising. The maximum surface area was calculated using the charge under the oxide stripping peak of the twelth voltammetric cycle to be 16.4 $m^2 g^{-1}$. The surface area calculated from the charge under the oxide stripping peak of the first voltammetric cycle was calculated to be 3.5 $m^2 g^{-1}$. This would have been the Pd surface area available during the first methane test. It can therefore be seen that voltammetric cycling in acid increase the surface area by 370 %. Following voltammetric cycling in acid the device was soaked in iso-propanol to remove the acid from the pores then dried thoroughly. The device was then retested in methane. The response following 1 h powered up in air is shown in fig 57.

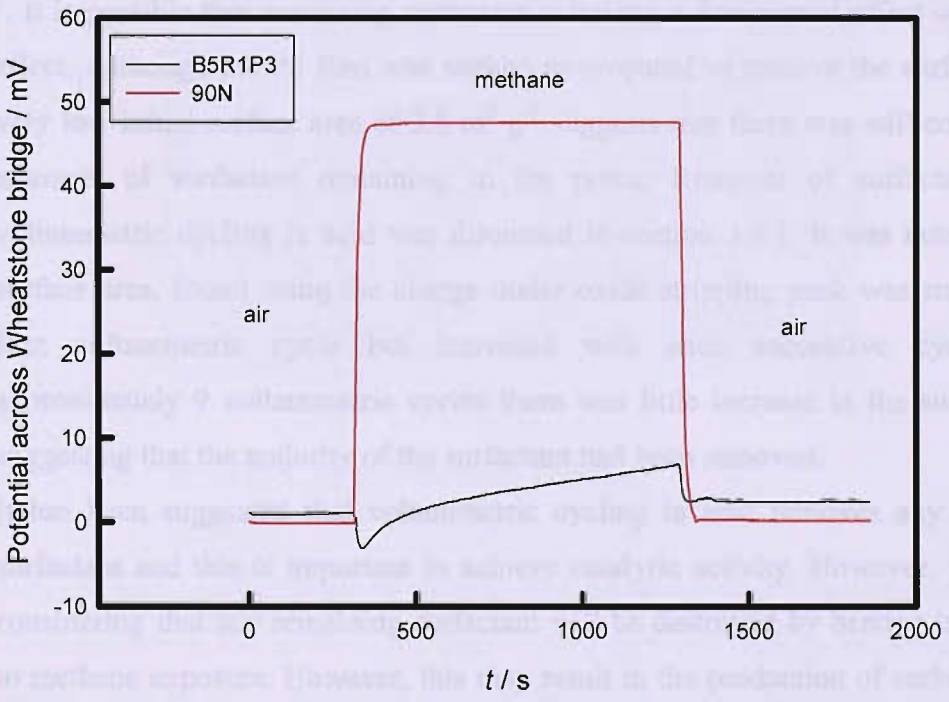

Fig 57 Methane response of an H_1-e Pd catalyst on an SRL 136 microhotplate, following voltammetric cycling in 1 M sulphuric acid. Please refer to fig 56 for deposition conditions.

Fig 57 shows the methane response of the H_1-e Pd film following voltammetric cycling in 1 M sulphuric acid. Upon exposure to methane the response is negative indicating a thermal response and no catalytic activity. There is then a gradual increase in the response. Upon switching back to air the response decreases, indicating that the palladium catalyst is now catalytically active. It is also noted that the baseline in air is more stable compare to prior to voltammetric cycling in acid.

Following voltammetric cycling in acid the palladium catalyst gave a positive, if modest response to methane. The device previously gave a negative response to methane. As reported earlier it was concluded that the device needs to be powered for a sufficient period of time for a positive methane response to be obtained. It can therefore be reasonably concluded that the voltammetric cycling has increased the catalytic activity of the palladium film, though it is possible that this is due to voltammetric cycling increasing the surface area of the film.

It is not clear why voltammetric cycling in acid increases the catalytic activity of the palladium film. It is noted that the surface area was significantly increased by voltammetric cycling. However, results in fig 55 showed that positive methane responses were obtained for H_1-e Pd films of relatively low surface areas of 9 m^2 g^{-1}. It is possible that remaining surfactant is having a detrimental effect on catalytic effect. Although the Pd film was soaked in propanol to remove the surfactant, the very low initial surface area of 3.5 m^2 g^{-1} suggests that there was still considerable amounts of surfactant remaining in the pores. Removal of surfactant during voltammetric cycling in acid was discussed in section 3.4.1. It was noted that the surface area, found using the charge under oxide stripping peak was small on the first voltammetric cycle but increased with each successive cycle. After approximately 9 voltammetric cycles there was little increase in the surface area, suggesting that the majority of the surfactant had been removed.

It has been suggested that voltammetric cycling in acid removes any remaining surfactant and this is important to achieve catalytic activity. However, it is worth considering that any remaining surfactant will be destroyed by heating in air, prior to methane exposure. However, this may result in the production of carbon dioxide and water which have been shown by Burch *et al.* [24] to have an inhibitory effect on methane activity. It may be more important that the surfactant is removed and that voltammetric cycling in acid is effective at doing so, rather than voltammetric cycling modifying the Pd in some way.

4.9 Changes to the H_1-e Pd film after methane testing

During methane sensing there will be changes to the palladium film as palladium oxide is formed.

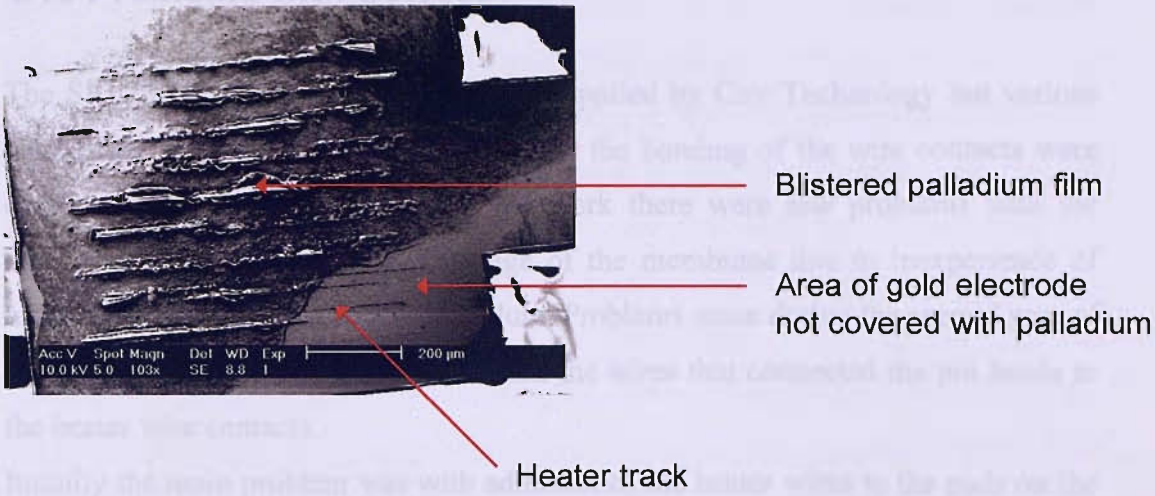

Fig 58 SEM image of an H_1-e Pd film following methane testing.

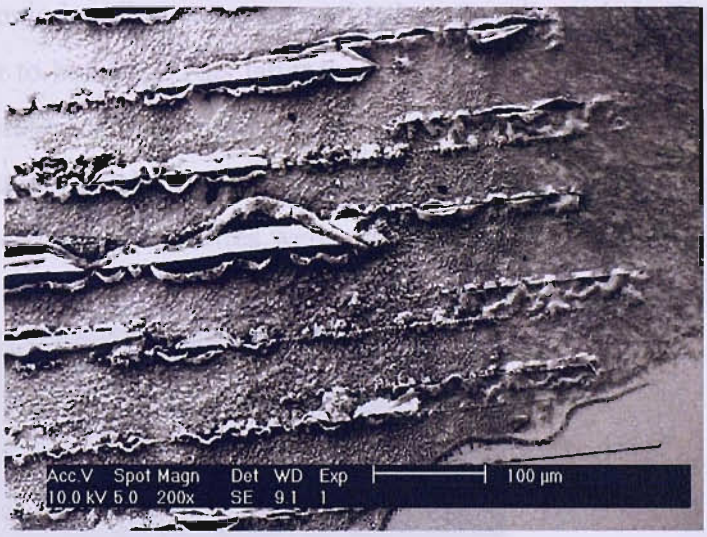

Fig 59 Close up of H_1-e Pd film depicted in fig 58.

It can be seen in figs 58 and 59 that the Pd film has become badly blistered directly above the heater tracks. Work by Lee[107] using infra red techniques showed that the hottest areas of the device were directly above the heater tracks. It therefore seems likely that this blistering is the result of excessive temperature. It is also possible that it is the result of a problem with the silicon nitride membrane and the Pt heater. As the two materials heat they will expand. It is possible they will expand at

sufficiently different rates that the mechanical stress becomes excessively large resulting in the observed blistering.

4.10 Problems with devices

The SRL136 and SRL162 devices were supplied by City Technology but various parts of the manufacturing process, namely the bonding of the wire contacts were outsourced. In the initial stages of the work there were few problems with the devices except for occasional breakage of the membrane due to inexperience of handling the devices and of the procedure. Problems arose during the second year of the project. The main problem concerned the wires that connected the pin heads to the heater wire contacts.

Initially the main problem was with adhesion of the heater wires to the pads on the membrane. The wires were observed to lift off from the pad. The wires were adhered to the pads by ultrasonic bonding. It was proposed that either the conditions of the ultrasonic bonding were not optimal or that the pads had not been properly cleaned prior to bonding. This latter theory was based on the presence of a residue on the membrane surface. These concerns were relayed to the supplier.

In the subsequent batch of devices received the wires were mainly breaking at the foot of the wire where the wires were ultrasonically bonded to the gold pad on the device. The SEM image in fig 60 shows an example of such a breakage.

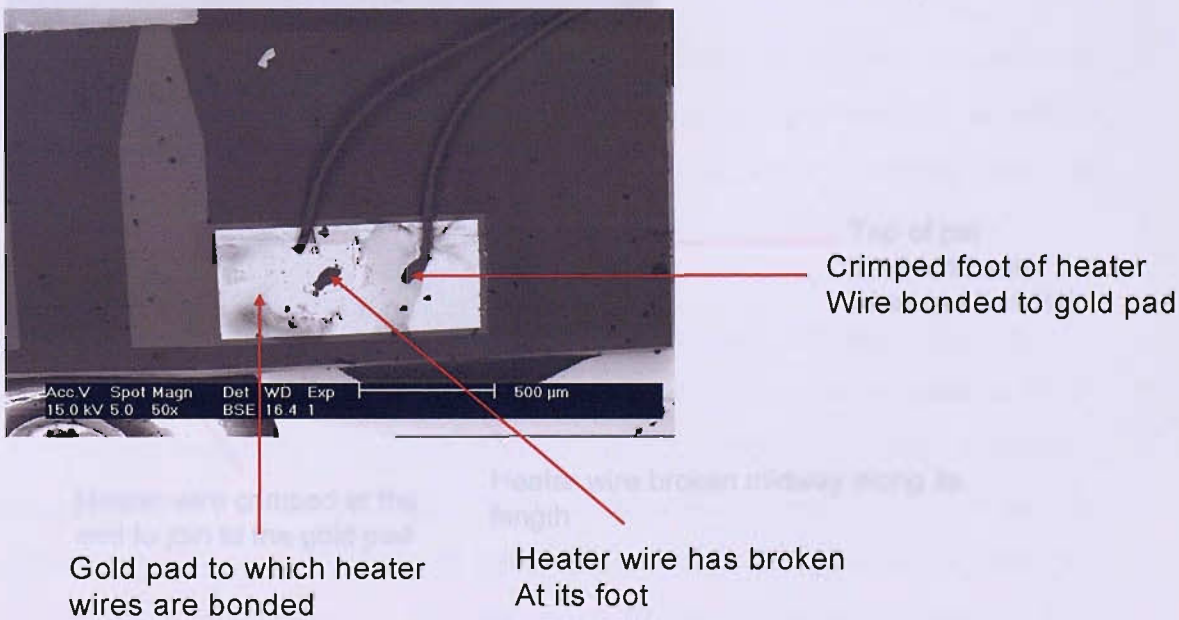

Fig 60. SEM image of an SRL 136 microhotplate device. It can be seen that a heater wire has broken close its foot.

This part of the wire will be weakest mechanically as the wire has a tight radius. It was proposed that the wire was breaking here as a result of mechanical stress caused by the movement of fluid during a stirred soak. The soak was changed to a non-stirred soak. However, an unstirred water soak was not sufficient to remove the surfactant from the pores. The water was therefore replaced with propan-2-ol which had previously been shown to be more effective at removing the surfactant. Despite the soak now being non-stirred breakages were still occurring. Considering the minimum mechanical forces involved in a non-stirred soak this was cause for concern. Following discussion with City Technology it was found that the frequency used for the ultrasonic bonding had been increased to compensate for the adhesion problems previously encountered. This higher frequency may have overstressed the wire, resulting in the breakages.

The adhesion of the wire to the pad and ultrasonic bonding issues were rectified. However, another problem with the wires developed. With this batch the heater wires broke midway along their length. In fig 61 it can be seen that the wires are still intact at the join with the pad on the far left of the image. The wires are also still bonded to the pin, just visible on the right of the image.

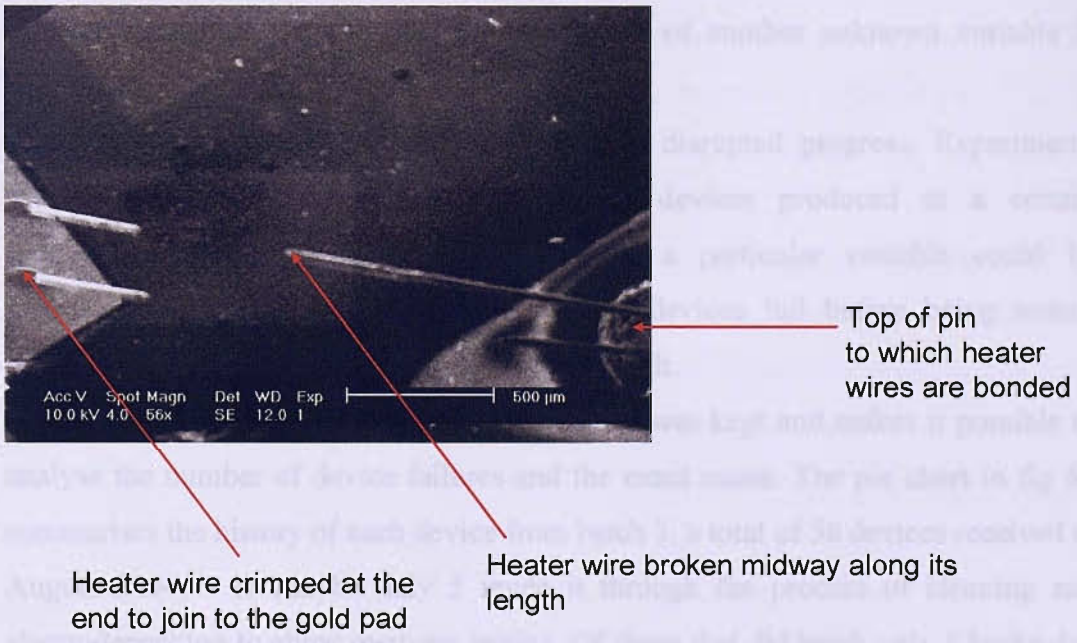

Fig 61. SEM image of the heater wires of an SRL136 device that have broken midway along their length.

It is likely that the weakest point of the wires will be the joints especially the crimp where the wire is bonded to the pad. It would seem likely that if the wires were breaking as a result of mechanical strain, they would break at one of these weak points. It was proposed that the breakages may have been due to a chemical reaction rather than a mechanical failure. However, it was thought that the wires were gold and therefore would not react with the acid used. In an electrodeposition of non-mesoporous Pd from a solution of 50 mM $(NH_4)_2PdCl_4$, 1 M HCl and 1 M NH_4Cl vigorous bubbling was observed originating from the wires. Subsequent examination revealed that the wires had broken along their length. Discussion with City Technology revealed that the gold coated wires had been replaced with aluminium. The reaction with the acidic deposition solution was the reaction of aluminium and acid, resulting in the evolution of hydrogen gas.

A number of other problems were encountered with the microhotplate devices. When the devices were powered up for methane testing they were balanced using a variable resistor in order to balance the Wheatstone bridge. Typically a value of 320 Ω was required to balance an SRL136 device and 420 Ω for an SRL162 device. On a number of SRL162 devices the resistance to balance the bridge was around 50 Ω. Examination of the device using SEM and optical microscopes revealed no obvious problems. However, when assessing the effect of changing a particular variable such as thickness of the Pd film the possible effect of another unknown variable is undesirable.

These problems were significant and seriously disrupted progress. Experiments were planned which required a number of devices produced to a certain specification so that the effect of changing a particular variable could be investigated. When a large proportion of the devices fail before being tested, assessing individual variables became very difficult.

A comprehensive history of all the devices used was kept and makes it possible to analyse the number of device failures and the exact cause. The pie chart in fig 62 summarises the history of each device from batch 3, a total of 56 devices received in August 2004. It can be only 5 made it through the process of cleaning and electrodeposition to allow methane testing. Of those that did break only 1 broke due to user error. In this case the reference electrode was brought down too hard onto the membrane when setting up the electrodeposition, resulting in the membrane breaking. This clearly indicates that the majority of breakages are a result of

manufacturing problems rather than user handling. A similar success rate was experienced with a further 3 batches of devices received over approximately 8 months which significantly impeded progress.

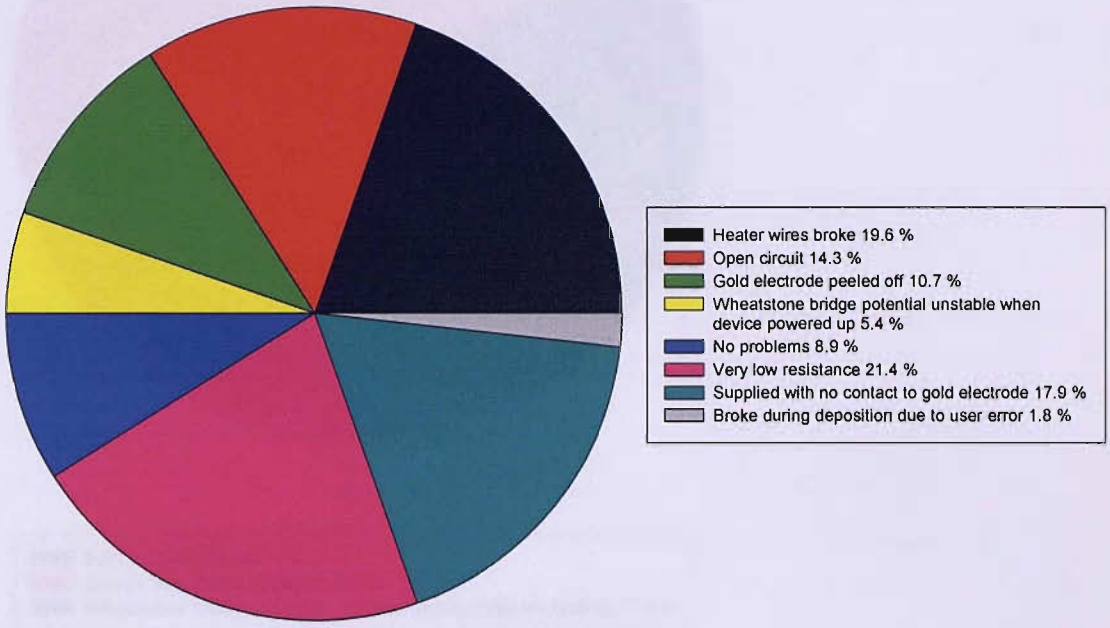

Fig 62. Pie chart summarising the history of each of the devices in batch 3. The batch contained a total of 56 devices comprising a mixture of SRL136 and SRL162 devices and was received in August 2004.

These results can be compared to a later batch of devices, batch 5 received in February 2005, once problems with the heater wires and ultrasonic bonding frequencies had been rectified. This batch consisted of 37 devices comprised of both SRL136 and SRL162 devices. The results are summarised in fig 63.

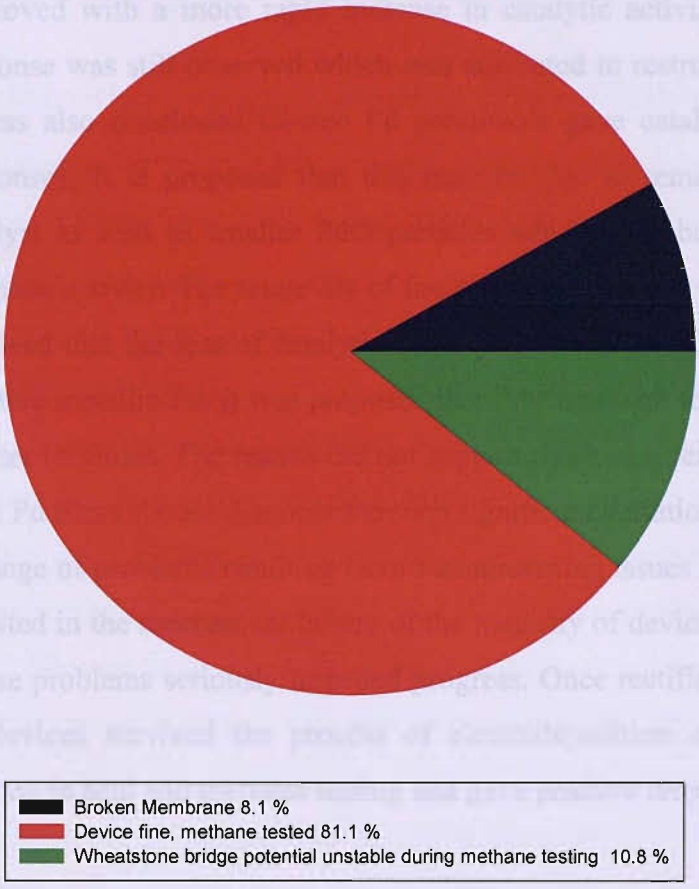

Fig 63. Pie chart summarising the end result of devices from batch 5. The batch was received in February 2005 and comprised 37 devices consisting of a mixture of SRL136 and SRl162 devices.

The results in fig 63 show a vast improvement in the numbers of devices surviving the cleaning and deposition process through to methane testing.

4.11 Conclusions

H_1-e Pd catalysts were electrodeposited onto silicon microfabricated microhotplates. Electrochemical characterisation confirmed high surface areas and the characteristic features of a nanostructured Pd acid cyclic voltammogram. The H_1-e Pd films gave positive responses to methane. The magnitude of the responses was typically between 10 and 30 mV, though it is unclear why there was such variation between similarly prepared films. The initial methane response was typically weak or negative. It was proposed that Cl present in the Pd precursor may be responsible for the poor initial activity. To investigate H_1-e Pd films from a Cl free Pd precursor

were prepared. It was found that the initial methane response was significantly improved with a more rapid increase in catalytic activity. A gradual increase in response was still observed which was attributed to restructuring of the Pd to PdO. It was also concluded Cl-free Pd precursors gave catalysts with larger methane responses. It is proposed that this may be due to remaining chloride in the Pd catalyst as well as smaller PdO particles which have been shown to give higher methane activity. The longevity of the methane response was also investigated. It is believed that the loss of catalytic activity is the result of the conversion of PdO to inactive metallic Pd. It was proposed that Pd films with low surface areas may have shorter lifetimes. The results did not support this and it remains unclear why similar H_1-e Pd films should demonstrate such significant variation in durability.

A range of problems resulting from manufacturing issues have been reported. These resulted in the mechanical failure of the majority of devices in a number of batches. These problems seriously impeded progress. Once rectified the significant majority of devices survived the process of electrodeposition of H_1-e Pd, voltammetric cycling in acid and methane testing and gave positive responses to methane.

5 Poisoning of catalysts with HMDS

5.1 Introduction to poisoning and inhibition of Pd catalysts

Palladium catalysts have been shown to be the most effective for the oxidation of alkanes of less than five carbon atoms and in particular for methane.[122] Pd is therefore well suited for use in a catalytic methane sensor. Perhaps the most common of existing flammable gas detector designs is the pellistor, a full description of which is given in section 1.1 The catalytic activity of a pellistor can be significantly reduced by small quantities of gas phase species.[123] Commercial pellistors have recently improved their resistance to poisons by using very high surface area catalysts. This has been achieved by increasing porosity and catalyst dispersion as well as by using the most appropriate catalyst.[7] The 90N pellistor used as a reference in these studies loses half of its catalytic activity in approximately 150 min when poisoned with 6 ppm hexamethyldisiloxane (HMDS), the standard poison used to test catalytic gas sensors. There is commercial interest in achieving higher poison resistance. In this chapter the poison resistance of a mesoporous Pd catalyst will be investigated and compared to that of a commercial pellistor. Ways of improving the poison resistance of mesoporous Pd catalysts will also be explored.

5.1.1 Definitions of poisoning

The terms poisoning and inhibition are frequently used, sometimes interchangeably. In this work a catalyst poison will be defined as a substance that causes a reduction in catalytic activity which does not recover when the substance is removed. In contrast, an inhibitor reduces catalytic activity, but performance improves when this substance is removed. In the previous section HMDS was found to irreversibly reduce catalytic activity of palladium catalysts for the oxidation of methane. It is therefore classified as a poison. In section 4.6.4.3 water was found to act as an inhibitor in that its detrimental effect on catalytic activity was reversed when it was removed from the gas feed.

5.1.2. Poisons of Pd catalysts for the oxidation of methane

Gas detectors are used to alert to the build up of a flammable gas and so prevent a possible explosion. Flame retardants are often used in environments where such detectors are commonly required and often contain materials such as halogenated

hydrocarbons, organosiloxanes and sulphur containing compounds which have a significant detrimental effect on their activity.[8,53 124-126] Cullis *et al.*[127] investigated the poisoning of a palladium sponge catalyst by chloromethanes. They reported a loss of catalytic activity which was attributed to the adsorbed halogen compounds being able to form dipoles with the negative charge facing outwards resulting in a reduction in the surface coverage of oxygen ions. Otto and Montreuil[6] carried out a study of the poisoning of palladium catalysts by chlorinated and brominated ethanes. They found that these substances had an inhibitory effect on catalytic activity which was attributed to competitive adsorption by the haloethanes on the catalyst active sites.

Cullis and Willatt[53] investigated poisoning of precious metal catalysts used for the oxidation of hydrocarbons. The H_1-e Pd catalysts operate at approximately 500 °C. At this temperature hexamethyldisiloxane, $(CH_3)_3Si\text{-}O\text{-}Si(CH_3)_3$ breaks down slowly forming a wide variety of products.[128] However, the decomposition is rapidly catalysed by transition metals.[129] In the presence of a transition metal catalyst the reaction proceeds via cleavage of the $Si\text{-}CH_3$ bond resulting in the formation of gaseous methane and polyorganosiloxane. The oganosiloxanes decompose to form silicon and carbon.[53] The extent to which these species penetrate the surface depends of the catalyst and its support.[53] It was reported that palladium adsorbs silicon more readily than platinum and is therefore poisoned to a greater extent by HMDS.

Gentry and Jones[8] also investigated the effect of HMDS on the catalytic oxidation of methane, propene, carbon monoxide and hydrogen over platinum and palladium catalysts. They used a coiled Pt wire as a heating element which was encapsulated by a support which was either γ-alumina silica or zeolite. This acted as the support for the Pd or Pt catalyst. The Pd catalyst was deposited onto the support by thermal decomposition of 0.1 M ammonium chloropalladate. A quantity of 50 μg of palladium was used. The geometric area of the catalyst bead was calculated to be 3 mm^2. The catalysts were poisoned with 40 ppm HMDS. In the case of the Pd catalyst a t_{50} value (the time taken for half of the catalytic activity to be lost) of less than 10 s was reported for both types of catalyst support. A Pt catalyst on an alumina support had an average half life of 108 +/- 40 s, considerably longer than that of a similarly prepared Pd catalyst. This result is consistent with the conclusions of Cullis and Willatt.[53] Interestingly the results showed that HMDS only had an

inhibitory effect on propene oxidation and only a negligible effect on hydrogen oxidation. It was concluded that the effect of hexamethyldisiloxane on catalytic activity depended on the type of active site involved. The authors report that in the case of a high energy site, as used in the oxidation of methane by palladium, the sites were rapidly poisoned. It was proposed that HMDS adsorbed irreversibly on to the most active catalytic sites, such as those used for the oxidation of methane or in the low temperature oxidation of propene and hydrogen oxidation. It was proposed that adsorption will lead to decomposition and the formation of a silicious adlayer. However, on low energy active sites such as those used for the oxidation of propene, reversible adsorption of HMDS occurred which inhibited catalytic activity but did not result in decomposition and irreversible poisoning of the active site. In the case of hydrogen oxidation the reaction has been shown to occur via an Eley-Rideal mechanism[130] which does not require strong chemisorption of hydrogen. They propose that the reaction may involve oxygen on active sites which are almost unaffected by HMDS.

Cullis and Willat[53] also investigated the poisoning of higher chain alkanes by HMDS. Their results are consistent with those of Gentry and Jones,[8] that HMDS had a smaller inhibitory effect on the oxidation of butane by a palladium catalyst compared to the effect on methane oxidation. It was proposed that this is a result of the lower reactivity of methane. Their proposal is consistent with that of Gentry and Jones,[8] that HMDS is irreversibly adsorbed on the high energy sites required for the oxidation of methane. Low energy sites have sufficient activity to catalyse the oxidation of more reactive longer chain alkanes such as butane, but HMDS is not irreversibly adsorbed to the surface.

Other inorganic compounds have also been shown to poison palladium catalysts. Hurtado *et al.*[124] carried out a study investigating the effect of inorganic compounds on the conversion of methane of a Pd / γ-alumina catalyst. They reported a significant decrease in methane conversion of 73.7 % upon the addition of 25 ppm H_2S. It is noted that they report a drop of 7.5% in methane conversion when no inorganic compound is added following an aging period of 50 h. This was attributed to the production of water during the reaction. A similar value was obtained for SO_2. The poisoning effect of these sulphur compounds was found to be mostly irreversible. They report that NH_3 and NO_2 give a small positive increase in

performance in the absence of sulphur compounds but have a detrimental effect in the presence of sulphur compounds.

In the case of water Hurtado *et al.*[124] found the poisoning effect to be around 14 % for a concentration of 20,000 ppm. Given the significantly larger concentration used it could be concluded that the poisoning effect of water is significantly less than that of the sulphur compounds. They also found that the poisoning effect of water was completely reversible, once the water was removed from the feed the methane conversion rate returned to the value obtained prior to its addition. It can therefore be concluded that water acts as inhibitor in the oxidation of methane over Pd catalysts.

When testing the poison resistance of catalysts for methane oxidation HMDS is generally used as the standard testing substance as it provides a source of voltatile Si compounds. HMDS will be used in these investigations to ascertain the poison resistance of H_1-e Pd films.

5.2 Poisoning of H_1-e Pd catalysts by HMDS

An investigation was carried out to determine the poison resistance of a H_1-e Pd catalyst relative to that of a 90N commercial pellistor. An H_1-e Pd catalyst was deposited onto an SRL136 header using the standard method of electrodepositing from an ammonium tetrachloropalladate Brij®56 template bath then voltammetrically cycling the Pd film in 1 M sulphuric acid. A deposition charge of 12.5 mC was passed in the electrodeposition of Pd. The device was tested in 2.5 % methane at the University of Southampton and gave a positive response. It was then powered down and stored. The device was poison tested with 20 ppm HMDS in 2.5 % methane with the assistance of Dr. G. Paxton at the City Technology laboratories several weeks later. There was no decrease in the magnitude of the methane response as a result of storage over this period of time. When exposed to the HMDS it was found that all catalytic activity was lost in a matter of seconds. This result is consistent with that obtained by Gentry and Jones.[8] They obtained a t_{50} value of less than 10 s using a palladium catalyst and using 40 ppm HMDS. It was therefore decided to use a lower concentration of HMDS. The aim was to obtain longer poisoning times so that the poisoning time contained more data points and would therefore be better defined. This would give a more accurate idea of how catalytic activity was lost, for example whether catalytic activity was lost immediately after

the addition of HMDS. Furthermore any differences in the poison resistance of different mesoporous Pd catalysts would be more clearly highlighted. The graph in fig 64 shows the response of a H_1-e Pd film to 2.5 % methane and HMDS 6 ppm in 2.5 % methane.

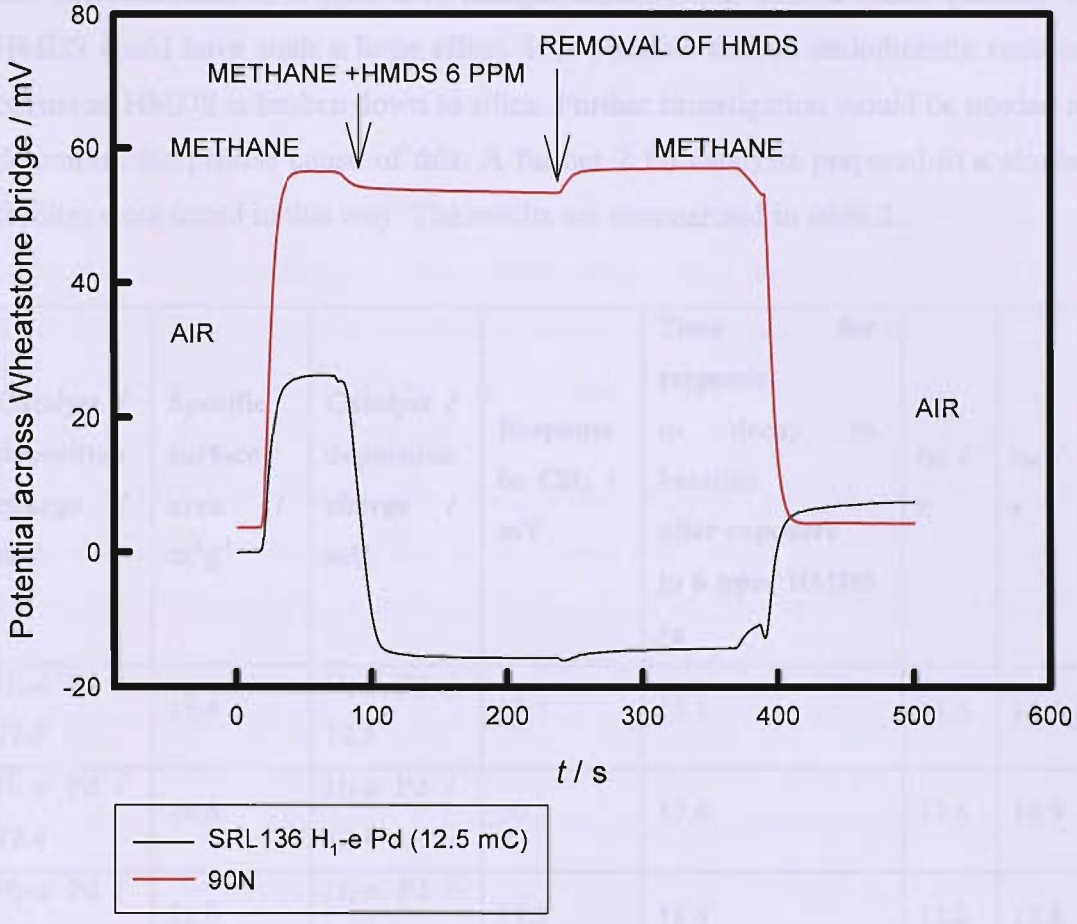

Fig 64. Response of H_1-e Pd on an SRL136 microhotplate to 2.5 % methane in air and HMDS 6 ppm. Please refer to fig 56 for preparation of the Pd film. The device was poison tested at the City Technology laboratories with the assistance of Dr. G. Paxton several weeks later.

It can be seen in fig 64 that the H_1-e Pd catalyst responds positively to methane giving a typical response of approximately 20 mV. After 70 s the methane response has stabilised and the poison, HMDS, 6ppm, was introduced to the gas flow. It can be seen that the methane activity of the Pd catalyst decreases rapidly and almost immediately, before the response stabilises at a value lower than the previous air baseline. At this stage the device is still being exposed to methane and HMDS. The lower baseline indicates that the Pd film has lost all catalytic activity and is now

giving a thermal response to methane. The activity of the 90N device falls by only 2 mV when exposed to HMDS. However, it is noted that the response of the 90N increases again when the HMDS is removed after approximately 250 s. It is not believed that this is a poisoning effect as all the evidence indicates that HMDS poisons Pd irreversibly. It is possible that HMDS has a cooling effect. Given the low concentration of 6 ppm it is thought unlikely that such a small quantity of HMDS could have such a large effect. It is possible that an endothermic reaction occurs as HMDS is broken down to silica. Further investigation would be needed to determine the precise cause of this. A further 2 Pd catalysts prepared in a similar fashion were tested in this way. The results are summarised in table 2.

Catalyst / deposition charge / mC	**Specific surface area / m^2g^{-1}**	**Catalyst / deposition charge / mC**	**Response to CH_4 / mV**	**Time for response to decay to baseline after exposure to 6 ppm HMDS / s**	**t_{50} / s**	**t_{90} / s**
H_1-e Pd / 12.5	19.4	H_1-e Pd / 12.5	13.7	15.1	11.5	14.5
H_1-e Pd / 12.4	24.8	H_1-e Pd / 12.4	10.2	17.6	13.6	16.9
H_1-e Pd / 12.5	21.0	H_1-e Pd / 12.5	17.5	18.4	12.2	17.8

Table 2. Summary of the poison resistance of H_1-e Pd catalysts. The poison used was HMDS 6 ppm in 2.5 % methane.

Table 2 shows that the specific surface areas of the Pd films are all of similar magnitude. Comparing the specific surface areas and the magnitude of the methane responses reveals there is no correlation between the two. Table two also shows the time taken for all methane activity to be lost and the t_{50} and t_{90} values. The t_{50} and t_{90} values represent the time taken for the catalysts to lose 50 and 90 % of their maximum catalytic response respectively. As well as giving a good comparison of the poison resistance of the different Pd films, these figures provide information

regarding the mechanism of how the catalytic activity is lost. For example activity may be lost rapidly at first before the rate slows down. In this case t_{50} would be relatively small and t_{90} relatively large. It can be seen that all values in table 2 are fairly similar. The similarity of the data indicates the results are accurate and therefore gives an accurate representation of the poison resistance of the H_1-e Pd catalysts. After approximately 320 s the gas supply was switched back to air, thus removing the supply of HMDS from the gas feed. Following 1 h in air the H_1-e Pd catalysts were retested in methane. All gave negative methane responses of approximately -20 mV, a similar magnitude to the response in fig 64 when the device is exposed to HMDS. The devices were tested again after a further 4 h and similar results were obtained. These results suggest that the H_1-e Pd catalysts have been irreversibly poisoned by HMDS which is consistent with the findings of Gentry and Jones[8] who reported that virtually no recovery of catalytic methane activity was observed for both Pd and Pt catalysts when poisoned by HMDS (40 ppm). A similar study by Cullis and Willatt[53] reported using palladium powder catalysts concluded that there was usually some recovery of catalytic activity. Their results show that prior to poisoning a response of 50 mV was obtained. Poisoning resulted in a complete loss of catalytic activity giving a response of 0 mV. Once HMDS was removed from the feed catalytic activity increased immediately and at an approximately linear rate. After approximately 30 min the response was approximately 8 mV. It is noted that the results obtained by Cullis and Willat indicate that no cooling effect was observed, i.e. the response falls to 0 mV in contrast to the negative value observed in fig 64. It is proposed that their catalyst might therefore still have some catalytic activity. There are two processes occurring simultaneously; the heating effect brought about by catalytic oxidation and a cooling effect due to the higher thermal capacity of methane. At 0 mV there must be some catalytic activity to counter the cooling effect of methane. If their catalyst did still have some methane activity following poisoning then this may explain the partial recovery in activity. This is contrast with the results obtained here and by Gentry and Jones [8]which both indicate no recovery of catalytic activity following poisoning by HMDS. The resistance of the H_1-e Pd catalysts to HMDS is very disappointing relative to that of the 90N and ways of improving the performance were investigated.

Poisoning by HMDS may result in silica forming on the Pd surface which may result in the pore openings becoming blocked. It is possible that rather than all active sites in the pores becoming blocked by silica, only the pore openings are blocked. If this occurs all active sites inside the pore become inaccessible to methane, thus resulting in a large decrease in catalytic activity. It was therefore proposed that creating a different catalyst structure in which the sealing of a pore opening does not cut off a large number of active sites may give an improvement in poison resistance. The cubic phase (V_1) consists of two separate, intertwined pores that have multiple openings. Consequently, the blocking of one pore opening does not result in all active sites in that pore becoming inaccessible.

5.3.1 Electrodeposition of cubic mesoporous Pd

Electrodeposited cubic mesoporous Pd will be referred to by the nomenclature V_1-e Pd. Consulting the phase diagram in fig 14 in section 3.2 it can be seen that the cubic phase exists over a narrow composition and temperature range which does not include room temperature. This poses no problems for the electrodeposition onto standard 1 mm diameter Au disc electrodes as the deposition can simply be thermostatically controlled using a flow cell. However, electrodeposition onto the devices is inherently more difficult. The deposition was carried out in an oven thermostatically controlled to 41°C +/- 2°C. This margin of error was acceptable as it does not pose the risk of entering a different phase. Electrodeposition was carried out by potential step from 0.4 to 0.1 V vs. SCE. An example of a current transient is shown in fig 65.

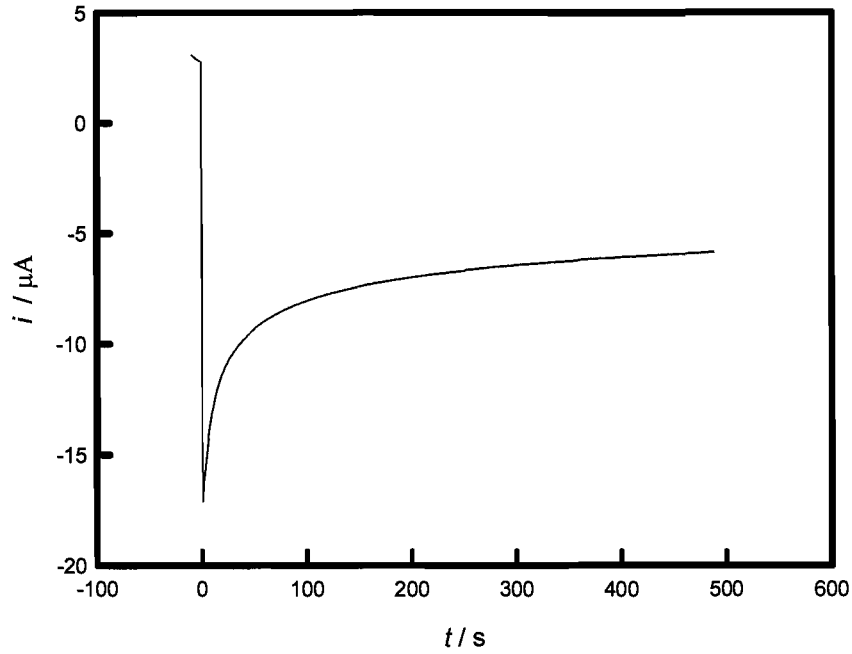

Fig 65. Graph showing the electrodeposition of V_1-e Pd onto an SRL 136 microhotplate at 40 °C. Deposition was carried out by potential step from 0.4 to 0.1 V vs. SCE. The template mixture consisted of 73 wt. % Brij®56, 3 wt % heptane, 17 wt % water and 7 wt % ammonium tetrachloropalladate.

Fig 65 shows that the peak current for the electrodeposition of V_1-e Pd onto a microhotplate is higher than that of the deposition of H_1-e Pd as shown in fig 48 but is of a similar order of magnitude. The viscosity of the deposition mixture in the cubic phase was significantly lower than that in the hexagonal phase. Indeed the mixture was sufficiently fluid that it was able to flow over the device surface. This had the advantage that it helped to ensure the electrode area was completely covered.

The lower viscosity of the template mixture did cause problems. The success rate of the deposition of V_1-e Pd onto microhotplates was very low at around 10 %, compared to around 95 % for the H_1-e Pd. The template mixture flowed over the surface of the device and came into contact with the wire contacts. Many of the current transients had large current spikes and jumps. Some of the deposition current transients had significant amounts of electrical noise, though this could be due to the fan and other electrical equipment inside the oven.

5.3.2 Characterisation of V_1-e Pd

Following electro-deposition the V_1-e Pd film was washed thoroughly in iso-propanol to remove all surfactant from the pores and also to clean the membrane. The Pd film was then voltammetrically cycled in 0.1 M sulphuric acid. The cyclic voltammogram was very similar to those obtained from H_1-e Pd films. The V_1-e Pd film was then rinsed in purified water and dried in an oven at 40 °C prior to gas testing.

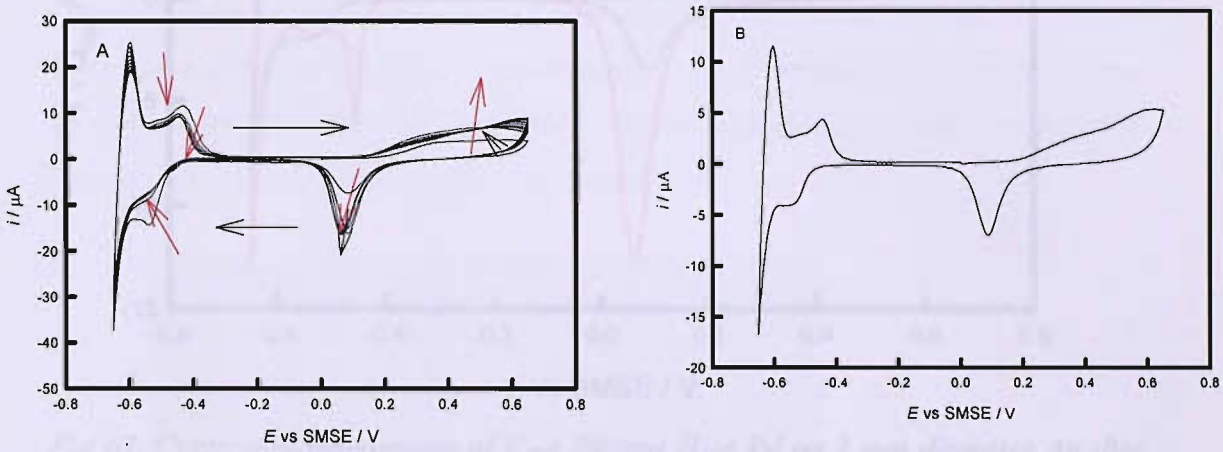

Fig 66a. A cyclic voltammogram of V_1-e Pd on a 1 mm diameter Au disc electrode in 1 M sulphuric acid. A scan rate of 20 mV / s was used. The graph shows the first ten voltammetric cycles. The electrodeposition is described in fig 65. Fig 66b. Cyclic voltammogram of the same V_1-e Pd film at a scan rate of 10 mV / s. The 11^{th} voltammetric cycle is shown. The red arrows indicate the trend in the cyclic voltammograms and the black arrow the sweep direction.

The surface area was calculated from the charge under the oxide stripping peak of fig 66a using the Rand and Woods constant[109] to be 17 $m^2 g^{-1}$ which is comparable to that of the H_1-e Pd films. Fig 66a shows cyclic voltammograms of V_1-e Pd on a 1 mm diameter Au disc electrode. It can be seen that the surface area increases significantly after the first voltammetric cycle, then stabilises. The resolution of the peaks in the hydride region at -0.5 V and -0.65 V vs. SMSE on the back scan and at -0.6 and -0.4 V vs. SMSE on the forward scan support the existence of a nanostructure as these features are not seen on non-nanostructured Pd films. It was

decided to overlay cyclic voltammograms of H_1-e Pd and V_1-e Pd for means of comparison.

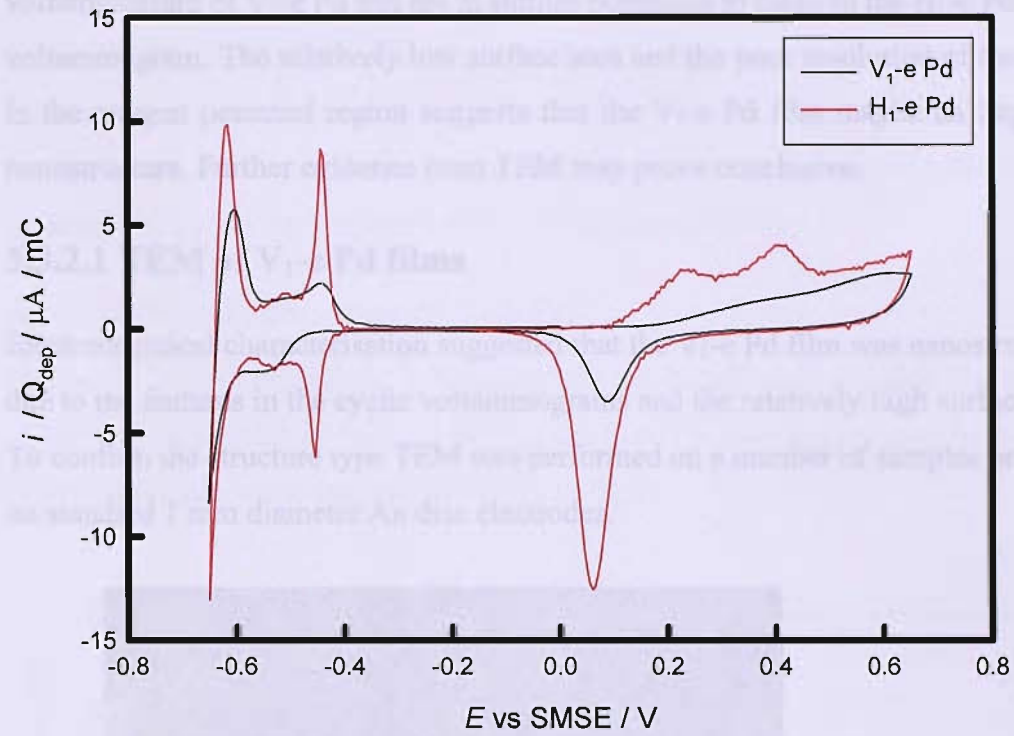

Fig 67. Cyclic voltammograms of V_1-e Pd and H_1-e Pd on 1 mm diameter Au disc electrodes in 1 M sulphuric acid. A scan rate of 20 mV / s was used in each case. The graph shows the eleventh voltammetric cycle in each case. The electrodeposition of the V_1-e Pd is described in fig 65. The H_1-e Pd was electrodeposited from a template mixture consisting of 47 wt. % Brij®56, 2 wt % heptane 12 wt % $(NH_4)_2$ $PdCl_4$ and 39 wt % water. A deposition charge of 3.5 mC was passed in the electrodeposition of the H_1-e Pd whilst 2.0 mC was passed in the electrodeposition of the V_1-e Pd..

Fig 67 shows the cyclic voltammograms of H_1-e Pd and V_1-e Pd on 1 mm diameter Au disc electrodes in 1 M sulphuric acid. As a lower deposition charge was used for the electrodeposition of H_1-e Pd it was decided to plot current / deposition charge for a fair comparison. The specific surface area of the H_1-e Pd film was calculated to be approximately 31 m^2 g^{-1}, whilst that of the V_1-e Pd was calculated to be approximately 7 m^2 g^{-1}. It is noted that this is significantly less than that obtained from the V_1-e Pd film in fig 66a. It can be seen that the H_1-e Pd has a significantly larger surface area. The cyclic voltammogram of the V_1-e Pd film does not contain

the two well resolved in the oxygen potential region present in the cyclic voltammogram of H_1-e Pd at 0.2 and 0.4 V vs. SMSE on the forward scan. However, the peaks in the hydrogen potential region are well resolved in the cyclic voltammogram of V_1-e Pd and are at similar potentials to those in the H_1-e Pd cyclic voltammogram. The relatively low surface area and the poor resolution of the peaks in the oxygen potential region suggests that the V_1-e Pd film maybe an imperfect nanostructure. Further evidence from TEM may prove conclusive.

5.3.2.1 TEM of V_1-e Pd films

Electrochemical characterisation suggested that the V_1-e Pd film was nanostructured due to the features in the cyclic voltammograms and the relatively high surface area. To confirm the structure type TEM was performed on a number of samples prepared on standard 1 mm diameter Au disc electrodes.

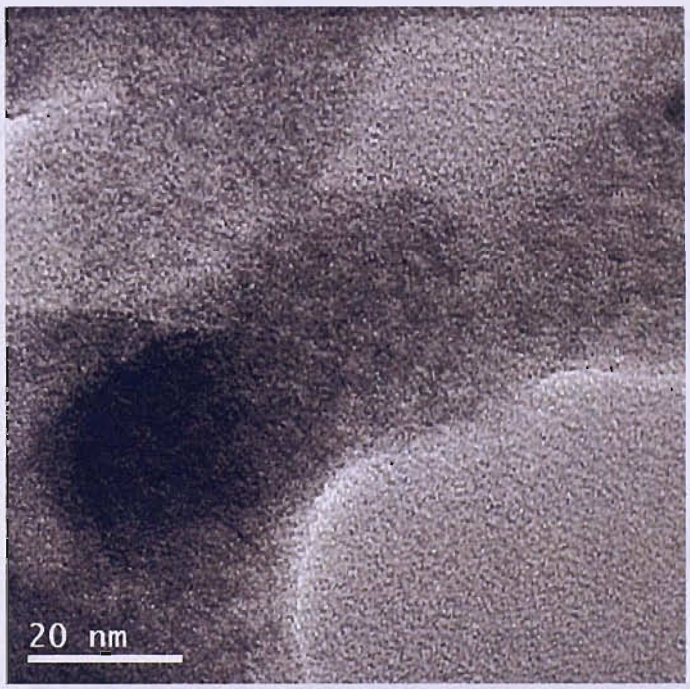

Fig 68. TEM image of a V_1-e Pd film. For details of the electrodeposition please refer to fig 65. A deposition charge of 0.40 μC / cm^2 was used.

The TEM image shown in fig 68 shows that some parts of the film are mesoporous, in particular the dark area above and to the right of the scale bar. The TEM does not confirm that the film has a regular nanostructure. It can be seen that the sample is very thin. In previous attempts at obtaining TEM images of V_1-e Pd the sample was

too thick to obtain an image. For this reason a thinner Pd film was deposited by passing a smaller charge in the electrodeposition. From the TEM the pore size was calculated to be approximately 2.6 nm and the pore separation approximately 2.4 nm. The evidence here does not confirm that a mesoporous cubic structure has been obtained. The cyclic voltammogram in fig 67 suggests that the film has some nanostructure but the relatively low surface area suggests an imperfect nanostructure has been produced. The TEM shows that some parts of the film are mesoporous but do not confirm a well ordered nanostructure.

5.3.3 Methane response of V_1-e Pd

Following electrodeposition, removal of the surfactant and carrying out an acid cyclic voltammogram of the V_1-e Pd film the film was methane tested. The response of a V_1-e Pd catalyst to methane is shown in fig 69.

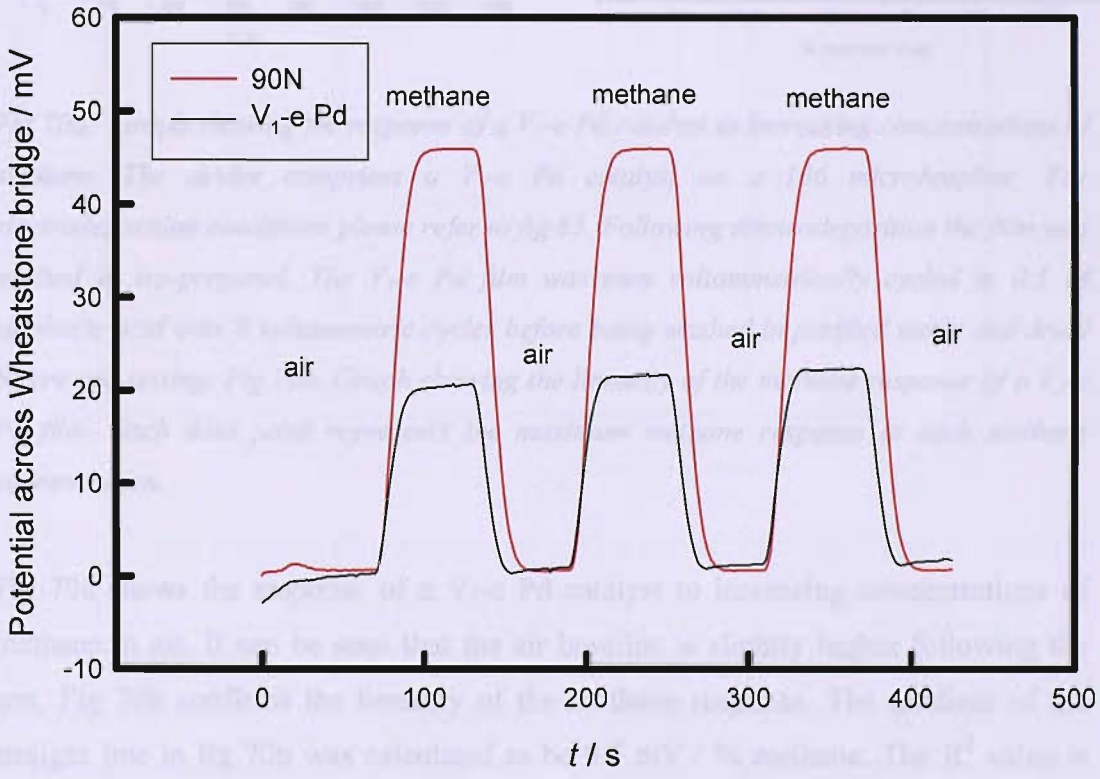

Fig 69. Methane response of a V_1-e Pd film. For deposition conditions please refer to fig 65, a deposition charge of 3.5 mC was passed. The device was powered in air for 1 h prior to methane testing at a gas flow rate of 400 cm^3 min^{-1}. Specific surface area was calculated to be 18 m^2g^{-1} using the charge under the oxide stripping peak and the Rand and Wood's constant.

Fig 69 shows the response of a V_1-e Pd film on an SRL136 microhotplate to methane. It can be seen that the response is of average magnitude at around 20 mV. This is similar to that of H_1-e Pd catalysts. The methane responses are reproducible and stable. The V_1-e Pd catalyst was then tested with different concentrations of methane in air to investigate the linearity of the response to methane concentration.

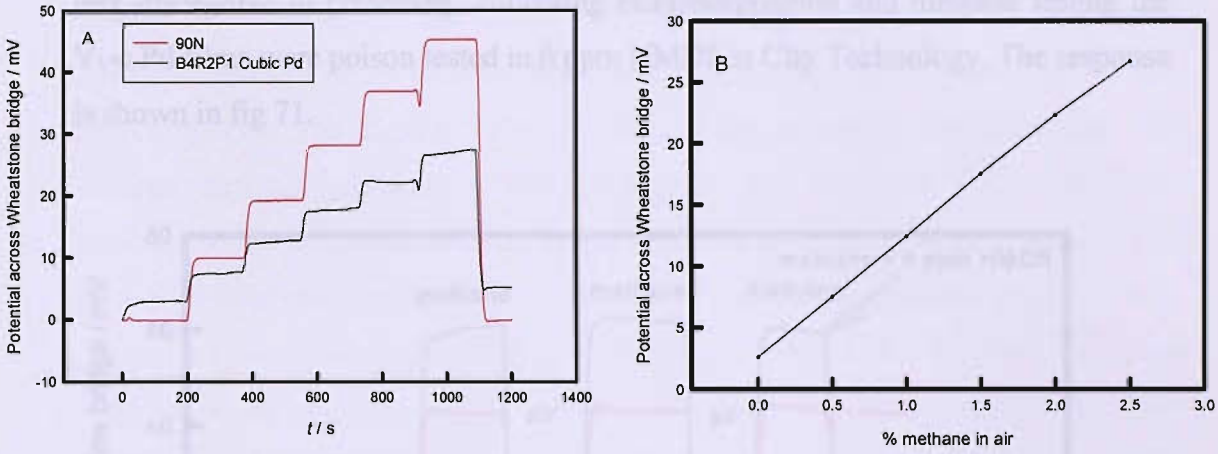

Fig 70a. Graph showing the response of a V_1-e Pd catalyst to increasing concentrations of methane. The device comprises a V_1-e Pd catalyst on a 136 microhotplate. For electrodeposition conditions please refer to fig 65. Following electrodeposition the film was washed in iso-propanol. The V_1-e Pd film was then voltammetrically cycled in 0.1 M sulphuric acid over 8 voltammetric cycles before being washed in purified water and dried before gas testing. Fig 70b. Graph showing the linearity of the methane response of a V_1-e Pd film. Each data point represents the maximum methane response at each methane concentration.

Fig 70a shows the response of a V_1-e Pd catalyst to increasing concentrations of methane in air. It can be seen that the air baseline is slightly higher following the test. Fig 70b confirms the linearity of the methane response. The gradient of the straight line in fig 70b was calculated to be 9.7 mV / % methane. The R^2 value is 0.999, confirming the catalyst has a linear response to methane. The gradient of the linear regression is very similar to the average gradient obtained for H_1-e Pd, discussed in section 4.6.4.4., which was calculated to be 8.5 mV / % methane. The average value for the H_1-e Pd from a chlorine free Pd template bath was 16.4 mV / % methane.

It was difficult to produce reproducible V_1-e Pd films mainly due to the flow of the template mixture. For this reason it was only possible to produce a few working devices with V_1-e Pd films.

5.3.4 Poison testing of V_1-e Pd

The motivation for producing V_1-e Pd films was to investigate the poison resistance to HMDS relative to a H_1-e Pd film. It was hoped that a different structure may be less susceptible to poisoning. Following electrodeposition and methane testing the V_1-e Pd films were poison tested in 6 ppm HMDS at City Technology. The response is shown in fig 71.

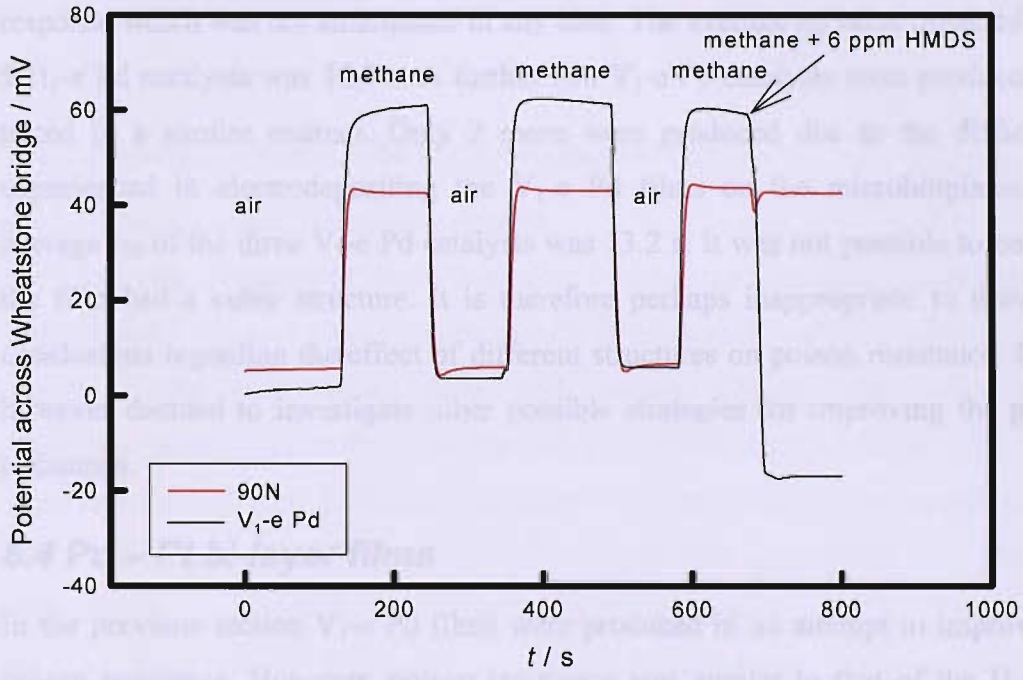

Fig 71. Graph showing the response of a V_1-e Pd catalyst (B4R2P1) to methane and HMDS. The device comprises a V_1-e Pd film on a 136 microhotplate. Cubic Pd was electrodeposited by potential step from 0.4 to 0.1 V vs. SCE at 40 °C. A deposition charge of 3.5 mC was passed. The catalyst was washed in iso-propanol following deposition to remove the surfactant. The catalyst was then voltammetrically cycled in 0.1 M sulphuric acid before being washed in purified water and dried before gas testing. Following methane testing the device was poison tested using 6 ppm HMDS in methane.

Fig 71 shows that when exposed to 6 ppm HMDS the V_1-e Pd film quickly loses all catalytic activity. The response falls below the previous air baseline, indicating that

the device is now giving a thermal response. It can be seen that the response of the V_1-e Pd in methane and HMDS is approximately -20 mV. A similar characteristic was observed in the poisoning of H_1-e Pd films by HMDS shown in fig 64. Fig 71 shows that the V_1-e Pd film lost all catalytic activity in 16 s. The t_{50} value was calculated to be 12 s and the t_{90} 14 s. The maximum methane response was 54 mV. The magnitude of the methane response is larger than that of a typical standard H_1-e Pd catalyst response of around 20 – 30 mV, however the average methane response of V_1-e Pd catalysts was still in the 20-30 mV range, though only five responses were obtained due to the inherent difficulties in producing the V_1-e Pd films on the microhotplates. The similar value of the average responses indicaties that the different structure did not on average improve the magnitude of the methane response which was not anticipated in any case. The average t_{50} value obtained from 5 H_1-e Pd catalysts was 12.7 s. A further two V_1-e Pd catalysts were produced and tested in a similar manner. Only 2 more were produced due to the difficulties experienced in electrodepositing the V_1-e Pd films on the microhotplates. The average t_{50} of the three V_1-e Pd catalysts was 13.2 s. It was not possible to confirm the film had a cubic structure. It is therefore perhaps inappropriate to draw any conclusions regarding the effect of different structures on poison resistance. It was however decided to investigate other possible strategies for improving the poison resistance.

5.4 Pd – Pt bi-layer films

In the previous section V_1-e Pd films were produced in an attempt to improve the poison resistance. However, poison resistance was similar to that of the H_1-e Pd catalysts. Other methods of improving the poisoning were therefore considered. One proposed solution was to protect the mesoporous Pd film with a protective layer. The silica may adsorb on to the top layer, leaving the Pd catalyst unaffected. The H_1-e Pd catalyst has a nanostructure consisting of a hexagonal array of pores each having a diameter of approximately 2.5 nm. The top layer would have to allow methane access to the Pd layer, thus a macroporous or a second nanostructured layer would be required. In previous work at the University of Southampton, H_1-e Rh was electrodeposited on top of H_1-e Pd by Marwan,[69 PhD thesis] who reported that the pores of the two layers interconnected. In this case it was decided to electrodeposit H_1-e Pt

on top of the H_1-e Pd layer to mimic the protection afforded to Pd in commercial pellistors.

5.4.1 Electrodeposition

The bi-layer was produced by electrodepositing a layer of H_1-e Pd onto the gold electrode, removing the surfactant, then applying the Pt template mixture on top of the H_1-e Pd. The Pt was then electrodeposited. A deposition charge of 5 mC was passed for the electrodeposition of each metal. The Pd was electrodeposited by applying a potential step of 0.4 to 0.1 V vs. SCE. The potential required for the electrodeposition of Pt was verified by carrying out a cyclic voltammogram of the Pt template mixture on a H_1-e Pd film on an Au 1 mm electrode. It was concluded that a potential of -0.1 V, as used for the electrodeposition of H_1-e Pt onto Au was suitable.

5.4.2 Characterisation of Pd-Pt bi-layer film

5.4.2.1 Electrochemical characterisation

A cyclic voltammogram of the bi-layer film in acid was undertaken to demonstrate that the electrolyte had access to both metals. If this was the case the voltammogram would contain contributions from both metals. Fig 72 shows the cyclic voltammograms of H_1-e Pd, H_1-e Pt and H_1-e Pd-Pt bi-layer films. The cyclic voltammogram of H_1-e Pd has a very sharp oxide stripping peak at approximately 0.45 V vs. SCE. The same feature in the cyclic voltammogram of the H_1-e Pt film is shifted to approximately 0.55 V vs. SCE and is considerably broader. The feature in the H_1-e Pd-Pt bi-layer film has characteristics of both films. The peak occurs at a potential between that of the Pd and Pt films and is broader than in the cyclic voltammogram of H_1-e Pd. This indicates that the electrolyte is in contact with both the Pd and Pt and therefore the pores in the bi-layer interconnect. Furthermore the charge passed in the oxide deposition and stripping for the H_1-e Pd-Pt bi-layer is larger indicating a larger surface area. Further evidence that both metals are in contact with the electrolyte is the larger double layer charging charge and the larger charge involved in the hydrogen region.

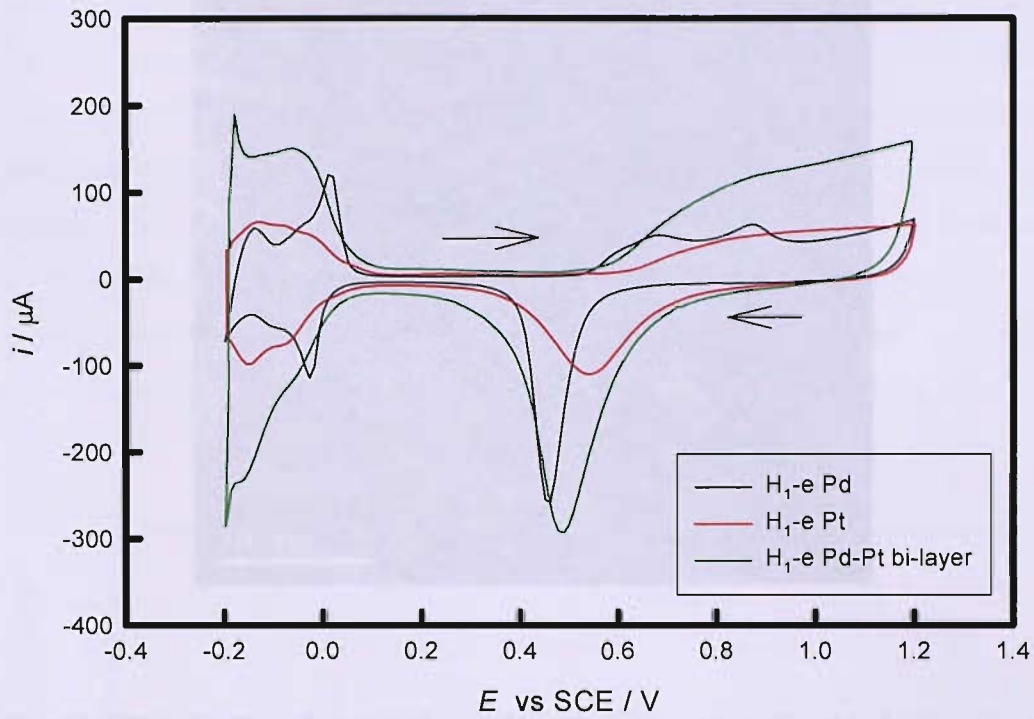

Fig 72. Cyclic voltammograms of H_1-e Pd, H_1-e Pt and H_1-e Pd-Pt bi-layer films in 1 M sulphuric acid. The Pd was electrodeposited by applying a potential step of 0.4 to 0.1 V vs. SCE. The H_1-e Pt was electrodeposited by applying a potential step from 0.5 to -0.1 V vs. SCE. A deposition charge of 5 mC was passed in each case. The H_1-e Pd-Pt bi-layer film was prepared by first electrodepositing H_1-e Pd then removing the surfactant with iso-propanol. The H_1-e Pt was then electrodeposited on top of the H_1-e Pd.

5.4.2.2. Characterisation by TEM

Electrochemical characterisation showed that the pores of the bi-layer film were interconnected as the acid cyclic voltammograms contained characteristic features of both Pd and Pt. A H_1-e Pd-Pt bi-layer film was prepared for inspection with TEM to confirm that the film was nanostructured.

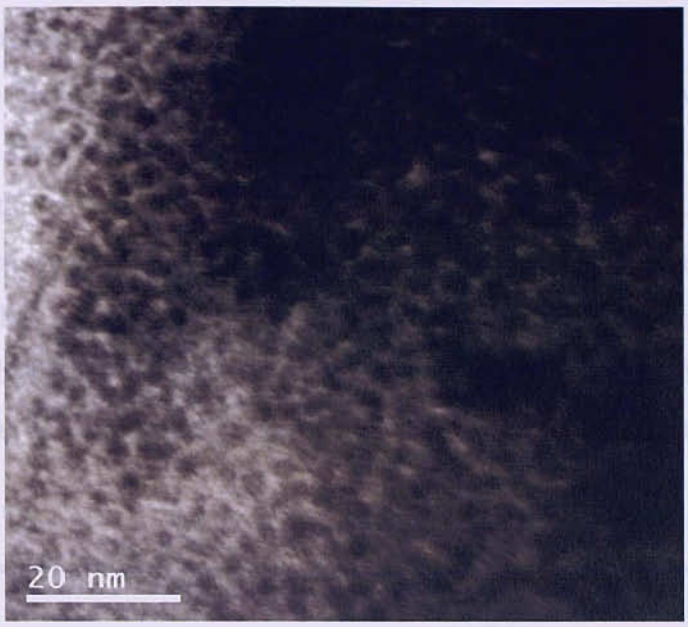

Fig 73 TEM of a H_l-e Pd-Pt bi-layer film. For deposition details please refer to fig 72. A deposition charge of 0.28 μC cm^{-2} was passed for both Pd and Pt.

Fig 73 shows a TEM of an H_l-e Pd-Pt bi-layer film. The pores can clearly be seen, though this image does not confirm a regular arrangement of pores in this part of the structure.

5.4.3 Methane testing of Pd-Pt bi-layer film

Platinum is also used as a catalyst for the oxidation of methane. However, Pt catalysts operate optimally at a higher temperature than Pd. Trimm and Lam[131] reported an operating range of 773 – 853 K for a Pt catalyst. The Pd catalysts produced here are heated to approximately 773 K, which is towards the upper end of the micro-hotplate's temperature range. An H_l-e Pt film was electrodeposited onto a microhotplate. The template mixture comprised 1 part by weight hexachloroplatinic acid to 1 part by weight water to 1.5 parts by weight Brij®56. Electrodeposition was carried out by applying a potential step of 0.4 to -0.1 V vs. SCE, a deposition charge of 3.5 mC was passed. The film was then washed in iso-propanol for 1 h then voltammetrically cycled in 1 M sulphuric acid over 8 voltammetric cycles. Using the same voltage from the power supply unit of 15 V to give the same temperature a methane response of -22 mV was obtained. The shape and magnitude of the

response was similar to that of a bare Au electrode shown in section 4.5.1. figs 35 and 36. The power supplied to the device was increased from 15 V to 16 V, close to the maximum for the device. A methane response of -16 mV was obtained, indicating that the Pt film had greater activity at this temperature, but that the total magnitude of the catalytic response was still less than the thermal response. It can therefore be reasonably assumed that at the standard temperature used there would be very limited, if any, methane activity from the Pt in the Pd-Pt bi-layer.

A H_1-e Pd-Pt bi-layer film was prepared on an SRL136 microhotplate and methane tested following 15 min powered up in air. The response is shown in fig 74.

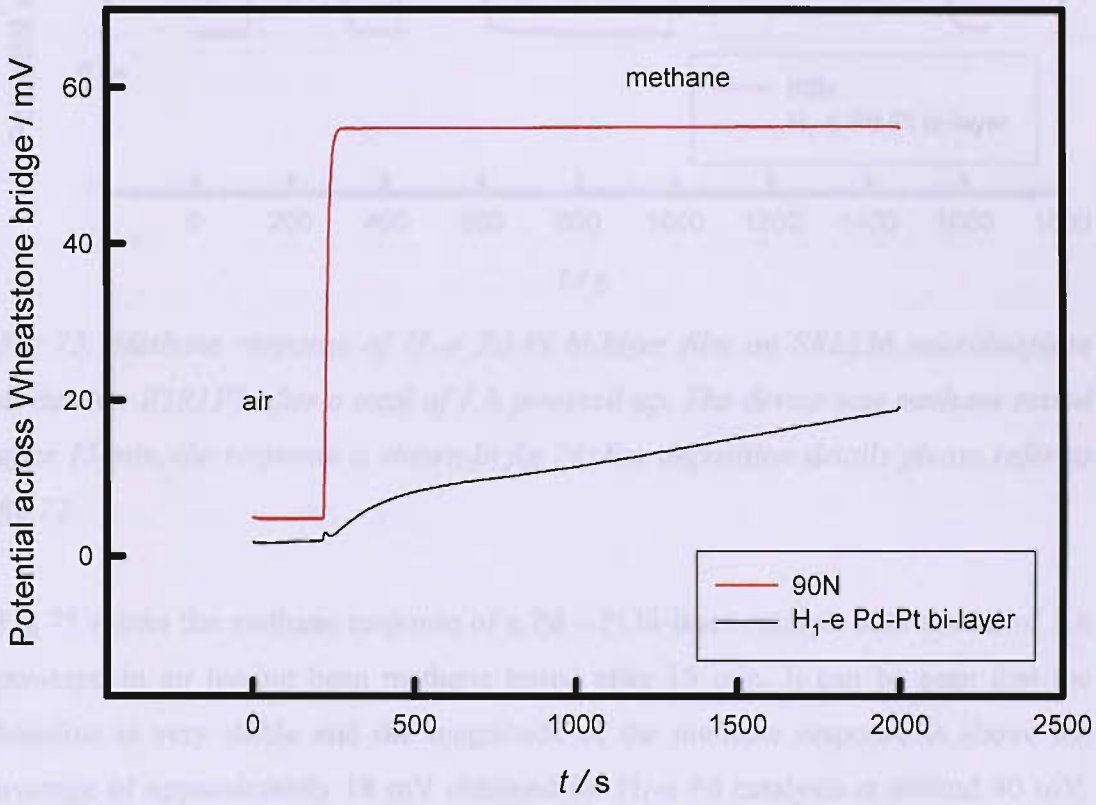

Fig 74. Methane response of an H_1-e Pd-Pt bi-layer film on SRL136 microhotplate device no. B3R1P7 after 15 min in air. For deposition details please refer to fig 72.

Fig 74 shows the catalytic activity of the Pd-Pt bi-layer film increasing with time. This is similar to the behaviour exhibited by H_1-e Pd catalysts. The device was powered in air for a further 45 min after which it was retested. The methane response is shown in fig 75.

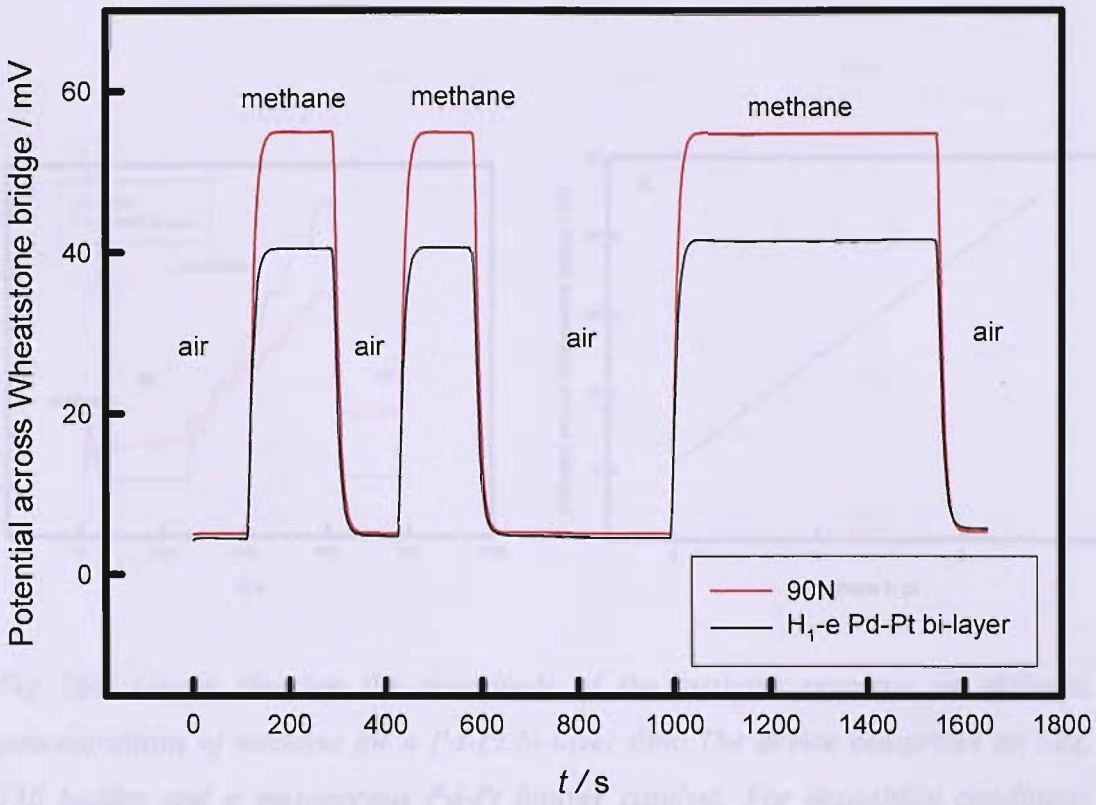

Fig 75. Methane response of H_1-e Pd-Pt bi-layer film on SRL136 microhotplate device no. B3R1P7 after a total of 1 h powered up. The device was methane tested after 15 min, the response is shown in fig 74. For deposition details please refer to fig 72.

Fig 75 shows the methane response of a Pd – Pt bi-layer catalyst after a total of 1 h powered in air having been methane tested after 15 min. It can be seen that the baseline is very stable and the magnitude of the methane response is above the average of approximately 18 mV obtained for H_1-e Pd catalysts at around 40 mV. The surface area of the Pd film was calculated prior to electrodeposition of the Pt layer to be 26 m^2g^{-1}. This is of similar magnitude to the surface area of H_1-e Pd films. This suggests that the larger methane response is not a result of an increased surface area. The methane responses are stable and reproducible.

The H_1-e Pd-Pt bi-layer film was then tested at different concentrations of methane to investigate the linearity of the response over the methane concentration range. The graph and linear fit are shown in figs 76a and 76b.

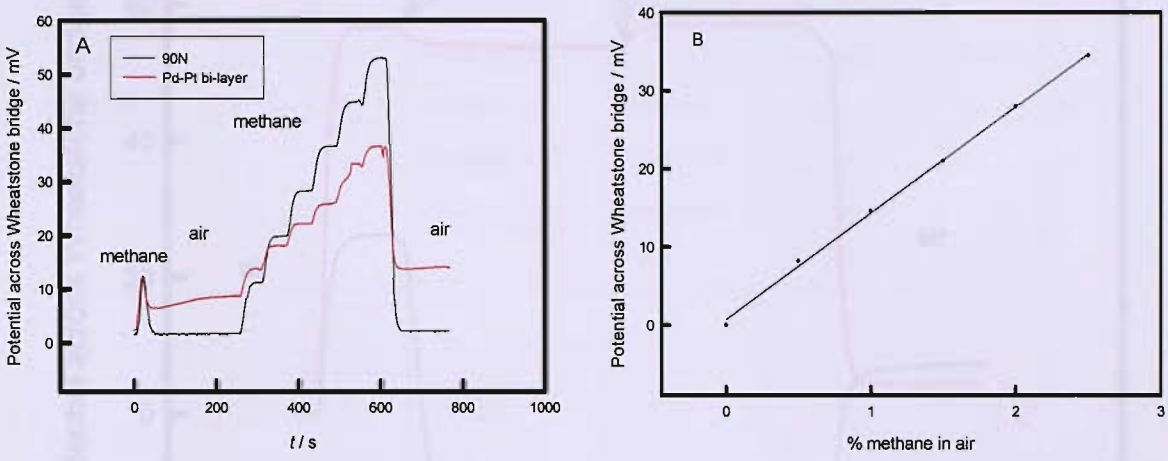

Fig 76a. Graph showing the magnitude of the methane response at different concentrations of methane for a Pd-Pt bi-layer film. The device comprises an SRL 136 header and a mesoporous Pd-Pt bilayer catalyst. For deposition conditions please refer to fig 75. Following electrodeposition the bi-layer film was washed in isopropanol for 1 h before being voltammetrically cycled in 1 M sulphuric acid over 8 cycles. Fig 74b shows the maximum methane response at each concentration along with a linear fit of the data.

Fig 76a shows that the magnitude of the methane response increases fairly linearly with methane concentration. The R^2 value of the data to the line of best fit is 0.990, confirming the catalyst has a linear response to increasing concentrations of methane.

5.4.4 Poison resistance of mesoporous Pd-Pt bi-layer catalyst

The motivation for developing the bi-layer catalyst was that it may offer an improved resistance to HMDS due to the Pt top layer preferentially adsorbing the silica, leaving the catalytically active Pd layer unaffected. Following methane testing the Pd-Pt bi-layer catalyst was poison tested at City Technology labs. The response to HMDS is shown in fig 77.

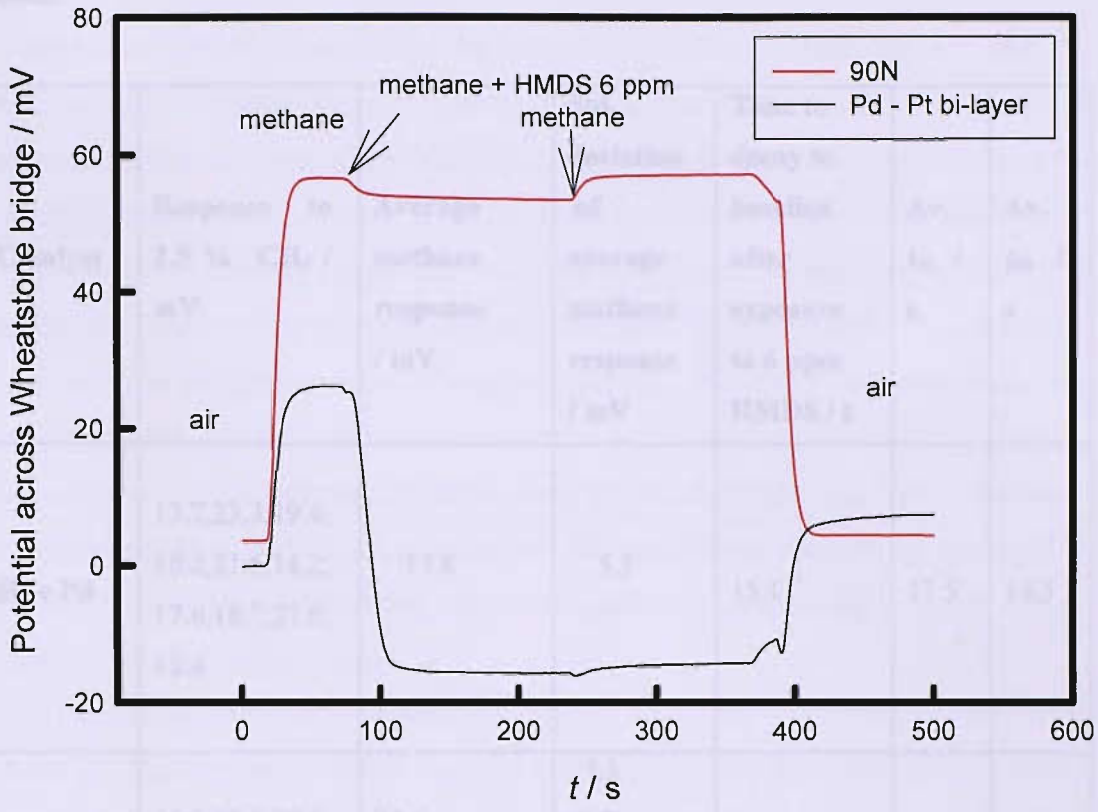

Fig 77. Response of H_1-e Pd-Pt bi-layer film on an SRL136 microhotplate to methane and HMDS 6 ppm. For deposition conditions please refer to fig 75. Following electrodeposition the bi-layer film was washed in isopropanol for 1 h before being voltammetrically cycled in 1 M sulphuric acid over 8 cycles. The film was then washed in purified water and allowed to dry. The device was exposed to methane upon which a positive response was recorded. The device was exposed to HMDS 6 ppm in methane immediately following a positive response to methane.

Fig 77 shows the response of a Pd-Pt bi-layer catalyst to methane and HMDS (6ppm). It can be seen that all methane activity is rapidly lost and the response stabilises at a value below the previous air baseline. This indicates that all catalytic activity has been lost and the response to methane is purely thermal. This is similar to the results obtained with H_1-e Pd and V_1-e Pd catalysts. It is noted that there is a small drop in the response of the 90N during exposure to methane and HMDS. It is proposed that this is most likely a flow rate effect but may be to an endothermic reaction involving HMDS.

The results in table 3 summarise the poisoning times of the different catalyst types used.

Catalyst	Response to 2.5 % CH_4 / mV	Average methane response / mV	Std. deviation of average methane response / mV	Time to decay to baseline after exposure to 6 ppm HMDS / s	Av. t_{50} / s	Av. t_{90} / s
H_1-e Pd	13.7,23.3,19.4, 10.2,21.6,14.2, 17.6,18.7,27.0, 12.4	17.8	5.3	15.1	11.5	14.5
Pd – Pt bi-layer	13.9,39.0,29.1, 28.7,21.8,29.6, 33.4,22.3,32.8, 35.6,	28.6 (30.2 excluding 13.9 mV result)	7.5 (5.7 excluding 1st result of 13.9 mV)	27.0	20.5	26.0
V_1-e Pd	7.6, 22.4, 19.8, 26.7, 12.4	17.8	7.7	16.5	12.2	14.8

Table 3. Summary of results of methane testing and poison testing of mesoporous catalysts on microhotplate devices.H_1-e Pd catalysts were electrodeposited by potential step from 0.4 to 0.1 V vs. SCE. A deposition charge of 5 mC was passed. Pd-Pt bi-layer catalysts were electrodeposited using a potential step of 0.4 to 0.1 V vs. SCE for the Pd and 0.4 to -0.1 V vs. SCE for the Pt. A deposition charge of 5 mC was passed for each layer. V_1-e Pd films were electrodeposited at 40°C by potential step from 0.4 to 0.1 V vs. SCE, a deposition charge of 5 mC was passed. In all cases Brij®56 was used as the surfactant.

The results in table 3 summarise the magnitude of the methane response and the time taken for all catalytic activity to be lost in 6 ppm HMDS in 2.5 % methane. It is noted that the average of the methane responses of the H_1-e and V_1-e Pd films are identical. The average methane response of the H_1-e Pd-Pt bi-layer catalysts is 60 % higher which represents a significant increase. It is noted that the standard deviation of the magnitude of the methane responses for H_1-e, V_1-e Pd and the H_1-e Pd-Pt bi-layer catalyst are fairly similar. It was proposed that the H_1-e Pt layer would have a negligible direct contribution to the catalytic activity of the bi-layer as Pt catalysts have been shown to operate optimally at temperatures higher than those used here. Experiments were carried out to determine the contribution from Pt by testing H_1-e Pt films. The results showed that they were inactive to methane at the temperatures used in these investigations.

The implications of adding an inactive layer on top of the catalyst were considered. Adding a Pt layer results in the methane molecules having further to travel to reach the Pd layer. If the reaction is mass transport limited inside the pores then this should result in a reduction in the rate of reaction. However, it can be seen that this is not the case. A common method for preparing palladium catalysts is by impregnating a support with a Pd precursor. The role of the support is to allow for the dispersal of the catalyst in its active state and to provide mechanical strength. The support can also contribute to the catalytic activity by reacting with or modifying the catalyst.

Whilst most of the research has focussed on the effect of the catalyst support there are some examples of work involving bimetallic systems in which Pd is used typically with a member of the platinum group.[114] Yamamoto and Uchida[132] investigated Pd-Pt catalysts on an alumina support in a gas mixture containing 3000 ppm hydrocarbon, 5 vol. % O_2 and approximately 14 vol. % water at 385 °C. The bimetallic catalyst was compared with Pd and Pt catalysts prepared using a similar method. The results showed a significant improvement both in terms of catalytic activity and durability. It is noted that the catalysts exhibited different behaviour with time powered up. The Pd catalyst on the alumina support initially lost 60 % of catalytic activity. After 15 h a conversion rate of 10 % was reported. The Pd-Pt catalyst again showed an initial loss of activity but this stabilised at a 50 %

conversion rate. Conversely, the Pt catalyst had lower initial activity but this had a constant conversion rate of 20 %. The results showed that increasing the amount of Pd resulted in an improvement in terms of both durability and activity. It was found that the promoting effect of Pt on catalytic activity was not related to the amount of Pt present. It was proposed that the higher durability was due to Pt preventing the sintering of Pd.

A similar study was carried out by Narui *et al.*[133] Catalysts comprising 0.5 wt. % Pd / Al_2O_3 and 0.5 wt. % Pd- 0.1 wt. % Pt / Al_2O_3 were prepared by impregnation of the alumina support with Pd and Pt acetylacetonate. The catalysts were tested in 0.5 vol. % methane in air. The results were consistent with those of Yamamoto in that the addition of Pt increased catalytic durability. Over 6 h catalytic activity of the Pd catalyst fell from a peak of around 89 % methane conversion obtained after 50 min on stream, to an approximate 50 % conversion rate after 6 h. The Pd-Pt / Al_2O_3 catalyst achieved a peak methane conversion rate of 98 % after approximately 15 min. This conversion rate was then maintained over 6 h. The authors investigated the bimetallic system using *ex situ* and *in situ* TEM measurements. It was concluded that the improved performance was due to a higher dispersion of the Pd-Pt particles and a reduction of particle growth. It is however noted that these investigations were carried out under vacuum and therefore under significantly different conditions.

Persson *et al.*[134] also investigating the methane activity of bi-metallic Pd-Pt catalysts. The results showed that the Pd catalyst had higher initial activity but this was rapidly lost. The Pd-Pt catalyst had lower initial activity but then exhibited little loss in activity. The improved long term response of the bimetallic catalyst is consistent with the results obtained by Narui *et al.*[133] However, the lower initial catalytic activity is not consistent with the results obtained here and those of Yamamoto and Uchida.[132]

The results in table 3 are consistent with those of Narui *et al.* in that the addition of Pt promotes the activity of a Pd catalyst. It is however still unclear exactly how Pt promotes the activity of a Pd catalyst. Considering the results of Narui and Yamamoto it seems clear that Pt promotes the long term response of the Pd catalyst. Earlier the loss of activity was discussed and it was suggested that this was a result of Pd conversion to PdO. It is possible that Pt prevents the conversion of Pd to PdO which may explain the improved long term response. It is possible that there is an

interaction effect which alters the state of the Pd film. It was first thought that as the film was a bi-layer any effect would be limited to the boundary between the two metals. However, at operating temperatures of 500°C there is likely to be a significant flux of Pt into the Pd bulk. Bartlett and Marwan[135] carried out an investigation in which small amounts of Pt were added to a H_I-e Pd film. The results showed that the addition of the Pt layer resulted in a significant increase in the rate of hydrogen absorption under electrochemical conditions. It was also noted that hydrogen adsorption was blocked by the presence of Pt on the surface. Finally it was noted that the addition of 0.3 monolayers of Pt resulted in the rate of electrochemical hydrogen evolution almost doubling. The effect of Pt could be further investigated by producing a Pd-Pt binary catalyst. This may result in a significant increase in the amount of Pd-Pt interaction and may further improve the magnitude and reproducibility of the methane response.

Table 3 shows that relative to the H_I-e Pd catalyst the Pd-Pt bi-layer catalyst has significantly improved the modest poison resistance. The Pt layer increases the poison resistance of the H_I-e Pd catalyst by 79 %. It is noted that the total thickness of the film has doubled as the same charge was used in the Pd and Pt layers as was used in the single Pd layer. However, it was decided most appropriate to keep the charge of the Pd layer the same, rather than halving the amount of Pd as in this way the total amount of catalytically active Pd was kept the same. As the thickness has doubled it will take the HMDS twice as long to reach the Pd which may account for the increased time taken to poison the catalyst. This implies that poisoning is limited by mass transport inside the pores. In order to investigate whether the increased thickness or the Pt layer were responsible for the increased poison resistance a further 5 H_I-e Pd-Pt bi-layer catalysts were produced with a total film thickness similar to that of the single layer H_I-e Pd films. The results are shown in table 4.

Catalyst	Charge passed in electro-deposition of each layer / mC	Response to CH_4 / mV	Average methane response / mV	Standard deviation of average methane response	Time to decay to baseline / s	Av. t_{50} / s	Av. t_{90} / s
H_1-e Pd-Pt bi-layer	2.5	28.7, 29.4, 34.5, 22.1, 35.8	30.1	2.4	23.5	16.5	22.0
H_1-e Pd–Pt bi-layer	5.0	13.9, 39.0, 29.1, 28.7, 21.8, 29.6, 33.4, 22.3, 32.8, 35.6,	28.6 (30.2 excluding 13.9 mV result)	7.5 (5.7 excluding 1st result)	27.0	20.5	26.0

Table 4 Summary of results of methane testing and poison testing of H_1-e Pd-Pt bi-layer catalysts. The bi-layer catalysts were electrodeposited using a potential step of 0.4 to 0.1 V vs. SCE for the Pd and 0.4 to -0.1 V vs. SCE for the Pt. A deposition charge of 2.5 mC was passed for each layer.

The data in table 4 shows that the average of the magnitude of the methane response of the thinner Pd-Pt bi-layer is similar to that of the thicker H_1-e Pd-Pt bi-layer catalysts used previously. Interestingly, the magnitude of the response is slightly higher. This suggests that in this instance the quantity of Pd catalyst does not affect the magnitude of the methane response. The implications of this result are fully discussed in section 5.9. It is also noted that the variation in the responses of the thinner Pd-Pt bi-layer films is lower. It is possible that the nanostructure is more regular in thinner films, resulting in a higher surface area and therefore giving a larger methane response. The poisoning times of the thinner H_1-e Pd-Pt bi-layer films though slightly shorter than those of twice the thickness, are of similar magnitude and are still significantly higher than those of the H_1-e and V_1-e Pd

catalysts. These results therefore suggest that the increased poisoning times of the H_1-e Pd-Pt bi-layer catalysts is not solely attributable to the films being thicker. It was discussed in section 5.1.2 that Pt is more resilient to poisoning by HMDS than Pd[8,53] due to Pd adsorbing more silica than Pt. It was not possible to compare the results obtained in this section with those of other authors as no results were found in the literature regarding the poison resistance of Pd-Pt bimetallic catalysts.

5.4.5 H_1-e Pt – Pd bi-layer films

In section 5.5.1 it was reported that H_1-e Pd-Pt bi-layer catalysts gave superior catalytic performance with respect to methane oxidation compared to standard H_1-e Pd catalysts. This was found to be consistent with the work of other authors,[132,133] though how Pt promotes Pd catalytic activity in this case is not fully understood. It was proposed that Pt was having a promoting effect on the Pd catalyst as it was found that Pt by itself had no catalytic activity at the temperature used. It was proposed that the interaction may not simply be confined to the boundary between the two metals but that there may be some migration of Pt into the bulk Pd as well as surface migration. It was also found that the Pt layer improved poison resistance. A Pd-Pt bi-layer film of similar thickness to a single layer H_1-e Pd film was found to have superior poison resistance. It was decided to investigate whether this result was dependent on the Pt film being the top layer.

The electro-depositions were carried out using the same method described in section 5.4.1 with the obvious exception being the H_1-e Pt layer was electrodeposited first. The films were made the same thickness as the single layer mesoporous films by passing a deposition charge of 2.5 mC for each layer. The film was then cleaned in iso-propanol and acid cycled in 1 M sulphuric acid. The acid cyclic voltammogram was very similar to that of the H_1-e Pd-Pt bi-layer film shown in fig 72. All peaks occurred at similar potentials. The methane response is shown below in fig 78.

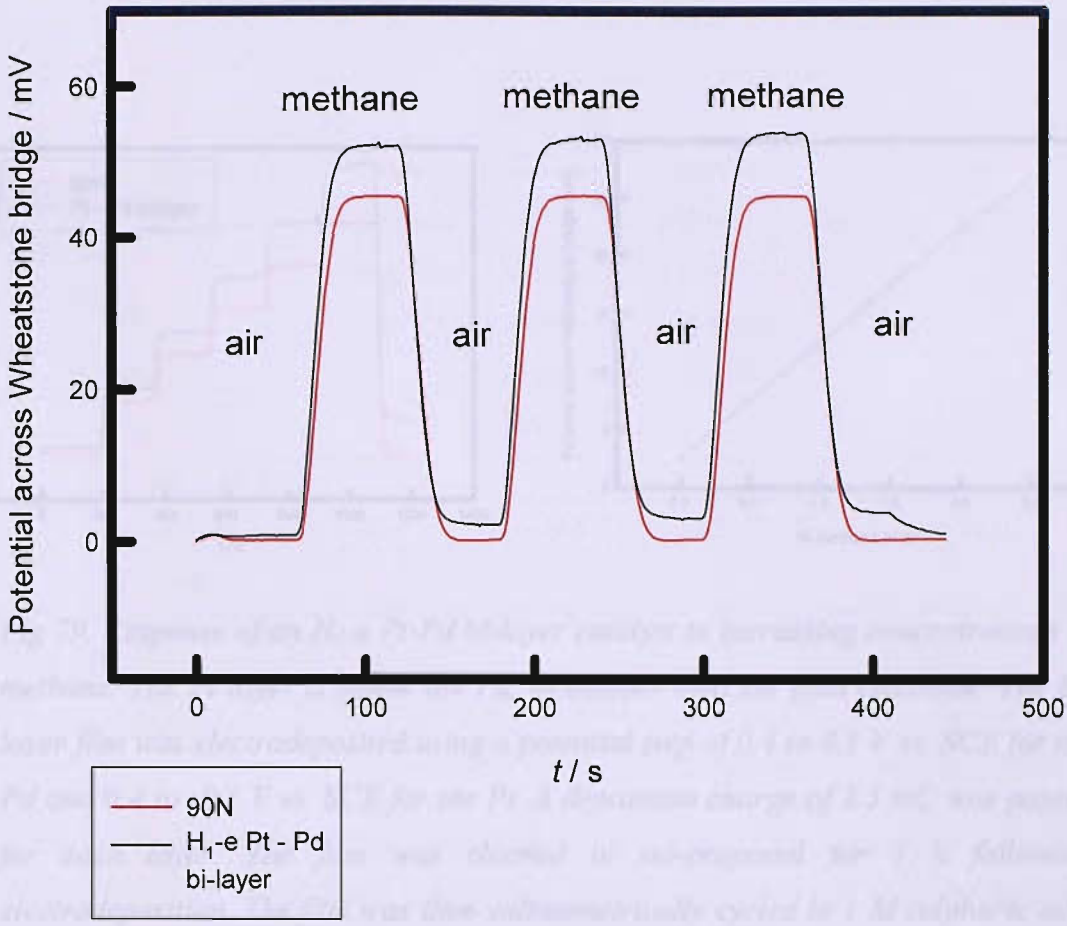

Fig 78. Methane response of an H_1-e Pt-Pd bi-layer film. The Pt layer is below the Pd, in contact with the gold electrode. For deposition details please refer to fig 75. A depositon charge of 2.5 mC was passed for both metals.

It can be seen from fig 78 that the H_1-e Pt-Pd bi-layer catalyst gave a positive response to methane of approximately 51 mV which was greater than that of the 90N device. It is noted that there is some baseline drift as the response in air does not return to the same baseline after exposure to methane. The H_1-e Pt-Pd film was tested at increasing concentrations of methane to investigate the linearity of the response to methane. The response is shown in fig 79.

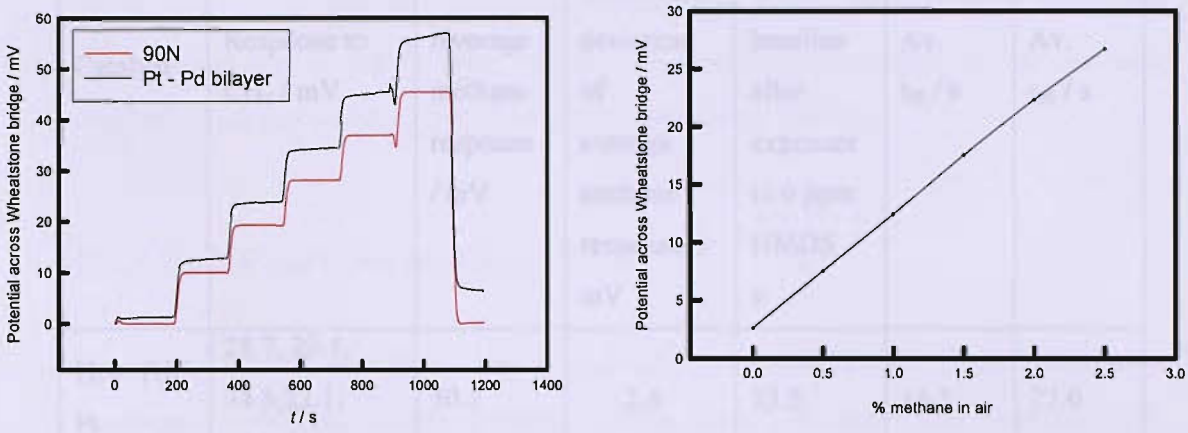

Fig 79. Response of an H_1-e Pt-Pd bi-layer catalyst to increasing concentrations of methane. The Pt layer is below the Pd, in contact with the gold electrode. The bi-layer film was electrodeposited using a potential step of 0.4 to 0.1 V vs. SCE for the Pd and 0.4 to -0.1 V vs. SCE for the Pt. A deposition charge of 2.5 mC was passed for each layer. The film was cleaned in iso-propanol for 1 h following electrodeposition. The film was then voltammetrically cycled in 1 M sulphuric acid over ten voltammetric cycles at 100 mV / s.

Fig 79 shows the methane response of a H_1-e Pt-Pd bi-layer film to increasing concentrations of methane. It can be seen that the film gives a linear response to increasing concentrations of methane. To allow for a comparison with the performance of the H_1-e Pd-Pt bi-layer catalysts a further 4 catalysts were prepared using the method described. The magnitude of the methane responses and the time taken to poison the catalysts with HMDS are given in table 5.

Catalyst	Response to CH_4 / mV	Average methane response / mV	Standard deviation of average methane response / mV	Average time to decay to baseline after exposure to 6 ppm HMDS / s	Av. t_{50} / s	Av. t_{90} / s
H_1-e Pd-Pt	28.7, 29.4, 34.5,22.1, 35.8	30.1	2.4	23.5	16.5	22.0
H_1-e Pt-Pd	51.0, 44.6, 29.3,35.9, 33.6	38.8	3.9	19.4	12.5	17.0

Table 5. Results showing the magnitude of the methane response and poisoning times of H_1-e Pt-Pd bi-layers and Pd-Pt bi-layer catalysts. The bi-layer catalysts were electrodeposited using a potential step of 0.4 to 0.1 V vs. SCE for the Pd and 0.4 to -0.1 V vs. SCE for the Pt. A deposition charge of 2.5 mC was passed for each layer. The films were cleaned in iso-propanol for 1 h following electrodeposition. The films were then voltammetrically cycled in 1 M sulphuric acid over ten voltammetric cycles at 100 mV / s.

The results shown in table 5 summarise the magnitude of the methane responses of the H_1-e Pt-Pd and Pd-Pt bi-layer films. The results show that the H_1-e Pt-Pd films, with Pd on the outside, gave larger catalytic responses to methane. The average methane response was 38.8 mV compared to 30.1 mV for the Pd-Pt films. It is not known why the Pt-Pd bi-layer films gave larger responses to methane. It is possible that an interaction between the Au and the Pt promotes the Pd activity. It is also possible that the reaction is mass transport controlled, in which case if Pd is on the outside the methane molecules will have less far to travel to reach the Pd active sites which may account for the higher response. This is discussed in detail in section 5.9. The poison resistance of the Pt-Pd bi-layer films was also determined by poisoning in 6 ppm HMDS. The results in table 5 show that the poison resistance of the H_1-e

Pt-Pd bi-layer with Pd on the outside is less than that of the Pd-Pt bi-layers. The t_{50} value of the H_1-e Pt-Pd bi-layer is 12.5 s which is similar to the value of 11.5 s obtained for H_1-e Pd shown in table 3. This suggests that the Pt layer on the top may act as a protective layer which is poisoned preferentially to the Pd, whilst having the Pd layer on top in the bi-layer whilst increasing the magnitude of the methane response does not result in the same poison resistance benefits.

5.4.6 H_1-e Pd-Pt binary films

In section 5.4.4 it was found that H_1-e Pd-Pt and Pt-Pd bi-layer films gave larger responses to methane than H_1-e Pd or V_1-e Pd films. This result was consistent with work by Yamamoto[132] and Narui.[133] It was proposed that Pt was promoting the catalytic activity of Pd. It was considered possible that the promoting effect of Pt on Pd may be further enhanced in a Pd-Pt alloy film. A template mixture was initially made containing 47 wt % Brij®56, 2 wt % heptane 6 wt % $(NH_4)_2$ $PdCl_4$, 6 wt % hexachloroplatinic acid and 39 wt % water. The template mixture was confirmed to be in the hexagonal phase at room temperature using an optical microscope. The aim was to electrodeposit a Pd-Pt binary film to maximise the interactions between Pd and Pt and so promote the activity of the Pd. The choice of deposition potential introduced several problems. H_1-e Pd films have been deposited at 0.1 V vs. SCE, whilst H_1-e Pt films were electrodeposited at -0.1 V vs. SCE. Initially the aim was to attempt to electrodeposit similar amounts of Pd and Pt. In a similar investigation by Guerin and Attard[73] a deposition potential of 0.2 V vs. SCE was used. The effect of deposition potential and temperature on the electrodeposition of H_1-e Pt were investigated by Elliott *et al.*[76] It was concluded that deviating by 0.2 V from the established deposition potential of -0.1 V vs. SCE for Pt compromised the nanostructure. However, it was considered highly probable that the same findings may well apply for Pd. Consequently a deposition potential of 0.0 V vs. SCE was selected so as to use a deposition potential as close as possible to the values used in these investigations of 0.1 V vs. SCE for Pd and –0.1 V vs. SCE and thereby minimise any detrimental effects on the nanostructure.

Fig 80 shows the electrodepositon of Pd-Pt onto a microhotplate from the aforementioned template mixture by potential step from 0.45 to 0.0 V vs. SCE.

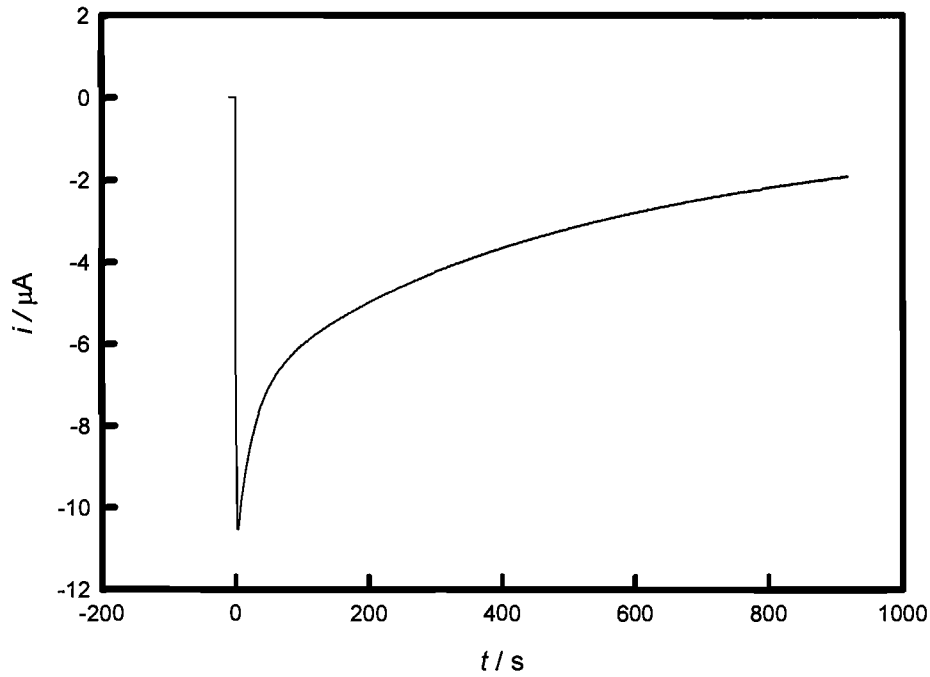

Fig 80. Electrodeposition of H_I-e Pd-Pt binary film from a template mixture comprising 47 wt % Brij®56, 2 wt % heptane 6 wt % $(NH_4)_2$ $PdCl_4$, 6 wt % hexachloroplatinic acid and 39 wt % water. A potential step of 0.45 to 0.0 V vs. SCE was applied and a deposition charge of 3.5 mC was passed.

Fig 80 shows the electrodepositon of a H_I-e Pd-Pt binary film onto a microhotplate. The current transient is very similar to that of the electrodeposition of H_I-e Pd onto a microhotplate shown in section 4.3 fig 31 in terms of both shape and magnitude of the current. Following electrodeposition the film was washed in iso-propanol for 1 h to remove the surfactant. The film was then voltammetrically cycled in 1 M sulphuric acid over 8 voltammetric cycles. The cyclic voltammogram is shown in fig 81.

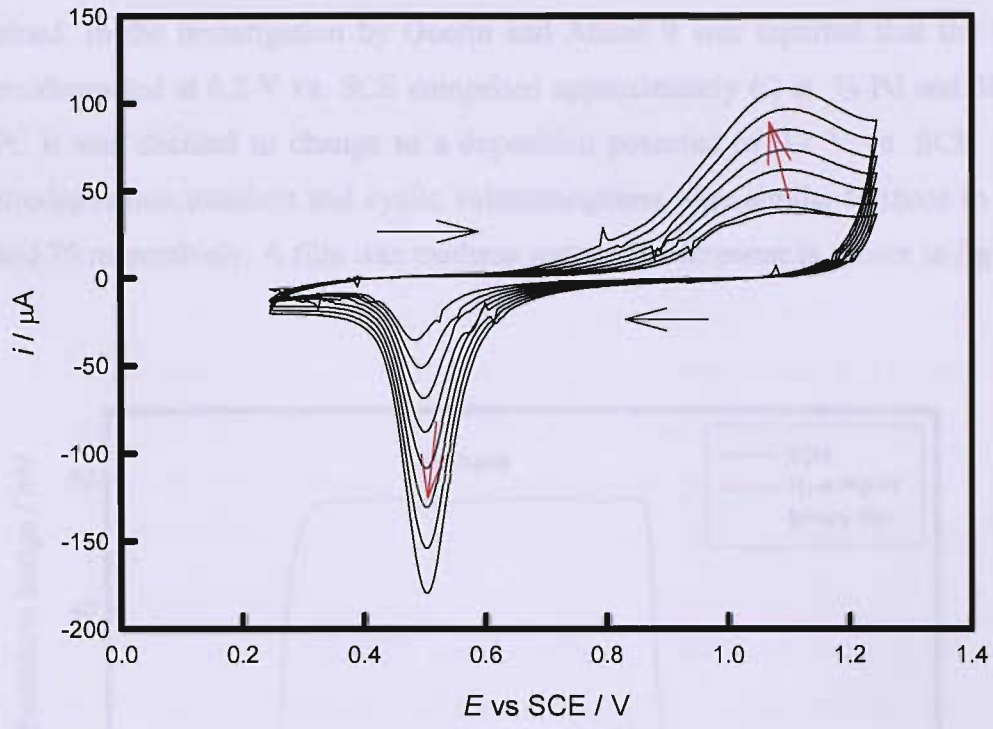

Fig 81. Cyclic voltammogram of a H_I-e Pd-Pt binary film in 1 M sulphuric acid. The cyclic voltammogram was carried out at room temperature using a scan rate of 200 mV / s, starting at 0.5 V vs. SCE then sweeping in the anodic direction. The electrodeposition conditions were the same as those described in fig 80.

Fig 81 shows eight cyclic voltammograms of an H_I-e Pd-Pt binary film in sulphuric acid. The black arrows indicate the scan direction and the red arrows the trend of the cyclic voltammograms. It can be seen that the surface area, calculated from the charge passed under the oxide stripping peak increases as voltammetric cycling progresses. A similar trait was observed in the cyclic voltammogram of an H_I-e Pd film shown in fig 4 section 3.4.1. It was considered not possible to accurately calculate the surface area using the charge under the oxide stripping peak. Although it would be possible to determine the relative amounts of Pd and Pt using EDS,[73] the Faradaic efficiency of the deposition is not known and hence the actual amount of metal deposited cannot be determined.

The H_I-e Pd-Pt binary films were then methane tested. The results were disappointing; five films were electrodeposited and all gave negative methane responses. In section 5.4.3 it was reported that H_I-e Pt films gave a negative

methane response at the temperatures used in these investigations. It is possible that the bulk of metal deposited was Pt resulting in the negative methane responses obtained. In the investigation by Guerin and Attard it was reported that the film electrodeposited at 0.2 V vs. SCE comprised approximately 62 at. % Pd and 38 at. % Pt. It was decided to change to a deposition potential of 0.2 V vs. SCE. The electrodeposition transient and cyclic voltammograms were similar to those in figs 78 and 79 respectively. A film was methane tested. The response is shown in fig 82.

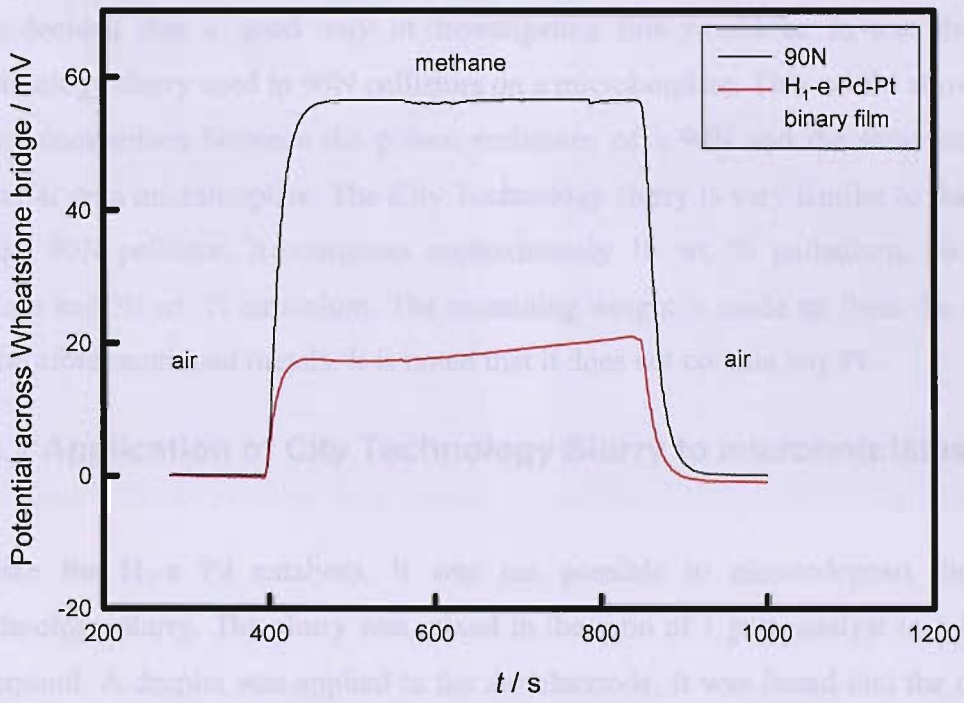

Fig 82. Methane response of an H_1-e Pd-Pt binary film on an SRL136 micro-hotplate. The electrodeposition conditions were the same as those described in fig 78. The response was taken following 1 h in air.

Fig 82 shows the methane response of an H_1-e Pd-Pt binary film. The response is positive with a maximum magnitude of approximately 22 mV. The response was taken following 1 h in air. The magnitude is similar to those obtained for H_1-e Pd films, but significantly less than those obtained for both the H_1-e Pd-Pt bi-layer and the H_1-e Pt-Pd bi-layer films. It was decided not to further persue the alloy films.

5.5 City Technology Catalysts

5.5.1 Motivation

The H_1-e and V_1-e Pd catalysts produced have exhibited poor resistance to HMDS compared to the commercial 90N pellistor. The difference in the poison resistance was very significant. It was proposed that the structure of the commercial pellistor with layers of catalyst sequentially added dropwise may be partly responsible. It was decided that a good way of investigating this would be to test the City Technology slurry used in 90N pellistors on a microhotplate. This would allow for a direct comparison between the poison resistance of a 90N and the same catalytic material on a microhotplate. The City Technology slurry is very similar to that used in the 90N pellistor. It comprises approximately 16 wt. % palladium, 30 wt % cerium and 30 wt. % zirconium. The remaining weight is made up from the oxides of the aforementioned metals. It is noted that it does not contain any Pt.

5.5.2 Application of City Technology Slurry to microhotplates

Unlike the H_1-e Pd catalysts, it was not possible to electrodeposit the City Technology slurry. The slurry was mixed in the ratio of 1 part catalyst to 1.8 parts α-terpinol. A droplet was applied to the Au electrode. It was found that the droplet spread over the membrane, though this did not cause any apparent problems. The mixture was cured by powering the microhotplate, first to 4 V for ten minutes, before gradually increasing the power to 14 V for 1 h. The device was then powered down and soaked in iso-propanol to remove the residue from the membrane. The main drawback with this method is that it does not allow for accurate control over the thickness which is possible using electrodeposition.

5.5.3 Characterisation of City Technology Catalyst

The structure of the catalyst was then investigated using SEM.

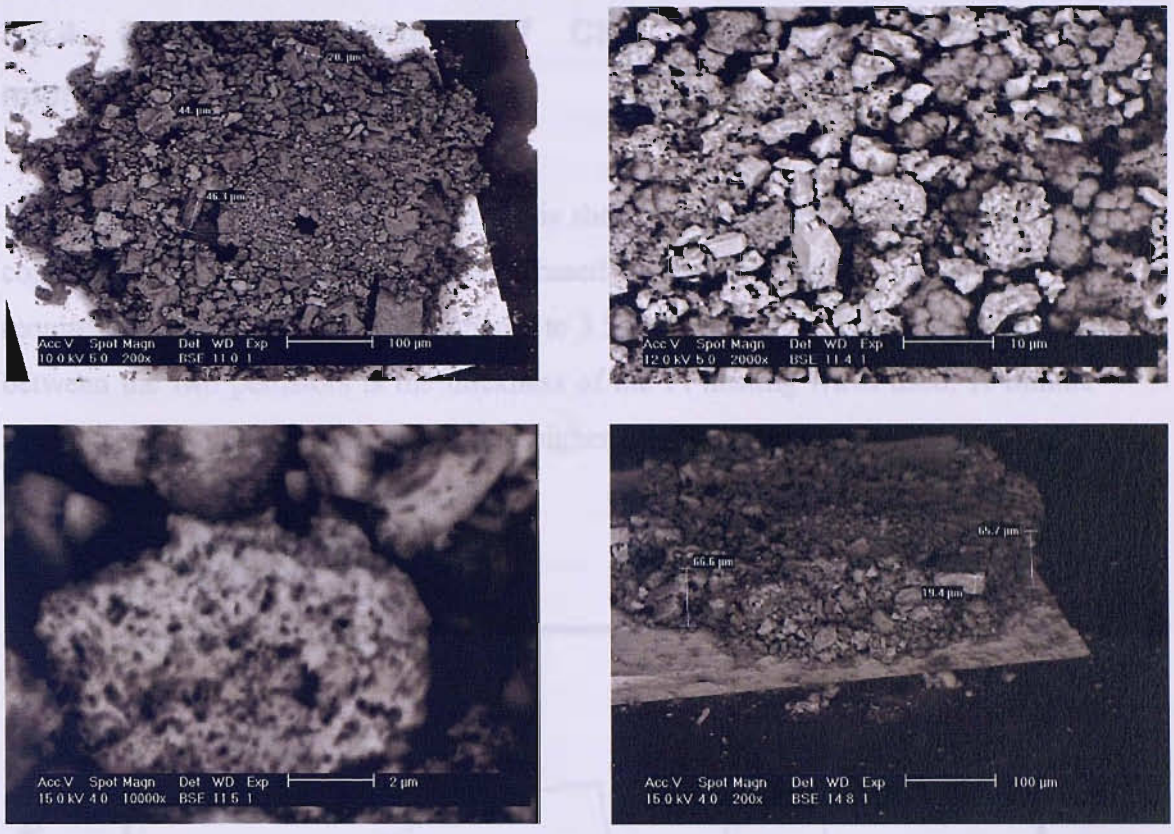

Fig 83. SEM images of a City Technology slurry catalyst on an SRL136 microhotplate. The slurry was mixed in the ratio of 1 part Catalyst to 1.8 parts α-terpinol. A droplet was applied to the Au electrode. The mixture was cured by powering the microhotplate, first to 4 V for ten minutes, before being gradually powered up to 14 V for 1 h. The device was then powered down and soaked in iso-propanol to remove the residue from the membrane.

The SEM images in fig 83 show that the catalyst consists of porous chunks of varying size. The sponge like structure will result in a very high surface area. The thickness of the film was determined by viewing the film at a tilt angle of 65° using SEM to be approximately 65 µm thick, though it is noted that the thickness varies throughout the film. The thickness of the film was determined by measuring The deposition method made it very difficult to ensure complete coverage was achieved and it can be seen that the catalyst does not cover the entire gold electrode. The pore diameter

can be seen to vary but values of approximately 200 nm were obtained. This is significantly greater than the 2.5 nm pore diameter of the H_1-e Pd films.

5.5.4 Methane response of City Technology slurry on microhotplates

The methane response after 5 min in air is shown in fig 84. It is noted that a 200N commercial pellistor was used. This is based on the same design as the 90N but requires a lower power of 2 V compared to 3.5 V for the 90N. The main difference between the two pellistors is the thickness of the Pt heating wires used. A thinner wire is used in the 90N, consequently a higher operating voltage is required though the corresponding current is lower. [3]

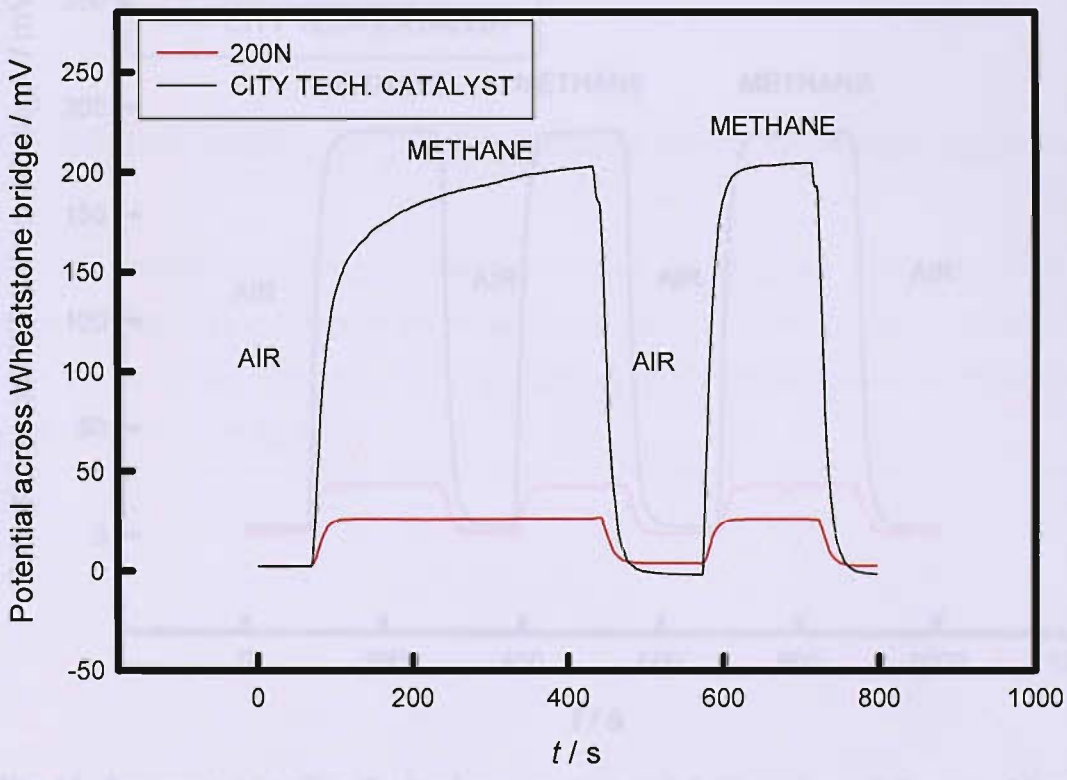

Fig 84. Methane response of City Tech catalyst on a microhotplate following 5 minutes in air. For detaisl of the application of the City Tech. catalyst please refer to fig 83. The device was then powered to 15 V. The 200N was powered to 2.0 V from the power supply.

It can be seen in fig 84 that the initial response of a City Tech catalyst rises rapidly at first then rises more gradually after reaching approximately 160 mV. The maximum response is immediately reached on the second exposure to methane. H_1-e Pd catalysts gave a negative or very weak initial response to methane before the response gradually increased. There is some similarity in the initial response in that a gradual increase in response over time is observed before the maximum response is obtained. It is proposed that this is due to the catalyst restructuring as Pd is converted to form palladium oxide, so that the required mixture of metallic Pd and Pd oxide is obtained.

The response of a City Tech slurry catalyst on a microhotplate after 1 h powered in air and methane is shown in fig 85.

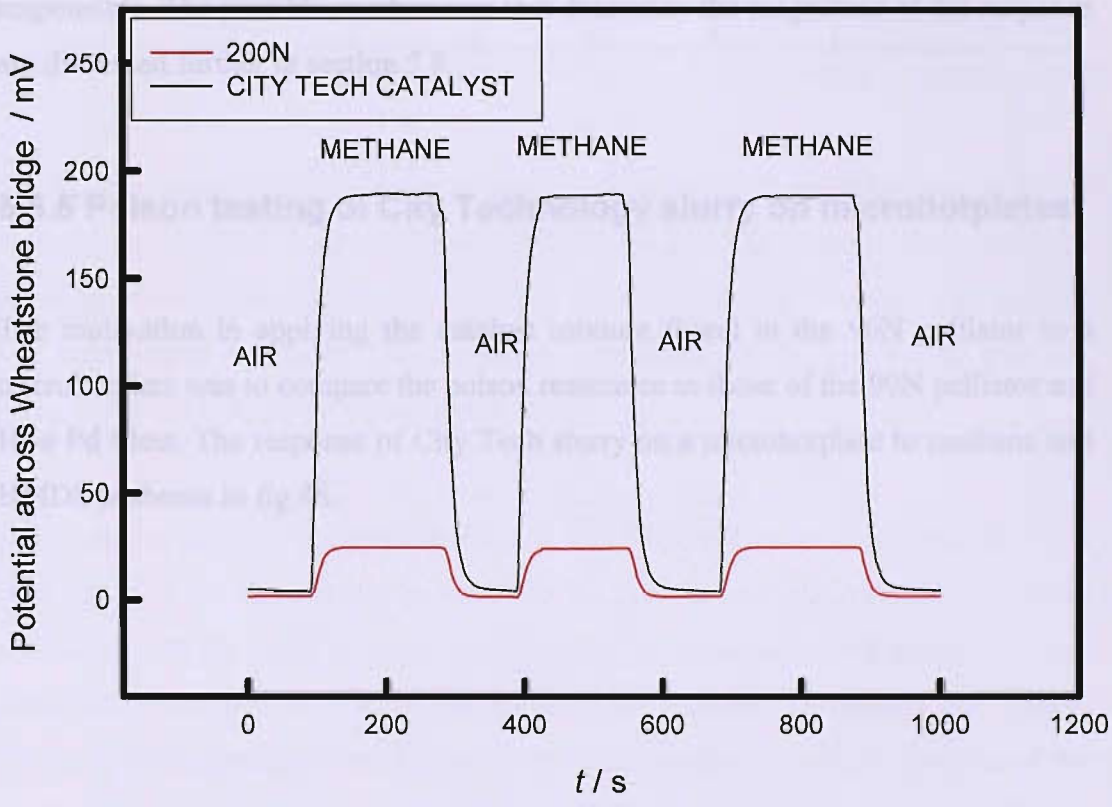

Fig 85. Response of a City Technology catalyst to 2.5 % methane following 60 min in air. The catalyst was tested for methane after 5 min then powered in air for the following 45 min. The catalyst was prepared as per fig 83. The 200N commercial pellistor was powered to 2.0 V from the power supply.

Fig 85 shows the methane response of a City Tech catalyst on a microhotplate following 60 min powered in air and methane. It can be seen that the magnitude of the response is significantly greater than that of the 200N or of any of the nanostructured Pd films prepared previously. It is also noted that the baseline and methane response are stable and the methane responses reproducible. The greater magnitude of this response relative to that of the nanostructured Pd catalysts requires explanation. The larger response suggests that rate of mass transport of methane to the catalyst may not be a limiting factor in determining the magnitude of the response of nanostructured Pd catalysts. It was proposed that the probable larger surface area of the City Tech catalyst may be responsible. However, earlier experiments showed that thicker H_1-e Pd catalysts did not result in larger methane responses. This therefore suggests that it is the composition of the catalyst, in particular the promoting effects of various additives such as Zr on the Pd that are responsible. The possible mechanisms that determine the magnitude of the response are discussed further in section 5.8.

5.5.5 Poison testing of City Technology slurry on microhotplates

The motivation in applying the catalyst mixture found in the 90N pellistor to a microhotplate was to compare the poison resistance to those of the 90N pellistor and H_1-e Pd films. The response of City Tech slurry on a microhotplate to methane and HMDS is shown in fig 86.

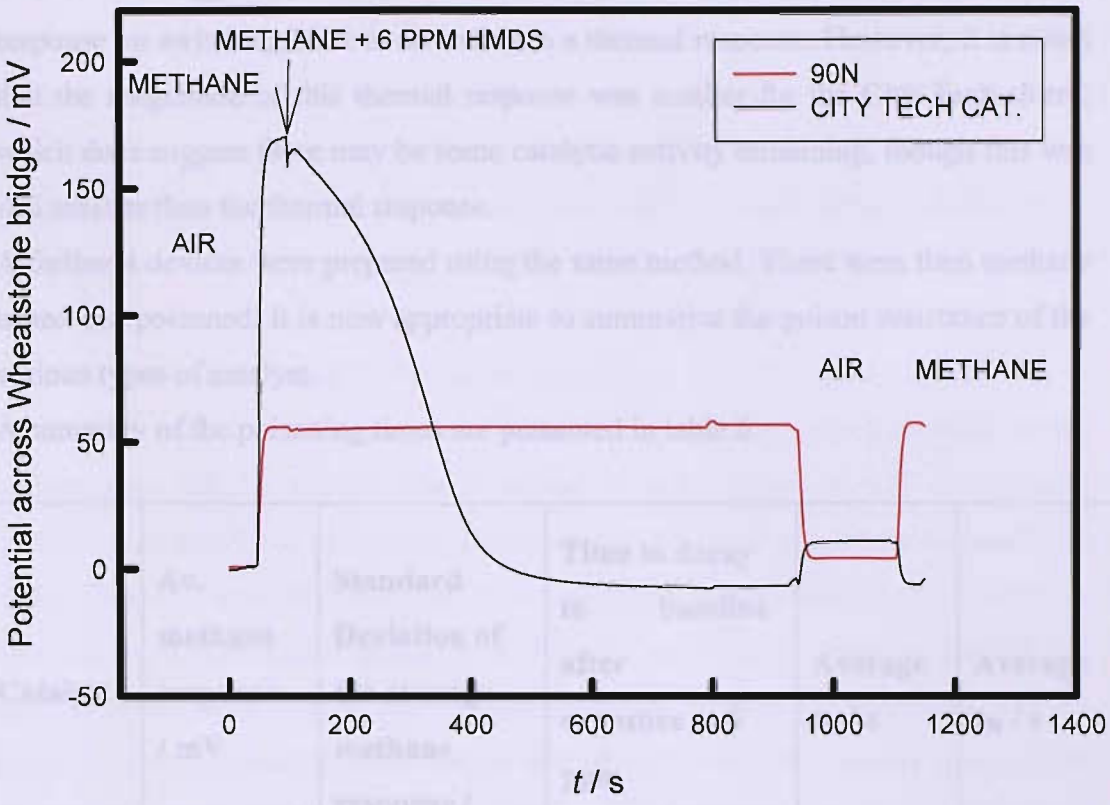

Fig 86. Response of City Technology catalyst on an SRL136 microhotplate to 2.5 % methane and HMDS 6 ppm following 60 min in air. The catalyst was tested for methane after 15 min then powered in air for the following 45 min. The catalyst was prepared as per fig 83. The device was then powered up to 15 V. The 90N was powered to 3.5 V from the power supply.

Fig 86 shows the City Technology catalyst was poisoned more slowly than both the H_1-e and V_1-e Pd films. It can be seen that the drop in methane response is gradual compared with the rapid decrease observed for the mesoporous Pd films. It is also noted that when the City Catalyst is poisoned the response in methane and HMDS stabilises at the previous air baseline. This is in contrast with the behaviour of the mesoporous Pd catalysts, such as that of an H_1-e Pd-Pt bi-layer catalyst in fig 64. Here it can be seen that the catalyst stabilised at a lower Wheatstone bridge potential than the air baseline. This suggests the City technology catalyst may still have some catalytic activity. However, it can be seen that the response in fig 86 increases once the gas supply is switched back to air. This indicates a thermal response; air has a lower heat capacity than methane hence the increase in the response.

These two observations are contradictory. The response stabilising at the previous air baseline suggests some catalytic activity might remain whilst the increase in response on switching back to air indicates a thermal response. However, it is noted that the magnitude of this thermal response was smaller for the City Tech slurry, which does suggest there may be some catalytic activity remaining, though this was still smaller than the thermal response.

A further 4 devices were prepared using the same method. These were then methane tested and poisoned. It is now appropriate to summarise the poison resistance of the various types of catalyst.

A summary of the poisoning times are presented in table 6.

Catalyst	**Av. methane response / mV**	**Standard Deviation of the average methane response / mV**	**Time to decay to baseline after exposure to 6 ppm HMDS / s**	**Average t_{50} / s**	**Average t_{90} / s**
H_1-e Pd	17.8	5.3	15.1	11.5	14.5
H_1-e Pd – Pt bi-layer	30.1	7.5	22.0	20.5	26.0
V_1-e Pd	17.8	7.7	16.5	12.2	14.8
City Tech Catalyst	160	8.4	370	205	296

Table 6. Summary of the poisoning times in 6 ppm HMDS in 2.5 % methane for different catalysts on SRL 136 microhotplates. The results represent the average of ten results for the H_1-e Pd and H_1-e Pd-Pt bi-layer catalyst and the average of 5 results for the City Technology slurry and V_1-e Pd.

The results in table 6 show that the City Tech catalyst has a significantly higher resistance to HMDS than the mesoporous Pd films. The t_{50} value is 205 s, compared to 20.5 s for a H_1-e Pd-Pt bi-layer, the highest of the mesoporous type Pd films. This represents an increase of 900 %. The increased resistance to HMDS could be explained in a number of ways. Firstly, it could be that the composition of the City Tech slurry comprising additives such as zirconium and cerium offers better performance. Due to the dispersed nature of the catalyst it is possible that Zr surrounding the Pd adsorbs the silica, therefore protecting the Pd. The poison resistance may also be partly due to the larger pore sizes. The pores can be seen in the SEM images in fig 83, and are of the order of 200 nm, therefore considerably greater than the 2.5 nm for the H_1-e and V_1-e Pd films. It will therefore be considerably easier for the pores in mesoporous Pd films to become blocked with silica. Finally, the poison resistance may simply be related to the amount of catalytic material. If there is more catalyst present it will take longer to poison. An SRL136 microhotplate has a 750 by 750 μm gold electrode. If the City Tech catalyst is 65 μm thick then the catalyst has a volume of 3.66×10^{-5} cm^3. This is only approximate as the thickness varies throughout the sample and complete coverage of the electrode is unlikely. A typical H_1-e Pd will be approximately 5 to 10 μm thick, resulting in a volume of approximately 2.8×10^{-6} cm^3 to 5.6×10^{-6} cm^3. Using the maximum volume of 5.6×10^{-6} cm^3 for the H_1-e Pd film results in the City Tech catalyst film having a 6.5 times greater volume. However, as already indicated the pores of the City Tech slurry are of the order of 200 nm in diameter compared to those of the H_1-e Pd film which are approximately 2.5 nm in diameter. This results in more of the volume comprising empty space. In addition it can be seen that the City Tech catalyst comprises many different sized pieces of catalyst which are not tightly packed. This further reduces the density of catalytic material in the City Tech catalyst. Furthermore the composition of the City Tech slurry contains approximately 16 wt % Pd. This suggests that the significantly improved poison resistance is likely to be a result of the more open structure.

The same theory of equating poison resistance to volume of catalytic material can be more appropriately applied to a comparison of a City Tech film catalyst on a microhotplate and a 90N pellistor. This is a fairer comparison as the same catalytic material is used in both cases. However, the density of the material in the 90N is

almost certain to be higher and this needs to be considered in the comparison. The 90N pellistor typically lasts for around 12 h in 6 ppm HMDS. The 90N contains a bead of catalyst with an approximate diameter of 1 mm. If the catalyst bead is treated as a sphere of diameter 1 mm then it has a theoretical volume of 5.24×10^{-4} cm^3. The volume of the 90N bead is therefore approximately 14.4 times greater than that of the City Technology catalyst on the microhotplate. Using the assumption that poison resistance can be related to the quantity of catalytic material and assuming similar densities it could be concluded that the 90N could be expected to last 14.4 times longer. Using the average poisoning time of 370 s in table 5 the poison resistance of the 90N should therefore be around 5300 s or 90 min, far shorter than the real poisoning time of around 12 h. There are a number of possible explanations. Firstly, it is highly probable that the density and hence the amount of catalytic material in the 90N pellistor is higher. Second, although the catalytic material is the same in both cases, it is arranged in different ways. The slurry on the 90N has an open structure. The 90N is made by sequentially adding droplets and building up the catalyst. This gives the catalyst a honeycomb structure which may reduce poisoning of the inner layers.

5.5.5.1 Effect of thickness of City Technology catalyst

In the previous section it was reported that the City Tech catalyst had superior resistance to HMDS than any of the various types of mesoporous Pd catalyst, but significantly less than the 90N which is made from similar material. It was proposed that the poison resistance may be related to the amount of catalytic material. In section 4.7 it was reported that thicker mesoporous Pd films gave less reproducible methane responses and often negative responses. It was therefore decided to investigate the affect of increasing the quantity of catalytic material on poison resistance by producing City Tech slurry catalysts of varying thickness. Unfortunately, the process of applying City Tech slurry to the micro-hotplates does not allow for precise control over film thickness. However, the thickness of the City Tech catalysts can be estimated using SEM. Four different thickness films were produced by applying 1, 2, 3 and 4 drops of catalyst slurry to an SRL136 micro-hotplate. The catalyst was cured after each addition of slurry and the microhotplate washed thoroughly in iso-propanol once the curing process had been completed. The thickness was then estimated using SEM. An SEM image of the City

Technology catalyst made by sequentially adding 4 drops of slurry is shown in fig 87.

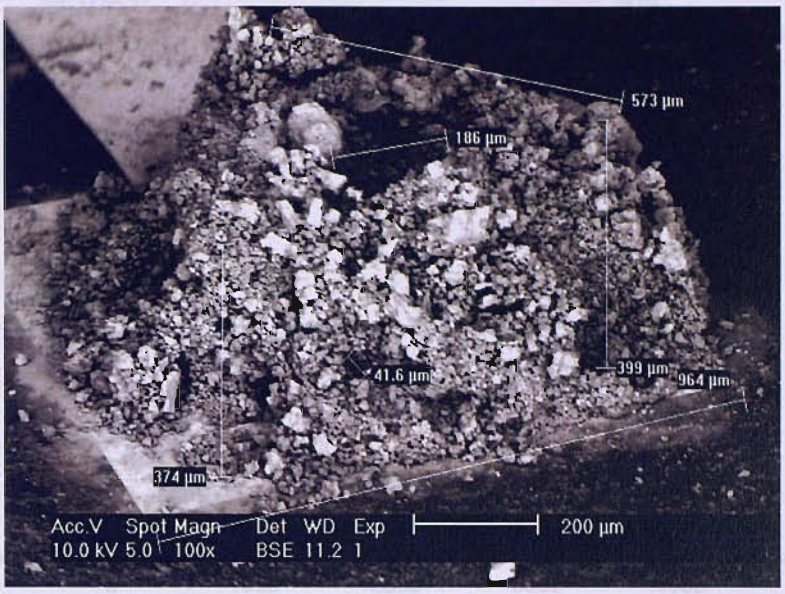

Fig 87. SEM images of City Technology catalyst on an SRL136 microhotplate. 4 droplets of catalyst slurry were added to the working electrode. For each addition the solvent was evaporated over one hour by heating to approximately 450°C. The device was cleaned after each addition using iso-propanol.

Fig 87 shows an SEM image of a City Tech slurry catalyst on an SLR136 microhotplate. It can be seen that the catalyst is comprised of wide range of different sized particles. There is a large channel down the middle of the catalyst. It is believed that this was formed during the curing process, when the solvent evaporated forcing gas up through the catalyst.

Following analysis by SEM the catalysts were methane, and then poison tested with HMDS. The response of a City Tech catalyst formed from 3 droplets of catalyst slurry is shown in fig 88.

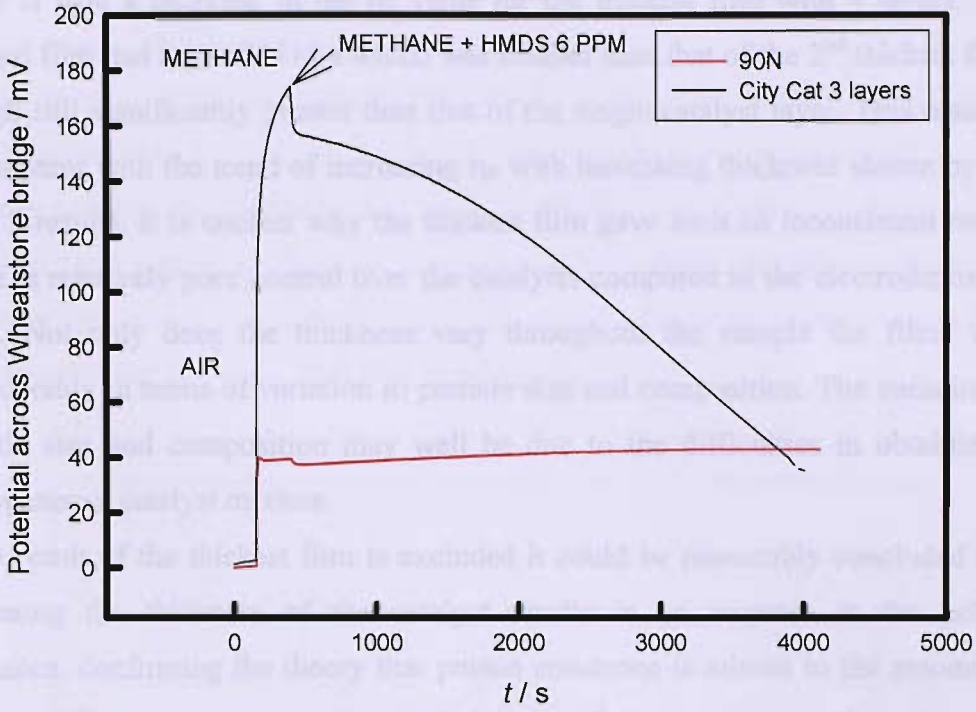

Fig 88. Response of a City Technology slurry catalyst on an SRL136 microhotplate to methane and HMDS 6 ppm. 4 droplets of catalyst slurry were added to the working electrode. For each addition the solvent was evaporated over one hour by heating to approximately 450°C. The device was cleaned after each addition using iso-propanol.

The maximum methane responses and poisoning times of City Tech slurry catalysts by HMDS are shown in table 7. Note that the total poisoning times were not obtained as the data logger reached its limit at approximately 4400 s. However it was possible to calculate t_{50} and t_{90} values.

No. layers / approx. thickness / µm	**Max. methane Response / mV**	t_{50} **/ s**	T_{90} **/ s**
4 / 400	164	1115	1808
3 / 270	172.7	2424.4	4350
2 / 180	157	1507	4041
1 / 65	160	205	296

Table 7 Summary results of City Tech slurry catalysts on SRL136 microhotplates.

The results in table 7 show an increase in t_{50} times for the first three thicknesses. There is then a decrease in the t_{50} value for the thickest film with 4 layers. The thickest film had a t_{50} of 1115 s which was smaller than that of the 2nd thickest film, though still significantly greater than that of the single catalyst layer. This result is inconsistent with the trend of increasing t_{50} with increasing thickness shown by the other 3 results. It is unclear why the thickest film gave such an inconsistent result. There is relatively poor control over the catalysts compared to the electrodeposited films. Not only does the thickness vary throughout the sample the films vary considerably in terms of variation in particle size and composition. The variation in particle size and composition may well be due to the difficulties in obtaining a homogeneous catalyst mixture.

If the result of the thickest film is excluded it could be reasonably concluded that increasing the thickness of the catalyst results in an increase in the poison resistance, confirming the theory that poison resistance is related to the amount of catalyst. The catalyst comprising 3 layers of catalyst lost all activity in approximately 1 h 20 minutes, still lower than that of the 90N. The volume of catalyst for 3 layers was approximately $1.5 \times 10^{-4} cm^3$ which is still approximately 3.5 times less than that of the 90N. This figure also does not take into account the volume of catalyst missing in the central channel and the fact that the catalyst has a pyramid type shape rather than cuboidal. These factors would result in the true volume of catalyst material present being considerably less.

It is interesting to note that the magnitude of the methane responses in table 7 are all similar. There is some variation but there is no trend of increasing magnitude with catalyst thickness. This is consistent with the results in section 4.7 which reported no relationship between surface area of mesoporous Pd catalysts and the magnitude of the methane response. This result certainly suggests that the reaction is mass transport limited, as an increase in the number of active sites has not resulted in an increase in reaction rate. This is discussed in detail in section 5.8.

5.6 Analysis of poisoned mesoporous Pd films

5.6.1 Electrochemical analysis

A number of different techniques were used to examine the mesoporous Pd films once they had been poisoned with HMDS. The aim was to try and establish how the Pd films had become poisoned. For example carrying out a cyclic voltammogram might reveal a significant decrease in electro-active surface area might suggest that the pores had become blocked by silica. An acid cyclic voltammogram of an H_1-e Pd film poisoned by 6 ppm HMDS is shown in fig 89.

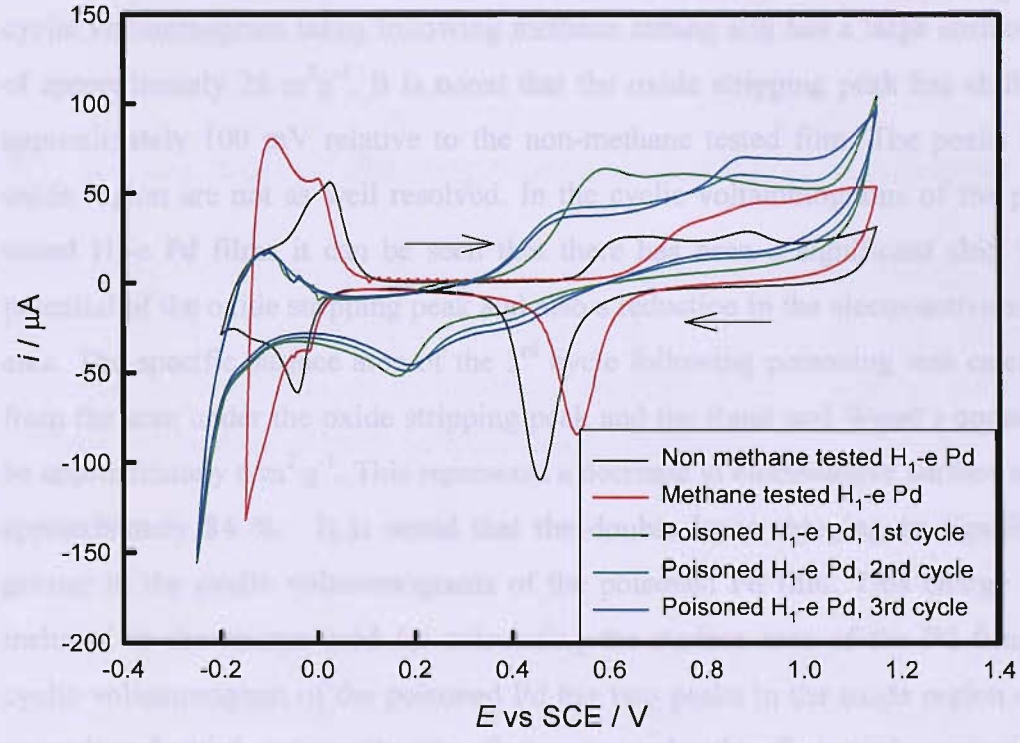

Fig 90. Cyclic voltammograms of an H_1-e Pd film on an SRL136 microhotplate. The cyclic voltammograms were carried out at room temperature in 1 M sulphuric acid at a scan rate of 100 mV / s starting from 0.2 V vs. SCE. The device gave a positive methane response of approximately 25 mV. The Pd film was then poisoned with 6 ppm HMDS. All catalytic activity was lost in approximately 15 s. The H_1-e Pd film was electrodeposited from a template mixture comprising 47 wt. % Brij®56, 2 wt % heptane 12 wt % $(NH_4)_2$ $PdCl_4$ and 39 wt % water. The Pd film was electrodeposited at room temperature by applying a potential step from 0.4 to 0.1 V vs. SCE. A deposition charge of 5 mC was passed. A cyclic voltammogram of the film following electrodeposition and prior to gas and poison testing is also shown. The arrows indicate the scan direction.

Fig 89 shows cyclic voltammograms of H_I-e Pd films before methane testing, following methane testing but prior to poison testing and following poisoning. A number of observations can be made. It can be seen that the cyclic voltammograms taken before methane testing and following methane testing have characteristic features of a nanostructured film. The cyclic voltammogram taken prior to methane testing has two well resolved peaks in the oxide region at approximately 0.65 and 0.9 V vs. SCE. The oxide stripping peak at approximately 0.45 V vs. SCE is also well defined. The surface area calculated from the charge under the oxide stripping peak using the Rand and Woods[109] constant to be approximately 38 $m^2 g^{-1}$. The cyclic voltammogram taken following methane testing still has a large surface area of approximately 28 $m^2 g^{-1}$. It is noted that the oxide stripping peak has shifted by approximately 100 mV relative to the non-methane tested film. The peaks in the oxide region are not as well resolved. In the cyclic voltammograms of the poison tested H_I-e Pd films it can be seen that there has been a significant shift in the potential of the oxide stripping peak and also a reduction in the electroactive surface area. The specific surface area of the 3rd cycle following poisoning was calculated from the area under the oxide stripping peak and the Rand and Wood's constant to be approximately 6 $m^2 g^{-1}$. This represents a decrease in electroactive surface area of approximately 84 %. It is noted that the double layer charging is significantly greater in the cyclic voltammograms of the poisoned Pd film. This charge is not included in the charge used for calculating the surface area of the Pd film. The cyclic voltammogram of the poisoned Pd has two peaks in the oxide region on the second and third scans. On the first scan only the first peak occurring at approximately 0.55 V vs. SCE is resolved. On the second and third scans it is noted that the first peak corresponding to the formation of oxide is shifted relative to the peak in the non-poisoned Pd film, by approximately 0.15 V to approximately 0.5 V vs. SCE. There are two peaks in the potential region associated with removal of the oxide at 0.4 and 0.18 V vs. SCE. It is proposed that the larger peak at 0.18 V vs. SCE corresponds to the removal of the oxide otherwise there will be a significant discrepancy in the charge passed in the formation of the oxide and its removal. The shift in potential of the oxide stripping peak is significant. It is possible that silica adsorbed during poisoning by HMDS is responsible for the observed shift in potentials of the features in the oxide region.

5.6.2. Raman Spectroscopy

Electrochemical characterisation of a poisoned Pd film showed that the surface area had been significantly decreased and that the some of the features in the voltammogram occurred at different potentials relative to the non-poisoned Pd film. The Pd films were also examined using SEM but no changes in the film were apparent. It was decided to examine the poisoned Pd films using Raman spectroscopy in an effort to determine the poisoning mechanism. Raman spectra were carried out of the Au electrode, the membrane, the Pd film prior to and following methane testing and finally after poisoning by HMDS. There was no significant variation between the spectra.

5.7 Comparison of the magnitude of methane responses

A variety of different types of methane catalyst have been produced with the aim of the investigating their resistance to poisoning by HMDS. In this section the magnitude of the responses to increasing concentrations of methane as well as methane responses at different temperatures are compared.

5.7.1 Comparison of methane responses at different methane concentrations

Three examples of each type of catalyst were tested at increasing concentrations of methane. The maximum response at each concentration was recorded and an average obtained. The results are shown in fig 90.

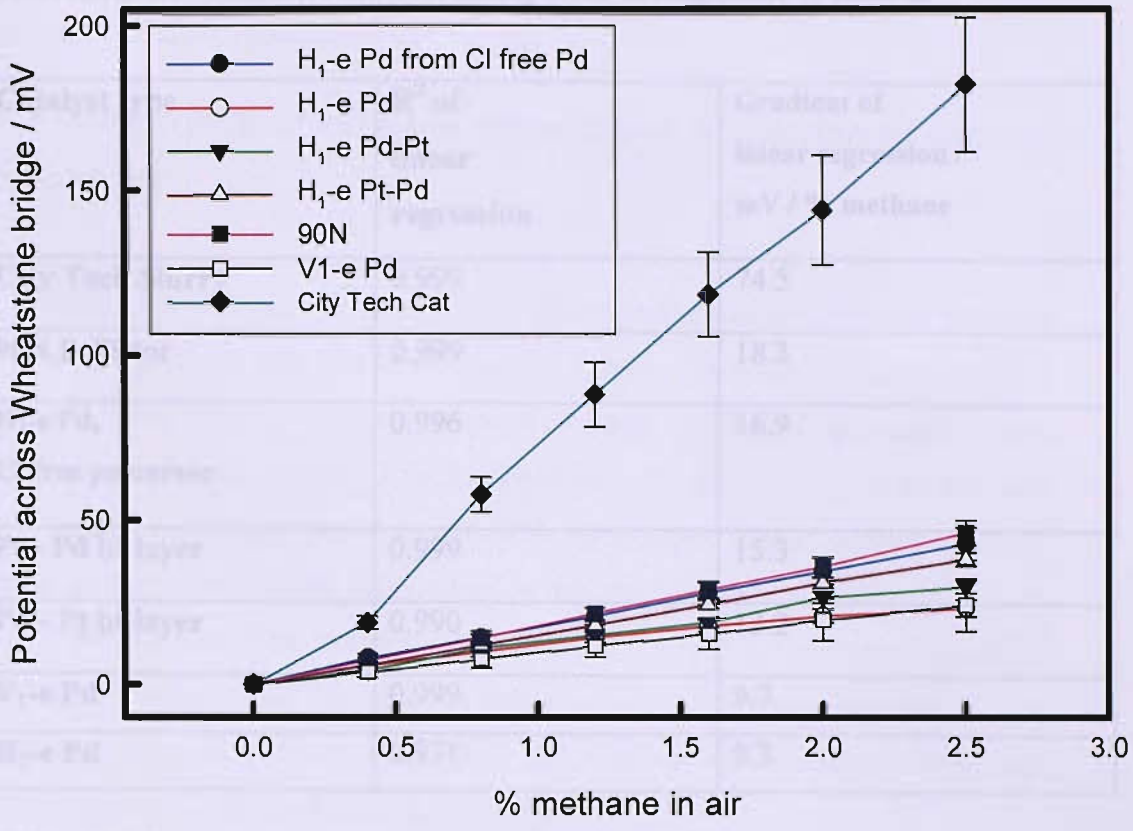

Fig 90. Graph showing the magnitude of the methane response of different catalyst types to increasing concentrations of methane in air. H_1-e Pd catalysts were electrodeposited at room temperature by potential step from 0.4 to 0.1 V vs. SCE. A deposition charge of 5 mC was passed. Pd-Pt bi-layer catalysts were electrodeposited at room temperature using a potential step of 0.4 to 0.1 V vs. SCE for the Pd and 0.4 to -0.1 V vs. SCE for the Pt. A deposition charge of 5 mC was passed for each layer. V_1-e Pd films were electrodeposited at 40°C by potential step from 0.4 to 0.1 V vs. SCE, a deposition charge of 5 mC was passed.H_1-e Pd catalysts, Cl free were electrodeposited at room temperature by potential step from 0.4 to 0.1 V vs. SCE from a template mixture in which the ammonium tetrachloropalladate was replaced with palladium nitrate hydrate. The City catalyst was applied from a mixture containing 0.45 g City Technology catalyst and 0.69 ml of α-terpinol. The catalyst was cured by powering the device to approximately 450 °C for one hour. After this time the micro-hotplate device was cleaned in iso-propanol and allowed to dry before another layer of catalyst was added. The error bars represent the standard deviation.

The results are summarised in descending order of magnitude in table 8.

Catalyst type	R^2 of linear regression	Gradient of linear regression / mV / % methane
City Tech Slurry	0.999	74.5
90N Pellistor	0.999	18.2
H_1-e Pd, Cl free precursor	0.996	16.9
Pt - Pd bi-layer	0.999	15.3
Pd - Pt bi-layer	0.990	12.2
V_1-e Pd	0.999	9.7
H_1-e Pd	0.971	9.3

Table 8. Table summarising the gradient and R^2 value of the linear regression from the data in fig 91 showing the magnitude of the methane response of different catalyst types to different concentrations of methane in air. For full description of deposition conditions please see fig 90.

The results in fig 90 and table 8 compare the magnitude of the methane responses for the various catalyst types produced. Fig 90 shows that of the mesoporous Pd catalysts it is the chlorine free H_1-e Pd catalyst that gave the highest methane response at each methane concentration. The gradient of the graph is 16.9 mV / % methane, which represents an 82 % increase over the average methane response of an H_1-e Pd film of similar thickness electrodeposited from the Cl containing Pd precursor. The results show that the average response of the V_1-e Pd film is very similar to that of the H_1-e Pd film. This indicates that the different structure gives no improvement in the magnitude of the methane response. The average gradients of the H_1 Pd-Pt and H_1-e Pt-Pd bi-layer catalysts is higher than those of mesoporous Pd except that of H_1-e Pd electrodeposited from the Cl-free Pd precursor. This suggests that the promoting effect of Pt on the methane response of Pd is less than the effect of a Cl- free Pd template bath. The City Tech slurry catalyst on an SRL136 micro-

hotplate gives by far the highest methane sensitivity. The sensitivity is approximately 4 times greater than that of the 90N pellistor which contains a similar make up of catalytic material.

5.7.2 Comparison of methane response as a function of catalyst temperature

An investigation was carried out into how the magnitude of the methane response varies with the power supplied to the device. Varying the power of the device is a useful way of controlling the temperature of the catalyst. The voltage supplied from the power supply was increased to the standard value of 15.0 V for an SRL136 microhotplate and then reduced in one Volt increments. It was considered more suitable to start at the highest temperature as this would give a positive response for the first temperature. The temperature at which there was no methane sensitivity would then become clear. The catalyst was allowed 5 minutes to stabilise at each temperature prior to methane testing and the baseline was readjusted after each change in voltage. The results are shown in fig 91.

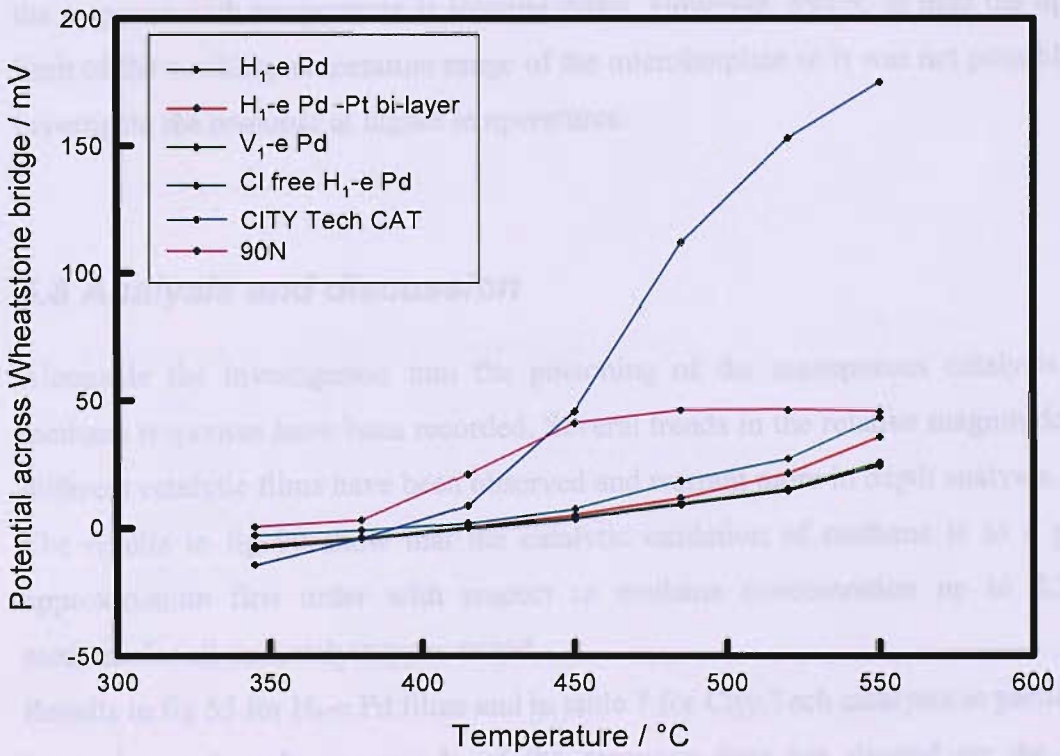

Fig 91 Graph showing methane response of different catalysts at different operating temperatures. For full deposition and preparation conditions please see fig 90.

Fig 91 shows the methane responses of the different types of catalyst produced. It can be seen that the graphs of all the mesoporous Pd catalysts have a similar shape. There are two slightly different trends within this group; the H_1-e and V_1-e Pd catalysts have fairly linear graphs up to 520°C where there is a larger increase in the magnitude of the response. This trend is also followed by the H_1-e Pd-Pt bi-layer and the Cl free H_1-e Pd, though they also show another earlier increase at 450 °C. This indicates that the latter two catalysts have slightly higher catalytic activity at lower temperatures.

The catalytic activity of the 90N starts at around 380 °C, increasing rapidly before levelling off at 450 °C. Unlike the mesoporous Pd catalysts it gives good catalytic activity at lower temperatures. Between 450 and 550 °C there is little increase in catalytic activity. The activity of the City Tech catalyst on a micro-hotplate increases after approximately 420 °C and increases rapidly. Unlike the 90N there is not such a pronounced levelling off, with catalytic activity still increasing at 550 °C. This trend suggests that the City Tech catalyst is not operating at its optimum temperature. Extrapolating the graph gives an approximate optimum temperature of 600 °C. The shape of the graph after 480 °C does suggest that the rate of increase of the response with temperature is slowing down. However, 550 °C is near the upper limit of the working temperature range of the microhotplate so it was not possible to investigate the response at higher temperatures.

5.8 Analysis and discussion

Alongside the investigation into the poisoning of the mesoporous catalysts the methane responses have been recorded. Several trends in the relative magnitudes of different catalytic films have been observed and warrant more in depth analysis.

The results in fig 90 show that the catalytic oxidation of methane is to a good approximation first order with respect to methane concentration up to 2.5 % methane for all the catalyst types tested.

Results in fig 55 for H_1-e Pd films and in table 7 for City Tech catalysts in particular have shown that the magnitude of the response does not depend on the film thickness and hence the number of active sites. This suggests that the reaction is controlled by the rate of mass transport inside the pores as increasing the number of

sites does not increase the reaction rate. H_1-e Pd-Pt bi-layer films were shown to give larger methane responses than H_1-e Pd film. (See fig 90) It was noted that at the temperatures used Pt was not catalytically active, though the Pt was believed to promote the activity of the Pd. This is inconsistent with the reaction being controlled by the rate of mass transport inside the pores the methane molecules have further to travel before reaching the active Pd sites. However, it is possible that the promotional effect of the Pt is more significant. Bi-layer films with Pd on top were also produced and were found to give higher responses than those with Pt on top, (See table 8) which again suggests the reaction is limited by mass transport inside the pores. This theory was also supported by results obtained from experiments in which the thickness of the Pd layer in a Pd-Pt bi-layer was increased. This showed no significant increase in the response with a thicker Pd film. In this case although the total thickness has increased the same number of Pd sites are still at the same distance below the pore opening. If the reaction rate was kinetically controlled then increasing the number of active sites would increase the reaction rate, this is therefore further evidence of a mass transport controlled reaction. It was decided to carry out some theoretical calculations in an attempt to investigate this theory.

The rate at which molecules enter the pore can be calculated using Knudsen effusion.[136]

$$Z_w A_o = pA_0 / (2\pi mkT)^{1/2} \qquad \textbf{(15)}$$

where,
$Z_w A_o$ is the number of molecules entering the pore in unit time
A_0 is the area of the pore mouth,
Z_w is the number of collisions per unit area per unit time.
m is the mass of the gas molecule.
p is the pressure

It is first necessary to calculate the number of pores in a typical mesoporous Pd film. A geometric surface area of 750 μm by 750 μm and a hexagonal array of pores were assumed. The number of pores was calculated to be 1.8×10^{10}. This assumes a perfect nanostructure and complete coverage of the electrode surface with Pd. The actual number of pores is likely to be less than this value as in many cases areas of

the electrode were not covered and it is likely that some parts of the film will not have a perfect nanostructure.

It is now possible to estimate the number of gas molecules entering the pores each second using equation 15. It is assumed that the pressure inside the cell is 1 atmosphere.

$$Z_w A_o n_{pores} = \frac{1.8 \times 10^{10} \times 1 \times 10^{5} \times \pi \times (1.5 \times 10^{-9})^2}{(2\pi \times 16 \times 1.6605 \times 10^{-27} \times 1.38 \times 10^{-23} \times 773)^{1/2}}$$

$$= 3 \times 10^{20} \text{ molecules entering pores each second.}$$

This figure will include air as well as methane. The concentration of methane is 2.5 %, it is therefore possible to estimate of the number of methane molecules entering the pores per second.

$$3 \times 10^{20} \times 0.025 = 7.5 \times 10^{18} \text{ s}^{-1}$$

It is then possible to estimate the amount of energy produced if these methane molecules are oxidised using the enthalpy of combustion of methane at 773 K. A value for the enthalpy of combustion of methane at 773 K was calculated using the 1st Law of Thermodynamics.[136]

$$\Delta H (T_2) = \Delta H (T_1) + {}_{T1}\int^{T2} \Delta C_p (T)\, dT \qquad \textbf{(16)}$$

where,

$\Delta H (T_2)$ is the enthalpy change at T_2, in this case 773 K

$\Delta H (T_1)$ is the enthalpy at T_1, in this case $T_1 = 298$ K

ΔC_p is the difference in the thermal heat capacities between the reactants and the products.

ΔH at 773 K for the combustion of methane was calculated to be -795.5 kJ mol^{-1}.

The possible amount of heat generated can now be estimated using the number of molecules entering the pores and enthalpy of combustion of methane.

$$\text{Heat generated} = \frac{7.5 \times 10^{18} \times 795.5}{6.02 \times 10^{23}}$$

$$= 10 \text{ W}$$

In section 4.5.1 the heat from a methane response of -20 mV was calculated to be approximately 1 mW. A positive response of about 20 mV is a good approximation for a typical response of an H_1-e Pd catalyst. It can therefore be seen by comparing the amount of heat produced with an estimated value for the maximum heat output that the reaction is not limited by the rate of mass transport of reactants.

The above calculations have suggested that the magnitude of the methane response is not determined by mass transport of methane in the catalyst layer. However, it was considered that the reaction may in fact be impeded by the diffusion of molecules into the pore due to the relatively small diameter of the pores. In section 5.5.3 City Tech catalysts applied to microhotplates were examined using SEM and found to have pore diameters in the region of 200 nm. This is significantly bigger than the 2.5 nm of a mesoporous Pd film. The results in fig 90 show that the City Tech catalysts gave significantly greater methane responses than any of the mesoporous Pd catalysts. It was considered possible that the smaller pore diameter of the mesoporous Pd films may be a factor in the lower methane response. Ryoo *et al.*[137] carried out investigations into the effect of mass transfer on the combustion of benzene and methane over palladium supported on porous materials. For metal catalysts supported on porous materials diffusion limitation becomes rate limiting when the rate of collisions with the pore walls are greater than intermolecular collisions. The methane molecule is significantly smaller than benzene hence restrictions on mass transport due to molecular size could be anticipated to be small. However, the Knudsen numbers for methane were significantly higher than those for benzene. It was concluded that the smaller molecular weight of methane results in the molecule moving more quickly. This will result in more frequent collisions with the pore walls which will result in slow mass transfer. Knudsen diffusion occurs when the collisions with the pore walls occur too frequently and reduce the rate of mass transfer. The Knudsen number, N_{kn}, is defined in equation 17;

$$N_{kn} = \lambda / 2r \qquad \textbf{(17)}$$

Where λ is the mean free path and r the radius of the pore.

The mean free path is defined in equation 18;[136]

$$\lambda = \frac{RT}{\sqrt{2}.\Pi d^2 N_A p} \qquad \textbf{(18)}$$

Where R is the ideal gas constant, T the temperature in K, d the diameter of the gas molecule / Å, N_A is Avogadro number and p is the pressure of the gas / kPa. The diameter of methane molecule is 4.0 Å and the pressure of the gas is atmospheric, P_o is 750 mm Hg or 100 kPa. The temperature is approximately 500°C, so T is 773 K. The mean free path, λ can now be calculated.

$$\lambda = \frac{RT}{\sqrt{2}.\Pi d^2 N_A P}$$

$$= 1.5 \text{ E-7 m}$$

$$= 1500 \text{ Å}$$

It is therefore possible to calculate N_{Kn} assumning a pore diameter of 2.5 nm = 25 Å

N_{Kn} = λ / 2r, where r is the radius of the pore / Å

= 1500 / (2 x 12.5)

= 60

Ryoo *et al.*[137] report that a Knudsen number of larger than 10 resulted in a reduction in the reaction rate as a result of diffusion limitation. It can therefore be seen that a reduction in the rate of the catalytic combustion of methane can be expected in mesoporous Pd films. The calculation was also carried out for the City Tech catalysts. A pore diameter of 200 nm was assumed.

N_{Kn} = λ / 2r, where r is the radius of the pore / Å

= 1500 / (2 x 1000)

= 0.75

It can be seen that there will be no rate reduction of methane oxidation by the City Tech slurry as a result of diffusion limitation.

Examining the magnitude of the methane responses in table 8 it is also noted that the methane responses of the City Tech catalysts are significantly greater than those of the 90N pellistor made from the same material. This suggests that the structure of the material may be important. The 90N is made by building up a catalyst layer. Consequently the catalyst may have a less open structure which may reduce diffusion. It is also possible that the pore diameter may be less resulting in a diffusion limited reaction rate.

It was also noted that the poisoning of the City Tech catalyst although far grater than that of the mesoporous Pd catalysts was significantly less than that of the 90N. It may be that the more open structure of the material which resulted in a larger response comprimises the poison resistance.

5.9 Summary

In this chapter the poison resistance of various types of mesoporous Pd as well as City Technology slurry catalysts has been investigated. Results showed that H_1-e Pd films were quickly and irreversibly poisoned by HMDS. It was proposed that the structure type might be responsible for the poor poison resistance and for this reason V_1-e Pd films were produced, though these showed similarly poor resistance. It was then decided to investigate the effect of adding a protective layer of Pt. It was found that this did result in a relatively significant increase in the poison resistance though the actual poison resistance was still poor compared to that of commercial pellistors. Catalysts were also made using City Technology slurry on microhotplates. These devices gave a more gradual loss of methane activity when poisoned by HMDS though they were still poisoned faster than the 90N pellistor. This result suggests that the structure of the 90N may be of fundamental importance given that the two devices had similar catalytic material. Experiments were carried out to investigate the effect of increasing the amount of catalytic material on the poison resistance. With the exception of one result it was found that increasing the amount of catalyst gave an increase in poison resistance. This result supported the proposed theory that the poisoning time may be related to the number of catalytically active sites available.

The relative magnitudes of the methane responses of the various catalysts was also investigated. It was found that the City Tech slurry on microhotplates had by far the largest methane sensitivity. It was noted that the sensitivity was far greater than that of the 90N. It was also noted that the City Tech slurry catalyst films of differing thickness all had similar maximum methane responses. Of the mesoporous catalysts the H_1-e Pd deposited from the Cl-free precursor had the highest sensitivity followed by the Pd-Pt bi-layer.

Experimental results suggested that mass transport may be the rate determining step in the catalytic combustion of methane over porous catalysts. Calculations were carried out in an effort to determine the rate determining step of the reaction. A theoretical value for the heat output was calculated based on the amount of methane

effusing into the pores. This was significantly larger than the energy involved in a typical methane response. This suggested that the reaction was not mass transport controlled. The possibility that the reaction rate may be limited by the effusion of methane into the pores was considered. Knudsen numbers were calculated for the City Tech and mesoporous catalysts and suggested that the reaction of methane in mesoporous films was limited by the rate of diffusion into the pores.

6 Responses and poisoning of mesoporous Pd films on micro-hotplates in other flammable gases

6.1 Introduction

In chapter 4 H_1-e Pd films were shown to give stable, reproducible responses to methane. In chapter 5 the poisoning of the methane response of H_1-e Pd, as well as other types of catalyst, by HMDS was investigated. It was concluded that H_1-e Pd, V_1-e Pd and H_1-e Pd-Pt bi-layer films were all quickly and irreversibly poisoned by HMDS. In this section the response of these catalysts to flammable gases is investigated. The motivation for this investigation is to compare the relative magnitudes of the responses as well as poisoning of the methane response by HMDS in different flammable gases.

Garcia *et al.* [138] investigated the oxidation of various short chain alkanes by 5 % Pd / Al_2O_3 catalysts and vanadium modified palladium catalysts. The results obtained showed that both types of catalyst exhibited catalytic activity for methane, ethane, propane and *n*-butane. At 500 °C the 5 % Pd / Al_2O_3 catalyst gave a 100 % conversion of all the gases, whilst the vanadium modified Pd catalyst gave 100 % conversions of all the gases with the exception of methane to which a 56 % conversion rate was reported. A study by Ryoo *et al.* [137] investigated the catalytic combustion of methane and benzene by Pd catalysts on porous supports. The investigation reported that benzene oxidation over supported Pd catalysts begins at 250 °C, with a 100 % combustion being achieved at approximately 500 °C for all of the catalysts tested.

6.1.1. Response of catalysts to methane, hydrogen and heptane.

Before investigating the catalytic responses of the catalysts to different flammable gases it was decided to determine the magnitude of the thermal responses. The observed responses when a catalyst is exposed to a flammable gas such as methane, is composed of the thermal response and the catalytic response as the two processes occur simultaneously. Consequently the true catalytic response is the observed response plus the thermal response. The thermal responses of bare SRL136 microhotplates to different flammable gases is shown in fig 92.

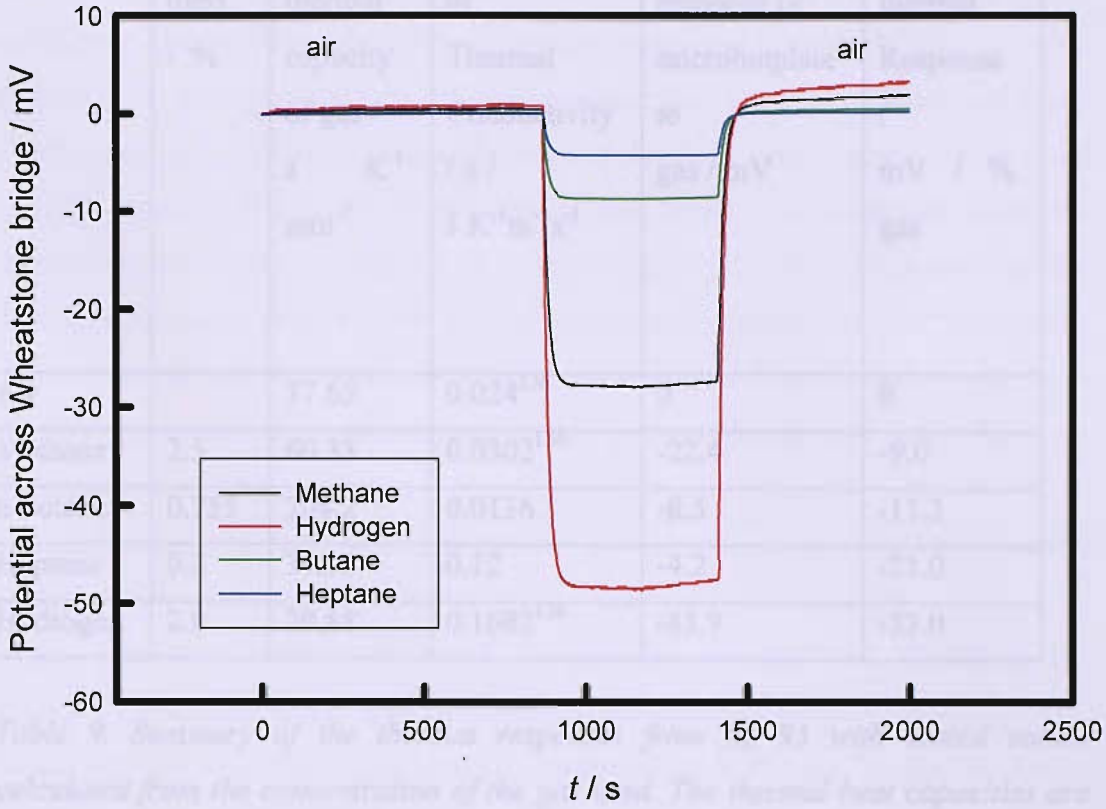

Fig 92. Response of an uncoated SRL136 microhotplate to different flammable gases. The device was powered at 15.0 V from the PSU and a gas flow rate of 400 cm^3min^{-1} was used. The following gas concentrations were used, methane 2.5 %, n-butane 0.755 %, hydrogen 2 % and heptane 0.2 %.

It can be seen in fig 92 that the magnitudes of the thermal responses varies significantly.

Gas	Conc. used / %	C_p / thermal capacity of gas / J K^{-1} mol^{-1}	Coefficient of Thermal Conductivity / κ / J $K^{-1}m^{-1}s^{-1}$	Thermal response of microhotplate to gas / mV	Scaled thermal Response / mV / % gas
Air		37.65	0.024[136]	0	0
Methane	2.5	60.33	0.0302[136]	-22.4	-9.0
n-butane	0.755	204.2	0.0136	-8.5	-11.3
Heptane	0.2	342.3	0.12	-4.2	-21.0
Hydrogen	2.0	29.88	0.1682[136]	-45.9	-23.0

Table 9. Summary of the thermal responses from fig 93 with scaled values calculated from the concentration of the gas used. The thermal heat capacities are also given calculated using equation 19.

The specific heat capacity, c_p

$$\mathbf{c_p = a + bT + cT^{-2}} \qquad \mathbf{(19)}$$

Where, T is the temperature in Kelvin and a, b and c are constants.
For air a = 28.1, b = 1.97 x 10^{-3} K^{-1}, c = 4.8 x 10^6 K^2,
And for methane, a = 23.64, b = 47.86 x 10^{-3} K^{-1}, c = -1.92 x 10^5 K^2
For hydrogen[136] a = 27.28, b = 3.26 x 10^{-3} K^{-1}, c = 0.5 x 10^5 K^2

Values of c_p for n-butane and heptane were obtained from CRC Handbook of chemistry and physics.
Values of the thermal responses are shown in table 9. Before they can be compared it is necessary to consider the concentrations of the gases used as at a larger gas concentration there will be more gas molecules present hence more heat will be lost. The thermal responses were scaled using the gas concentrations. It can be seen that the scaled thermal responses of the hydrocarbon gases scale according to the specific heat capacities of the gases. However, the thermal response for hydrogen was the largest yet the heat capacity of hydrogen was calculated to be lower than

air. However, the thermal conductivities of the gases also needs to be considered as these also consider the relative speeds of the different gas species. Values of the coefficient of thermal conductivity, κ, are also presented in table 9. It can be seen that the value for hydrogen is significantly greater than those of methane and air. It is proposed that as hydrogen is a diatomic molecule it consequently has a small thermal capacity. But it can move quickly due to its low molecular mass and therefore has a higher coefficient of thermal conductivity. It is proposed that the thermal response is related to the thermal conductivity rather than just the thermal capacity as the relative speeds of the gas molecules also needs to be taken into account when considering the amount of heat removed by the gas molecules from the surface.

The magnitudes of the thermal responses have been established. The catalytic responses were then investigated.

Three types of catalyst were tested for sensitivity to methane, hydrogen and heptane. These were H_1-e Pd, an H_1-e Pd – Pt bi-layer and a City Technology slurry. In addition a 90N pellistor was used as a reference in each case. It was decided to test for methane in the same test to obtain a reference response. An example of each is shown in figs 93, 94 and 95 respectively.

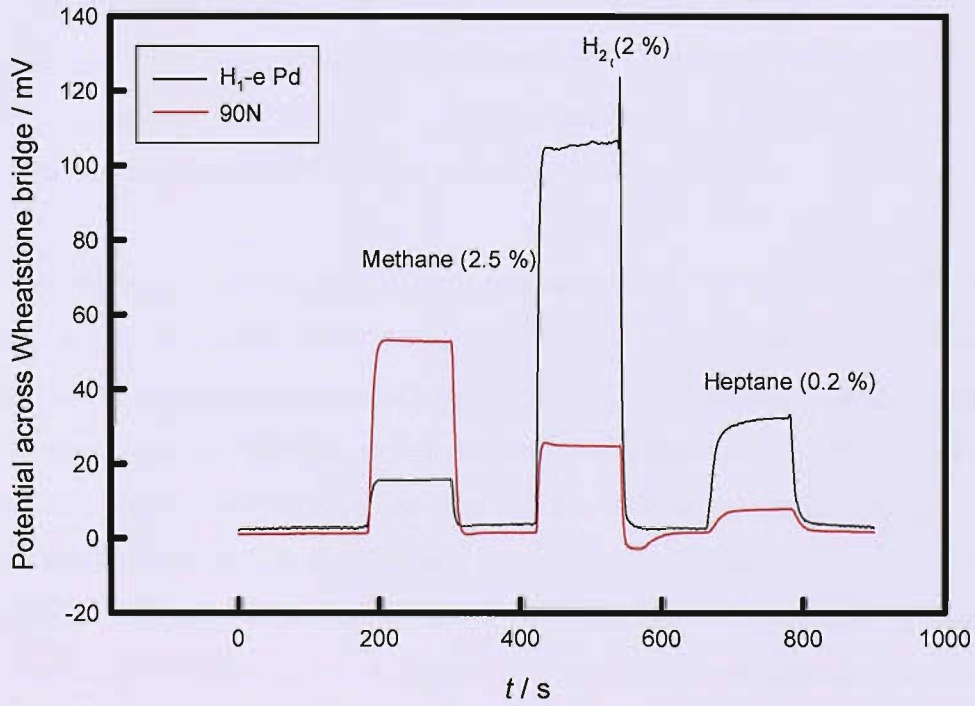

Fig 93. Response of an H_1-e Pd catalyst on an SRL136 micro-hotplate to methane, hydrogen and heptane. For details of the deposition please refer to fig 56.

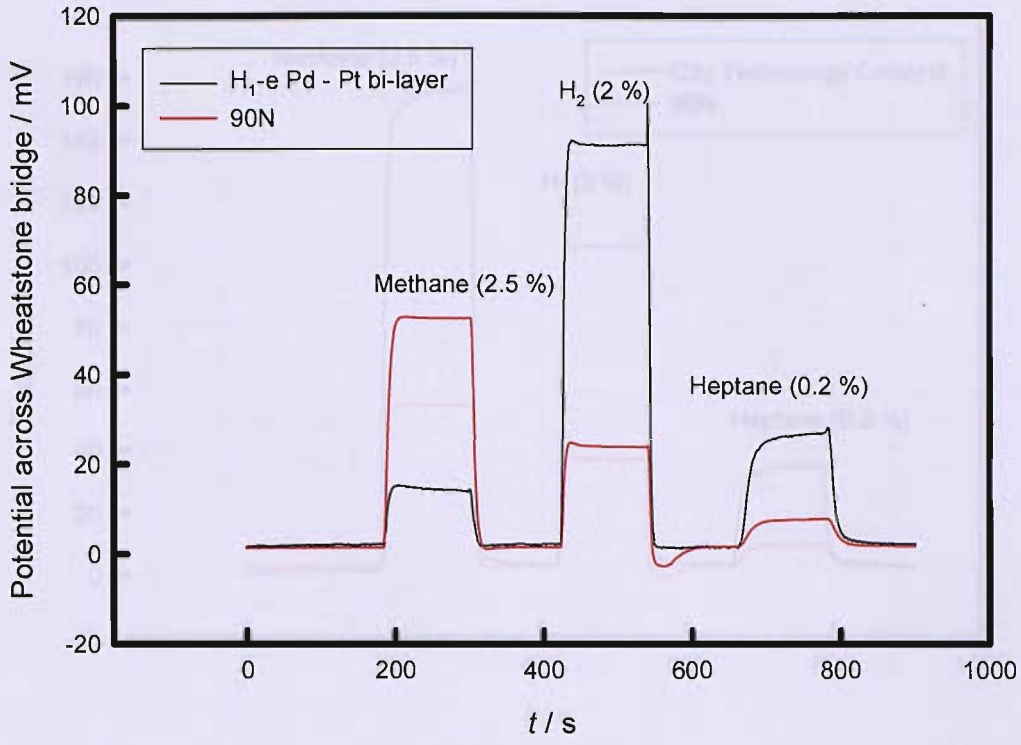

Fig 94. Response of an H_1-e Pd-Pt bi-layer film on an SRL136 micro-hotplate to methane, hydrogen and heptane. Testing was carried out at City Technology labs. For details of the deposition please refer to fig 75.

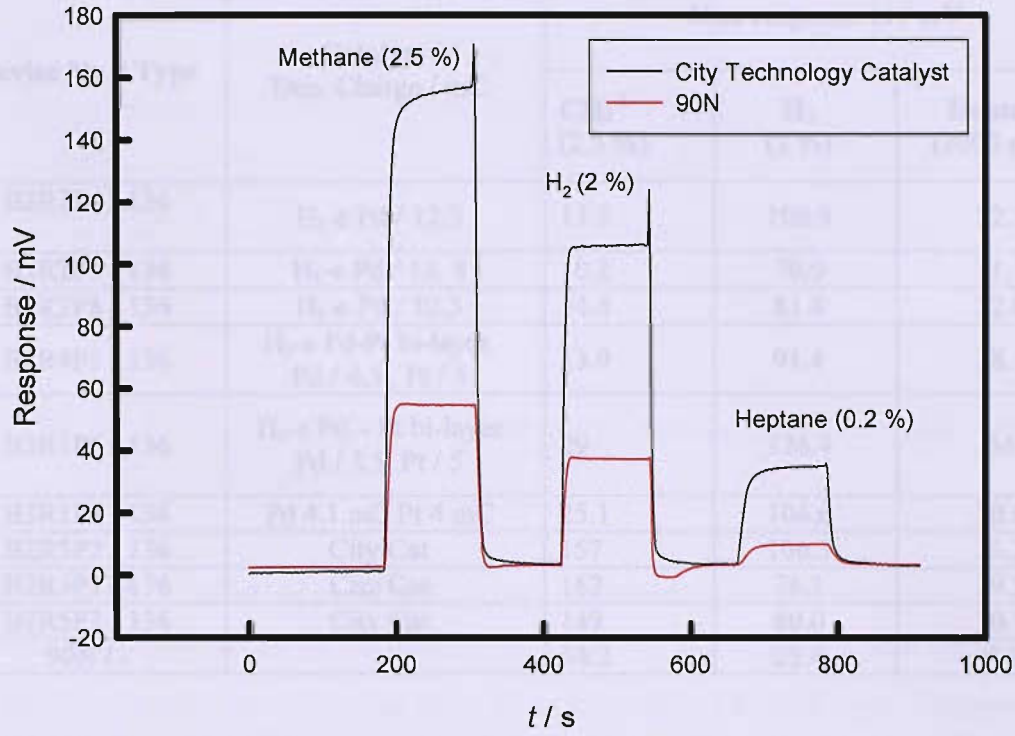

Fig 95. Response of a City Tech Catalyst on an SRL136 micro-hotplate to methane, hydrogen and heptane. This response was obtained at City Tech labs. A droplet of catalyst mixture was applied to the Au electrode. The device was then powered to 4 V for ten minutes, before powering up to 15 V for one hour. The device was then powered down and rinsed in iso-propanol for 10 minutes prior to drying at 40 °C for 10 minutes. The device was then powered to 15 V and exposed to methane. A positive response of 160 mV was recorded.

The methane, hydrogen and heptane responses of an H_1-e Pd, H_1-e Pd-Pt bi-layer and a City Tech catalyst are shown in figs 93, 94 and 95 respectively. However, different concentrations of gases were used and it is inappropriate to compare the relative responses without considering the concentrations. For the H_1-e Pd and H_1-e Pd-Pt bi-layer catalysts it can be seen that the catalyst has the greatest sensitivity to hydrogen then heptane and the least sensitivity to methane. This contrasts with the trend exhibited by both the 90N and City Tech catalysts which show greatest sensitivity to methane, then hydrogen then heptane. These responses and those of other similarly prepared catalysts are summarised in table 10.

Device No. / Type	Catalyst / Dep. Charge / mC	Max response to / mV		
		CH_4 [1] (2.5 %)	H_2 (2 %)	Heptane (2000 ppm)
B2R2P4 / 136	H_1-e Pd / 12.5	13.7	106.9	32.5
B2R2P6 / 136	H_1-e Pd / 12. 4	10.2	70.9	31.1
B2R2P8 / 136	H_1-e Pd / 12.5	14.4	81.4	32.0
B1R4P5 / 136	H_1-e Pd-Pt bi-layer. Pd / 4.5 , Pt / 5	13.9	91.4	28.1
B3R1P6 / 136	H_1-e Pd – Pt bi-layer Pd / 5.5, Pt / 5	29	126.4	34
B3R1P7 / 136	Pd 4.1 mC Pt 4 mC	25.1	106.6	30.6
B2R5P2 / 136	City Cat	157	106.3	35.2
B2R5P1 / 136	City Cat	162	76.1	29.2
B2R5P3 / 136	City Cat	149	80.0	30.1
90N / -	-	54.2	23.4	9.1

Table 10. Summary of the responses of catalysts to methane, hydrogen and heptane at City Technology labs.

Catalyst	Average Response to / mV		
	CH_4 [2] (2.5 %)	H_2 (2 %)	Heptane (0.2 %)
H_1-e Pd	12.8 (1.3) 5.1	86.4 (10.7) 43.2	31.9 (0.4) 159.5
H_1-e Pd-Pt bi-layer	22.7 (4.5) 9.1	108.1 (10.1) 54.1	30.9 (1.7) 154.5
City Cat	156 (3.8) 62.4	87.5 (10.5) 43.8	31.5 (1.5) 157.5
90N	54.2 21.7	23.4 11.7	9.1 45.5

Table 11. Average of 3 responses of the various types of catalyst to methane, hydrogen and heptane. The result for the 90N is for the same device. The standard error is shown in brackets after each average. The response normalised to the concentration of the gas in mV / % of gas is shown in red.

[1] prior to H_2 testing
[2] prior to H_2 testing

	Ratio of average sensitivities to average methane sensitivity		
Catalyst	CH_4	H_2	Heptane
H_1-e Pd	1	8.5	31.3
H_1-e Pd-Pt bi-layer	1	6.0	17.0
City Cat	1	0.7	2.5
90N	1	0.5	2.1

Table 12. Ratio of responses to hydrogen and heptane to methane calculated for responses shown in table 10.

The results in tables 11 show the average responses of the different catalysts to the different gases as well as the average sensitivity in mV / % gas which are shown in red. The results show that the H_1-e Pd and the H_1-e Pd-Pt bi-layer catalysts have high sensitivity to heptane then hydrogen and then methane. It is noted that with the exception of the 90N the average sensitivities to heptane and to a lesser extent hydrogen are similar. This is in contrast to the methane sensitivities which vary significantly.

Aryafar and Zaera[17] investigated the kinetics of alkane oxidation over nickel, palladium and platinum catalysts. The results showed a good correlation between C–H bond energies and reactivities. It was proposed that the initial activation of the alkane was therefore the rate limiting step. The results showed that C-H bond energy decreased with increasing hydrocarbon chain length an observation supported by other authors.[21,22] This is consistent with the results obtained here which show that both the H_1-e Pd and the H_1-e Pd-Pt bi-layer catalysts exhibit higher sensitivity to heptane than methane. However, the results in tables 10, 11 and 12 show that both the 90N and the City Tech. catalyst exhibited significantly higher sensitivity to methane than heptane.

The results in table 10 show that the City Tech catalyst slurry on the microhotplates gave a very large response to methane compared to both the 90N and the different mesoporous Pd catalysts. The mesoporous Pd and City Tech slurry catalysts gave very similar responses to both hydrogen and heptane and for both gases the responses of the City Technology catalyst were significantly greater than those of

the 90N. It is noted from table 12 that the ratios of the hydrogen and heptane responses to methane of both the City Tech catalyst and the 90N pellsitor are similar. This indicates that using the same catalytic material on different platforms has not changed the relative sensitivities.

The magnitude of the response and the thickness of the catalyst film are shown in table 10. Devices B2R2P4 and B2R2P6 were both prepared by passing 12.4 mC in the electrodeposition of H_1-e Pd. The devices gave methane responses of 13.7 and 10.2 mV respectively. In this case the responses are similarly though poor reproducibility was often noted for similarly prepared H_1-e Pd films. In the H_1-e Pd-Pt bi-layer catalysts charges of 4.5, 5.5 and 4.1 mC were passed in the electrodeposition of Pd. Methane responses of 13.9, 29 and 25.1 mV were obtained respectively. The range of responses is greater indicating fairly poor reproducibility. The results also show that thinner Pd catalysts gave higher methane responses assuming no catalytic contribution from the Pt layer.

Variation in magnitudes of responses

Examining the results shows that the magnitude of the response of similar catalyst types varies significantly. For example H_1-e Pd catalysts of similar thicknesses gave methane responses varying by approximately 34 %. The variation in the hydrogen response was approximately 50 % whilst the variation in the heptane response was 4 %. These values were calculated using the difference between the smallest and the largest response and dividing by the smallest response. The variation in the responses of the H_1-e Pd-Pt bi-layer catalysts were calculated in the same way. The variation in the methane responses was 109 %, 38 % for hydrogen responses and the variation in heptane responses was 21 %. The variation of the responses of the City Tech catalysts were also calculated. The variation in methane responses was 3.8 %, hydrogen 40 %, and a variation in heptane responses of 21 %. A significant variation in the responses of the City Tech catalysts may be expected due to their nature of their fabrication which does not ensure that the same composition is used and also that the same amount of catalyst is applied.

The reason for the variation of the responses of the mesoporous catalysts is unclear. The template mixtures were electrodeposited from similarly prepared template mixtures that were well mixed to ensure good homogeneity. Similar deposition charges were used to give films of similar thickness. It is likely that in some cases

the nanostructure was imperfect and this may account for some of the variation. However, it is noted that whilst variation to one gas may be significant the variation of the same catalyst to a different gas is significantly less. For example H_1-e Pd catalysts varied in magnitudes of methane response by 34 %, whilst the variation of the heptane responses was only 4 %. It is therefore difficult to propose any reason for the variation the response to one gas type when the catalyst exhibits significantly less variation to another gas.

6.2 Linearity of responses

In the previous section H_1-e Pd, H_1-e Pd-Pt bi-layer and City Tech catalysts were shown to give catalytic responses to methane, hydrogen and heptane. In this section the linearity of the responses to hydrogen and heptane will be investigated.

6.2.1. Hydrogen

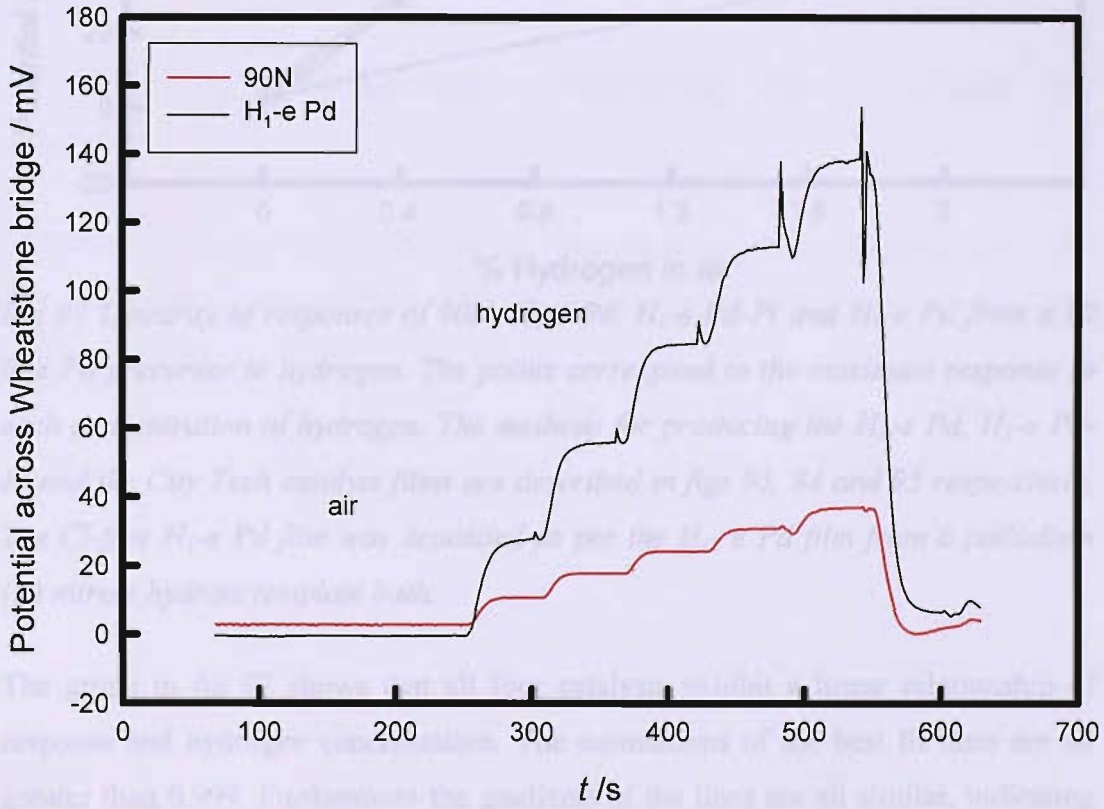

Fig 96. Response of an H_1-e Pd catalyst on an SRL136 micro-hotplate to increasing concentrations of hydrogen. Concentrations of 0, 0.4, 0.8, 1.2, 1.6 and 2.0 % hydrogen in air were used .The H_1-e Pd film was electrodeposited as per fig 56.

Fig 96 shows the response of an H_1-e Pd catalyst to increasing concentration of hydrogen. An H_1-e Pd-Pt bi-layer, a H_1-e Pd film from a chloride free precursor and a City Tech catalyst were tested in a similar way. A graph summarising the results is shown in fig 97.

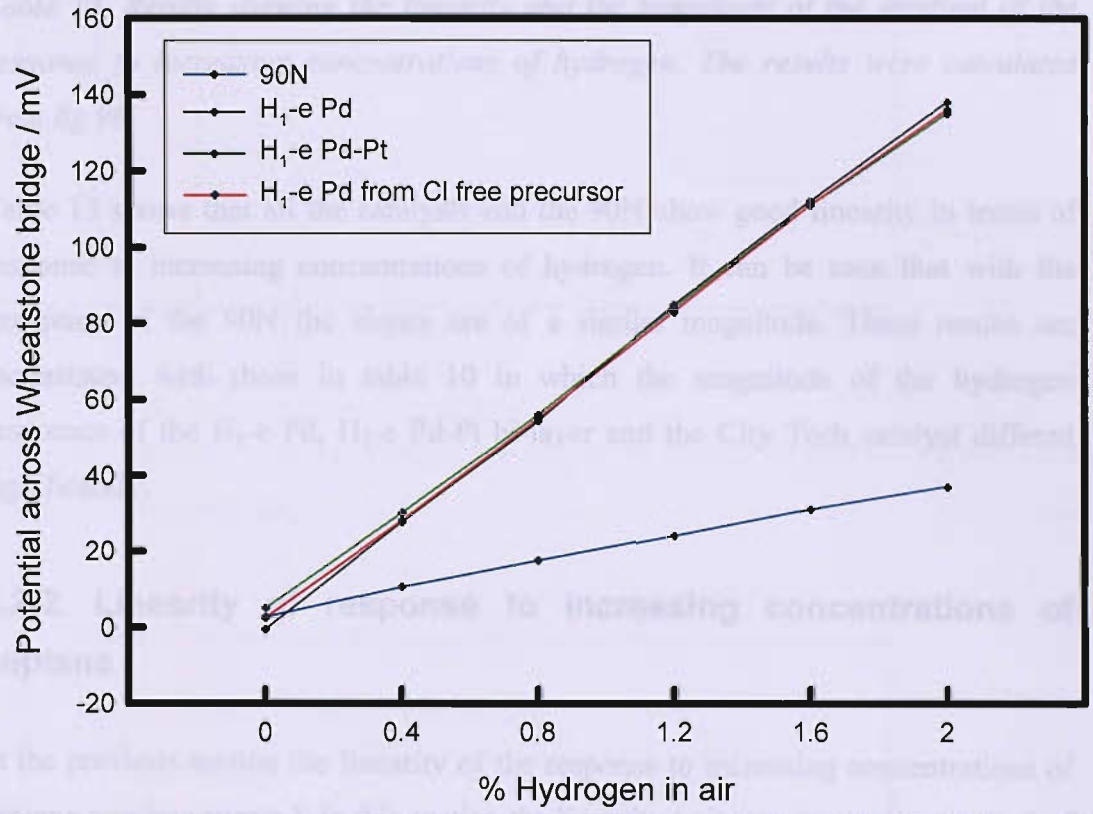

Fig 97 Linearity of responses of 90N, H_1-e Pd, H_1-e Pd-Pt and H_1-e Pd from a Cl free Pd precursor to hydrogen. The points correspond to the maximum response to each concentration of hydrogen. The methods for producing the H_1-e Pd, H_1-e Pd-Pt and the City Tech catalyst films are described in figs 93, 94 and 95 respectively. The Cl-free H_1-e Pd film was deposited as per the H_1- e Pd film from a palladium (II) nitrate hydrate template bath.

The graph in fig 97 shows that all four catalysts exhibit a linear relationship of response and hydrogen concentration. The correlations of the best fit lines are all greater than 0.999. Furthermore the gradients of the lines are all similar, indicating that the different catalysts had similar catalytic activity for hydrogen. This is interesting as when testing for methane the same H_1-e Pd film deposited from a Cl-free Pd precursor had a notably higher response.

Catalyst	90N	H_1-e Pd from Cl free Pd precursor	H_1-e Pd	H_1-e Pd-Pt bi-layer
R^2 of linear fit	0.998	0.999	0.999	0.999
Gradient mV / % H_2	17.1	69.7	67.5	65.8

Table 13. Results showing the linearity and the magnitude of the gradient of the response to increasing concentrations of hydrogen. The results were calculated from fig 98.

Table 13 shows that all the catalysts and the 90N show good linearity in terms of response to increasing concentrations of hydrogen. It can be seen that with the exception of the 90N the slopes are of a similar magnitude. These results are inconsistent with those in table 10 in which the magnitude of the hydrogen responses of the H_1-e Pd, H_1-e Pd-Pt bi-layer and the City Tech catalyst differed significantly.

6.2.2. Linearity of response to increasing concentrations of heptane

In the previous section the linearity of the response to increasing concentrations of heptane was investigated. In this section the linearity to increasing concentrations of hydrogen is reported.

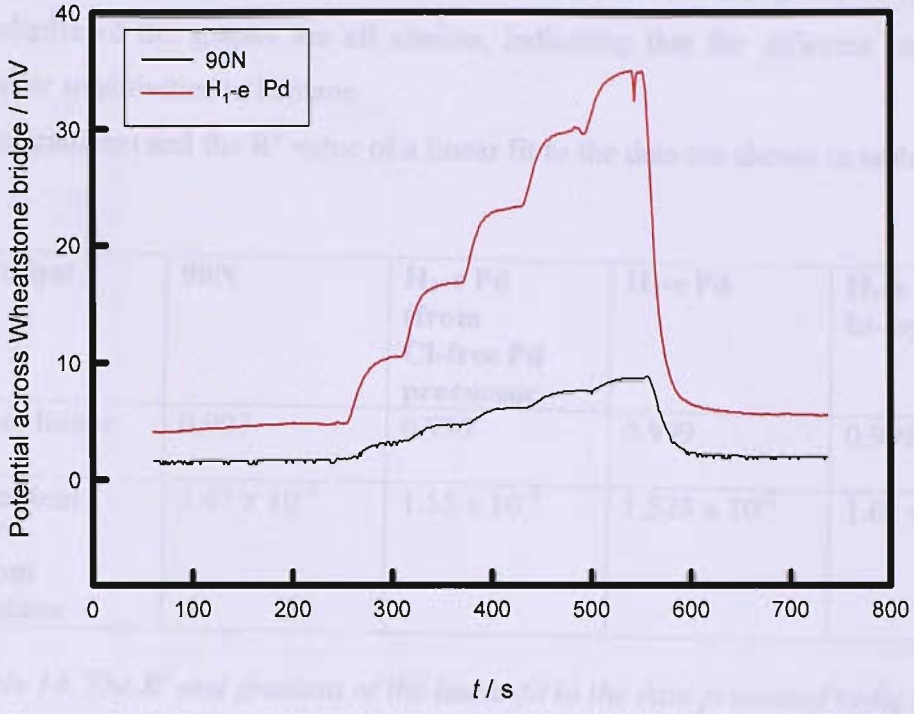

Fig 98. Response to increasing concentrations of heptane of an H_1-e Pd film on an SRL136 microhotplate.

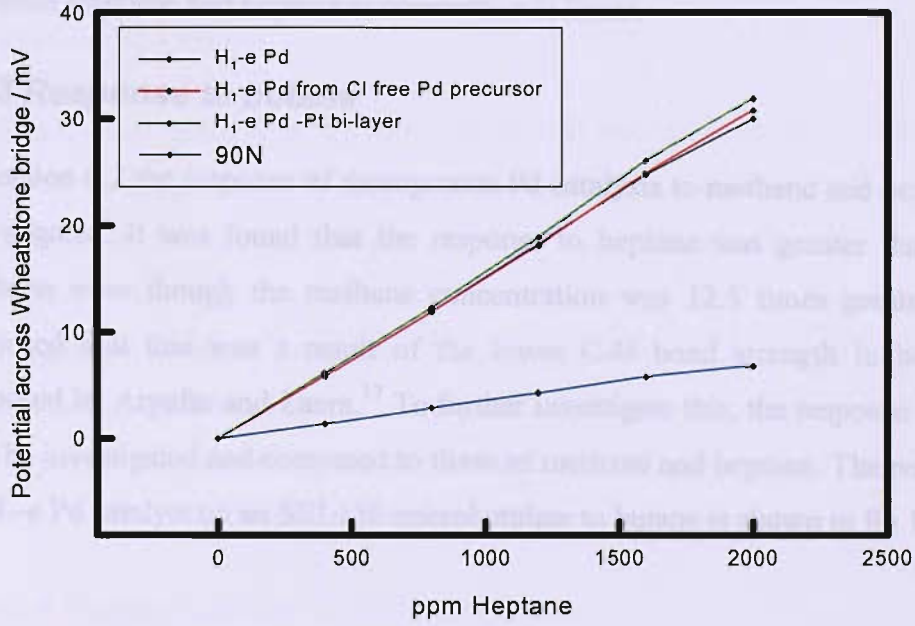

Fig 99. Linearity of heptane responses. The points correspond to the maximum response to each concentration of heptane. The methods for producing the H_1-e Pd, H_1-e Pd-Pt and the City Tech catalyst films are described in figs 94, 95 and 96 respectively.

Fig 99 shows that all of the catalysts gave linear responses to increasing concentrations of heptane. It can be seen that with the exception of the 90N the gradients of the graphs are all similar, indicating that the different catalysts had similar sensitivities to heptane.

The gradients and the R^2 value of a linear fit to the data are shown in table 14.

Catalyst	**90N**	**H_1-e Pd (from Cl-free Pd precursor**	**H_1-e Pd**	**H_1-e Pd-Pt bi-layer**
R^2 of linear fit	0.997	0.999	0.999	0.999
Gradient / mV / ppm heptane	3.47×10^{-3}	1.55×10^{-2}	1.524×10^{-2}	1.62×10^{-2}

Table 14. The R^2 and gradient of the linear fit to the data presented in fig 100, of the relationship between response and concentration of heptane.

The results in table 14 of the linear fit to the data indicate that the relationship between response and heptane concentration is linear.

6.3 Response to butane

In section 6.2 the response of mesoporous Pd catalysts to methane and heptane was investigated. It was found that the response to heptane was greater than that of methane even though the methane concentration was 12.5 times greater. It was proposed that this was a result of the lower C-H bond strength in heptane as proposed by Aryafar and Zaera.[17] To further investigate this, the response to butane will be investigated and compared to those of methane and heptane. The response of an H_1-e Pd catalyst on an SRL136 microhotplate to butane is shown in fig 100.

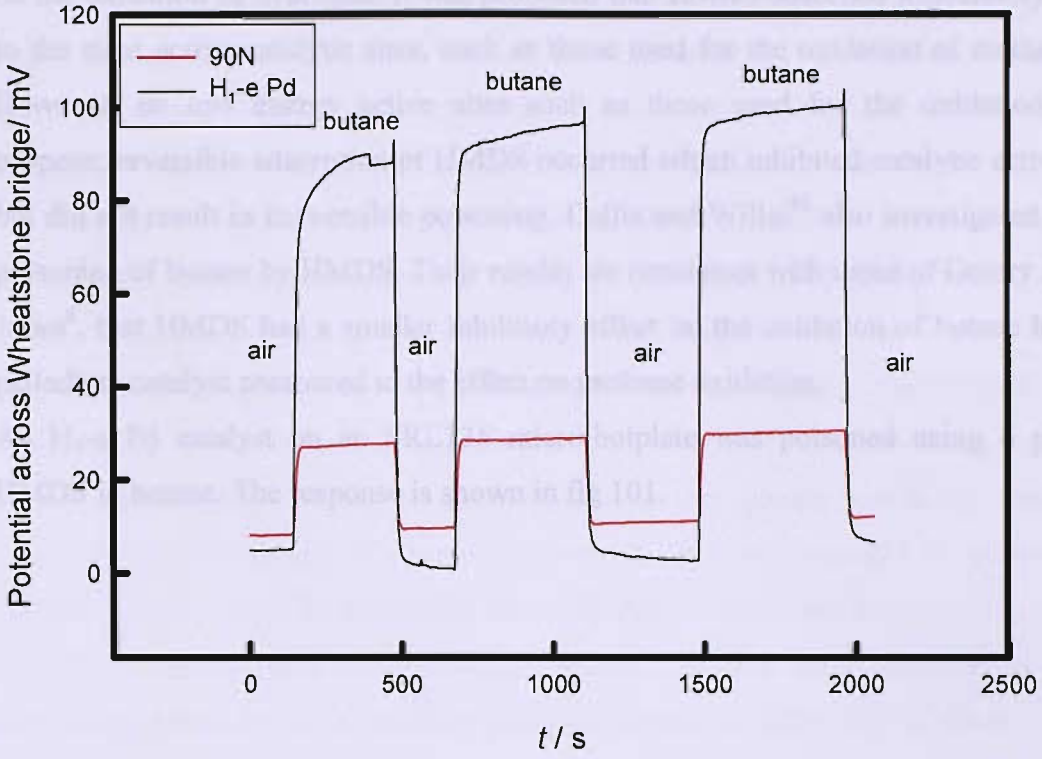

Fig 100. Response of an H_1-e Pd catalyst on an SRL136 microhotplate to butane (0.755 %). For details of the preparation of the Pd film please refer to fig 56. The surface area was calculated to be 15.8 m^2g^{-1}. The catalyst gave a positive response of 50 mV to methane.

The butane response in fig 100 is stable and reproducible. The maximum response is approximately 85 mV, considerably higher than the maximum methane response of 50 mV. The sensitivities are 113 mV / % butane and 20 mV / % methane. The ratio of the butane to methane sensitivity is 5.6. This is less than the ratio of methane to heptane sensitivity of approximately 31 shown in table 12. This is consistent with the findings of Aryafar and Zaera. The relative magnitudes of the responses are further discussed in section 6.6.

6.4 Poisoning by HMDS in butane

Part of the motivation for investigating the responses to other flammable gases such as butane and heptane was to investigate how the poison resistance to HMDS compared to that in methane. In section 5.1.2 the poisoning of low and high energy active sites was discussed. Work by Cullis and Willat[53] reported that HMDS only

had an inhibitory effect on the catalytic oxidation of propene and a negligible effect on the oxidation of hydrogen. It was proposed that HMDS adsorbed irreversibly on to the most active catalytic sites, such as those used for the oxidation of methane. However, on low energy active sites such as those used for the oxidation of propene, reversible adsorption of HMDS occurred which inhibited catalytic activity but did not result in irreversible poisoning. Cullis and Willat[53] also investigated the poisoning of butane by HMDS. Their results are consistent with those of Gentry and Jones[8], that HMDS had a smaller inhibitory effect on the oxidation of butane by a palladium catalyst compared to the effect on methane oxidation.

An H_1-e Pd catalyst on an SRL136 micro-hotplate was poisoned using 6 ppm HMDS in butane. The response is shown in fig 101.

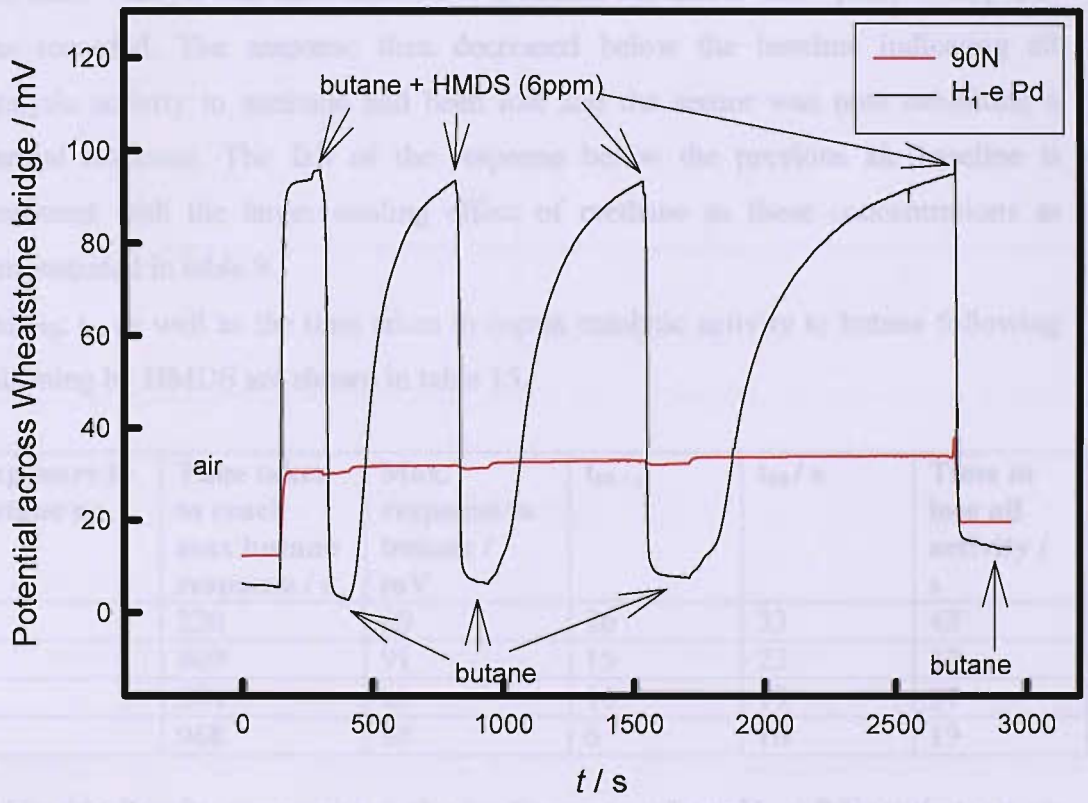

Fig 101. Response of an H_1-e Pd catalyst on an SRL136 microhotplate to butane 0.755 %, and HMDS (6 ppm). For full details of the deposition of the Pd film please refer to fig 56.

Fig 101 shows the repeated poisoning of a mesoporous Pd catalyst by HMDS in butane. It can be seen that catalytic activity is lost very quickly. It is noted that the response returns to the air baseline and not below as observed in the poisoning of H_1-e Pd catalysts by HMDS in methane. A smaller cooling effect was anticipated based on the thermal response of a bare SRL136 microhotplate of -8.5 mV shown in table 9. Once the response had reached the baseline the supply of poison was stopped. It can be seen that once the supply of poison is stopped the response gradually increases, reaching the same maximum response recorded prior to poisoning. It is remembered that H_1-e Pd catalysts showed no signs of regaining any catalytic activity to methane following poisoning by HMDS. The catalyst was then poisoned a second time. Again, all catalytic activity was quickly lost though was regenerated when the supply of poison was removed. This was repeated a third time. From these results it can be concluded that with respect to butane the mesoporous Pd catalyst is quickly poisoned by HMDS but on removing the HMDS catalytic activity is regained. HMDS is therefore acting as an inhibitor rather than a poison.

The same catalyst was then exposed to methane. An initial small positive response was recorded. The response then decreased below the baseline indicating all catalytic activity to methane had been lost and the sensor was now exhibiting a thermal response. The fall of the response below the previous air baseline is consistent with the larger cooling effect of methane as these concentrations as demonstrated in table 9.

The t_{50}, t_{90} as well as the time taken to regain catalytic activity to butane following poisoning by HMDS are shown in table 15.

Exposure to butane no.	**Time taken to reach max butane response / s**	**Max. response to butane / mV**	**t_{50} / s**	**t_{90} / s**	**Time to lose all activity / s**
1	220	90	26	33	43
2	409	91	15	23	32
3	574	86	16	19	27
4	968	88	6	16	19

Table 15. Results summarising the performance of an H_1-e Pd catalyst on an SRL136 microhotplate following poisoning by HMDS in butane. The H_1-e Pd film was electrodeposited as per fig 56.

The results in table 15 show that the magnitude of the butane responses following repeated poisoning by HMDS are similar. It is also noted that the time taken to regain all catalytic activity to butane increases with each exposure to HMDS. Furthermore, the t_{50}, t_{90} and the time taken to lose all activity decrease with each addition of HMDS. A graph showing the time taken to regain butane activity after each addition of HMDS is shown in fig 102.

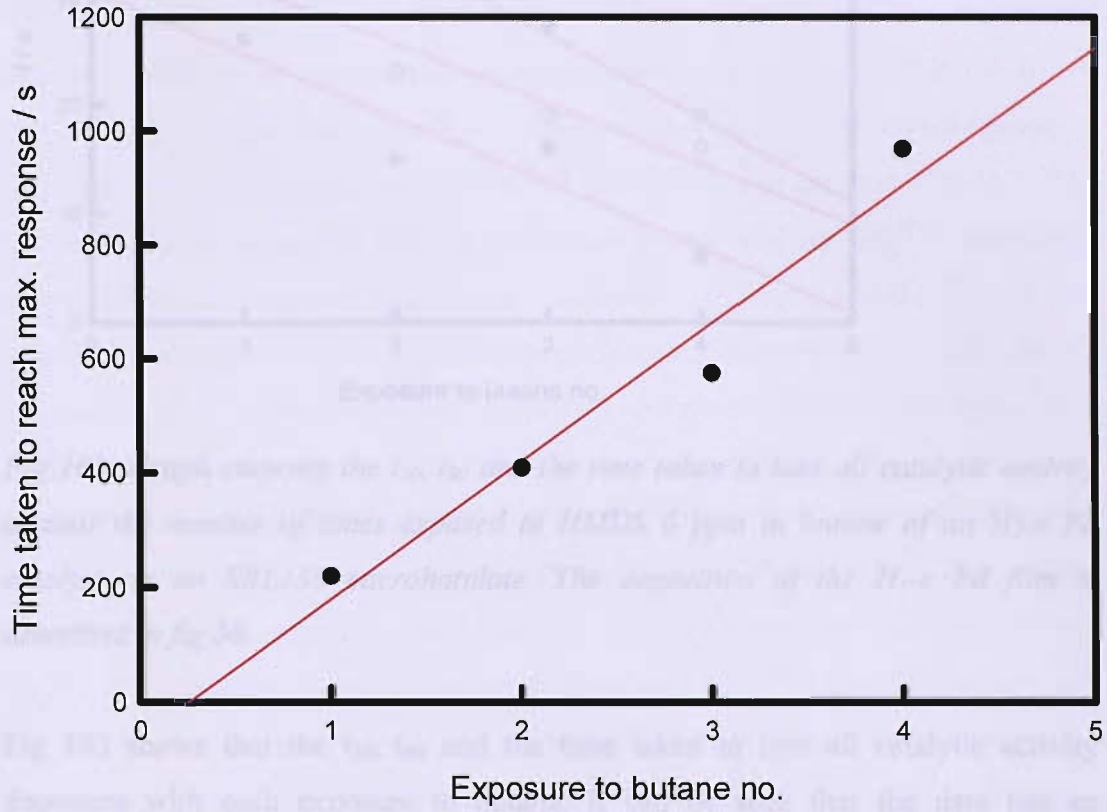

Fig 102. Graph showing the time taken for all butane activity to be regained following repeated poisoning by HMDS 6 ppm of an H_1-e Pd catalyst on an SRL136 microhotplate. The H_1-e Pd film was deposited as per fig 101.

Fig 102 shows the time taken to regain all activity to butane following repeated poisoning by HMDS. It can be seen that the graph has an approximate linear fit.It can be seen that full catalytic activity is regained though this takes longer with each exposure to HMDS. This suggests that with each successive exposure to poison more active sites are being poisoned due to the weak adsorbtion of the poison. Alternatively, it maybe that it becomes harder to remove the poison with each successive exposure. A graph of the t_{50}, t_{90} and the time taken to lose all catalytic

activity was also plotted against the number of times the catalyst was exposed to butane and is shown in fig 103.

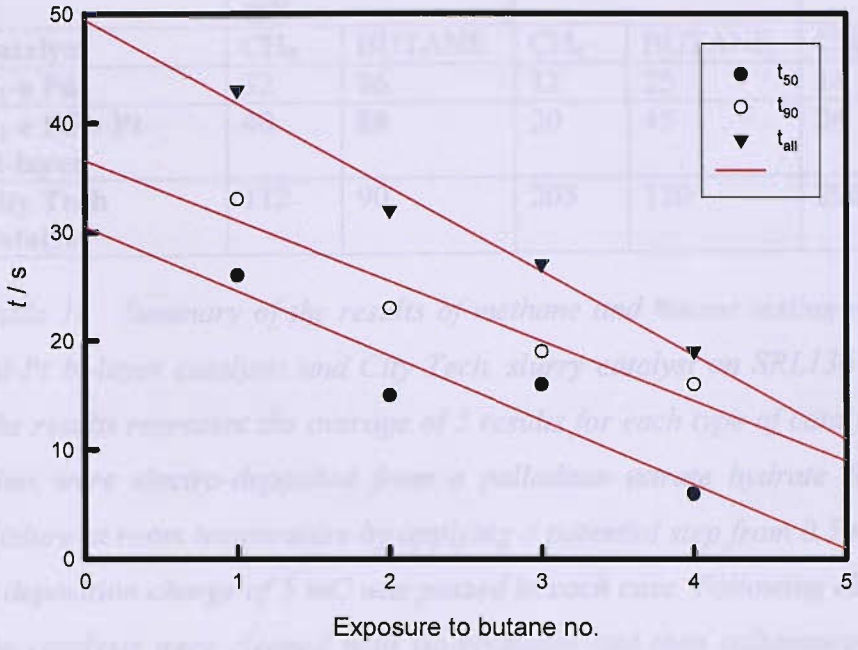

Fig 103. Graph showing the t_{50}, t_{90} and the time taken to lose all catalytic activity against the number of times exposed to HMDS 6 ppm in butane of an H_1-e Pd catalyst on an SRL136 microhotplate. The deposition of the H_1-e Pd film is described in fig 56.

Fig 103 shows that the t_{50}, t_{90} and the time taken to lose all catalytic activity decreases with each exposure to butane. It can be seen that the data has an approximate linear fit. The t_{50}, t_{90} and t_{all} values all decrease with each subsequent addition of HMDS indicating a drop in poison resistance.

Comparing these results with those of H_1-e Pd catalysts poisoned by HMDS in methane reveals that the poisoning times are longer. A similar mesoporous Pd catalyst had t_{50} and t_{90} values in methane of 11.5 and 14.5 s. After first exposure to butane the respective times are 26 and 33 s, which represents an increase of approximately 100%. A number of other H_1-e Pd, H_1-e Pd-Pt bi-layer and City Tech catalysts were tested in a similar manner. All exhibited the trends described above. A summary of the maximum response, the t_{50}, t_{90} and time taken to lose all catalytic activity values in butane are shown in table 16.

	MAX RESPONSE / mV		t_{50} HMDS 6 ppm / s		t_{90} HMDS 6 ppm / s	
Catalyst	CH_4	BUTANE	CH_4	BUTANE	CH_4	BUTANE
H_1-e Pd	32	86	12	25	14	29
H_1-e Pd – Pt Bi-layer	40	88	20	45	24	50
City Tech Catalyst	112	90	205	120	296	465

Table 16. Summary of the results of methane and butane testing of H_1-e Pd, H_1-e Pd-Pt bi-layer catalysts and City Tech. slurry catalyst on SRL136 microhotplates. The results represent the average of 3 results for each type of catalyst. The H_1-e Pd films were electro-deposited from a palladium nitrate hydrate Brij®56 template mixture at room temperature by applying a potential step from 0.5 to 0.1 V vs. SCE. A deposition charge of 5 mC was passed in each case. Following electro-deposition the catalysts were cleaned with iso-propanol and then voltammetrically cycled in 0.1 M sulphuric acid. In the H_1-e Pd-Pt bi-layer the H_1-e Pd film was electro-deposited from a palladium nitrate hydrate Brij®56 template mixture at room temperature by applying a potential step from 0.5 to 0.1 V vs. SCE. A deposition charge of 5 mC was passed in each case. The H_1-e Pt layer was electrodeposited onto the H_1-e Pd layer from a hexachloroplatinic acid– Brij®56 template mixture at room temperature by applying a potential step of 0.5 to -0.1 V vs. SCE. A deposition charge of 5 mC was passed in each case. Following electro-deposition the catalysts were cleaned with iso-propanol and then voltammetrically cycled in 0.1 M sulphuric acid. The City Tech. slurry catalysts were formed from 1 drop of slurry mixture comprising 0.45 parts catalyst powder to1.8 parts solvent. The catalysts were cured by increasing the voltage from the power supply to 4.0 V for 10 min before increasing gradually to 15.0 V for 1 h. The residue was then removed from the membrane by cleaning with iso-propanol.

The results in table 16 summarise the poison resistance of the different types of catalysts to methane and butane. First it is noted that the maximum butane responses for H_1-e Pd and H_1-e Pd-Pt bi-layer catalysts are significantly higher than the maximum methane response; the ratio of methane to butane response is 2.69 for the H_1-e Pd catalysts and 2.2 for the H_1-e Pd-Pt bi-layer catalysts. Conversely, the City

Technology slurry catalysts have higher methane responses. In this case the ratio is 0.80.

The City catalyst has a larger t_{50} value in methane whilst the t_{90} value is higher in butane, indicating a rapid initial decrease in activity followed by a more gradual loss of the final part of activity.
The t_{50} and t_{90} values for the H_1-e Pd and H_1-e Pd-Pt bi-layer catalysts are higher in butane. Although the values for butane differ they are both significantly higher than those for methane.

The individual responses of the H_1-e Pd catalysts are shown in table 17.

Device no.	**Catalyst**	**Specific surface area / $m^2 g^{-1}$**	**Max response /mV**		**t_{50} HMDS 6 ppm / s**		**t_{90} HMDS 6 ppm / s**	
			CH_4	Butane	CH_4	Butane	CH_4	Butane
B4R6P9	H_1-e Pd	14.6	26	86	12	24	14	30
B4R3P5	H_1-e Pd	15.8	50	90	12.5	26	14.5	33
B4R3P6	H_1-e Pd	10.4	20	82	11	19	13	24

Table 17. Summary of the responses and poisoning by HMDS of H_1-e Pd catalysts on SRL136 microhotplates to methane and butane. The H_1-e Pd films were electro-deposited from a palladium nitrate hydrate Brij®56 template mixture at room temperature by applying a potential step from 0.5 to 0.1 V vs. SCE. A deposition charge of 5 mC was passed in each case. Following electro-deposition the catalysts were cleaned with iso-propanol and then voltammetrically cycled in 0.1 M sulphuric acid.

It can be concluded that poisoning of H_1-e Pd catalysts by HMDS in butane is reversible. Upon removal of HMDS from the gas supply all catalytic activity is regained. The time taken to regain all activity increases with each subsequent addition of HMDS. The resistance to HMDS decreases with each subsequent exposure to HMDS as shown by the increasing t_{50} and t_{90} values shown in table 15. Finally, H_1-e Pd catalysts showed significantly higher butane sensitivity compared

Finally, H_1-e Pd catalysts showed significantly higher butane sensitivity compared to methane activity. The ratio of the average butane to methane sensitivities was calculated to be 9.

6.5 Hydrogen response of poisoned H_1-e Pd films

In the previous section the poisoning of H_1-e Pd catalysts by HMDS in butane was investigated. It was found that the poisoning was reversible. In section 5.1.2 it was reported that work by Cullis and Willat[53] showed that HMDS had a negligible effect on hydrogen oxidation. It was decided to investigate these findings using an H_1-e Pd catalyst to build up a better understanding of the poisoning of the Pd catalyst in different gases.

To establish whether indeed HMDS had a negligible effect on the oxidation of hydrogen, an H_1-e Pd catalyst was poisoned in HMDS and methane before being exposed to hydrogen for the first time. The response is shown in fig 104.

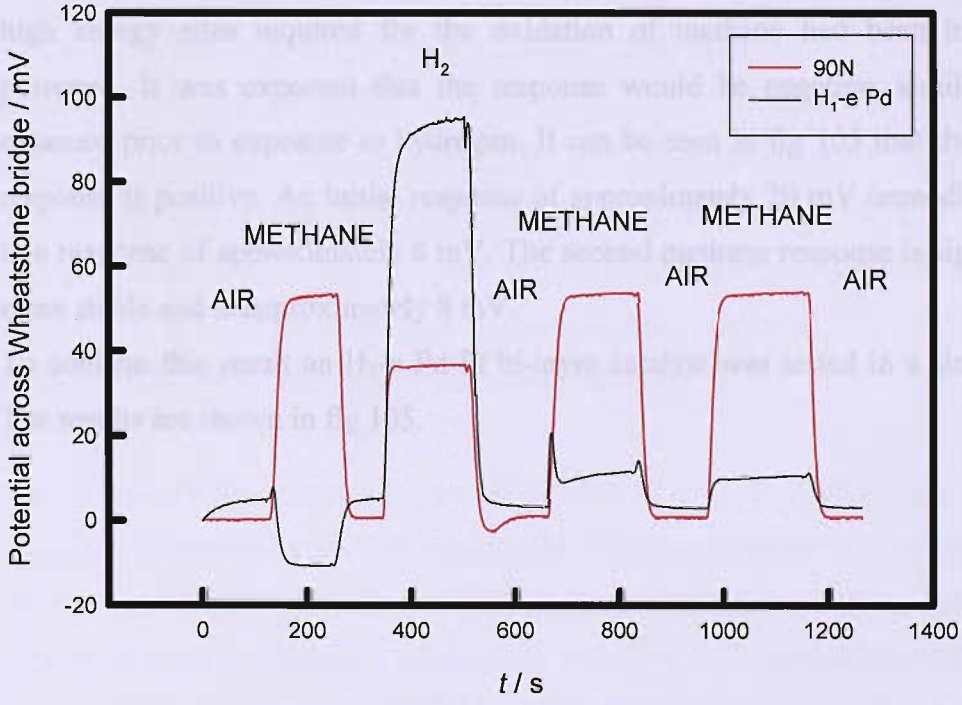

Fig 104. Response of H_1-e Pd on an SRL136 micro-hotplate to 2.5 % methane and 2 % hydrogen following poisoning by HMDS (6 ppm). The catalyst lost all activity to methane following poisoning by HMDS. The H_1-e Pd film was electrodeposited as per fig 102 deposition charge of 12.5 mC was passed.

Fig 104 shows the response of an H_1-e Pd catalyst to both methane and hydrogen following poisoning by HMDS. It can be seen that methane response is negative, indicating that there is no catalytic activity to methane. The thermal response is due to methane having a higher thermal capacity than air. Following exposure to methane the gas supply was switched back to air. The response can be seen to return to approximately the same air baseline. Hydrogen (2 %) was then introduced to the device. It can be seen that the response is immediately positive. The magnitude of the response is approximately 90 mV. Table 11 shows that the average hydrogen response of a non-poisoned H_1-e Pd catalyst was 88 mV, though it is noted that this average is based on only 2 results of 106.9 and 70.9 mV. Even so the magnitude of the response clearly suggests that little if any hydrogen sensitivity has been lost. This result is consistent with the findings of Cullis and Willat[53] that HMDS has a negligible effect on hydrogen activity.

Following exposure to hydrogen the H_1-e Pd catalyst was exposed to methane to confirm that the device was still catalytically inactive to methane. This would further support the theory that the low energy sites had not been poisoned whilst the high energy sites required for the oxidation of methane had been irreversibly poisoned. It was expected that the response would be negative, similar to that obtained prior to exposure to hydrogen. It can be seen in fig 105 that the methane response is positive. An initial response of approximately 20 mV immediately falls to a response of approximately 8 mV. The second methane response is significantly more stable and is approximately 8 mV.

To confirm this result an H_1-e Pd-Pt bi-layer catalyst was tested in a similar way. The results are shown in fig 105.

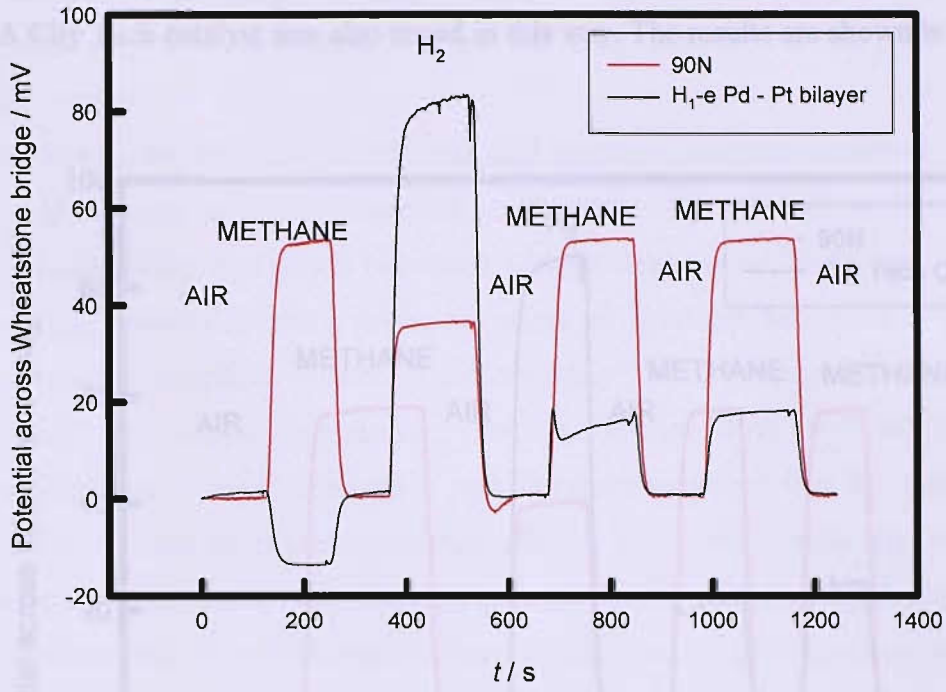

Fig 105. Response of device of H_I-e Pd-Pt bi-layer catalyst on an SRL136 microhotplate to methane and hydrogen following poisoning by HMDS (6ppm). Poisoning resulted in a loss in all catalytic activity to methane. The H_I-e Pd was electrodeposited as per fig 102. A H_I-e Pt layer was electrodeposited onto the H_I-e Pd layer from the hexachloroplatinic acid Brij®56 template bath at room temperature by applying a potential step from 0.5 to -0.1 V vs. SCE. A deposition charge of 4 mC was passed. The film was then soaked in iso-propanol for 1 h. The H_I-e Pd-Pt bi-layer film was then voltammetrically cycled in 1 M sulphuric acid from 0 to 0.65 V vs. SMSE over 8 voltammetric cycles.

Fig 105 shows the response of an H_I-e Pd-Pt bi-layer to methane and hydrogen following poisoning by HMDS. As with the response of the H_I-e Pd layer in fig 105 the methane response is negative indicating no catalytic activity to methane. The catalyst then gave a positive response to hydrogen of approximately 85 mV. The average value of a non-poisoned H_I-e Pd-Pt bi-layer was 106.9 mV. This suggests that some catalytic activity may have been lost, but the possible loss is small. Again exposure to methane following hydrogen exposure yielded positive responses. It is noted that the methane responses are considerably more stable and of a greater magnitude than those of the H_I-e Pd catalyst in fig 104. The magnitude is approximately 20 mV. Prior to poisoning a methane response of approximately 33

mV was recorded. This therefore represents a partial but nonetheless significant recovery of methane activity.

A City Tech catalyst was also tested in this way. The results are shown in fig 106.

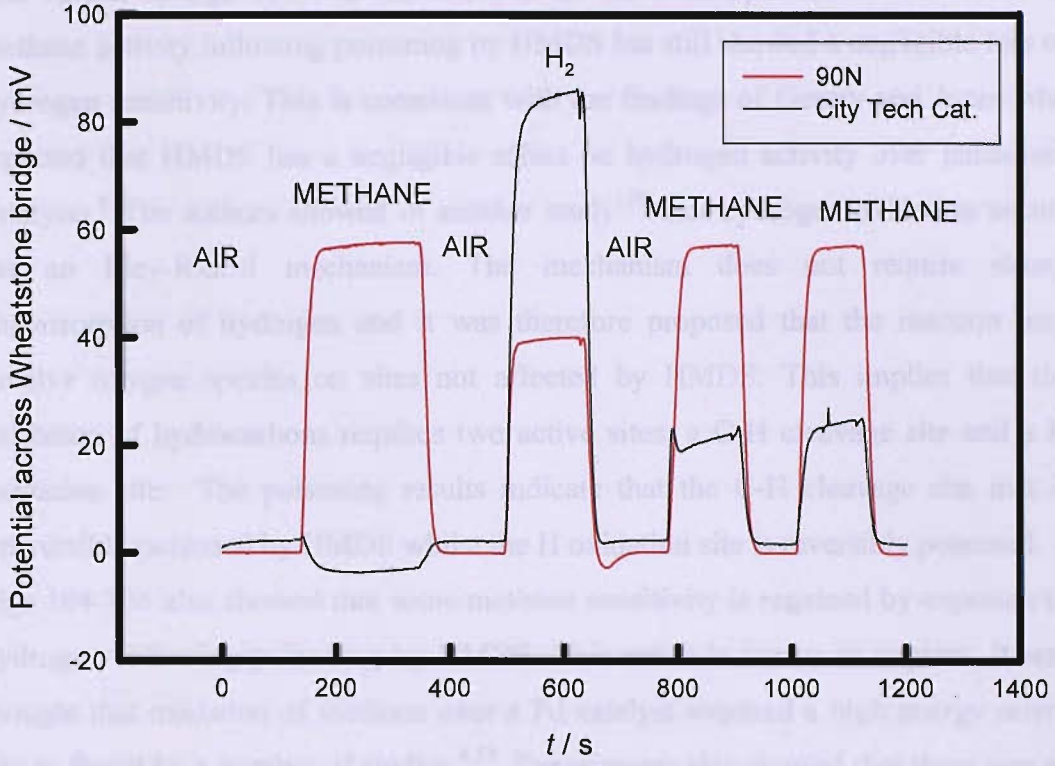

Fig 106. Response of City Technology catalyst on an SRL 136 microhotplate to methane and hydrogen following poisoning by HMDS (6ppm). Poisoning resulted in a loss of all methane activity. The catalyst was deposited as per fig 96.

Fig 106 shows that the City Tech catalyst also gave a positive response to hydrogen following a negative response to methane. The hydrogen response was approximately 85 mV, similar in magnitude to those from the H_1-e Pd and H_1-e Pd-Pt bi-layer in figs 105 and 106 respectively. Table 11 shows that an average hydrogen response of 91.2 mV was obtained for non-poisoned City Tech catalysts. This suggests that little hydrogen activity has been lost. Following exposure to hydrogen the catalyst was exposed to methane. It can be seen that the City Tech catalyst positive responses to methane. It is noted that the shape of the first methane responses are similar in figs 104, 105 and 106; there is an initial spike which decreases before increasing slowly. In all three cases the second methane response was more stable. The second methane response of the City Tech catalyst in fig 106 is approximately 20 mV, similar to that of the H_1-e Pd-Pt bi-layer catalyst in fig

105. Table 11 shows that the average methane response of a non-poisoned City Tech catalyst is around 160 mV. The City Tech catalyst has therefore recovered a smaller proportion of normal methane sensitivity compared to the H_1-e Pd-Pt bi-layer catalyst.

The results in figs 104-106 showed that all three catalysts exhibited a loss of methane activity following poisoning by HMDS but still showed a negligible loss of hydrogen sensitivity. This is consistent with the findings of Gentry and Jones who reported that HMDS has a negligible effect on hydrogen activity over palladium catalysts.[8] The authors showed in another study[130] that hydrogen oxidation occurs via an Eley-Rideal mechanism. The mechanism does not require strong chemisorption of hydrogen and it was therefore proposed that the reaction may involve oxygen species on sites not affected by HMDS. This implies that the oxidation of hydrocarbons requires two active sites; a C-H cleavage site and a H oxidation site. The poisoning results indicate that the C-H cleavage site that is irreversibly poisoned by HMDS whilst the H oxidation site is reversibly poisoned.

Figs 104-106 also showed that some methane sensitivity is regained by exposure to hydrogen following poisoning by HMDS. This result is harder to explain. It was thought that oxidation of methane over a Pd catalyst required a high energy active site as found by a number of studies.[8,53] Experiments also showed that there was an increase in the magnitude of the methane response following hydrogen testing *prior* to poisoning. The results are shown in table 18.

Catalyst / deposition charge / mC	**Max Response / mV**				**Time to decay to baseline after exposure to 6 ppm HMDS / s**	**t_{50} / s**	**t_{90} / s**	**CH_4 poisoning / mV**	**CH_4 After H_2 / mV**
	CH_4 [3]	H_2	heptane	CH_4 [4]					
H_1-e Pd / 12.5	13.7	106.9	32.5	20.0	15.1	11.5	14.5	-18	7.7
H_1-e Pd - Pt / 4.5 / 5	13.9	91.4	28.1	24.0	27.0	20.5	26.0	-15.2	17.4
City Cat	162	106.3	35.2	52.3	172.4	71.2	144.0	-6	23.4

Table 18. Summary of results obtained investigating catalytic activity to methane, hydrogen and heptane and resistance to HMDS.

[3] prior to H_2 testing
[4] in poison test. Post H_2 testing, before poisoning

The results in table 18 show a significant increase in the magnitude of the methane response following exposure to hydrogen before poison testing. The H_1-e Pd catalyst gave a methane response of 13.7 mV then a response of 106.9 mV to hydrogen. A subsequent methane response of 20.0 mV was obtained. This represents an increase of 46 %. Similarly an H_1-e Pd-Pt bi-layer catalyst gave a methane response of 13.9 mV, a hydrogen response of 91.4 mV followed by a methane response of 24.0 mV, representing an increase of 73 %. Conversely, it is noted that the methane response of the City Tech catalyst falls following exposure to hydrogen. A study by Su *et al.*[139] investigated the reduction of PdO by H_2. The report concluded that the reduction of PdO by H_2 proceeds in a shellwise manner. However, if the shell is kept thin, oxygen can penetrate the metal layer and reoxidise it to PdO. The report also investigated the reduction of PdO by CH_4. The report concluded that the reaction proceeded via a nucleation mechanism and that the presence of metallic Pd was essential to dissociate the CH_4. In section 1.2.4 the optimum state of Pd catalysts for the oxidation of methane was discussed at length. It was shown that there is still disagreement over the optimum form of the catalyst. A study by Carstens *et al.*[140] investigated factors affecting the catalytic activity of Pd supported on ZrO_2 for the combustion of methane. The report concluded that the optimum state of the catalyst was achieved when 6-7 monoloayers of PdO were formed. A similar result was obtained by Burch and Urbano.[19] The results showed that catalytic activity could be increased by partially reducing the surface of the PdO to form small regions of metallic Pd. The report concluded that metallic Pd is more effective at dissociating CH_4. These effects cannot be sustained as the metallic Pd is oxidised back to PdO. These findings and conclusions are consistent with the results obtained here. It was noted that prior to poisoning by HMDS exposure to H_2 resulted in a significant increase in the magnitude of methane sensitivity. It is therefore proposed that the increase in activity following exposure to hydrogen is the result of reduction of some of the PdO to metallic Pd. The catalyst will therefore contain both metallic and palladium oxide which was shown by Thevenin *et al.* to be the optimal form of the catalyst.[38]

6.6 Summary and discussion

In this chapter responses to methane, hydrogen, heptane and butane of H_1-e Pd, H_1-e Pd-Pt bi-layer and City Tech catalysts have been investigated. In this section the responses are presented in graphical form to summarise the results in this chapter. For all the graphs presented in this section the result for each catalyst type represents the average of 3 results.

Maximum response

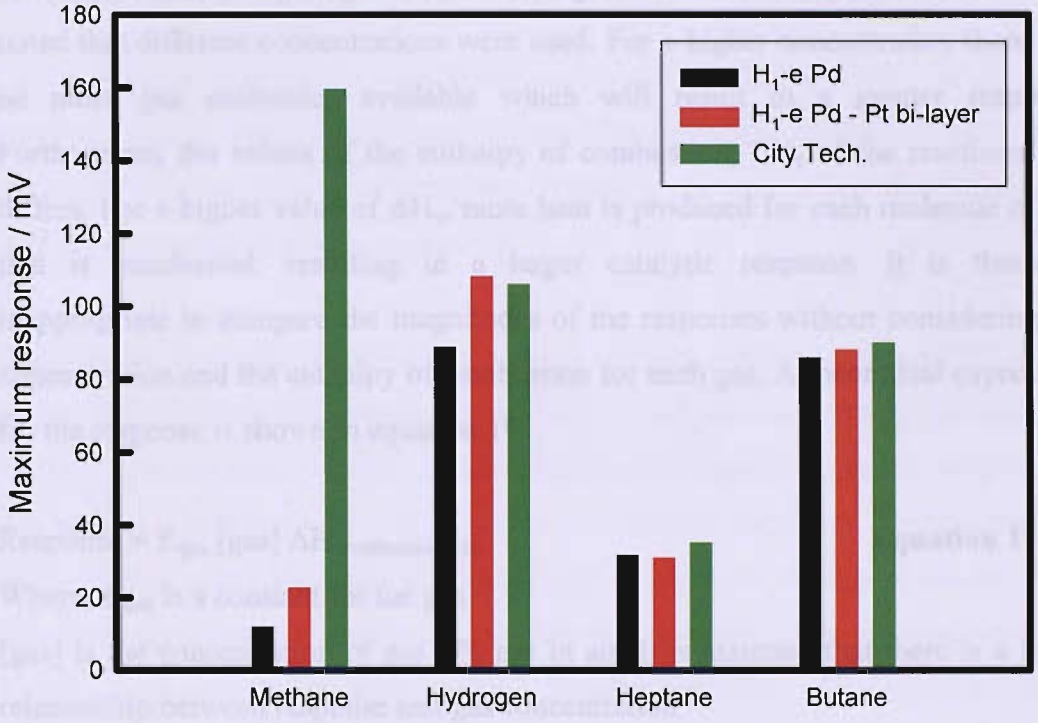

Fig 107 Graph showing the maximum response of each catalyst type to different flammable gases. Each result is the average of 3 results. All catalysts were prepared on SRL136 micro-hotplates. The H_1-e Pd films were electrodeposited from the Brij®56 ammonium tetrachloropalladate template mixture. A deposition charge of 5 mC was passed in each case. The H_1-e Pd-Pt bi-layers were electrodeposited using a Brij®56 ammonium tetrachloropalladate and Brij®56 hexachloroplatinic acid template mixture respectively. A deposition charge of 5 mC was passed for each layer. The City Tech catalysts were prepared by applying one droplet of catalyst slurry. The slurry was cured by powering to 4 V for 10 min before increasing the power to 15 V for 1 h.

Fig 107 shows the maximum responses to methane, hydrogen, heptane and butane. It can be seen that in the case of methane the City Tech catalyst gave a significantly greater response than the mesoporous Pd catalysts. In chapter 5 the Knudsen diffusion numbers for methane in the City Tech catalyst and the mesoporous Pd films were calculated and suggested that diffusion was limiting the rate of reaction of methane in the mesoporous Pd catalysts. It can be seen that the responses of the different catalysts to the other flammable gases are very similar. The similar responses of the City Tech and H_1-e Pd catalysts in particular suggests that in these cases the reaction may not be controlled by diffusion.

However, when comparing the relative magnitudes of the responses it should be noted that different concentrations were used. For a higher concentration there will be more gas molecules available which will result in a greater response. Furthermore, the values of the enthalpy of combustion, ΔH_c of the reactions also differs. For a higher value of ΔH_c, more heat is produced for each molecule of gas that is combusted, resulting in a larger catalytic response. It is therefore inappropriate to compare the magnitudes of the responses without considering the concentration and the enthalpy of combustion for each gas. A theoretical expression for the response is shown in equation 19.

$$\text{Response} = K_{gas}\,[\text{gas}]\,\Delta H_{\text{combustion gas}} \qquad \textbf{Equation 19}$$

Where; K_{gas} is a constant for the gas

[gas] is the concentration of gas / % gas in air. It is assumed that there is a linear relationship between response and gas concentration

$\Delta H_{\text{combustion gas}}$ is the heat of combustion for the gas / kJ / mol

Values of K_{gas} can be calculated from the magnitude of the catalytic response, the gas concentration of the gas and the value of $\Delta H_{\text{combustion gas}}$. It is then possible to compare values of K_{gas} calculated from the response obtained with theoretical values. These were calculated and are shown in table 19.

Gas	Conc. used / %	ΔH_c / kJ / mol	Thermal response of microhotplate to gas / mV	Catalytic response / mV	Total Catalytic response / mV	$K_{gas\ experimental}$
Methane	2.5	-890	-22.4	12.0	34.4	0.015
n-butane	0.755	-2874	-8.5	86.0	94.5	0.044
Heptane	0.2	-4847	-4.2	31.8	36	0.037
Hydrogen	2.0	-285.9	-45.9	88.9	134.8	0.24

Table 19. Summary of the conditions and results from the testing of H_1-e Pd catalysts with a range of flammable gases. The magnitude of the responses from come from fig 108. The total catalytic response is the sum of the thermal reponse and the observed catalytic response.

It can be see that when the gas concentration and ΔH_c values are considered the K_c values for methane and butane are consistent with the findings of Aryafar and Zaera.[17] Their results showed a good correlation between C–H bond energies and reactivities. It was proposed that the initial activation of the alkane was therefore the rate limiting step. The results showed that C-H bond energy decreased with increasing hydrocarbon chain length an observation supported by other authors.[21,22] The $K_{gas\ experimental}$ value for heptane is smaller than that of n-butane which is inconsistent with this theory. The values are however similar which suggests that the theory might not hold for long chain alkanes.

The $K_{gas\ experimental}$ for hydrogen is much greater than those of the hydrocarbons tested. When poisoned H_1-e Pd films were tested in hydrogen it was found that the hydrogen response was not affected by HMDS. Gentry and Jones [130] showed that hydrogen oxidation occurs via an Eley-Rideal mechanism which does not require strong chemisorption of hydrogen. It was proposed that the oxidation of hydrogen occurs on different active sites than the oxidation of hydrocarbons. It is possible that the kinetics on this active site are faster resulting in the larger response.

Poisoning by HMDS in methane and butane

The catalysts were also poisoned by HMDS in other flammable gases. Fig 108 shows the time taken to lose all activity, t_{100}, as well as t_{50} and t_{90} values of H_1-e Pd, H_1-e Pd-Pt bi-layer and a City Tech catalyst.

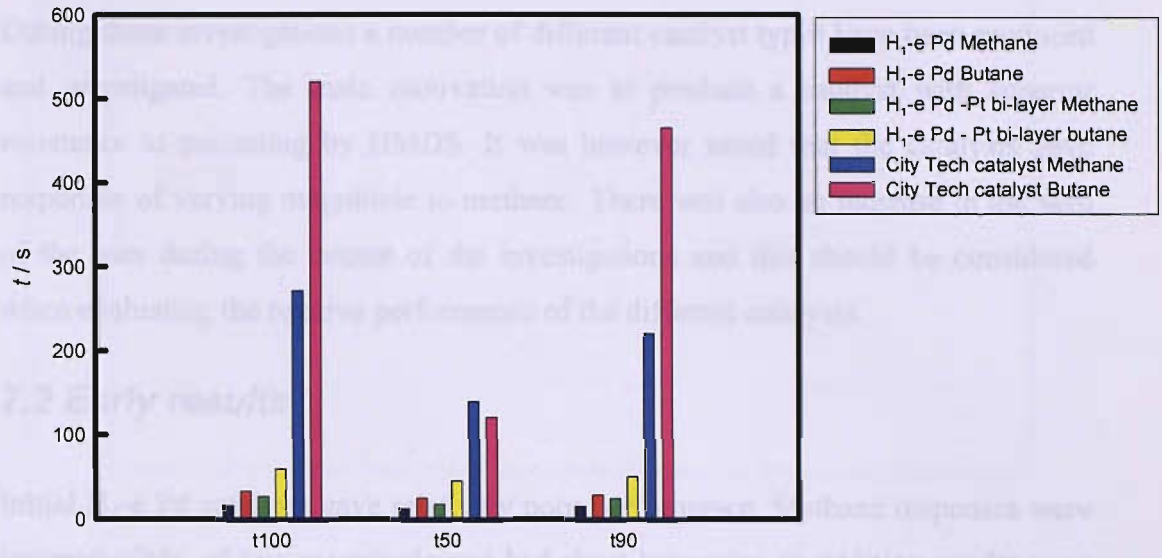

Fig 108 Graph showing the poisoning times to HMDS (6ppm) of various catalysts in methane in and butane. Each result is the average of 3 results. All catalysts were prepared on SRL136 micro-hotplates. For deposition details please refer to fig 107.

It can be seen in fig 108 that all of the catalysts had better resistance to HMDS in butane than in methane. The t_{100}, t_{50}, and t_{90} values are all greater in butane. It was proposed that this is because low energy active sites are used for the oxidation of butane whereas high energy sites are required for the oxidation of methane. It has been reported that whilst HMDS binds irreversibly to high energy sites, resulting in irreversible poisoning, the binding to low energy sites is reversible, so sensitivity can be regained. It is noted that for both methane and butane the City Tech catalyst gave far superior resistance to HMDS. It is proposed that this is a result of the optimised composition containing Zr and other additives. It is also highly possible that the more open porous structure improves poison resistance by making it harder for the pores to become blocked.

7 Optimum mesoporous methane catalyst

7.1 Introduction

During these investigations a number of different catalyst types have been produced and investigated. The main motivation was to produce a catalyst with superior resistance to poisoning by HMDS. It was however noted that the catalysts gave responses of varying magnitude to methane. There was also an increase in the skill of the user during the course of the investigations and this should be considered when evaluating the relative performance of the different catalysts.

7.2 Early results

Initial H_1-e Pd catalysts gave relatively poor performance. Methane responses were irreproducible, of low magnitude and had short longevity. In addition results were compromised by poor quality control in the manufacture of the microhotplates. The methane response of an early H_1-e Pd catalyst is shown in fig 109.

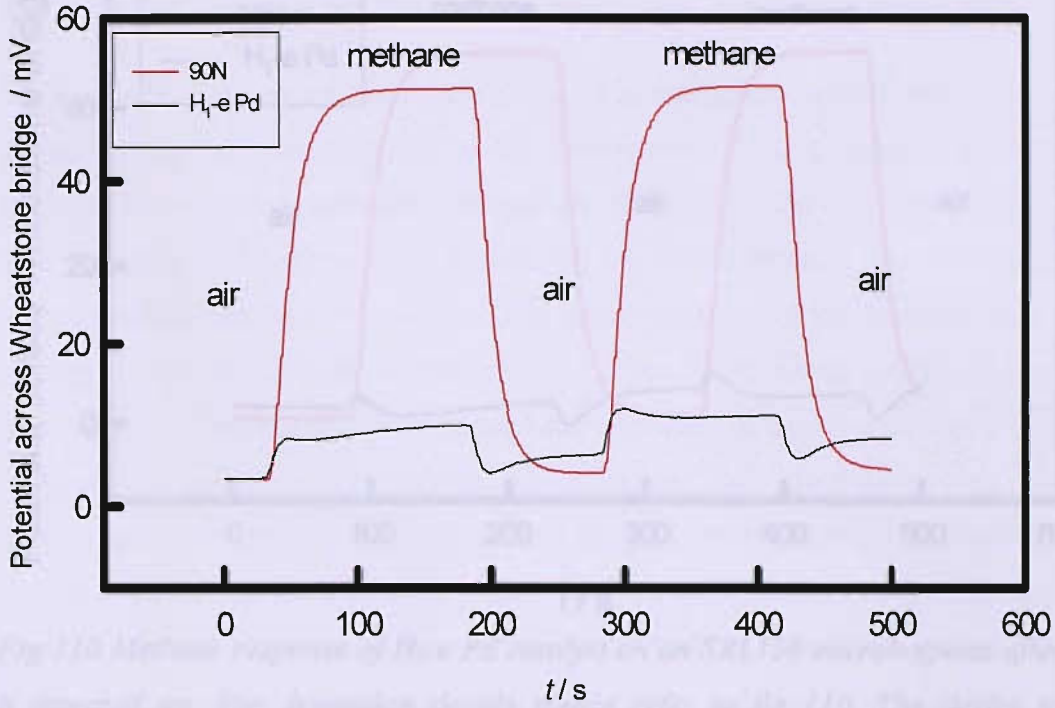

Fig 109 Methane response of H_1-e Pd catalyst no SRL136B1R2P13. The H_1-e Pd was electrodeposited from the standard Brij®56 - ammonium tetrachloropalladate template mixture using chronoamperometry and applying a potential step of 0.4 to 0.1 V vs. SCE. A deposition charge of 3.5 mC. The surfactant was removed using iso-propanol. The H_1-e Pd film was then voltammetrically cycled in 1 M sulphuric acid until maximum surface area was obtained after 8 voltammetric cycles. The device was powered in air for 30 min prior this response being obtained.

The graph in fig 109 shows the methane response of an H_1-e Pd catalyst after 30 min in air. It can be seen that the magnitude of the response is poor, approximately 6 mV. The air baseline is also fairly unstable, though this may be due to the microhotplate and not the Pd catalyst. The catalyst was tested after a further 30 min in air. The response is shown in fig 110.

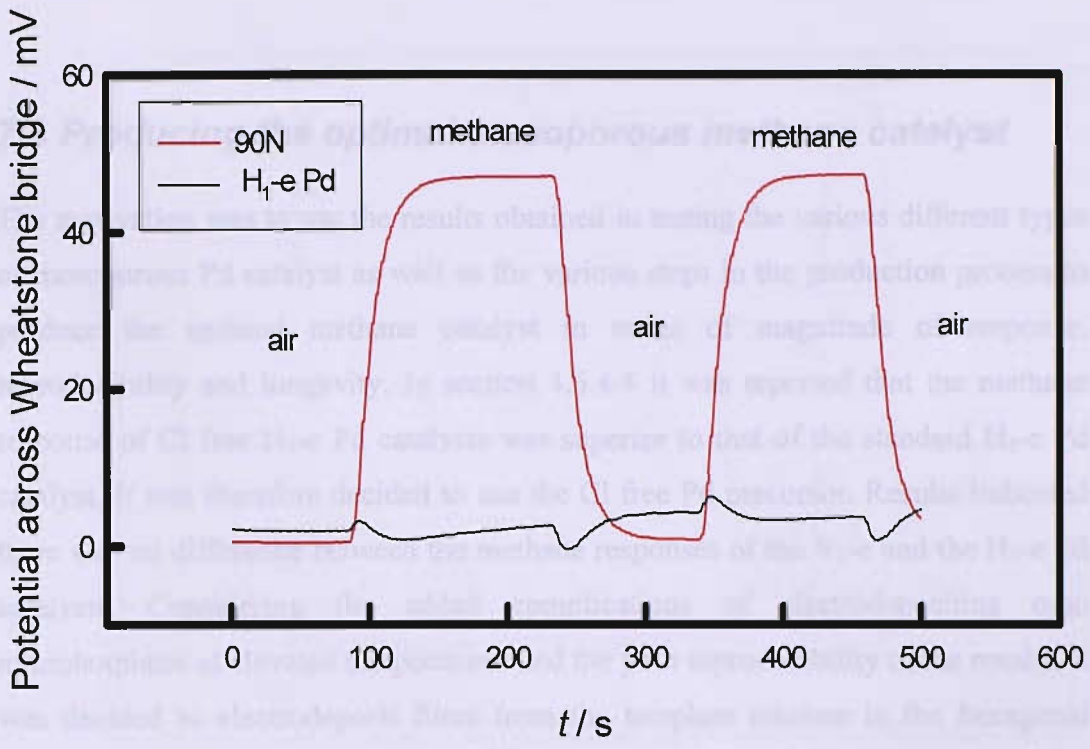

Fig 110 Methane response of H_1-e Pd catalyst on an SRL136 microhotplate after 1 h powered up. For deposition details please refer to fig 110. The device was powered in air for 1 h prior to this response being obtained and was methane tested after 30 min.

The graph in fig 110 shows the methane response after 1 h in air. It can be seen that the magnitude of the methane response of the H_1-e Pd catalyst has decreased compared to the response after 30 min shown in fig 109. It is also noted that the positive methane response is not maintained. After the initial positive response, the response decreases to the air baseline. When the gas supply is switched back to air, the response decreases, before increasing again. In summary the response in both methane and air is unstable and the methane response is weak. The device was retested after a further 30 min in air and a negative response was obtained. This indicates that catalytic activity has been lost and that the response is now purely thermal.

7.3 Producing the optimal mesoporous methane catalyst

The motivation was to use the results obtained in testing the various different types of mesoporous Pd catalyst as well as the various steps in the production process to produce the optimal methane catalyst in terms of magnitude of response, reproducibility and longevity. In section 4.6.4.4 it was reported that the methane response of Cl free H_1-e Pd catalysts was superior to that of the standard H_1-e Pd catalyst. It was therefore decided to use the Cl free Pd precursor. Results indicated there was no difference between the methane responses of the V_1-e and the H_1-e Pd catalysts. Considering the added complications of electrodepositing onto microhotplates at elevated temperatures and the poor reproducibility of the results, it was decided to electrodeposit films from the template mixture in the hexagonal phase. In section 5.5.1 it was reported that H_1-e Pd-Pt bi-layer films gave superior methane responses to the standard H_1-e Pd catalyst. Although the difference was modest it was found that results were also more reproducible using bi-layer catalysts. Results also showed that having the Pt as the bottom layer further increased the magnitude of the response. A catalyst consisting of a H_1-e Pt-Pd bi-layer with the Pd electrodeposited from the Cl free precursor was therefore designed based on the results obtained. Investigations into the effect of the thickness of the mesoporous metal films on the magnitude of the response proved inconclusive. It was therefore decided to use the standard 5 mC deposition charge for each layer.

It was found that mesoporous metal films had low surface areas if the surfactant was not fully removed. It was concluded that the optimum procedure was a stirred soak in iso-propanol soak for at least 1 h. In section 4.8 it was reported that voltammetric cycling in sulphuric acid was beneficial in terms of the magnitude of the methane response and also in terms of obtaining consistent methane responses. This step was therefore also included in the production process. The methane response of the optimised catalyst after 30 min in air is shown in fig 111.

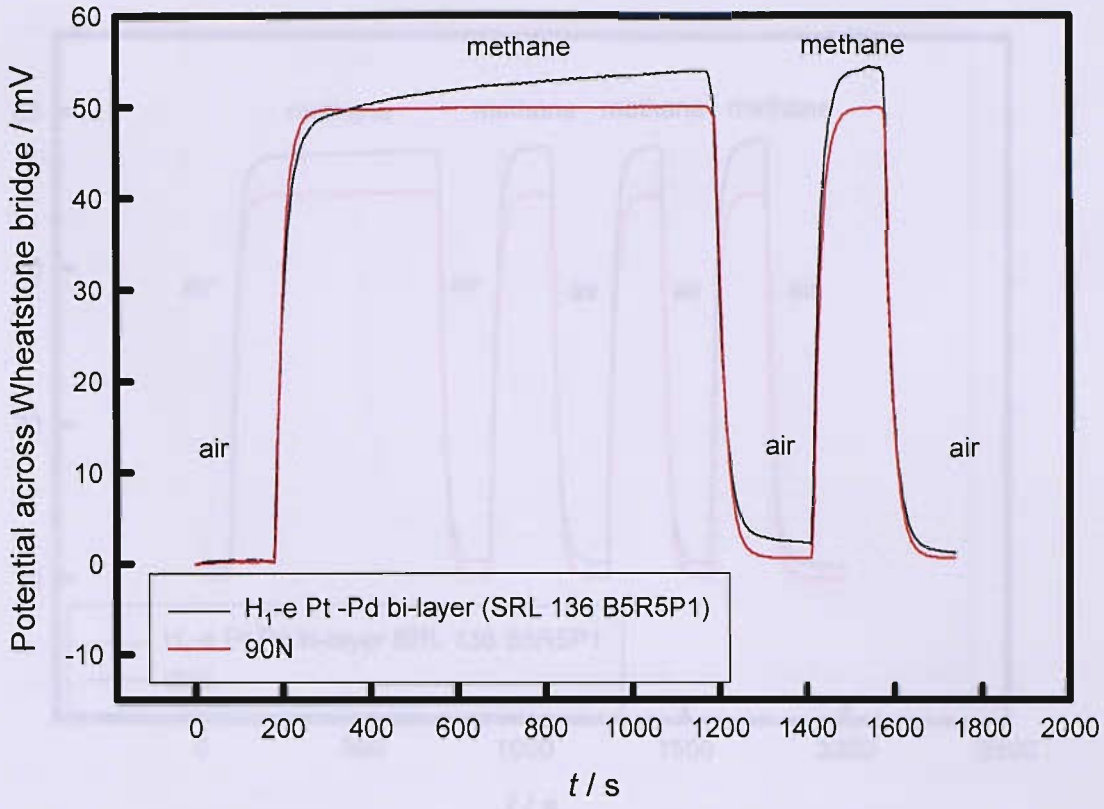

Fig 111 Methane response of a H_1-e Pt-Pd bi-layer catalyst. The device comprises a 136 header unit with a mesoporous Pd-Pt bilayer catalyst. The Pd was electrodeposited from the Cl free template mixture by potential step from 0.5 to 0.1 V vs. SCE. A deposition charge of 5.0 mC was passed. The surfactant was then removed using iso-propanol. The platinum layer was electrodeposited from a Brij®56 - hexachlorplatinic acid template bath in the hexagonal phase by potential step from 0.5 to -0.1 V vs. SCE and the surfactant subsequently removed using iso-propanol. The film was then voltammetrically cycled in 1 M sulphuric acid over 8 voltammetric cycles when maximum surface area was obtained. The device was powered in air for 30 min prior to this result being obtained.

The graph in fig 111 shows the methane response of the optimal H_1-e Pt-Pd catalyst after 30 min in air. It can be seen that the magnitude of the response is greater than that of the 90N. The gas supply was then switched back to air. A second methane response shown in fig 112 was taken after a further 5.5 h.

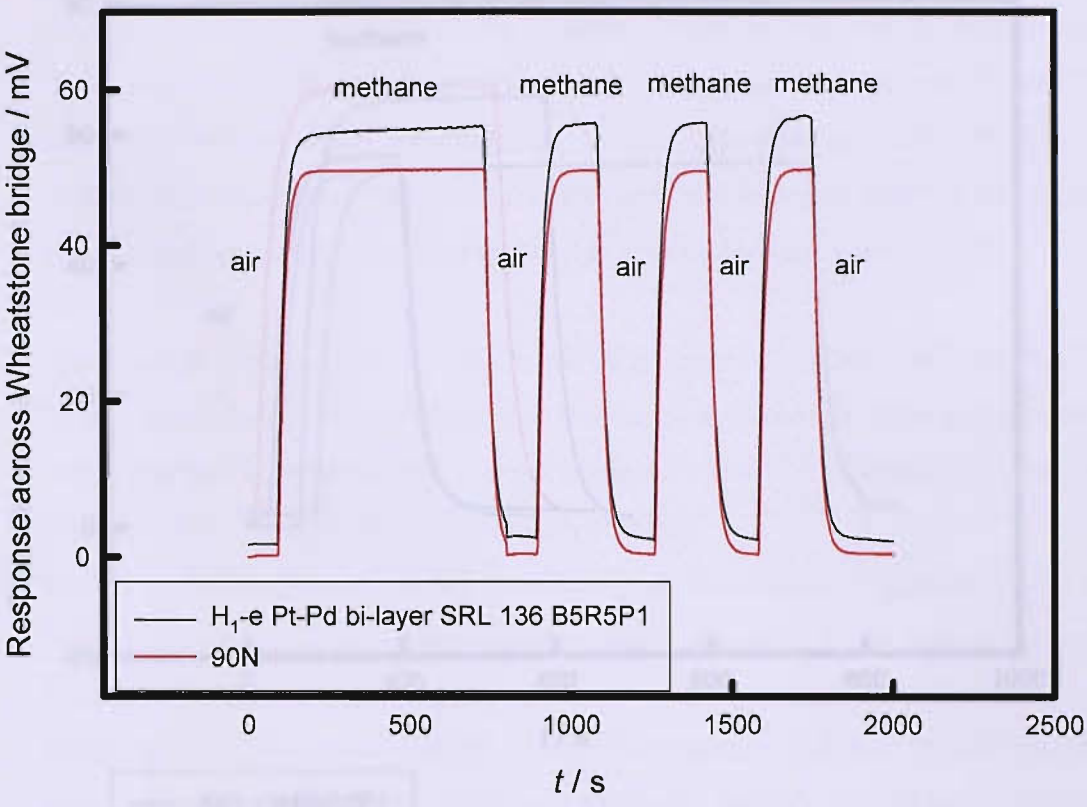

Fig 112. Methane response of a H_1-e Pt-Pd bi-layer catalyst. The fabrication of the catalyst is described in fig 111. The device was powered in air for 6 h prior to this graph being obtained. A methane response was obtained after 30 min in air.

The graph in fig 112 shows the methane response of an H_1-e Pt-Pd bi-layer catalyst after 30 min in air. The resistance required to balance the Wheatstone bridge was not readjusted following the initial methane response shown in fig 111. This indicates that there has been no baseline drift. It is noted from fig 112 that the magnitude of the methane response of the H_1-e Pt-Pd bi-layer catalyst exceeds that of the 90N. The methane response is stable and reproducible. Furthermore the reproducibility of responses of different films was excellent. Five similar devices were produced and similar responses were obtained. The methane responses are shown in fig 113 and summarised in table 20.

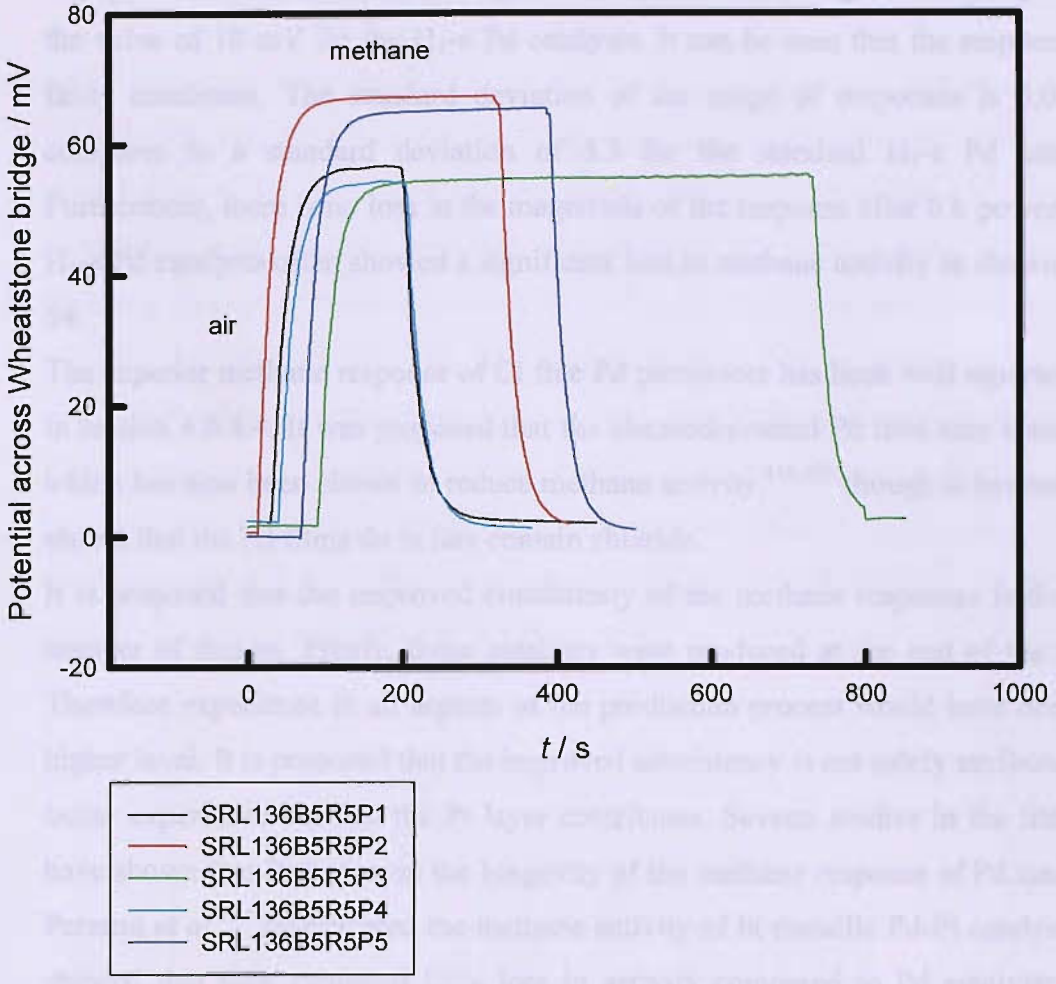

Fig 113. Graph showing the methane responses of H_I-e Pt-Pd bi-layer catalysts after 30 min in air powered at 15 V with a gas flow rate of 400 cm^3 min^{-1}. The fabrication of the catalysts is described in fig 111.

Device Number	SRL136 B5R5P1	SRL136 B5R5P2	SRL136 B5R5P3	SRL136 B5R5P4	SRL136 B5R5P5
Maximum response to 2.5 % CH_4 / mV	56.7	67.1	55.3	54.4	65.4

Table 20. Summary of the maximum methane response of H_I-e Pt-Pd bi-layer catalysts.

The results in table 20 show the maximum methane responses of H_1-e Pt-Pd bi-layer catalysts after 6 h. The average response is 60 mV. This is significantly higher than the value of 18 mV for the H_1-e Pd catalysts. It can be seen that the responses are fairly consistent. The standard deviation of the range of responses is 6.0. This compares to a standard deviation of 5.3 for the standard H_1-e Pd catalysts. Furthermore, there is no loss in the magnitude of the response after 6 h powered up. H_1-e Pd catalysts often showed a significant loss in methane activity as shown in fig 54.

The superior methane response of Cl free Pd precursors has been well reported here in section 4.6.4.4. It was proposed that the electrodeposited Pd film may contain Cl which has also been shown to reduce methane activity,[116,121] though it has not been shown that the Pd films do in fact contain chloride.

It is proposed that the improved consistency of the methane responses is due to a number of factors. Firstly, these catalysts were produced at the end of the study. Therefore experience in all aspects of the production process would have been at a higher level. It is proposed that the improved consistency is not solely attributable to better experience but that the Pt layer contributes. Several studies in the literature have shown that Pt improves the longevity of the methane response of Pd catalysts. Persson *et al.*[134] investigated the methane activity of bi-metallic Pd-Pt catalysts and showed that they exhibited little loss in activity compared to Pd catalysts. This result is consistent with those obtained by Narui *et al.*[133] who concluded that the improved performance was due to a higher dispersion of the Pd-Pt particles and a reduction of particle growth. In studies by Simplico *et al.*[121] the catalytic activity of methane catalysts was shown to be inversely related to particle size. The most active catalysts had the smallest PdO particle size and the highest PdO dispersion as well as the highest PdO decomposition temperature. The high catalytic activity of the catalyst prepared here can be explained in terms of particle size. The use of the Cl-free Pd precursor will give a smaller particle size than a Cl-containing Pd precursor such as ammonium tetrachloropalladate.[121] Furthermore the addition of Pt has been shown to restrict particle size growth which accounts for the improved longevity of the responses.

7.3.1 Largest methane response

In the previous section the optimal H_1-e Pd catalyst was designed and produced. An SRL136 microhotplate was used as these were found to give the most reproducible results during the investigations. An alternative model, the SRL162 was also supplied by City Technology. This microhotplate was similar in all aspects but feature a smaller gold electrode area of 3.25 x 10^{-3} cm^2 compared to 5.625 x 10^{-3} cm^2 for the standard SRL136. The significantly smaller surface area made the electrodeposition process more difficult, consequently reproducibility with these devices was poor. However, it was found that these devices often gave higher methane responses when operating at similar temperatures. It was decided to make a number of optimal H_1-e Pt-Pd catalysts on SRL162 microhotplates. The response after 6 h powered up is shown in fig 114.

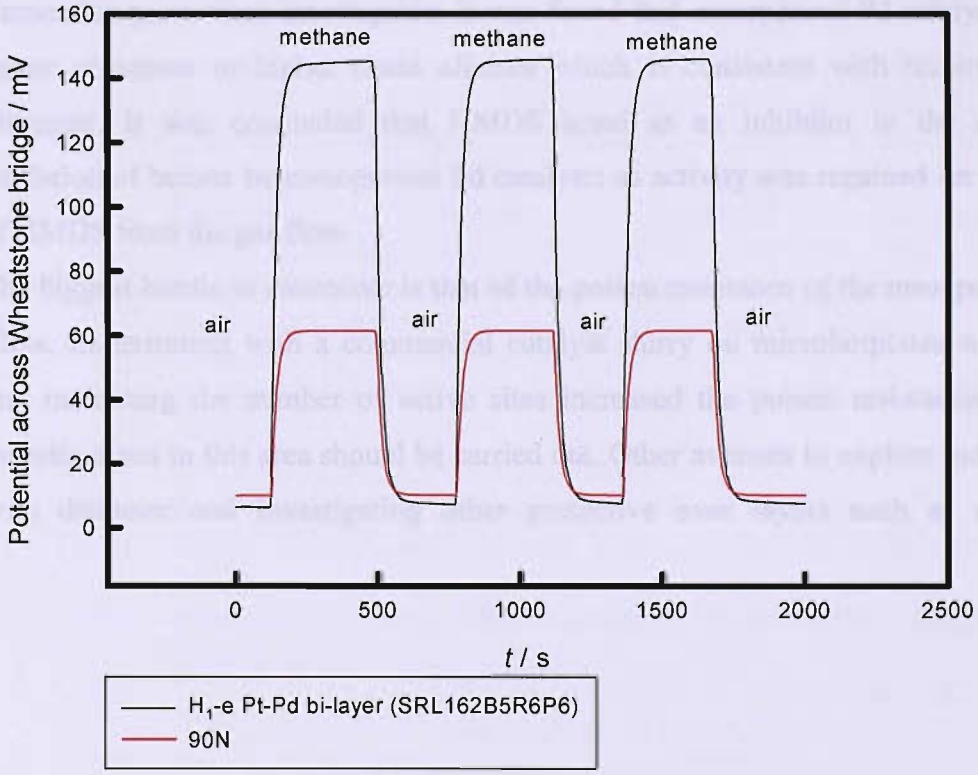

Fig 114. Response of a H_1-e Pt-Pd bi-layer catalyst on an SRL162 microhotplate after 6 h powered at 15 V from the PSU with a gas flow rate of 400 cm^3 min^{-1}. For deposition details please refer to fig 111.

The H_1-e Pt-Pd bi-layer catalyst was tested after 30 min and gave a similar sized response, indicating that there has been no loss in activity. The catalyst gave a reproducible, stable methane response and a stable air baseline. The magnitude of the methane response is significantly greater than that of the 90N.

7.4 Summary and future work

In summary significant progress has been made in producing reproducible, stable catalytic methane responses with mesoporous Pd catalysts. This was achieved by developing the skills required in the key stages of electrodepositing the mesoporous palladium films, as well as developing the optimum form of the catalyst. Investigations were carried out to improve the poison resistance of the mesporous Pd films. The methane response of standard H_1-e Pd catalysts was found to be rapidly and irreversibly poisoned by HMDS. Modifying the structure and using protective overlayers had a negligible effect on poison resistance. The responses to other flammable gases were investigated. It was found that mesoporous Pd catalysts gave larger responses to higher chain alkanes which is consistent with results in the literature. It was concluded that HMDS acted as an inhibitor in the catalytic oxidation of butane by mesoporous Pd catalysts as activity was regained on removal of HMDS from the gas flow.

The biggest hurdle to overcome is that of the poison resistance of the meosporous Pd films. Experiments with a commercial catalyst slurry on microhotplates suggested that increasing the number of active sites increased the poison resistance. Futher investigations in this area should be carried out. Other avenues to explore include the pore diameter and investigating other protective over layers such as zirconia.

References

(1) Online report. The Fuel Industry: Wood, Coal, and Domestic Gas; http://www.psigate.ac.uk/newsite/reference/plambeck/chem1/p01264a.htm.

(2) Moseley, P. T. *Meas. Sci. Technol.* **1997**, *8*, 223.

(3) City Technology report

(4) City Technology 90N CiTipel specification data sheets

(5) Guerin, S. PhD thesis, University of Southampton, 1999.

(6) Otto, K., Montreuil, C.N. *Environ. Sci. Technol.* **1976**, *10*, 154.

(7) Ehrhardt J-J, C. L., Jamois D,. *Sensors and actuators B* **1997**, *40*, 117.

(8) Gentry S, J. A. *J.appl. Chem. Biotechnol.* **1978**, *28*, 727.

(9) Gentry S.J., W., A. *Sensors and actuators* **1984**, *5*, 727.

(10) Anderson, R. B., Stein, K.C., Feenan, J.J., Hofer, L.J.E., *Ind. Eng. Chem.* **1961**, *53*, 809.

(11) Roberts, R. E., Roberts, J.B., *J. Air Pollut. Control Assoc.* **1976**, *26*, 353.

(12) Spivey, J. J. *Ind. Eng. Chem. Res.* **1987**, *26*, 2165.

(13) Nishino, A. *Catal. Today* **1991**, *10*, 107.

(14) Krill, W. V., Kesserling, J.P., Chu, E.K., Kendall, R.M., *Mech. Eng* **1980**, *102*, 28.

(15) Pfefferle, W. C. *J. Energy* **1978**, *2*, 142.

(16) Enga, B. E., Thompson, D.T., *Plat. Met. Rev* **1979**, *23*, 134.

(17) Aryafar, M., Zaera, F. *Catalysis Letters* **1997**, *48*, 173.

(18) Burch, R.; Crittle, D. J.; Hayes, M. J. *Catalysis Today* **1999**, *47*, 229.

(19) Burch, R.; Urbano, F. J. *Applied Catalysis a-General* **1995**, *124*, 121.

(20) Schwartz, A., Holbrook, L.L., Wise, H. *J. Catal* **1971**, *21*, 199.

(21) Hiam, L., Wise, H., Chaikin, S., *Journal of Catalysis* **1968**, *9/10*, 272.

(22) Drozdov, V. A., Tsyrulnikov, P.G., Popovskii, V.V., Bulgakov, N.N., Moroz, E.M., Galeev, T.G., *React. Kinet. Catal. Lett.* **1985**, *27*, 425.

(23) Lee, J. H., Trimm D.L., *Fuel processing technology* **1995**, *42*, 339.

(24) Burch, R.; Urbano, F. J.; Loader, P. K. *Applied Catalysis a-General* **1995**, *123*, 173.

(25) Ciuparu, D.; Altman, E.; Pfefferle, L. *Journal of Catalysis* **2001**, *203*, 64.

(26) Cullis, C. F. W., B.M. *J. Catal.* **1983**, *83*, 267.

(27) Baldwin, T. R. B., R. *Appl. Catal.* **1990**, *66*, 337.

(28) Hicks, R. F. Q., H.H.; Young, M.L.; Lee, R.G. *J. Catal.* **1990**, *122*, 295.

(29) Ribeiro, F. H.; Chow, M.; Dallabetta, R. A. *Journal of Catalysis* **1994**, *146*, 537.

(30) Shi, C.-K., Yang, L-F., Wang, Z-C., He, X-E., Cai, J-X., Li, G., Wang., X-S. *Appl. Catal. A.* **2003**, *243*, 379.

(31) Epling, W. S., Hoflund, G.B.,. *J. Catal* **1999**, *182*, 5.

(32) Burch, R. *Catal. Today* **1997**, *35*, 27.

(33) Farrauto, R. J., Hobson, M.C., Kennelly, T., Waterman, E.M., *Appl. Catal. A.* **1992**, *81*, 227.

(34) Burch, R., Loader, P.K., Urbano, F.J.,. *Catal. Today* **1996**, *27*, 243.

(35) Oh, S. H. M., P.J.; Siewert, R.M. *Appl. Catal. B* **1991**, *132*, 287.

(36) Hicks, R. F. Q., H.H.; Young, M.L.; Lee, R.G. *J. Catal.* **1990**, *122*, 295.

(37) Lyubovsky, M.; Pfefferle, L. *Catalysis Today* **1999**, *47*, 29.
(38) Thevenin, P. O.; Pocoroba, E.; Pettersson, L. J.; Karhu, H.; Vayrynen, I. J.; Jaras, S. G. *Journal of Catalysis* **2002**, *207*, 139.
(39) Ciuparu, D.; Lyubovsky, M. R.; Altman, E.; Pfefferle, L. D.; Datye, A. *Catalysis Reviews-Science and Engineering* **2002**, *44*, 593.
(40) Hoflund, G. B.; Hagelin, H. A. E.; Weaver, J. F.; Salaita, G. N. *Applied Surface Science* **2003**, *205*, 102.
(41) Campbell, K. D., Lunsford J.H., *J. Phys. Chem.* **1988**, *92*, 5792.
(42) Campbell, K. D., Moralesand, E., Lunsford J.H., *J. Am. Chem. Soc* **1987**, *109*, 7900.
(43) Martir, W., Lunsford, J.H., *J. Am. Chem. Soc* **1981**, *103*, 3728.
(44) Mims, C. A., Hall, R.B., Rose, K.D., Myers, G.R., *Catal. Lett.* **1989**, *2*, 361.
(45) Nelson, P. F., Lukey, C.E., Cant, N.W., *J. Phys. Chem.* **1988**, *92*, 6176.
(46) Choudhary, V. R., Rane, V.H.,. *J. Catal* **1991**, *130*, 411.
(47) Soklovskii, V. D. *Catal. Lett.* **1986**, *32*, 159.
(48) Garrone, E., Zecchina, A., Stone, F.S., *J. Catal* **1980**, *62*.
(49) Driscoll, D. J., Martir, W., Wang, J-X., Lunsford, J.H., *J. Am. Chem. Soc* **1985**, *107*.
(50) Otsuka, K., Murakami, Y., Wada, Y., Said, A.A., Morikawa, A,. *J. Catal* **1990**, *121*, 122.
(51) Finocchio, E., Busca, G., Lorenzelli., Willey, R.J., *J. Catal* **1995**, *151*, 204.
(52) Kikuchi, R.; Maeda, S.; Sasaki, K.; Wennerstrom, S.; Eguchi, K. *Applied Catalysis a-General* **2002**, *232*, 23.
(53) Cullis, C. F. W., B.M. *Journal of Catalysis* **1984**, *86*, 187.
(54) Fujimoto, K., Ribiero, F.H., Avalos-Borja. M., Iglesia, E., . *J. Catal* **1998**, *179*, 431.
(55) Davis, M. E. *Nature* **1993**, *364*, 391.
(56) Raimondi, M. E., Seddon, J.M., . *Liquid Crystals* **1998**, *26*, 305.
(57) Nettleship, I. *Key. Eng. Materials* **1996**, *122*, 305.
(58) Collins, P. J. *Liquid Crystals*; Princeton University Press: Princeton, NJ, 1990.
(59) Coleman, N. R. B. PhD thesis, University of Southampton, 1999.
(60) Mitchell, D. J., Tiddy G.J.T., Waring, L., Bostock, T., Mcdonald, M.P., *J.Chem.Soc., Faraday Trans. 1* **1983**, *79*, 975.
(61) Kresge, C. T., Leonowicz, M.E., Roth, W.J., Vartuli, J.C., Beck, J.S. *Letters to Nature* **1992**, *359*, 710.
(62) Attard, G. S., Glyde, J.C., Goltner, C.G., . *Nature* **1995**, *378*, 366.
(63) Attard, G. S., Goltner, C.G., Corker, J.M., Henke, S., Templer R.H. *Angew. Chem. Int. Ed. Engl.* **1997**, *36*, 1315.
(64) Greenwood, N. N., Earnshaw, A. *Chemistry of the Elements*, 1st ed.; Pergamon Press: Oxford, 1985.
(65) Ahmadi, T. S., Wang, Z.L., Heglein, El-Sayed, M.A., *Chem. Mater.* **1996**, *8*, 1161.
(66) Attard, G. S.; Bartlett, P. N.; Coleman, N. R. B.; Elliott, J. M.; Owen, J. R.; Wang, J. H. *Science* **1997**, *278*, 838.
(67) Bartlett, P. N.; Gollas, B.; Guerin, S.; Marwan, J. *Physical Chemistry Chemical Physics* **2002**, *4*, 3835.

(68) Attard, G. S., Bartlett, P.N., Coleman, N.R.B., Elliott, J.M., Owen, J.R. *Langmuir* **1998**, *14*, 7340.
(69) Marwan, J., PhD thesis, University of Southampton, 2002,.
(70) Lewis, F. A. *The Palladium Hydrogen system*; Academic Press: New York, 1967.
(71) Cioffi, N., Torsi, L., Sabbatini, L., Zabonin, P.G., Bleve-Zacheo, T. *J. Electroanal chem.* **2000**, *488*, 42.
(72) Baldauf, M., Kolb, D.M. *Electrochim Acta* **1993**, *38*, 2145.
(73) Guerin, S.; Attard, G. S. *Electrochemistry Communications* **2001**, *3*, 544.
(74) Rand, D. A. J., and Woods, R. *J. Electroanal chem.* **1972**, *36*, 57.
(75) Rand, D. A. J., Woods, R. *Electroanalytical chemistry and interfacial electrochemistry* **1972**, *35*, 209.
(76) Elliott, J. M., Attard, G.S., Bartlett, P.N., Coleman, N.R.B., Merckel, D.A.S., Owen, J.R. *Chem. Mater.* **1999**, *11*, 3602.
(77) Naohara, H., Ye, S., Uosaki, K., *J. Electroanal chem.* **1999**, *473*, 2.
(78) Naohara, H., Ye, S., Uosaki, K., *J. Phys. Chem.* **1998**, *102*, 4366.
(79) Kibler, L. A., Kleinert, M., Kolb, D.M., *Surface Science* **2000**, *461*, 155.
(80) Kibler, L. A., Kleinert, M., Randler, R., Kolb, D.M., *Surface Science* **1999**, *443*, 19.
(81) Ye, S., Uosoki, K., Thermodynamics and electrified interfaces. In *Encyclopedia of Electrochemistry,* Bard, A. J., Gileadi, Urbakh, M., Ed.; Wiley-VCH, 2002; Vol. 1.
(82) Quayum, M. E., Ye, S., Uosaki, K., *J. Electroanal chem.* **2002**, *520*, 126.
(83) Tsirlina, G. A., Petrii, O.A., Safonova, T.Y., Papisov, I.M., Vassiliez, S.Y., Gabrielov, A.E. *Electrochemica Acta* **2002**, *47*, 3749.
(84) Safonova, T. Y., Khairullin, D.R., Tsirlina, G.A., Petrii, O.A., Vassilev, S.Yu. *Electrochemica Acta* **2005**, *50*, 4752.
(85) Bolzan, A. E.; Martins, M. E.; Arvia, A. J. *Journal of Electroanalytical Chemistry* **1984**, *172*, 221.
(86) Hoare, J. P. *J. Electrochem. Soc* **1964**, *111*, 610.
(87) Perdriel, C. L., Custidiano, E., Ariva, A.J.,. *J. Electroanal chem.* **1988**, *246*, 165.
(88) Hoare, J. P., Thacker, R., Wiese, C.R., . *J. Electroanal chem.* **1971**, *30*, 15.
(89) Schuldiner, S., Warner, T.B., *J. Electrochem. Soc.* **1965**, *112*, 212.
(90) Thacker, R. *J. Electroanal chem.* **1971**, *30*, 1.
(91) Warner, T. B., Schuldiner, S., *J. Electrochem. Soc* **1965**, *112*, 853.
(92) Dall'Antonia, L. H.; Tremiliosi-Filho, G.; Jerkiewicz, G. *Journal of Electroanalytical Chemistry* **2001**, *502*, 72.
(93) Conway, B. E., Jerkiewicz, G., . *J. Electroanal chem.* **1993**, *357*, 47.
(94) Mengoli, G., Bernardini, M., Fabrizio, Manduchi, Zannoni, G. *J. Electroanal chem.* **1996**, *403*, 143.
(95) Zhang, W.-S., Zhang, X-W., Li, H-Q. *J. Electroanal chem.* **1997**, *434*, 31.
(96) *Electroanalytical Chemistry,* Gilman, S. I. B., A.J., (Ed.), Ed.; Arnold: London, 1967; Vol. 2, pp 111.
(97) Breiter, M. W. *Electrochemical processes in fuel cells*; Springer-Verlag: New York, 1969; Chap. 6.

(98) Imokawa, T., PhD thesis, University of Southampton, 2002.
(99) Simon, I., Barsan, N., Bauer, M., Weimar, U., *Sensors and actuators B* **2001**, *73*, 1.
(100) Krebs, P., Grisel, A. *Sensors and actuators B,* **1993**, *13-14*, 155.
(101) Gall, M. *Sensors and actuators B* **1993**, *15-16*, 260.
(102) www.thermometrics.com.
(103) Aigner, R., Dietl, M., Katterloher, R., Klee, V. *Sensors and actuators B* **1996**, *33*, 151.
(104) Briand, D., Krauss, A., van der Schoot, B., Weimar, U., Barsan, N.,Gopel, W., de Rooij, N.F.,. *Sensors and actuators B* **2000**, *68*, 223.
(105) Capone, S., Siciliano, P., Barsan, N., Weimar, U., Vasanelli,L., *Sensors and actuators B* **2001**, *78*.
(106) Cerda, J., Ciera, A., Vila, A., Cornet, A., Morante, J.R., *Thin solid films* **2001**, *391*, 265.
(107) Lee, S. M., PhD thesis, University of Southampton, 2002.
(108) Hoare, J. P. *Journal of the Electrochemical Society* **1984**, *131*, 1808.
(109) Rand, D. A. J., and Woods, R. *J. Electroanal chem.* **1971**, *31*, 29.
(110) Triantafyllopoulou, R., Chatzandroulis, S., Tsamis, C., Tserepi, A. *Microelectronics Engineering* **2006**.
(111) Baroncini, M., Placidi, P., Cardinali, G.C., Scorzoni, A. *Sensors and actuators A* **2004**, *115*, 8.
(112) Semenov, N. N. "Some problems of chemical kinetics and reactivity," 1958.
(113) Peri, S. S.; Lund, C. R. F. *Journal of Catalysis* **1995**, *152*, 410.
(114) Gelin, P.; Primet, M. *Applied Catalysis B-Environmental* **2002**, *39*, 1.
(115) Baldwin, T. R. B., R. *Appl. Catal.* **1990**, *66*, 359.
(116) Roth, D.; Gelin, P.; Primet, M.; Tena, E. *Applied Catalysis a-General* **2000**, *203*, 37.
(117) Tonetto, G.; Ferreira, M. L.; Damiani, D. E. *Journal of Molecular Catalysis a-Chemical* **2001**, *171*, 123.
(118) Euzen, P.; Le Gal, J. H.; Rebours, B.; Martin, G. *Catalysis Today* **1999**, *47*, 19.
(119) Monteiro, R. S., Dieguez, L.C., Schmal, M. . *Catal. Today* **2001**, *65*, 77.
(120) Sekizawa, K., Widjaja, H., Maeda, S., Ozawa, Y., Eguchi, K. *Applied Catalysis a-General* **2000**, *200*, 211.
(121) Simplicio, L. M. T., Brandao, S.T., Sales, E.A., Lietti, L., Bozon-Verduraz, F. *Applied Catalysis B-Environmental* **2006**, *63*, 9.
(122) Ordonez, S., Hurtado, P., Sastre, H., Diez, F.V. *Appl. Catal. A* **2004**, *259*, 41.
(123) Colin, L., Cassuto, A., Ehrhardt, J.J., Ruiz-Lopez, M.F., Jamois, D., *Applied Surface Science* **1996**, *99*, 245.
(124) Hurtado P, O. S., Sastre H, Diez F, *Appl. Catal. B* **2004**, *47*, 85.
(125) Jones, J. M., Dupont, V.A., Brydson, R., Fullerton, D.J., Nasri, N.S., Ross, A.B., Westwood, A.V.K. *Catalysis Today* **2003**, *81*, 589.
(126) Hoyos, L. J., Praliaud, H. and Primet, M. *Appl. Catal. A.* **1993**, *98*, 125.
(127) Cullis, C. F., Keene, D.E., Trimm D.L.J., *J. Catal.* **1970**, *19*, 378.
(128) Kuzminskii, A. S., Goldovskii, E.A., Dudenkova, S.V., Sunitsa, L.L., Orlov, V. Yu., Int. Symp. Organosilicon Chem Sci. Commun., **1965**, Prague.

(129) Akhrem, I. S., Christovalova, N.M., Mysov, E.I., Volpin M.E., *Zh. Obshch. Khim.* **1972**, *42*, 1868.
(130) Gentry S.J., F., J.G., Jones, A. *J. Chem. Soc. Farady Trans. I* **1974**, *70*, 600.
(131) Trimm D.L, L. C. W. *Chemical Engineering Science* **1980**, *35*, 1405.
(132) Yamamoto, H., Uchida, H.,. *Catal. Today* **1998**, *45*, 147.
(133) Narui, K., Yata, H., Furuta, K., Nishida, A., Kohtoka, Y., Matsuzak, T., *Appl. Catal. A.* **1999**, *179*, 165.
(134) Persson, K., Ersson, A., Manrique Carrera, A., Jayasuriya, J., Fakhrai, R., Fransson, T., Jaras, S. *Catalysis Today* **2005**, *100*, 479.
(135) Bartlett, P. N., Marwan, J. *Physical Chemistry Chemical Physics* **2004**, *6*, 2895.
(136) Atkins, P. W. *Physical Chemistry*; Oxford University Press, 1998.
(137) Ryoo, M.-W., Chung, S-G., Kim, J-H., Song, Y.S., Seo, G., *Catalysis Today* **2003**, *83*, 131.
(138) Garcia, T., Solsona, B., Murphy, D.M., Antcliff, K.L., Taylor. S.H.,. *J. Catal* **2005**, *229*, 1.
(139) Su, S. C.; Carstens, J. N.; Bell, A. T. *Journal of Catalysis* **1998**, *176*, 125.
(140) Carstens, J. N.; Su, S. C.; Bell, A. T. *Journal of Catalysis* **1998**, *176*, 136.
(141) Atkins, P.W., *Physical Chemistry*, Sixth edition, Oxford University Press, 1998.